

Advanced Metallopolymer Architectures in Solution and on Surfaces

Zur Erlangung des akademischen Grades eines

DOKTORS DER NATURWISSENSCHAFTEN

(Dr. rer. nat.)

Fakultät für Chemie und Biowissenschaften

Karlsruher Institut für Technologie (KIT) - Universitätsbereich

genehmigte

DISSERTATION

von

Dipl.-Chem. Christiane Lang

aus

Karlsruhe, Deutschland

Dekan: Prof. Dr. Peter Roesky

Referent: Prof. Dr. Christopher Barner-Kowollik

Korreferent: Prof. Dr. Peter Roesky

Tag der mündlichen Prüfung: 17.04.2014

Die vorliegende Arbeit wurde von Januar 2011 bis März 2014 unter Anleitung von Prof. Dr. Christopher Barner-Kowollik am Karlsruher Institut für Technologie (KIT) - Universitätsbereich angefertigt.

Erklärung

Ich erkläre hiermit, dass ich die vorliegende Arbeit im Rahmen der Betreuung durch Prof. Dr. Christopher Barner-Kowollik selbstständig verfasst und keine anderen als die angegebenen Quellen und Hilfsmittel verwendet habe. Wörtlich oder inhaltlich übernommenen Stellen sind als solche kenntlich gemacht und die Satzung des Karlsruher Instituts für Technologie (KIT) zur Sicherung guter wissenschaftlicher Praxis wurde beachtet.

Des Weiteren erkläre ich, dass ich mich derzeit in keinem weiteren laufenden Promotionsverfahren befinde und auch keine vorausgegangenen Promotionsversuche unternommen habe.

Karlsruhe, den 02.03.2014

Christiane Lang

Publications Arising from the Present Thesis

1. C. Lang, C. Kiefer, E. Lejeune, A. S. Goldmann, F. Breher, P. W. Roesky and C. Barner-Kowollik, *Polym. Chem.*, 2012, **3**, 2413-2420.
2. C. Lang, K. Pahnke, C. Kiefer, A. S. Goldmann, P. W. Roesky and C. Barner-Kowollik, *Polym. Chem.*, 2013, **4**, 5456.

Abstract

The current thesis presents the design and synthesis of new metal-containing materials supported on polymers or solid substrates, respectively, employing highly efficient ligation techniques.

For the incorporation of Pd complexes into polymer systems, the copper catalyzed azide alkyne cycloaddition (CuAAC) is employed. Well-defined linear polymers exhibiting azide side-groups are obtained *via* radical addition fragmentation chain transfer copolymerization (RAFT) of 3-azidopropyl methacrylate with methyl methacrylate or *p*-chloromethyl styrene with styrene and subsequent azide transformation, respectively. The content of functional comonomer ranges between 13 and 57 % controlled by the variation of the initial monomer composition. A model study on the ligation of propargyl alcohol with the azide polymers evidences fine control over the amount of ligated sites *via* the added amount of the alkyne species. For the ligation of the metal complexes, full conversion of the azide side groups is targeted.

The CuAAC ligation of *N,N'*-bis(2,6-diisopropylphenyl)propiolamidine affords side-chain functionalized polymers with absolute weight-averaged molar masses up to $M_w = 30 \text{ kg}\cdot\text{mol}^{-1}$ derived from static light scattering (SLS) measurements. The metallopolymers are obtained *via* subsequent loading with $[\text{Rh}(\text{cod})\text{Cl}]_2$. SLS measurements attest molar masses up to $M_w = 46 \text{ kg}\cdot\text{mol}^{-1}$ for the metallopolymers.

Quantitative CuAAC ligation with 2-ethynyl pyridine and subsequent metal loading with $[\text{Pd}(\text{cod})\text{Cl}_2]$ in methylene chloride affords polymers with high loading efficiencies up to 84 % determined *via* nuclear magnetic resonance (NMR) spectroscopy and elemental analysis. The obtained metallopolymers exhibit absolute weight-averaged molar masses up to $M_w = 20 \text{ kg}\cdot\text{mol}^{-1}$ derived SLS measurements.

Metal complexes directly incorporated into the polymer backbone are obtained upon poly(CuAAC) ligation of bifunctionalized azides with 2,6-diethynylpyridine. A small molecule model study is conducted in order to optimize the polymerization conditions. Soluble polymers with absolute weight-averaged molar masses (SLS) close to $M_w = 56 \text{ kg}\cdot\text{mol}^{-1}$ are obtained employing 2,7-diazido-9,9-dioctyl fluorene as the azide monomer. Subsequent metal loading with $[\text{Pd}(\text{cod})\text{Cl}_2]$ affords metallopolymers with loading efficiencies up to 95 %, yet decreased solubility preventing absolute molar mass determination *via* SLS. The calculated molar mass of the metallopolymer is close to $M_w = 78 \text{ kg}\cdot\text{mol}^{-1}$.

For the modification of silicon substrates with spatial resolution, a self-assembled monolayer (SAM) of phenacylsulfide is irradiated with UV light employing a photo mask. The uncovered phenacylsulfide molecules decompose and the generated thioaldehydes are trapped *in-situ* by ligand or metal complex containing dienes. The successful immobilization of a $\text{Pd}(\text{bipy})$ and an $\text{Au}(\text{PPh}_3)\text{Cl}$ complex is confirmed *via* spatially resolved time-of-flight secondary ion mass spectrometry (ToF-SIMS).

Zusammenfassung

In der vorliegenden Arbeit werden Konzepte zur Entwicklung neuartiger Metallkomplex-haltiger Materialien mithilfe von hoch-effizienten Kupplungsreaktionen, wie der kupfer-katalysierten Alkin-Azid Cycloaddition (CuAAC) oder licht-induzierten DIELS-ALDER Reaktionen, vorgestellt.

Für die Funktionalisierung von Polymer-Seitenketten mit Metallkomplexen werden wohl-definierte azidhaltige Copolymere mittels radikalischer Additions-Fragmentierungs Kettentransferpolymerisation (radical addition chain transfer, RAFT) aus 3-Azidopropyl Methacrylat und Methyl Methacrylat, beziehungsweise aus 4-Chloromethyl Styrol und Styrol mit anschließender Azidumwandlung hergestellt. Das relative Verhältnis im Copolymer zwischen funktionalisiertem und nicht-funktionalisiertem Comonomer und somit der statistische Abstand zwischen zwei benachbarten funktionellen Gruppen kann durch die Zusammensetzung des anfänglichen Reaktionsgemisches kontrolliert werden. Die hergestellten Copolymere weisen einen zwischen 13 % und 57 % funktionelles Comonomer auf. In einer Modellstudie wird die Effizienz der CuAAC Ligation durch die teilweise Anbindung

von Propargylalkohol an die Azid-Seitenketten belegt. Der Anteil der reagierenden Seitengruppen ist über die zugeführte Menge des Alkins steuerbar. Für die Anbindung der rhodium- und palladium-haltigen Metallkomplexe wird jedoch eine vollständige Umwandlung aller Azid-Seitengruppen angestrebt.

Durch die Anbindung des Liganden *N,N'*-bis(2,6-diisopropylphenyl)propiolamidin werden Polymere mit absoluten gewichts-gemittelten molaren Massen von bis zu $M_w = 30 \text{ kg}\cdot\text{mol}^{-1}$ erhalten. Die Bestimmung der molaren Masse erfolgt mittels statischer Lichtstreuung (SLS). Die anschließende Beladung der Ligand-Polymere mit $[\text{Rh}(\text{cod})\text{Cl}]_2$ liefert schließlich die rhodium-haltigen Metallopolymere mit absoluten gewichts-gemittelten Massen (*via* SLS) von bis zu $M_w = 46 \text{ kg}\cdot\text{mol}^{-1}$

Nach der quantitativen Anbindung von 2-Ethynylpyridin an die Azidpolymere mittels CuAAC und der Metall-Beladung mit $[\text{Pd}(\text{cod})\text{Cl}_2]$ in Dichloromethan werden die palladium-haltigen Metallopolymere mit bis zu 84 % der maximal möglichen Metallbeladung erhalten. Das ergeben die Analysen mittels Kernresonanzspektroskopie (NMR) und Elementaranalyse übereinstimmend. Das absolute gewichts-gemittelte Molekulargewicht der Metallopolymere, bestimmt mithilfe SLS, beträgt bis zu $M_w = 20 \text{ kg}\cdot\text{mol}^{-1}$.

Durch die kupferkatalysierte Polyaddition von bifunktionellen Aziden und Alkinen können Metallkomplexe direkt in das Polymerrückgrat eingebaut werden. Hierzu wird ein äquimolares Gemisch aus 2,6-Diethynylpyridin mit verschiedenen Diaziden umgesetzt. Die Optimierung der Reaktionsbedingungen in Bezug auf den verwendeten Kupferkatalysator und das Lösemittel erfolgt mittels niedermolekularer Test-Reaktionen. Lösliche Polymere mit absoluten gewichts-gemittelten Molekulargewichten (SLS) von etwa $M_w = 58 \text{ kg}\cdot\text{mol}^{-1}$ werden durch die Polyaddition von 2,6-Diethynylpyridin mit 2,7-Diazido-9,9-dicylfluorene in Anwesenheit von Cu^I Komplexen in THF erhalten. Die anschließende Metallbeladung mit $[\text{Pd}(\text{cod})\text{Cl}_2]$ ergibt Metallopolymere mit bis zu 95 % der maximal möglichen Beladung, bestimmt *via* NMR und Elementaranalyse. Aufgrund nicht ausreichender Löslichkeit kann das Molekulargewicht der Metallopolymere nicht direkt mittels SLS bestimmt werden. Aus dem Molekulargewicht des unbeladenen Polymers und dem Beladungsgrad wird das Molekulargewicht auf etwa $M_w = 78 \text{ kg}\cdot\text{mol}^{-1}$ abgeschätzt.

Die orts aufgelöste Oberflächenmodifizierung von Silizium-Substraten mit Metallkomplexen ist bisher auf Tintenstrahldruck- oder Photolithografische-Verfahren beschränkt. In der vorliegenden Arbeit wird ein neues Konzept basierend auf der licht-induzierten Modifikation von selbst-anordnenden Monolagen (self-assembled monolayer, SAM) vorgestellt. Als Ligationsmethode wird der UV-induzierte Zerfall von Phenacylsulfid mit anschließender hetero DIELS-ALDER Cycloaddition zwischen dem intermediären Thioaldehyd und einem entsprechend funktionalisierten Dien verwendet. Die Diene enthalten entweder nur den Liganden oder bereits den vollständigen Metallkomplex. Auf diese Weise können zwei verschiedene Metallkomplexe, ein Pd(bipy) Komplex und ein Au(PPh₃)Cl Komplex, auf der Oberfläche immobilisiert werden. Die erhaltenen Oberflächen werden mittels Flugzeit-Sekundärionenmassenspektrometrie (ToF-SIMS) analysiert.

Contents

Introduction.....	1
Theoretical Background and Literature Overview.....	5
2.1. Metallopolymers.....	6
2.1.1. Polymers with Side-Chain Attached Metal Complexes.....	7
2.1.2. Main-Chain Metallopolymers	11
2.2. Spatially Resolved Surface Modification.....	19
2.2.1. Photo-Active Self-Assembled Monolayers on Various Substrates.....	20
2.2.2. Suitable Reactions for the Photochemical Patterning of Activated Substrates.....	21
2.2.3. Metal Patterns and Metal Complexes on Surfaces	29
Metal-Containing Side-Chain Functionalized Polymers.....	35
3.1. Side-Chain Functionalization of Poly(methyl methacrylate)s.....	38
3.1.1. Glycidyl Methacrylate Copolymers	38
3.1.2. RAFT-Endgroup Transformation.....	42
3.1.3. 3-Azidopropyl Methacrylate Copolymers	44
3.1.4. Test CuAAC Reactions of Azide Functionalized Poly(methacrylate)s with Propargyl alcohol	47
3.1.5. CuAAC Reaction of Azide Functionalized Poly(methacrylate)s with an Amidine Ligand.....	50
3.2. Side-Chain Functionalization of Poly(styrene)s.....	54
3.2.1. Synthesis of Azide-Containing Polystyrene	54
3.2.2. Reactivity Study of the CuAAC Reaction with Propargyl Alcohol.....	57
3.2.3. CuAAC Reaction with a Rh-Complexing Ligand and Subsequent Rh-Containing Polymers	61
3.2.4. Generation of a Pd-Complexing Ligand by CuAAC Ligation with 2-Ethynylpyridine and Subsequent Pd-containing Polymers.....	68
Metal-Containing Main Chain Functionalized Polymers.....	79
4.1. Synthesis of Suitable Alkyne Monomers.....	82
4.2. Low-Molecular Model Study for CuAAC Catalyst Activity Testing.....	84
4.3. CuAAC Driven Polymerization Reactions	91
4.3.1. Synthesis of Bifunctionalized Azide Linkers	91

Contents

4.3.2.	CuAAC-Polymerization of 1,3-Dipropynyl-imidazolium bromide (5) with Azide Linkers	92
4.3.3.	CuAAC Polymerization of 2,6-Dietylnyl pyridine (6) with Azide Linkers	93
4.4.	Palladium Loading of the Poly(triazole).....	97
	Spatially Controlled Surface Immobilization of Metal Complexes.....	101
5.1.	Phenacysulfide Derivatives	103
5.2.	Diene Functionalized Ligands and Metal Complexes	107
5.3.	Photo-Ligation in Solution	112
5.4.	Surface Patterning.....	115
	Concluding Remarks and Outlook.....	121
	Experimental Section	123
7.1.	Materials	124
7.2.	Measurements	126
7.3.	Syntheses	128
7.3.1.	Syntheses of Low Molar Mass Compounds	128
7.3.2.	Syntheses of Polymers.....	138
7.3.3.	Surface Preparation.....	150
	References	151
	List of Publications	167
	Conference Contributions.....	168
	Danksagung.....	169



Introduction

Organometallic compounds are versatile reagents employed, for example, in catalysis, photovoltaics, biology, or medicine.¹⁻⁵ The combination of an inorganic metal center with a layer of organic ligands generates unique properties such as the ability to switch between several oxidation states of the metal center or to solubilize metal ions in organic solvents. However, the quantitative separation of low molar metal complexes employed as catalysts in an organic synthesis from the subsequent product is challenging.⁶ In contrast, catalysts supported on solid substrates such as nanoparticles, microspheres, or polymers are readily separable from the reaction product *via* filtration or precipitation.⁷⁻⁹ Moreover, polymeric materials with incorporated organometallic moieties can feature new properties caused by the interaction of the metal centers in spatial proximity. Completely conjugated polymers with incorporated metals exhibit, for example, luminescence, magnetism or electrical conductivity.¹⁰⁻¹³ In terms of organometallic compounds supported on linear polymer chains, the metal complexes are either located on the side chains of the polymer or directly integrated into the polymer backbone. In addition to supramolecular

metallopolymers, main-chain ligand polymers can be distinguished where the metal ions are not directly participating in the backbone formation. Typical examples include polymers of interlinked SCHIFF-base or *N* heterocyclic chelate complexes, polymerized *via* polycondensation or polyaddition reactions. Please refer to section 2.1 for a more detailed literature review on linear metallopolymers.

The current thesis introduces strategies for both approaches to immobilize metal complexes on polymer supports. For the side-chain functionalization, well-defined linear polymer precursors were prepared *via* radical addition fragmentation chain transfer polymerization (RAFT) exhibiting azide moieties located at the polymer side chains. The statistical distance between two functional groups can be controlled by the copolymerization with a non-functionalized comonomer in varying ratios. The ligation efficiency of the copper catalyzed azide alkyne cycloaddition (CuAAC) is evidenced *via* the addition of propargyl alcohol. CuAAC ligation of *N,N'*-bis(2,6-diisopropylphenyl)propiolamidine and subsequent loading with [Rh(cod)Cl]₂ affords rhodium-containing metallopolymers of high molar masses. The ligation of 2-ethynylpyridine *via* CuAAC with the azide-containing polymers affords a bidental ligand composed of the pyridinyl and the triazole ring at the side chains. Subsequent metallation is carried out employing [Pd(cod)Cl₂] as the metal precursor. The modular approach enables the detailed analysis of the efficiency of each individual reaction step.

The poly(CuAAC) ligation of bifunctionalized azides with 2,6-diethynyl pyridine was employed for the synthesis of tridental *N* chelate. Comparable to the side-chain functionalization, the triazolyl rings participate in the complexation of the Pd^{II} ions introduced *via* the metal precursor [Pd(cod)Cl₂] subsequently to the polycycloaddition.

The modification of well-defined surfaces (*e.g.* silicon, glass or gold wafer) attract strong interest due to the possibility to spatially define where a compound is immobilized onto the surface. The immobilization of metal complexes *via* inkjet printing or lithographic techniques requires a complex experimental setup and is material-intensive.^{14,15} Alternatively, the spatially resolved immobilization of compounds onto photo-active self-assembled monolayers (SAMs) *via* light-triggered

ligation reactions with low experimental and material expense have already been successfully demonstrated for the ligation of small molecules, polymers and peptides. For a detailed literature review please refer to section 2.2. To date, however, there are no examples reported for the spatially resolved immobilization of metal complexes onto SAMs.

The present thesis introduces a new approach *via* the UV-triggered decomposition of phenacylsulfide and *in-situ* DIELS–ALDER trapping of the formed thioaldehyde with functional dienes. For the spatially resolved immobilization of the metal complexes onto a silicon substrate, pre-functionalized with a SAM of phenacylsulfide, the surface was partially irradiated in the presence of the diene employing a photo-mask. The Pd(bipy) and Au(PPh₃)Cl complexes were introduced in a modular fashion first, ligating only the ligand with subsequent metal loading as well as by direct ligation of the metal complex.

The presented approaches to immobilize metal complexes on polymer chains or solid substrates extend the scope of synthetic methods for the design of metallopolymeric material and metal loaded surfaces employing highly efficient ligation techniques such as CuAAC and photo-induced DIELS–ALDER reactions.

2

Theoretical Background and Literature Overview

In the following, an overview of the past and present literature focussed on metallopolymers and the patterning of substrate surfaces is presented.

Metallopolymers provide a high structural variety from linear polymers to multi armed star polymers, polymer networks or dendritic structures. Within the linear metallopolymers, side-chain metallopolymers are distinguished from main-chain metallopolymers, and the metallopolymers derived from polymeric ligands.

The literature review on spatially resolved surface modifications is mainly focussed on photo-triggered modifications of self-assembled monolayers (SAM) in general, the immobilization of metals and metal complexes onto surfaces with spatial resolution employing ink-jet printing and lithographic techniques, as well as the global immobilization of self-assembled mono- and multi layered metal complexes.

2.1. Metallopolymers

The interdisciplinary overlap at the interface of organic and inorganic chemistry is also reflected in polymer chemistry by establishing a new class of materials, so-called metallopolymers. These materials do not necessarily only combine the individual properties of polymers and organometallics, respectively, but exhibit new characteristics induced by an interaction between the metal ions incorporated into the polymer chains. Figure 1 depicts the possible structural variety of metallopolymers obtained *via* different strategies to incorporate a metal ion – most often stabilized by organic ligands – into a polymeric material. The additional diversity both in the nature of the polymer and the organometallic complexes enables the generation of tailored functional materials for applications, *e.g.* in catalysis, photo- or electrochemistry.

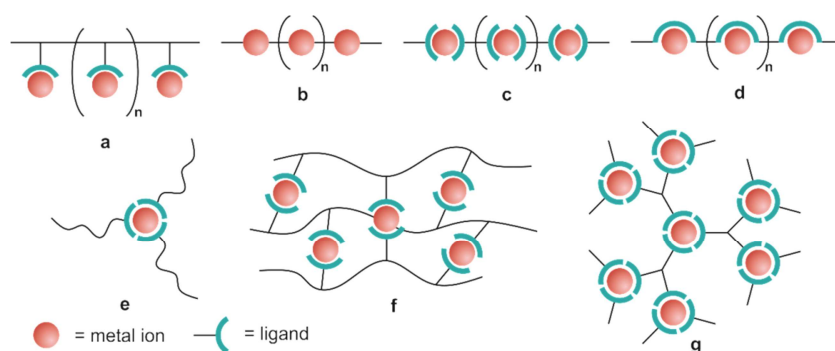


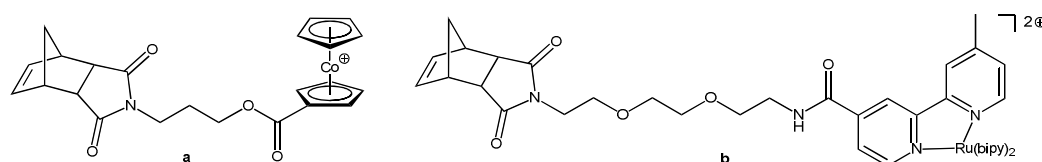
Figure 1. General structures of metallopolymers. Linear polymers can be equipped with metal complexes located at the side chains (a). Poly(metallayne)s exhibit metal-alkyne σ -bonds in their polymeric backbone (b), while supramolecular metallopolymers are constructed *via* dynamic ligand-metal coordination along the polymer backbone (c). In metallopolymers derived from polymeric ligands (d), however, the polymer backbone is established from covalently linked ligands, which can be metallated previous or past to the actual polymerization. Non-linear structures are based on the coordination of metal ions with additionally functionalized ligands. Upon metal addition, star polymers (e) are derived from polymers featuring a ligand-endgroup, polymeric networks (f) are obtained from polymers equipped with multiple ligand functionalities along a polymer backbone, and dendritic structures (g) are formed employing multi-armed ligands.

Due to the wide scope of polymeric materials with incorporated metals, the following review will be limited on linear polymers as depicted in Figure 1a-d with disregard to multidimensional structures, such as multi armed star polymers, polymer networks, hyperbranched, or dendritic polymers as depicted in Figure 1e-f. For detailed reviews on the latter materials, the reader is referred to the relevant literature.¹⁶⁻¹⁹

Within the linear metallopolymer structure family, the position of the metal complexes can be distinguished between side-chain (Figure 1a) and main-chain locations which in turn can be subdivided into three classes. Polymers with covalently bound metals (Figure 1b) in the backbone – realized *via* metal-acetylene σ -bonds – are termed poly(metallaynes). Employing a metal-coordinating ligand, the polymer can be generated *via* coordinative and dynamic bonds as implemented in supramolecular metallopolymers (Figure 1c). The incorporation of bifunctional metal coordinating ligands along the polymer backbone affords polymeric metal ligands (Figure 1d). The functionalization with metal ions can either be conducted in a reaction step previous, simultaneous, or past to the polymerization. In the following, some examples for the above noted classes of linear metallopolymers will be reviewed without claiming to be exhaustive. An additional section addresses the special sub-class of supramolecular metallopolymers, the poly(metalloarenes).

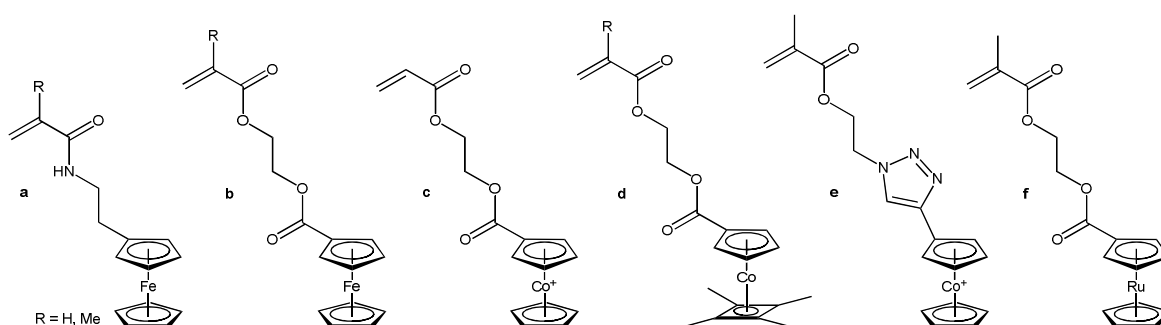
2.1.1. Polymers with Side-Chain Attached Metal Complexes

Side-chain functionalized polymers (Figure 1a) can be derived either by post-polymerization transformation or by employing the pre-synthesized functional monomer directly in the polymerization process. Advantages of the pre-polymerization approach are the facile characterization and the possibility to separate the product from by-products by conventional organic synthetic methods, *e.g.* column chromatography or distillation. For example, the ring-opening metathesis polymerization (ROMP) of monomers pre-functionalized with cobaltocene or Ru(bipy) is realized *via* ester or amide binding units between the precursor-monomer and the functionalized metal complex (Scheme 1).^{20,21}



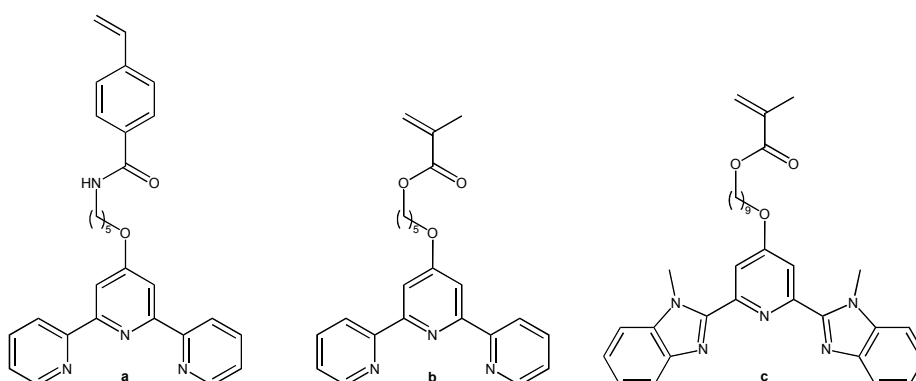
Scheme 1. Suitable monomers for the ring-opening metathesis polymerization (ROMP) containing cobaltocene (a) or Ru(bipy) complexes (b).^{20,21}

Within radical polymerizations, the functionalized monomers are most-often based on typical species such as styrenics, acrylates or methacrylates. Ferrocene and cobaltocenium-containing acrylates and methacrylates can be obtained *via* esterification or copper catalyzed alkyne-azide cycloaddition (Scheme 2) and are polymerized in conventional or controlled radical polymerization reactions, such as atom-transfer radical polymerization (ATRP) or reversible addition fragmentation chain transfer (RAFT) polymerization.²²⁻²⁸



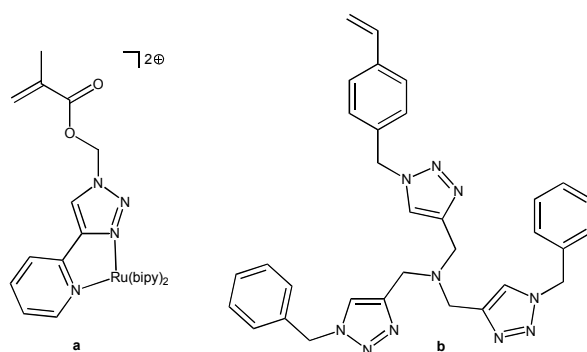
Scheme 2. Acrylic and methacrylic monomers equipped with metallocene moieties.²²⁻²⁸

The polymerization of monomers already functionalized with the metal ligand represents an intermediate between the pre- and the post-polymerization approach. Suitable monomers are, for example, terpyridine functionalized styrene (Scheme 3a) or methacrylate (Scheme 3b), as well as methacrylate modified with a di(benzimidazolyl)pyridine ligand (Scheme 3c). After nitroxide mediated polymerization (NMP), ATRP or RAFT polymerization, the metallopolymers are obtained in a subsequent metallation step, e.g. with Cd^{II} , Cu^{II} , Zn^{II} , or Co^{II} ions.²⁹⁻³¹



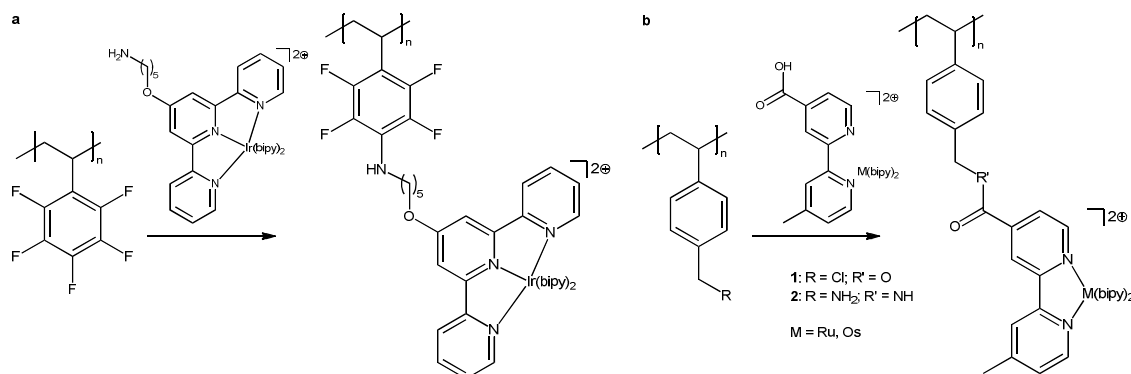
Scheme 3. Styrenic and methacrylic monomers equipped with tridental ligands suitable for NMP, ATRP or RAFT polymerization and subsequent metallation.²⁹⁻³¹

The triazolyl ring formed in the CuAAC ligation is additionally applicable as a ligating unit, *e.g.* together with an adjacent pyridinyl ring for the coordination of Ru^{II} in methacrylates (Scheme 4a),³² or in the styrenic tris(benzyl triazolyl methyl) amine ligand (Scheme 4b).³³



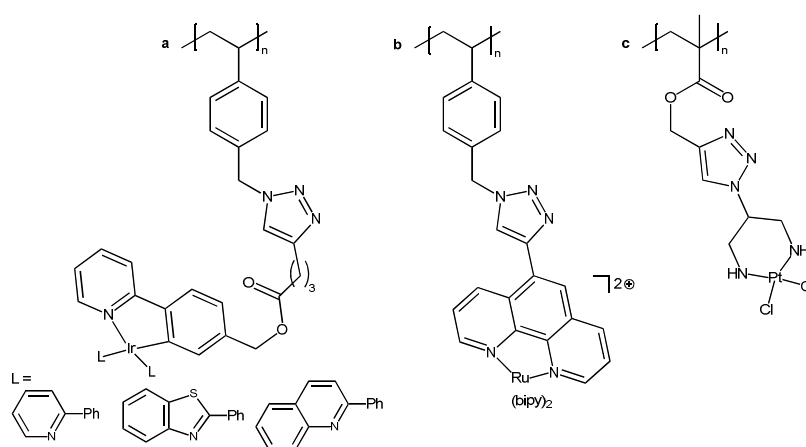
Scheme 4. Monomers with multidentate ligand moieties composed of the triazolyl ring formed upon CuAAC ligation with nitrogen-containing compounds.

The post-polymerization functionalization of precursor polymers with metal complexes is more demanding in terms of the modification reactions. For complete functionalization of the present side groups, the employed reactions need to be highly efficient and by-products should be easily separable, *e.g.* by precipitation of the polymer. Substituted poly(styrene)s are suitable precursor polymers for the post-polymerization functionalization. For example, the *para*-substitution of a poly(pentafluoro styrene) with an amino-functionalized Ir^{II} containing complex is depicted in Scheme 5a.³⁴ Side chains equipped with Ru^{II} or Os^{II} complexes can be obtained by the post-polymerization reaction of chloride- or amine-functionalized poly(styrene)s with carboxylic acid metal complexes (Scheme 5b).³⁵⁻³⁸



Scheme 5. Post-functionalization of modified polystyrene. (a) Substitution of poly(pentafluoro styrene) with an amino-functionalized Ir^{II} complex.³⁴ (b) Attachment of carboxylic acid metal complexes onto chloride- or amine-functionalized poly(styrene)s.³⁵⁻³⁸

With characteristics such as high efficiency and orthogonality to many functional groups, the CuAAC reaction is a suitable post-polymerization reaction. Polymerization of 4-vinyl benzyl chloride *via* conventional free-radical or RAFT polymerization and subsequent azide-transformation with sodium azide affords the precursor polymers for ligation of alkyne-functionalized Ir(2-pyridine benzyl) (Scheme 6a) or Ru(phenanthroline) (Scheme 6b) complexes.^{39,40} Inversely, methacrylate based polymers with triazole-linked *cis*-Pt(1,3-diaminopropyl) complexes (Scheme 6c) are obtained from alkyne side-chain functionalized poly(methyl methacrylate).⁴¹



Scheme 6. Post-functionalized metallopolymers *via* CuAAC ligation of metal complexes with azide functionalized poly(styrene) (a,b) or alkyne-functionalized poly(methyl methacrylate) (c).

A general challenge in the characterization of metallopolymers is the determination of the molar mass. Since the charged species interact with the column material, gel permeation chromatography (GPC) often affords falsified or non-reproducible results.⁴² As an exclusion, poly(metallocene)s can be readily analyzed *via* GPC since the metal centers do not significantly interact with the GPC column material enabling GPC analysis of polymers with molar masses up to $M_n = 61 \text{ kg}\cdot\text{mol}^{-1}$.^{20,24-26,28} Alternative determination of the molar mass of the metallopolymer can be conducted *via* nuclear magnetic resonance spectroscopy (NMR), or static light scattering (SLS),^{21,22,27} yet most-often the molar mass of the metallopolymers is derived indirectly from the molar mass of the metal-free precursor polymer and the results of measurements determining the loading of the polymers.^{31,33,34,39-41}

2.1.2. Main-Chain Metallopolymers

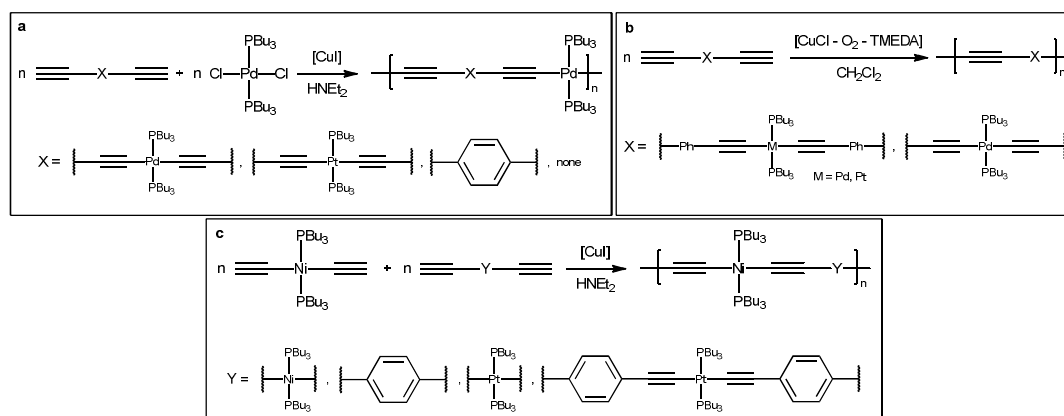
Polymeric Metallaynes

The incorporation of metals into a polymeric backbone by carbon-metal σ -bonds (Figure 1b) characterizes the group of poly(metallayne)s. Due to their rigid structure and high electron density along the polymer backbone, these polymers are often employed in optoelectronic fields, *e.g.* optical power limiters (OPL), or organic solar cells.^{43,44}



Scheme 7. Schematic structure of poly(metallayne)s.

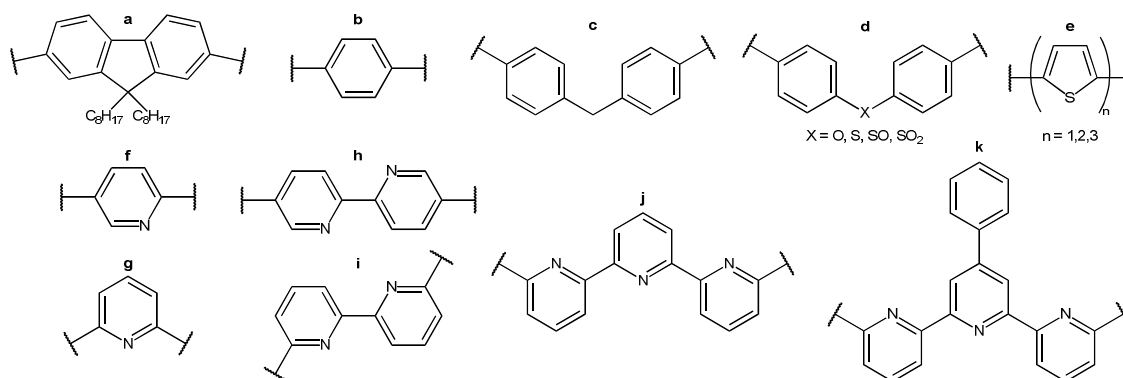
The general structure of poly(metallayne)s is depicted in Scheme 7. The metallopolymers are composed of the metal center covalently bound to acetylene units. In addition, the metal can be stabilized by ligands, or an optional spacer can be incorporated in order to tune the properties of the resulting polymer. Poly(metallayne)s are accessible *e.g.* by Cu-catalyzed dehydrohalogenation (Scheme 8a),^{45,46} oxidative self-coupling employing a catalytic mixture of CuCl and O₂ (Scheme 8b),⁴⁷ or alkynyl ligand exchange reaction (Scheme 8c).⁴⁸



Scheme 8. Synthesis of poly(metallayne)s *via* Cu-catalyzed dehydrohalogenation (a), oxidative self-coupling (b), or alkynyl ligand exchange (c).

The beneficial properties of Pt^{II} ions in terms of opto-electronic applications account for the dominance of metallaynes with Pt^{II} ions as metal centers that are most often stabilized by phosphorous ligands. As spacer moieties conjugated systems are preferred in order to benefit from the conjugated metal-acetylenic structure. The

repertory of spacers includes, for example, fluorene (Scheme 9a),⁴³ phenylene and bridged diphenylenes like diphenylmethane, diphenylether, diphenylsulfide, or diphenylsulfoxide (Scheme 9b-d).⁴⁹⁻⁵² Pyridine, bipyridine, or terpyridine (Scheme 9f-k), as well as thiophene, bithiophene, or terthiophene (Scheme 9e) are suitable structures for the metallaynes interlinked by heterocyclic spacers.⁵³⁻⁵⁶



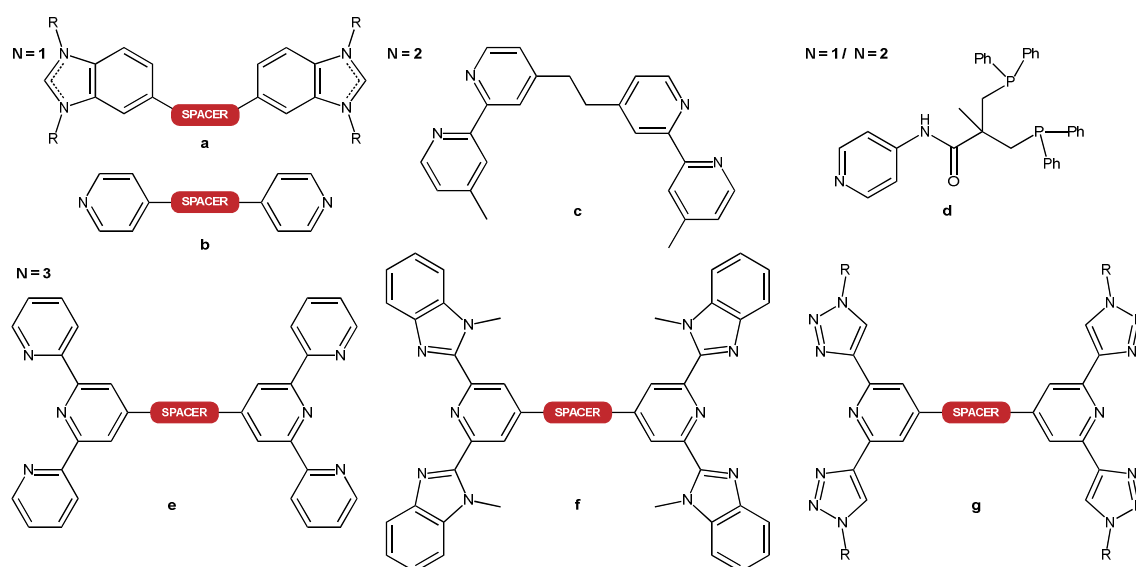
Scheme 9. Suitable spacers for the incorporation into poly(metallayne)s. Fluorene (a), phenylene (b), diphenyl methane (c), diphenyl ether, diphenyl sulfide, diphenyl sulfoxide, diphenyl sulfone (d), thiophene, bithiophene, terthiophene (e), imidazole (f,g), bipyridine (h,i), terpyridine (j), and 4'-phenyl-terpyridine (k).^{43,49-56}

Various other spacers are collated in detailed review articles, *e.g.* by Ho *et al.*,⁵⁷ or Long *et al.*⁵⁸ Besides the Pt-containing poly(metallayne)s, comparable compounds with Pd^{II}, Ni^{II}, Co^{II}, Hg^{II}, or Au^{II} have been reported.^{43,59,60} The molar mass of the metallopolymers can be adjusted to the application requirements. High molar masses up to 87 kg·mol⁻¹ with a dispersity of 1.8 are, for example, attained for Pt-polymers with bipyridyl spacers.⁵⁴

Supramolecular Metallopolymers

Supramolecular polymers (Figure 1c) in general feature non-covalent bonds within the lateral polymer chain. Besides employing hydrogen bonding moieties, supramolecular bonding can be realized by the incorporation of metal (chelate) complexes into the polymeric backbone to form supramolecular metallopolymers. For the polymerization of a pre-synthesized metal complex suitable polymerization protocols can be employed that are also applicable for other specialized monomers, *e.g.* the SUZUKI coupling of bis(terpyridine)Ru^{II} complexes with bifunctional fluorene linkers,⁶¹ or the electropolymerization of bis(2,6-di(quinolin-8-yl)pyridine)Ru^{II}

complexes.⁶² On the other hand, the polymerization of metal ligands by the addition of a metal precursor is unique for supramolecular metallopolymers. Suitable monomers feature two metal binding units linked by a spacer (Scheme 10). Most commonly nitrogen-containing heterocycles are employed as ligands, such as *N* heterocyclic carbenes or pyridine derivatives. Benzimidazolyl ligands (Scheme 10a) for example coordinate to Pd^{II} or Pt^{II} ions building polymers with molar masses of $M_n = 8000 \text{ g}\cdot\text{mol}^{-1}$ and a dispersity of $\mathcal{D} = 1.3$. As a spacer, fluorene moieties were employed to increase the solubility of the polymers.⁶³ The addition of a pre-formed Sn-ferrocene adduct to bis(pyridine)s (Scheme 10b) interlinked without a spacer, or by a propylene or vinylene spacer unit, provides bimetallic supramolecular metallopolymers.⁶⁴ Anthracene-linked bis(pyridine)s are employed to form silver-containing polymers upon reaction of the ligand with silver nitrate.⁶⁵ Examples of bidental ligands for the synthesis of supramolecular metallopolymers are bis(dipyridine)s (Scheme 10c) or bis(diphenylphosphine)s (Scheme 10d). The former was coordinated with Ru^{III} providing trimers of Ru^{II} and Ru^{III} metal complexes⁶⁶ while the latter is able to coordinate Cu^{II}, Ag^{II}, Au^{II}, Pt^{II} or Pd^{II} ions by the combination of the bis(diphenylphosphin) ligand from one molecule and the pyridinyl moiety of an adjacent ligand molecule.⁶⁷

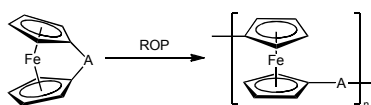


Scheme 10. Examples of building blocks for supramolecular metallopolymers. (a) Bis(benzimidazolyl),⁶³ (b) bis(pyridine),⁶⁴ (c) bis(bipyridine),⁶⁶ a combination of pyridine and diphenylphosphine,⁶⁷ (e) bis(terpyridine),⁶⁸⁻⁷¹ (f) bis(dibenzimidazolyl pyridine),^{72,73} and (g) bis(di(triazolyl)pyridine).⁷⁴

The tridental ligands are most frequently employed as metallocupramolecular building blocks. The terpyridine moiety (Scheme 10e), for example, can be linked *via* fluorene, quinoxaline, bis(ureido pyrimidine), or phenylene spacers and coordinates metal ions such as Ru^{II}, Zn^{II}, or Fe^{II}.⁶⁸⁻⁷¹ Bis(benzimidazolyl pyridine)s (Scheme 10f) with a poly(butadiene) spacer form supramolecular metallopolymers with Zn^{II},⁷³ or act as crosslinking units of linear conjugated polymer chains *via* the coordination of Zn^{II} or Cu^{II} ions.⁷⁵ New tridental ligands are obtained by the copper catalyzed azide-alkyne cycloaddition (CuAAC) of diethynylpyridine and two azide molecules. The ditopic ligands (Scheme 10g) with a conjugated π -system as spacer forms metallopolymers by the ligation of Ru ions. The obtained polymers exhibit molar masses of $M_n = 35 \text{ kg}\cdot\text{mol}^{-1}$ with a dispersity of $\mathcal{D} = 3.30$.

Poly(metalloarene)s

Metalloarenes are well-studied organometallic compounds most often featuring high stability and facile derivatization at the aromatic rings. The most prominent representative – ferrocene – was reported in 1952 for the first time.^{76,77} Shortly thereafter, the first reports on poly(ferrocene)s followed highlighting the interest in organometallic polymeric materials.^{78,79} In time not only the synthesis of novel small molecule metalloarenes but also different protocols for the polymerization of metalloarenes were developed. The ring-opening polymerization (ROP) of strained metalloarenophanes, for example, gives 1,1'-linked poly(metalloarene)s. The bridging element defines the angle between the planes of the two aromatic rings and induces ring strain. It is the higher the more distorted the rings are and thus, the monomer is more reactive to a ring-opening reaction. The radical ROP can be initiated thermally,⁸⁰ photolytically,^{81,82} or by a transition metal catalyst.⁸³ The addition of strong bases like ⁿBuLi initiates the anionic ROP.⁸⁴



Scheme 11. Ring-opening polymerization (ROP) of ferrocenophanes. Examples of bridging elements and polymerization conditions are collated in Table 1.

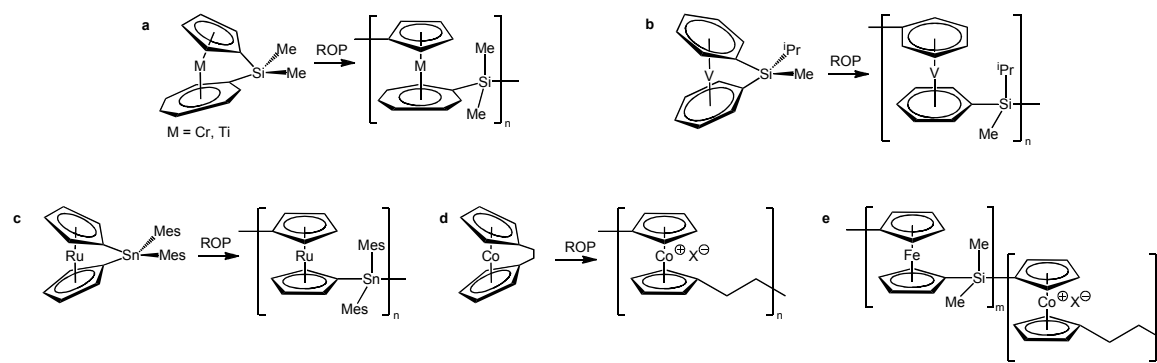
A variety of ferrocenophanes and their respective polymers exists. Scheme 11 schematically depicts the ROP of bridged ferrocenophanes and Table 1 collates some examples of bridging elements, as well as the polymerization conditions and the obtained molar mass (M_n) and dispersity (\mathcal{D}) of the respective poly(ferrocene)s.

Table 1. Bridging elements of ferrocenophanes, polymerization conditions of the respective ring-opening polymerization and obtained molar masses and polydispersities of the poly(ferrocene)s.

A	R	polymerization conditions	M_n^a kg·mol ⁻¹	\mathcal{D}^a	Lit.
C₂R₄	H, Me, ⁱ Pr, Ph	photolytic ROP (NaCp + h·ν)	12.8	1.30	85
SiR₂	C≡C ^t Bu	catalytic ROP (PtCl ₂)	multimodal		86
		thermal ROP (160 - 185 °C)	multimodal		
		photolytic ROP (NaCp + h·ν)	43.1	1.15	
PR	^t Bu, CH ₂ ^t Bu, CH ₂ SiMe ₃	photolytic ROP (NaCp + h·ν)	88.3	1.40	87
GeR₂	Me	anionic ROP (ⁿ BuLi)	33.7	1.05	88

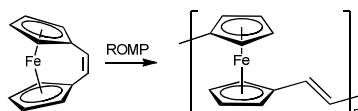
^a For clarity only one selected example is collated per reference.

Other metalloarenophanes are, for example, SiR₂ bridged complexes of Cr^{II}, Ti^{II}, or V^I, as well as ruthenocenophanes and cobaltocenophanes to provide the respective linear metallopolymers after ring-opening polymerization as depicted in Scheme 12.⁸⁹⁻⁹³ In addition, block-copolymers are accessible for example by the subsequent ROP of a ferrocenophane and a cobaltocenophane (Scheme 12e).⁹⁴



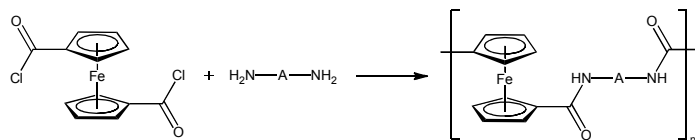
Scheme 12. Ring-opening polymerization of (a) *ansa*-[1]silacyclopentadienyl-cycloheptatrienyl chromium and titanium complexes,^{89,90} (b) *ansa*-[1]-sila-bis(benzyl) vanadophorane,⁹¹ (c) *ansa*-[1]-tin ruthenocenophane,⁹² and (d) *ansa*-[2]ethyl cobaltocenophane.⁹³ (e) A ferrocene-*block*-cobaltocene copolymer obtained *via* ROP.⁹⁴

The ring-opening metathesis polymerization (ROMP) of *ansa*-[2]-vinylene ferrocenophane in the presence of suitable organometallic catalysts provides conjugated organometallic polymers (Scheme 13).^{95,96}



Scheme 13. Ring-opening metathesis polymerization (ROMP) of *ansa*-[2]-vinylene ferrocenophane provides a conjugated metallopolymer with the metal center directly incorporated into the polymer backbone.

Alternating copolymers are accessible *via* polycondensation reactions, *e.g.* of 1,1'-ferrocenedicarbonyl chloride with bis(amine)s as depicted in Scheme 14. As variable linkers, sulfonyl phenylene,⁹⁷ siloxane,^{98,99} or aniline derivatives¹⁰⁰ can be employed, as well as phenylene or cyclohexyl linkers to mention but a few examples. Polyesters are obtained employing dialcohols instead of the bis(amine) moieties.⁹⁹



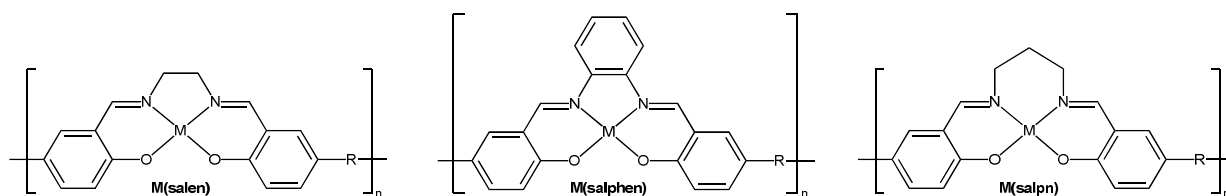
Scheme 14. Polycondensation reaction of 1,1'-ferrocenedicarbonyl chloride with bis(amine)s.

Further, novel polymerization strategies such as SONOGASHIRA coupling or the copper(I) catalyzed azide-alkyne cycloaddition (CuAAC) of multifunctional monomers have been successfully employed to synthesize poly(metalloarene)s.¹⁰¹⁻¹⁰³ In addition to the polymers where the metalloarene unit is incorporated into the polymer backbone, side-chain metalloarene functionalized polymers, *e.g.* poly(acrylate)s and poly(methacrylate)s with ferrocene or cobaltocenium side groups,²²⁻²⁵ have been synthesized successfully as well as dendrimeric metalloarene structures.¹⁰⁴

Polymeric Ligands and Derived Metallopolymers

Metallopolymers composed of a polymeric metal ligand backbone and therein coordinated metal ions (Figure 1d) draw considered attention since they offer high flexibility in the synthetic strategies in addition to their specific electronical and optical characteristics. A pre-synthesized metal complex can be polymerized directly ensuring full metal loading. On the other hand, the metal-free ligand polymer can be synthesized and characterized previous to the metal loading which can possibly provide air- or moisture sensitive materials. In addition, a precursor polymer can be loaded with different metal ions with minimal synthetic efforts.

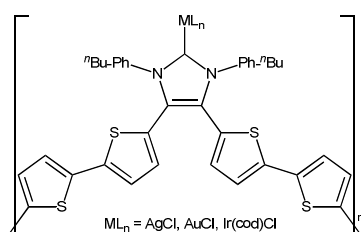
SCHIFF-base ligands (Scheme 15) such as *N,N'*-bis(salicylidene) ethylenediamine (salen) or the related compounds salphen and salpn feature a N_2O_2 coordination pocket suitable for divalent metal ions like Zn^{II} , Co^{II} , Ni^{II} , $(VO)^{II}$, Cu^{II} , Ni^{II} , Cd^{II} , or Mn^{II} , which can be introduced by the respective acetates or chlorides.¹⁰⁵



Scheme 15. Salene-type metal complexes incorporated into the polymer backbone.¹⁰⁵

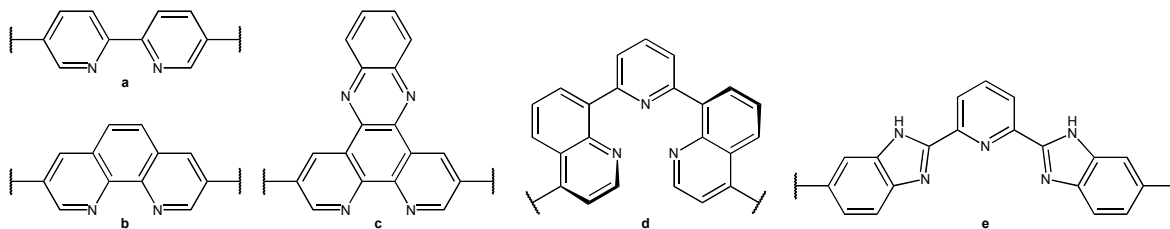
The incorporation of these moieties into a polymeric backbone is realized *via* condensation,¹⁰⁶⁻¹⁰⁸ SONOGASHIRA coupling,¹⁰⁹ elimination,¹¹⁰ or electropolymerization of suitable bifunctional monomers.^{111,112} According to the various synthetic routes the linkages between the salen-type ligands are versatile, *e.g.* fused aromatic rings,^{106,107} thiophene bridges,^{111,112} or acetylenes.¹⁰⁹ The incorporation of comonomers *via* polycondensation reactions provides functionalized polyethers, polyesters, or polyurethanes.¹¹³⁻¹¹⁵

Electropolymerization of bis(bithiophene) substituted NHC-metal complexes provide Ag^{II} , Au^{II} , or Ir^{II} containing metallopolymers (Scheme 16). They exhibit varying electrochromic properties dependant on the employed metal complex.^{116,117}



Scheme 16. Metal-NHC complex containing polymer obtained *via* electropolymerization.

A further multifaceted group of metallopolymers is derived from the metal-loading chelate-ligands incorporated into the polymeric backbone. Typical ligands employed in the polymer synthesis are bipyridine (bipy), phenanthroline (phen), dipyrrophenazine, diquinolinepyridine, and dibenzimidazolyl pyridine (Scheme 17).^{62,118-121}



Scheme 17. Ligand motifs of chelate-metallopolymers. Bipyridine (a), phenanthroline (b), dipyrrophenazine (c), diquinoline pyridine (d), and dibenzimidazolyl pyridine (e).

Besides some examples with other metal centers,¹¹⁸ complexes with Ru^{II} are most studied due to their beneficial electronical and optical features. Conjugated polymers with Ru(bipy) units, for example, are likely suitable materials for photosensitizers, photoconductors, charge-transport species, or light emitters,¹²²⁻¹²⁸ while Ru(phen)-containing metallopolymers could be successfully employed as donor species in photovoltaic devices.¹¹⁹ Other applications, *e.g.* light emitting devices with Ru(dipyridophenazine) or Ru(dibenzimidazolyl pyridine) containing metallopolymers,^{62,121} as well as photoredox-active films composed of polymers with Ru(diquinoline pyridine) complexes in the backbone also exploit the unique optoelectronic features of the conjugated metallopolymers.¹²⁰

2.2. Spatially Resolved Surface Modification

The generation of substrate surfaces exhibiting spatial resolution is of high interest, *e.g.*, in tissue engineering,¹²⁹ biomedical applications,¹³⁰⁻¹³² the design of new “smart” materials with stimuli responsive (super-) hydrophilic / hydrophobic properties,^{133,134} as well as the development of materials for electronic devices.^{135,136} Typical techniques to generate patterned surfaces include lithographic methods,^{15,137} inkjet printing,¹³⁸ microcontact printing,^{139,140} and the photochemical modification of substrates. The lithographic patterning of substrates (Figure 2a) is based on the partial removal of a pre-coated polymer layer applying a mechanical force or light.^{141,142} An optional functionalization of the uncovered surface can be carried out, *e.g.* with bioactive substances.^{143,144} Subsequently, the remaining polymer layer can be removed, if required. For microcontact printing (Figure 2b), a stamp is incubated with the molecules to be attached to the surface. The stamp is subsequently applied to the substrate and the molecules transfer from the stamp to the substrate. The employed ink can either contain the targeted molecules,¹⁴⁵ or precursors such as polymerization initiators,¹⁴⁰ or functionalized linkers, *e.g.* for subsequent CuAAC, DIELS–ALDER, or thiol-ene ligations.¹³⁹

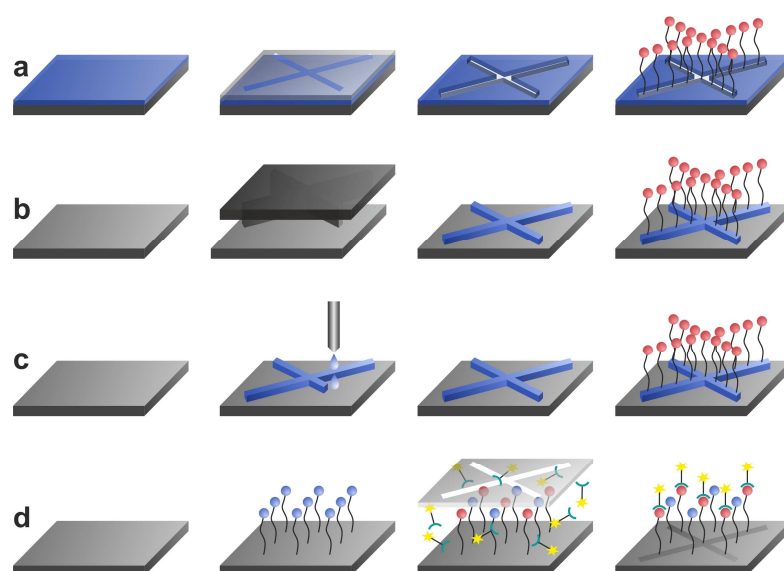


Figure 2. Modification techniques for surface patterning. (a) Lithography, (b) microcontact printing, (c) inkjet printing, and (d) photochemical reactions.

Inkjet-printed substrates (Figure 2c) are prepared from fluids containing the targeted molecules that are applied to the surface and subsequent solvent evaporation. Thus, variable patterned substrates, *e.g.* with immobilized metal-organic frameworks (MOFs), polymers or biochemical valuable substances, can be produced.¹⁴⁶⁻¹⁴⁸ The photochemical patterning of substrates (Figure 2d) covered with a photo-active self-assembled monolayer (SAM) is based on the light-triggered activation of those photo-active moieties on the surface that are not covered with the employed shadow mask. The next section will focus on suitable reactions for the photo-patterning of SAMs as a versatile and readily realizable approach followed by a review of surface analytic techniques.

2.2.1. Photo-Active Self-Assembled Monolayers on Various Substrates

Typical substrate materials are polymer films, carbon allotropes (carbon nanotubes, fullerenes, or graphene), gold, silver, silicon, glass or indium tin oxide (ITO) wafers, or biosubstrates, *e.g.* composed of cellulose or hyaluronic acid. The basic immobilization of a suitable SAM for the subsequent photo-ligation on the substrate depends on the available binding sites on the substrate surface. For polymer film modification, side chain or endgroup functionalities of the polymers can be employed, *e.g.* the chlorine side groups of poly(vinylbenzyl chloride) copolymerized with divinylbenzene or the bromine endgroups in functionalized poly(propylene) obtained *via* plasma-polymerization.^{149,150} If the photo-reactive group is stable under the polymerization conditions, it can be directly incorporated into the polymeric film material.¹⁵¹ Alternatively, the surface functionalization of non-modified polymer substrates can be realized *via* UV irradiation in the presence of perfluoro derivatives.¹⁵² For the functionalization of cellulose or hyaluronic acid substrates the free hydroxyl functions can be utilized in esterification reactions.^{153,154} Inorganic substrates like glass, gold, or silicon wafers are often employed for surface modification reactions due to their defined and smooth surface properties facilitating surface analytics. Here, the special affinity of thiols to gold,¹⁵⁵⁻¹⁵⁸ or of silanes to glass, ITO and silicon, respectively, are exploited to attach reagents onto the surface.¹⁵⁹⁻¹⁶⁵ Another approach to attach functional molecules onto various surfaces mimics the strong

adhesion of mussels *via* the catechol groups of *L*-3,4-dihydroxyphenylalanine (*L*-DOPA).¹⁶⁶

The basic functionalized substrates can then be reacted in the respective photoreactions which will be introduced in the following section.

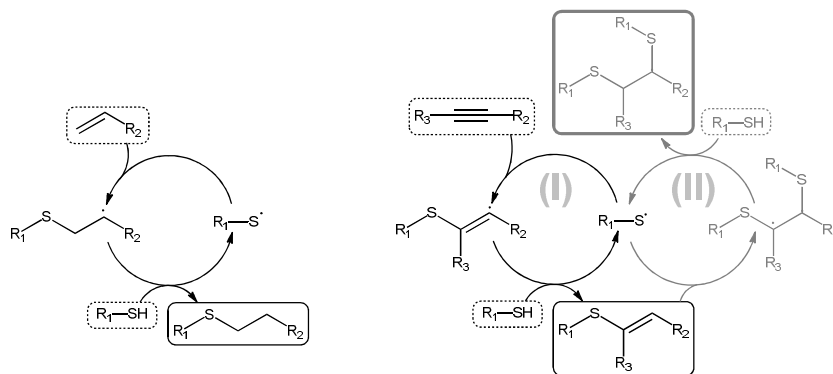
2.2.2. Suitable Reactions for the Photochemical Patterning of Activated Substrates

In principle, every reaction that is activated by light can be employed for the photo-patterning of surfaces following the procedure depicted in Figure 2D. Restrictions may arise from the material that is supposed to be functionalized and the feasibility to immobilize the photo-reactive groups onto the surface. The employed photoreaction should be orthogonal to additional functionalities of the ligated compounds and proceed in high yields. Potentially generated by-products can only be removed by washing and ultrasonication if they are not attached to the substrate surface. In the following, the three dominating reaction types for light-induced surface functionalization will be introduced, namely the addition of thio-radicals to alkenes or alkynes (thiol-ene and thiol-yne reaction), 1,3-dipolar cycloadditions, and DIELS–ALDER cycloadditions.

Thiol-ene and Thiol-yne Reaction

The radical addition of thiols to alkenes or alkynes, respectively, is – besides the application as a polymerization technique¹⁶⁷⁻¹⁶⁹ – a versatile tool for the modification of polymer chains such as chain-end functionalization, cross-coupling, as well as the formation of stars or dendrimers.¹⁷⁰⁻¹⁷² Especially for biochemical applications the thiol-ene and thiol-yne reaction represent viable alternatives to the widely exploited copper catalyzed cycloaddition of azides and alkynes since there are no heavy metal catalysts required and the functional groups are readily available.¹⁷³⁻¹⁷⁶ The addition mechanisms are depicted in Scheme 18. In both cases, a thiol-radical is formed *via* proton abstraction by a radical initiator. The addition of the unsaturated moiety in *anti*-MARKOVNIKOV position and subsequent proton abstraction from a second thiol affords the thioether product.¹⁷⁷ If terminal alkynes are employed as the unsaturated

species, the addition of another thiol can occur following the same mechanism as depicted in Scheme 18, right hand side.¹⁷⁸ Typically employed radical initiators are *N,N*-azobisisobutyronitrile (AIBN) for thermal initiation at 60 °C, or 2,2-dimethoxy-2-phenylacetophenone (DMPA) which is activated upon irradiation at $\lambda = 365$ nm,¹⁷⁹⁻¹⁸¹ but there exist also examples of initiator-free thiol-ene reactions *via* irradiation at $\lambda = 365$ nm or 254 nm, respectively.^{182,183}



Scheme 18. Reaction scheme for the radical thiol-ene (left) and thiol-yne addition (right). The optional addition of a second thiol in the thiol-yne reaction as depicted in the second cycle is restricted to terminal alkynes with $R_3 = H$.

The patterning of sugar molecules both *via* the thiol-ene and the thiol-yne approach can be realized employing thiol functionalized sugars to surfaces equipped with a self-assembled monolayer of alkenes or alkynes. Irradiation in water at $\lambda = 365$ nm in the presence of DMAP as the radical initiator affords the modified substrate which can serve as a biosensor (Figure 3a,b).¹⁵² The biocompatibility of the thiol-ene ligation method is illustrated by the attachment of alkene or alkyne derivatized proteins onto a thiol containing surface. Successful patterning could be proven by incubating the surfaces with fluorescent labelled streptavidin (Figure 3c).^{160,184} A study of side-chain functionalization of alkyne-containing polymethacrylates directly on the substrate surface in order to obtain polymer brushes indicates the limits of the thiol-yne surface modification (Figure 3d). Surface analysis was conducted *via* infrared spectroscopy and film thickness measurements. The incomplete disappearance of the vinyl sulfide vibration in the IR spectra of the product substrates as well as a minor increase in film thickness than expected allowed for the qualitative conclusion that – especially the addition of the second thiol to the intermediate vinyl sulfide – is the more challenging the more sterically demanding the thiol is.¹⁵⁹

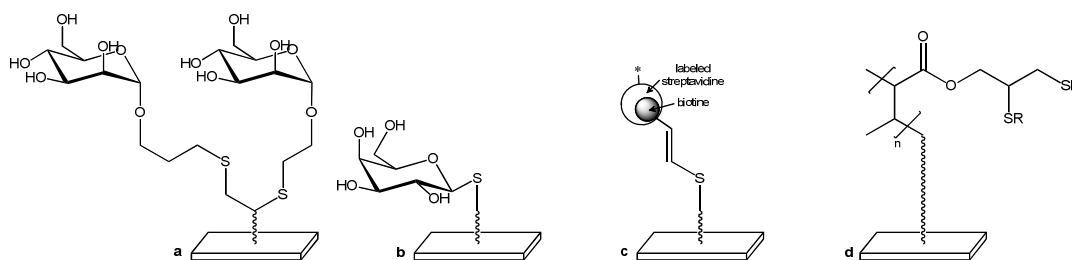
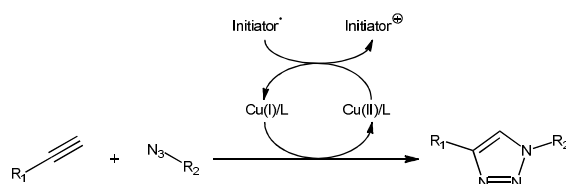


Figure 3. Examples for the spatially resolved functionalization *via* thiol-ene and thiol-yne reaction. Synthesis of biosensors is realized patterning thiolated sugar molecules onto an alkyne (a) or an alkene (b) SAM.¹⁵² The immobilization of biotinyne alkyne on thiol-containing surfaces is detected *via* streptavidin recognition (c).^{160,184} Polymer brushes are obtained after the thiol-yne reaction of alkyne containing poly(methacrylate) with various thiols (d).¹⁵⁹

In summary, the thiol-ene and thiol-yne ligation on surfaces are versatile tools particularly for biochemical applications since they proceed without the addition of heavy metal catalysts and produce biocompatible adducts. On the other hand, the formation of free radicals in the reaction mixture may cause undesired side reactions altering the expected properties of the modified substrates. In these cases, a cycloaddition reaction could be a promising alternative.

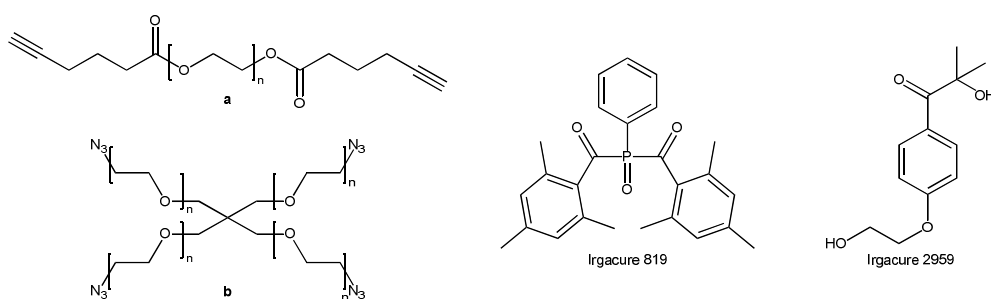
1,3-Dipolar Cycloadditions

The significant interest in 1,3-dipolar cycloaddition reactions and especially in the copper catalyzed alkyne-azide cycloaddition (CuAAC) for the modification of valuable compounds is displayed in a wide range of applications.¹⁸⁵⁻¹⁸⁷ To extend the scope of applications to spatially controlled surface modifications, the reaction needs to be photo-induced. In order to implement this photo-control into the CuAAC reaction, a photo-active catalytic system consisting of a Cu(II) complex and a photoinitiator can be employed. The initiator decomposes upon UV irradiation and the generated radicals reduce the Cu(II) complex to the catalytic active Cu(I) species (Scheme 19). There are no restrictions concerning the employed alkynes and azides except that they should be stable under UV irradiation.



Scheme 19. Copper-catalyzed 1,3-dipolar cycloaddition of alkynes and azides. The catalytic active Cu(I) species is obtained *via* reduction of Cu(II) by a photoinitiator radical.

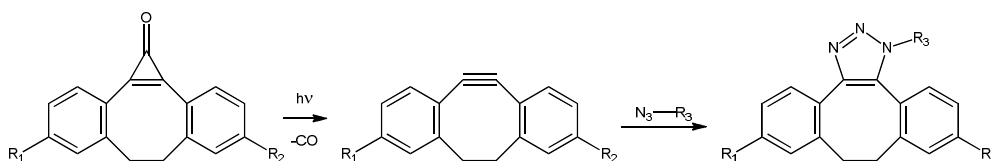
Following this approach, multifunctional alkynes could be ligated to an azide pre-functionalized surface with spatial control as proven by optical microscopy, scanning electron microscopy (SEM), and atomic force microscopy (AFM). The additional alkyne functionalities served as crosslinking positions induced by the initiator radicals.¹⁵⁰ In another study, the substrate patterning with triazolyl-hydrogels was realized employing multifunctional alkynes and azides (Scheme 20a,b). As suitable photoinitiators bis-acylphosphine oxide (Irgacure 819) and 1-[4-(2-hydroxyethoxy)-phenyl]-2-hydroxy-2-methyl-1-propan-1-one (Irgacure 2959) were employed. The successful patterning could be visualized by AFM and fluorescence microscopy.¹⁸⁸



Scheme 20. Triazolyl linked hydrogels are obtained employing multifunctionalized alkynes (a) and azides (b). The employed photoinitiators bisacylphosphine oxide (Irgacure 819) and 1-[4-(2-hydroxyethoxy)-phenyl]-2-hydroxy-2-methyl-1-propan-1-one (Irgacure 2959) are depicted on the right side of the scheme.¹⁸⁸

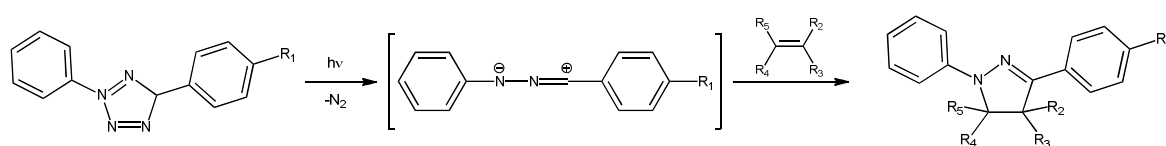
In both cases, however, there is not only a requirement of a heavy metal catalyst but also of the presence of free radicals reducing the employed Cu(II) complexes. As already stated, this may cause undesired side reactions in addition to the biotoxicity of the copper complexes.

Attempts to avoid copper in the reaction mixture are based on the copper-free cycloaddition of azides to cyclooctynes. The photo-control is realized *via* the protection of the alkyne by a cyclopropenone ring. Irradiation at $\lambda = 350$ nm induces decarbonylation of the cyclopropenone and the release of the cyclooctyne which can then react with an azide (Scheme 21). Employing fluorescent marked azides, the patterning of cyclopropenone pre-functionalized substrates can be visualized *via* fluorescence microscopy.¹⁶⁵ Depending on the application, the absence of any additives in the reaction mixture may compensate the limitations of the alkyne moiety on cyclooctyne derivatives.



Scheme 21. Photo-induced deprotection of cyclopropenone protected cyclooctynes and copper-free cycloaddition with azides.

Another 1,3-dipolar cycloaddition is the nitril-imine mediated tetrazole-ene cycloaddition (NITEC). Although it is much less employed compared to the CuAAC in general, it represents a robust, effective and additive-free alternative. In addition, the reaction is *per se* a light-triggered reaction and does not need to be modified for the application in photo-controlled surface patterning. First described by Huisgen and Sustman in 1967,¹⁸⁹ the reaction found its niche in biochemical applications such as protein modification,¹⁹⁰⁻¹⁹² *in-vivo* protein-labelling of *E.coli* cells,¹⁹³ or DNA folding.¹⁹⁴ The reaction principle is depicted in Scheme 22. UV irradiation at around $\lambda = 300$ nm induces the release of nitrogen from the tetrazole ring and thus, the formation of the intermediate nitrile-imine. Subsequent 1,3-dipolar cycloaddition with an inactivated or electron deficient alkene affords the adduct linked by a 4,5-dihydro-1*H*-pyrazole ring.¹⁹⁵ The wavelength of the photo-activation can be tuned between $\lambda = 254$ nm and 365 nm depending on the substituents of the *N*-phenyl ring.¹⁹⁶ The substituted tetrazoles are obtained *via* 1,5-dipolar cycloaddition of phenylsulfonylhydrazones with arenediazonium salts.¹⁹⁷



Scheme 22. The nitril-imine mediated tetrazole-ene cycloaddition (NITEC) of alkenes and *in-situ* formed nitril-imines upon UV irradiation.

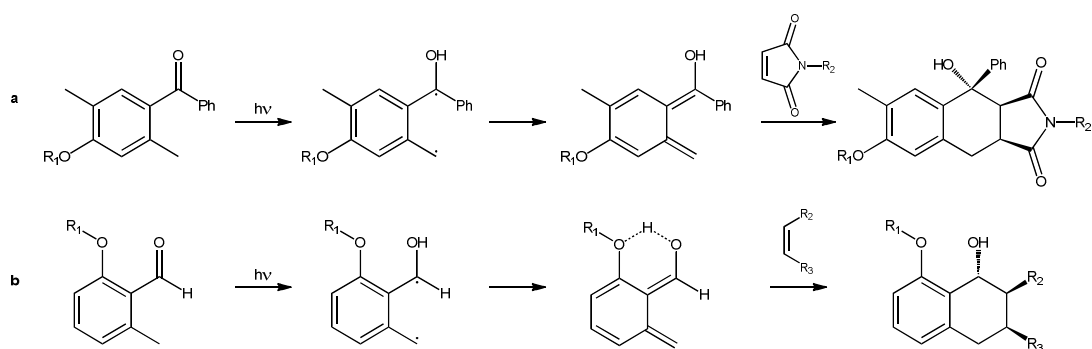
The application of the NITEC concept in the realm of surface modification was for example shown in the grafting of maleimide terminated poly(methyl methacrylate) onto cellulose and silicon substrates pre-functionalized with a tetrazole containing self-assembled monolayer.¹⁶³ The immobilization of azobenzene derivatives on a tetrazole functionalized silicon substrate *via* NITEC afforded light-responsive substrates exploiting the *cis/trans* isomerization of the azobenzene unit.¹⁶⁴ The orthogonality of the ligation reaction at $\lambda = 290$ nm and the isomerization at

$\lambda = 355$ nm was proven by contact angle measurements. Underlining the benefit in biocompatibility compared to the CuAAC reaction, a spatially controlled cell-adhesion on poly(dopamine) functionalized substrates was achieved in our team by blocking distinct surface areas with polymer brushes exhibiting anti-fouling properties *via* the NITEC reaction.¹⁹⁸ As NITEC is a pro-fluorescent reaction, the cycloadducts can readily be visualized by fluorescence microscopy.

DIELS–ALDER Reactions

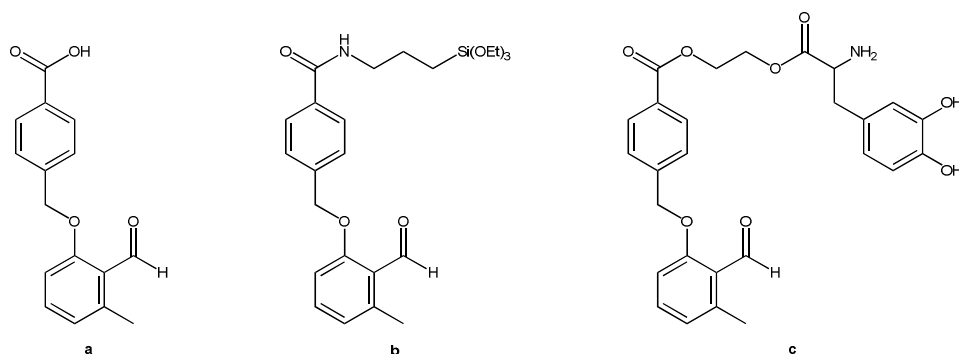
Comparable to the CuAAC reaction, the DIELS–ALDER reaction represents a powerful and widely employed synthetic tool for the synthesis of low molecular compounds as well as polymeric systems. It is robust, atom-efficient and tolerant towards other functional groups. It proceeds at ambient or slightly elevated temperature in solvents that are benign or can readily be evaporated from the reaction mixture. The products are of high purity and regioselectivity. The reaction thus complies not only with the criteria for low molecular *click* reactions, as stated by SHARPLESS *et al.*,¹⁹⁹ but also with the extended criteria for polymer conjugations from BARNER-KOWOLLIK and co-workers.²⁰⁰ Not surprisingly, the reaction is also employed for surface modifications without spatial control.²⁰¹⁻²⁰³ The light-triggered formation of either the diene or the dienophile provides additional photochemical control over the reaction enabling the spatially resolved immobilization of compounds on substrate surfaces.

The light-triggered enolization of *o*-methyl ketones or -aldehydes affords dienes that are able to react with a dienophile in a [4+2]-cycloaddition reaction. The top reaction in Scheme 23 depicts the reactive hydroxy-*o*-quinodimethane (photoenol) intermediate obtained upon UV irradiation of the *o*-methyl ketone and the subsequent DIELS–ALDER adduct with maleimide as the dienophile. UV irradiation induces $n\pi^*$ singlet-excitation of the *o*-methyl ketone with subsequent intersystem crossing to the triplet-excited $n\pi^*$ state. After proton abstraction a triplet diradical is formed which can rearrange to the intermediate hydroxy-*o*-quinodimethane diene (photoenol) as a mixture of *E* and *Z* isomers. Only the *E* isomer is able to react with a dienophile to the targeted cycloadduct while the *Z* isomer rearranges rapidly to the starting ketone *via* [1,5]-sigmatropic shift.²⁰⁴⁻²⁰⁷



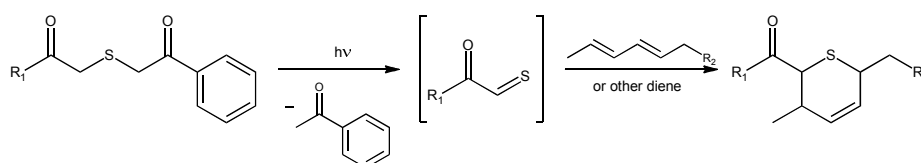
Scheme 23. Reaction mechanism of the light-triggered hydroxy-*o*-quinodimethane (photoenol) formation from *o*-methylphenyl ketones and -aldehydes. From the diradical intermediate a mixture of *E* and *Z* isomers is formed of which only the *E* isomer undergoes subsequent DIELS–ALDER reaction with a suitable dienophile (a). 2nd generation photoenols stabilize the DIELS–ALDER reactive *E* isomer of the diene *via* hydrogen bonding (b).

In addition to the photo-triggered formation of 2-naphthoquinone-3-methides from 3-(hydroxymethyl)-2-naphthol and subsequent DIELS–ALDER cycloaddition introduced by POPIK *et al.*,²⁰⁸ successful polymer-polymer conjugation was obtained by the reaction of *o*-methyl phenyl ketone-derivatized polymers with maleimide end-capped polymers under UV irradiation in solution.^{209,210} For surface modification, a screening of alternative photoenol precursors revealed an increased reactivity employing 2-formyl-3-methoxyphenyl (FMP) derivatives, the so-called second generation photoenols (Scheme 23b). In contrast to the first generation of photoenol precursors (Scheme 23a), the second generation is able to stabilize the *E* isomer of the diene *via* hydrogen bonding and thus exhibits a higher efficiency in the DIELS–ALDER reaction.¹⁶¹ Besides improved reactivity in polymer-polymer conjugation,²¹¹ this precursor also allows for the spatially resolved surface modification. The immobilization of the photo-active FMP is depending on the substrate. Immobilization on cellulose or hyaluronic acid surfaces is realized *via* esterification with a carboxylic acid derivative of FMP,¹⁵³ while silicon substrates can be functionalized with a triethoxysilyl ether derivative.¹⁶¹ Mimicking the attachment strength of maritime mussels, various substrates, *e.g.* gold, polymer films, or graphite, can be functionalized employing a dopamine functionalized FMP.¹⁶⁶ The subsequent cycloaddition of polymers or peptides equipped with a maleimide functional group affords spatially resolved functionalized substrates that were visualized by ToF-SIMS analysis.^{153,161,166}



Scheme 24. Modified photoenol precursors for the attachment onto substrates. (a) carboxylic acid function for immobilization on cellulose or hyaluronic acid (A),¹⁵³ triethoxysilyl ether for silicon surfaces (b),¹⁶¹ and dopamine functionalized 2-formyl-3-methylphenoxy (FMP), which can be attached to various surfaces (c).¹⁶⁶

The inverted strategy is based on the light-triggered formation of a dienophile and subsequent DIELS–ALDER reaction with a diene. As a suitable dienophile precursor phenacylsulfide was identified which decomposes upon UV irradiation at around $\lambda = 355$ nm in acetophenone and a highly reactive thioaldehyde which undergoes DIELS–ALDER cycloaddition with variable dienes.¹⁶² There are no restrictions to the choice of the diene, neither for the reaction of diene functionalized polymers in solution, nor for the respective surface patterning on silicon substrates. Successful coupling was achieved in both cases with cyclic dienes such as cyclopentadiene and cyclohexadiene, as well as with open chain dienes, e.g. 2,3-dimethyl butadiene, sorbic acid, and sorbic alcohol.



Scheme 25. Photo-induced decomposition of phenacylsulfide derivatives and subsequent hetero DIELS–ALDER reaction of the thioaldehyde with dienes.

An alternative approach to trap the highly reactive thioaldehyde is to employ nucleophiles, *e.g.* amines, hydroxylamines, or thiols, instead of dienes affording thioamides, oximes or disulfides, respectively.²¹²

In summary, the well-equipped toolbox for the spatially resolved patterning of surfaces opens the route to a variety of applications. With respect to the requirements and conditions, a light-triggered reaction can be chosen that does not interfere with the compounds to be immobilized onto the surface. The accessibility of the required counterpart may also have an influence on the choice of the photoreaction.

2.2.3. Metal Patterns and Metal Complexes on Surfaces

Substrate-immobilized metal-containing compounds find attraction in diverse fields from electronic and optic devices to catalytic active materials.²¹³⁻²¹⁸ In the following section, special focus will be placed on the patterned immobilization of metals and metal nanoparticles onto surfaces and on the surface-immobilization of metal complexes *via* molecular self-assembly.

Substrates with Patterned Metals and Metal Nanoparticles

The immobilization of metals or metal nanoparticles on substrates is especially attractive for applications in electronics as so-called nano-wires. A readily performable and material-efficient approach is the inkjet printing of suspended metal nanoparticles onto a substrate as illustrated in Figure 2C.²¹⁹ Upon heating, the suspending solvent mixture evaporates and the metal atoms are sintered. Employing this technique, conductive silver and copper lines could be printed onto glass substrates.^{220,221} The line thickness of inkjet printed wires is strongly dependent on the employed conditions, *e.g.* the initial particle size in the ink, the droplet size which is restricted by the size of the printing nozzle, and the sintering conditions. Typical line widths are limited to the double-digit μm range. Employing a laser beam for subsequent sintering after inkjet printing of gold nanoparticles onto a glass substrate afforded a line width of 6 μm .²²²

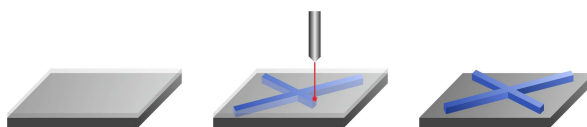


Figure 4. Schematic depiction of the electron beam lithography. A substrate pre-casted with a solution of metal salt is irradiated with an electron beam inducing reduction of the metal ions. After development, the reduced metal nanoparticles remain on the substrate while the precursor solution is removed.

Line-widths up to the double-digit nm range are obtained employing the electron-beam lithographic technique. Herein, a precursor solution containing metal salts is casted onto the substrate. Irradiation with an electron beam reduces the metal ions at the targeted positions. After removal of the unreacted precursor and thermal development, the metal nanoparticles are immobilized spatially resolved on the

substrate surface (Figure 4). In this way, palladium and gold nanowires were obtained from thiolate precursors.^{223,224} Employing stabilizing additives also other nanowires composed of metals or alloys like Ag, Cu, Pb, or AuCu, are accessible. The development in a controlled environment can additionally afford the respective metal nitride, -oxide, or -sulfide patterns.²²⁵ Comparable to the inkjet-printing, electron beam lithography is a mask-free technique offering more flexibility in the form of the patterns.

Light-triggered lithography employing photo-masks compensates this constriction by a non-demanding experimental set-up. Thus, it only requires a light source emitting at the correct wavelength besides the photo-mask. Figure 5 depicts the principle of the photolithography technique (left side). A mask is placed on a substrate coated with a precursor, *e.g.* a cross-linkable polymer. After irradiation, the unprotected parts are cross-linked and immobilized while the residual, unreacted polymer can be removed.

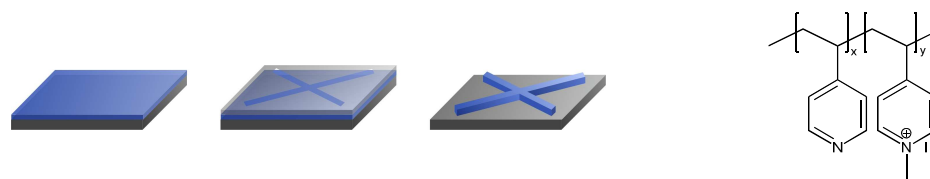
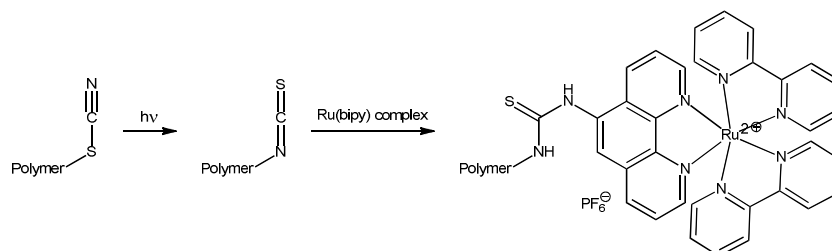


Figure 5. Schematic depiction of the UV-induced crosslinking of a pre-coated cross-linkable polymer film. After irradiation, the unreacted polymer can be removed (left). For Au and Pd nanoparticle immobilization, partially quaternized poly(vinyl *N* methylpyridine) is employed (right).

For the patterning of Au and Pd nanoparticles onto substrates, partially quaternized poly(vinyl *N* methylpyridine) (PMVP) is suitable (Figure 5, right). Due to the favorable electronic structure, the metal nanoparticles only immobilize on the PVMP-functionalized parts of the substrate surface. Subsequent reactions, *e.g.* the Pd-catalyzed reduction of Ni or the ligation of thiols on the patterned gold nanoparticles, respectively, attest the viability of the particles immobilized on the surface.^{226,227}

A slightly modified approach is employed for the ligation of a Ru(bipy) complex based on the UV-induced isomerization of thiocyanates. The substrate is coated with thiocyanate side-chain functionalized polymer and covered with a photo-mask. The irradiated parts isomerize to the reactive isothiocyanate which reacts in a subsequent step with an amine functionalized ruthenium complex as depicted in Scheme 26. The modified substrates show high photoluminescence.²²⁸



Scheme 26. UV-induced isomerization of a thiocyanate to the reactive isothiocyanate. Subsequent reaction with an amine functionalized Ru(bipy) complex immobilizes the complex on the polymer.

Self-Assembled Mono- and Multilayers of Metal Complexes

The direct functionalization of substrates with self-assembling metal complexes reduces the synthetic effort compared to the photolithography of casted polymer films circumventing the addition of the targeted compound to a polymer support. The potential applications of substrates patterned with metal complexes range from catalytic to electronic or photochemical applications just as their soluble correspondents, yet with the addition of spatial control. For example, a sequence of reactions could be catalyzed on a single substrate without interference of the different catalysts since they are spatially separated on the substrate. Until now, however, there are no examples of patterned self-assembling metal complexes reported. In lieu thereof, the self-assembly of metal complexes on surfaces without spatial resolution will be highlighted in the following section.

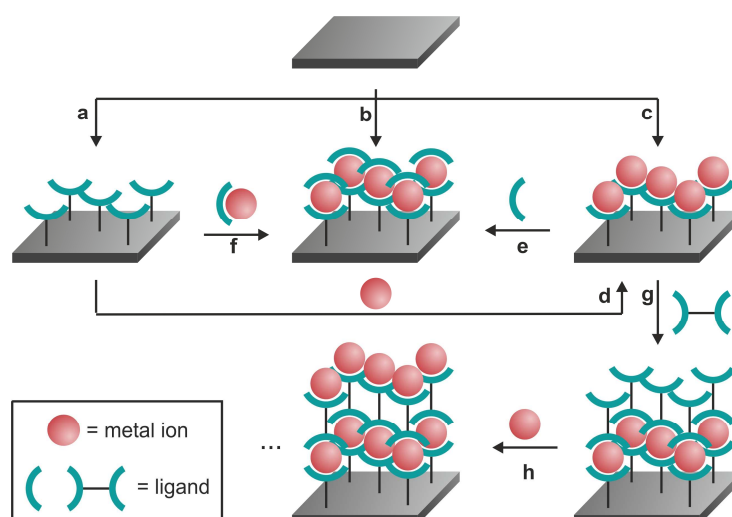
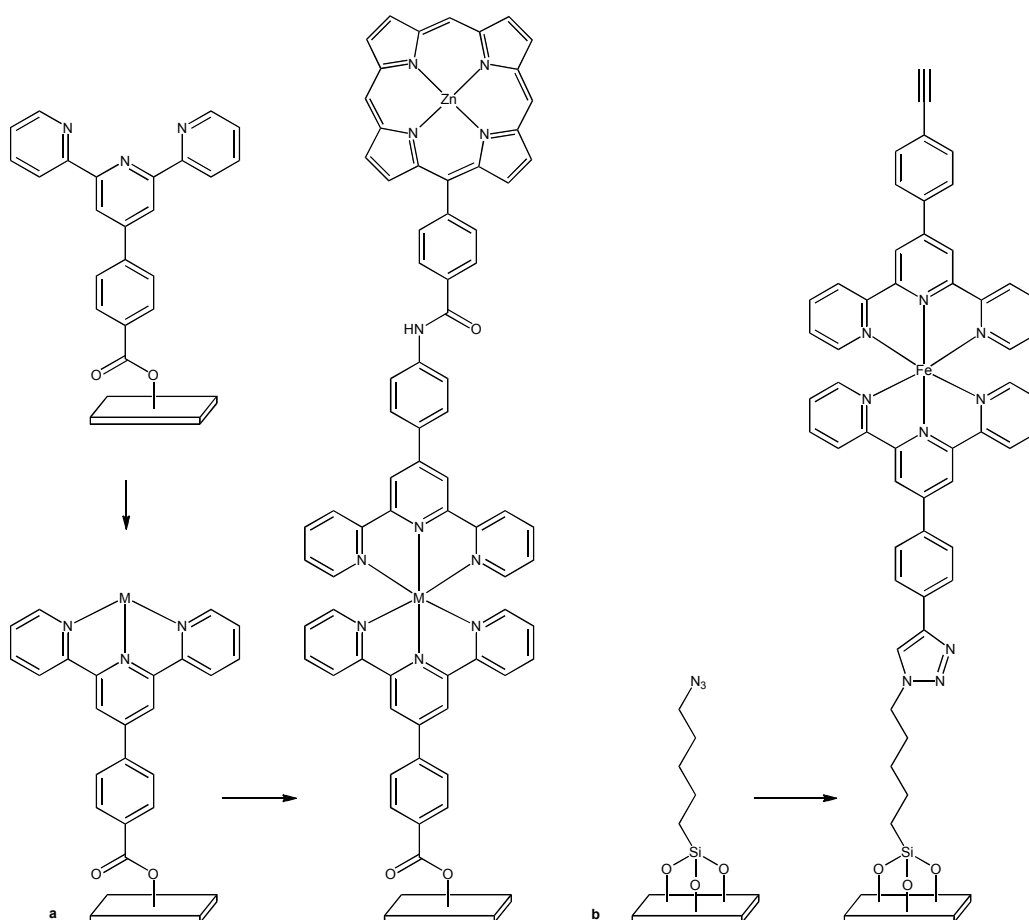


Figure 6. Self-assembled layers of metal complexes on substrates. Suitable self-assembling monolayers (SAM) are composed of metal ligands (a), closed metal complexes (b), or open metal complexes (c). Closed metal complexes can be subsequently derived *via* the successive addition of a metal center (d) and a second ligand (e) or by the addition of a metal center already equipped with a second ligand (f). Multilayers are obtained *via* the sequential addition of bifunctional ligands (g) and metal centers (h).

Figure 6 schematically depicts the construction of self-assembled metal complexes. Monolayers can be obtained *via* sequential addition of the components or by direct attachment of the complete complex onto a pre-functionalized substrate. The reaction steps in the sequential immobilization consist of the preparation of a SAM of metal-binding ligands (Figure 6a) and the successive loading with a metal (d) and a second ligand (e). Depending on the accessibility and stability of the compounds the loading of the ligand SAM with a metal center is only possible if it is already equipped with a second ligand (f). The attachment of a complete metal complex is most often realized by the conventional surface modification procedures, e.g. CuAAC or DIELS–ALDER ligation. The immobilized complex can already be equipped with a second ligand (b) or not (c), or be followed by an optional subsequent attachment of a second ligand (e).



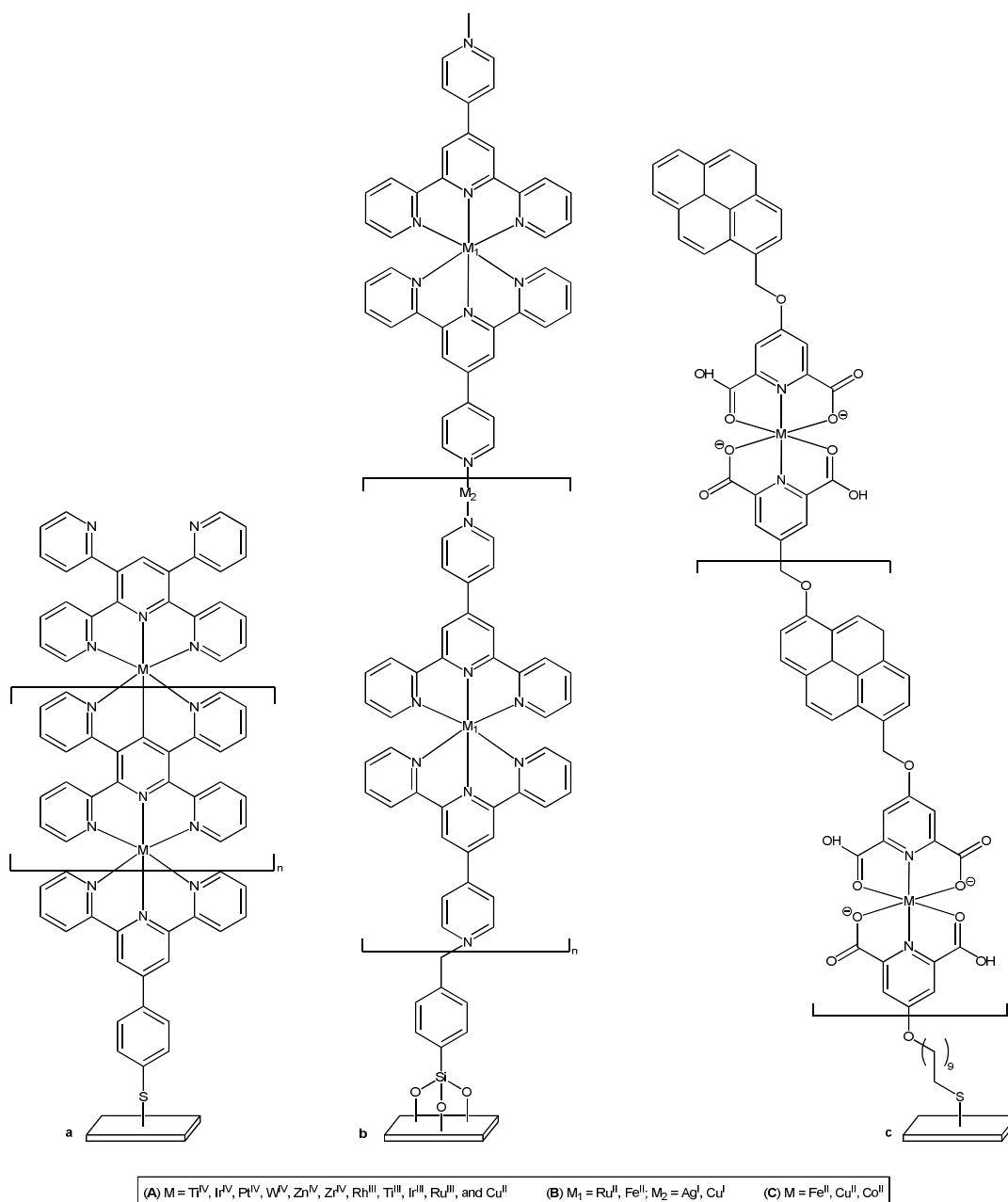
Scheme 27. Self-assembled monolayers of metal complexes. (a) Sequential immobilization of the ligand, the metal center, and finally a second ligand.²²⁹ (b) Direct attachment of a Fe(terpy)₂ complex onto an azide functionalized SAM.²³⁰

As an example, the sequential preparation of a bis(terpyridine)metal complex on an indium tin oxide (ITO) substrate is depicted in Scheme 27a. After self-assembly of the carboxylic acid functionalized terpyridine ligand, Fe^{II}, Co^{II} and Zn^{II} metal ions are introduced and the second terpyridine ligand – terminated by a Zn(porphyrin) complex – is added successively.²²⁹ The direct immobilization of a complete metal complex following the sequence depicted in Figure 6b, on the other hand, reduces the reaction steps on the substrate surface at the expense of flexibility in the choice of the metal center. For example, an alkyne bifunctionalized Fe(terpy)₂ complex is ligated *via* CuAAC reaction onto an azide pre-functionalized substrate (Scheme 27b).²³⁰ A change of the metal center on the substrate into Ir or Zn is only possible after removing the Fe center by immersing the substrate in hydrochloric acid. This afforded the free terpyridine ligand on the surface which then could be reloaded employing Ir(terpy) or Zn(terpy) precursors.

Alternating addition of metal precursors and bifunctionalized ligands to an initial SAM of ligands affords multilayers of metal complexes as depicted in Figure 6g and h. Scheme 28 depicts three examples of metal complex multilayers. A variety of metal centers was tested in the modular ligation with tetra-2-pyridinyl pyrazine (tppz) as the bridging ligand starting from a gold substrate functionalized by an initial terpyridine containing SAM (Scheme 28a). Successful growing of at least five layers was achieved with Ti^{IV}, Ir^{IV}, Pt^{IV}, W^{IV}, Zn^{IV}, Zr^{IV}, Rh^{III}, Ti^{III}, Ir^{III}, Ru^{III}, and Cu^{II}.²³¹

Scheme 28b depicts bimetallic multilayer complexes composed of alternating Ru(terpy)₂ and Ag(py)₂ or Cu(py)₂ moieties, respectively. For this purpose, a Ru(4'-pyridinyl terpyridine)₂ was attached to a self-assembled monolayer of trichloro(4-chloromethyl phenyl) silane on glass and silicon substrates. The bridging Ag^I or Cu^{II} metal ions were introduced *via* immersing the substrates with a solution of AgNO₃ or Cu(NO₃)₂, respectively, before the addition of the second layer of Ru(4'-pyridinyl terpyridine)₂.²³² Other ligands that are not based on the terpyridyl moiety, such as 1,6-bis(2',6'-dicarboxypyridyl-4'-oxymethyl)pyrene were also successfully employed for the preparation of multi-layered metal complexes (Scheme 28c). Successive immersion of the substrate with FeBr₃, CuBr₂, or CoBr₂ solutions, respectively, and addition of the bifunctional ligand afforded substrates with at least three metal complex layers.²³³ In summary, the self-assembly of metal

complexes on substrate surfaces is feasible, yet very time-consuming. Especially for the modular approach to obtain self-assembled multilayered metal complexes each successive step takes several hours of reaction time in order to achieve as high conversions as possible. As already mentioned, there is also no spatial resolution which would expand the potential applications enormously.



Scheme 28. Multilayer metal complexes *via* sequential ligation of metal ions and bifunctional ligands. (a) Initial SAM of terpyridine ligand onto gold substrate is successively loaded with various MCl_n salts and the bridging ligand tetra-2-pyridinyl pyrazine (tppz).²³¹ (b) $\text{Ru}(4'\text{-pyridinyl-terpyridine})_2$ complexes immobilized on silicon substrate are bridged *via* Ag^+ or Cu^{2+} metal ions.²³² (c) Gold substrate with a multilayer of Fe^{III} , Cu^{II} , or Co^{II} complexes *via* the bridging ligand 1,6-bis(2',6'-dicarboxypyridyl-4'-oxymethyl)pyrene.²³³

3

Metal-Containing Side-Chain Functionalized Polymers

The side-chain modification of polymers enables the attachment of a large number of functionalities onto a single polymer chain with a significant influence on the polymer properties *i.e.* the electronic structure,²³⁴ solubility,²³⁵ hydrophobicity,^{236,237} or pH- and thermo-responsiveness.²³⁸⁻²⁴¹ Suitable polymers are accessible by the polymerization of monomers that feature at least one additional functionality besides the polymerizable unit. To prevent side reactions, the additional functionality has to comply with the polymerization conditions. On the other hand, the type of polymerization should be selected to be compatible to the additional functionality, even if in principle all types of polymerizations are applicable. Commercially available

Metal loading and elemental analysis of the palladium polymers were performed in collaboration with C. Kiefer and Prof. P. Roesky (KIT). The synthesis and characterization of the *N,N'*-bis(2,6-diisopropylphenyl)propiolamidine ligand and the loading of the polymers with Rh were performed in collaboration with S. Gallardo-Gonzalez and Prof. Breher (KIT). Parts of this chapter were reproduced with permission from C. Lang, C. Kiefer, E. Lejeune, A. S. Goldmann, F. Breher, P. W. Roesky and C. Barner-Kowollik, *Polym. Chem.*, **2012**, *3*, 2413-2420. Copyright The Royal Society of Chemistry.

monomeric precursors can be transformed to the desired moiety either before or after the polymerization. For the first approach more reaction types can be employed to modify the precursor since purification and characterization by standard organic synthesis techniques is feasible. On the other hand, a loss of valuable functionalized material has to be taken into account if the polymerization not conducted to full conversion. The pre-polymerization functionalization approach is thus only preferred either if the monomers are readily accessible or if the required transformation cannot be employed after the polymerization.

The so-called post-polymerization functionalization of the side chains is more restrictive towards the employed reactions requiring quantitative transformations. Purification and characterization of the polymers can be more challenging. On the other hand, the subsequent ligation of the functionality offers a modular approach where different moieties can be attached to the same pre-synthesized polymer.²⁴² Typical structures for the post-polymerization functionalization are active esters,^{243,244} ketones,²⁴⁵ isocyanates,^{246,247} or epoxides.^{248,249} A set of highly efficient reactions including DIELS—ALDER,²⁵⁰⁻²⁵⁵ thiol-ene,^{256,257} or the copper catalyzed cycloaddition of azides and alkynes (CuAAC), which often fulfil the click-criteria implemented for polymer chemistry, are not surprisingly frequently employed.²⁰⁰

In the following, the syntheses of side-chain functionalized polymers featuring palladium and rhodium complexes are presented. The distance between two functionalities is tuned *via* the initial monomer composition of the functionalized monomers and their non-functionalized analogs generating statistical copolymers.

Well-defined polymers and good control over molar mass were obtained employing the reversible-addition-fragmentation chain transfer (RAFT) polymerization with various chain transfer agents. As side-chain ligation strategy, the copper catalyzed 1,3-dipolar cycloaddition of azides and alkynes was selected.

Interestingly, during the azide transformation of the chloride functionalized RAFT polymers, discoloring was observed. Section 3.1.2 addresses the investigation of the reaction mechanism of the RAFT end-group upon reaction with sodium azide by mass spectrometry on poly(methyl methacrylate), P(MMA).

The relative amount of functionalized comonomer in the polymers was deduced *via* nuclear magnetic resonance (NMR), the molar mass and the molar mass distribution

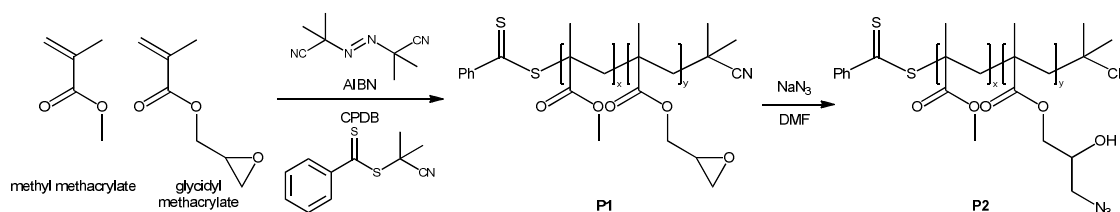
was obtained *via* gel-permeation chromatography (GPC). Absolute weight-averaged molar masses were determined for the unloaded and metal-loaded polymers by static light scattering (SLS) measurements and a subsequent ZIMM-plot analysis. The methacrylate based polymers were additionally characterized employing electrospray ionization mass spectrometry coupled to a size exclusion chromatography system (SEC-ESI-MS).

3.1. Side-Chain Functionalization of Poly(methyl methacrylate)s

For the synthesis of azide functionalized poly(methacrylate)s, two strategies were followed, namely the azide transformation of poly(methyl methacrylate-*co*-glycidyl methacrylate), P(MMA-GMA), and the direct copolymerization of methyl methacrylate (MMA) with 3-azidopropyl methacrylate (AzPMA).

3.1.1. Glycidyl Methacrylate Copolymers

The synthetic strategy of the first approach includes the RAFT-mediated copolymerization of methyl methacrylate and the commercially available glycidyl methacrylate (GMA) using azo-bis-(isobutyronitril) (AIBN) as radical initiator and cumyl dithiobenzoate (CPDB) as chain-transfer agent at 60 °C. Subsequent azide transformation of the obtained poly(methyl methacrylate-*co*-glycidyl methacrylate) (**P1**) with sodium azide in dimethylformamide (DMF) should afford **P2** with 2-hydroxy-3-azidopropyl side groups as depicted in Scheme 29.



Scheme 29. RAFT-Copolymerization of MMA and GMA with AIBN as radical initiator and CPDB as RAFT agent affords polymer **P1**. Azide transformation *via* reaction of **P1** with sodium azide in DMF yields the azide functionalized polymer **P2**.

The overall SEC-ESI-MS spectrum of **P1** (Figure 7a) shows a single distribution of the copolymer both for the double charged and the single charged species. The observed isotopic pattern of the peaks agrees with the theoretically expected pattern, as shown exemplarily for the peak of [(MMA₈GMA₄)CPDB · Na]⁺ in Figure 7b. All observed peaks can be assigned to the different monomer compositions (Figure 7c). According to the SEC-MS results, no unfunctionalized polymer chains are observed.

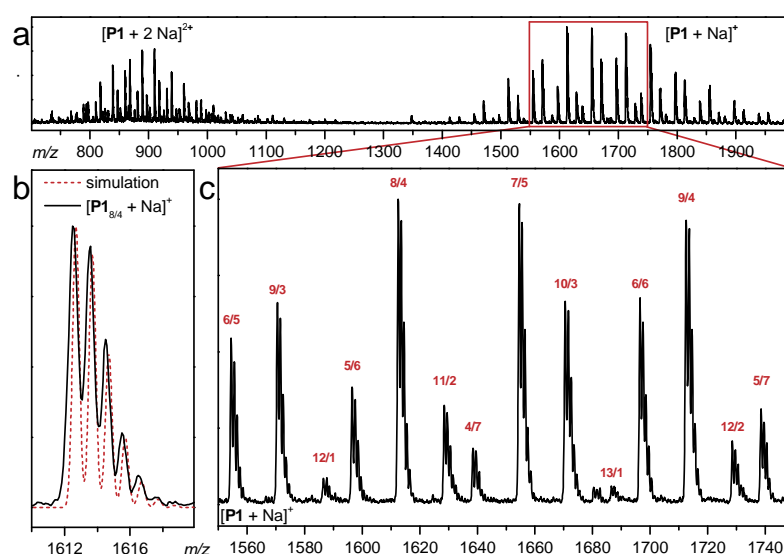


Figure 7. (a) SEC-ESI-MS spectrum of poly(MMA-GMA), **P1**. (b) Comparison of the simulated and measured peak at 1612.50 m/z assigned to the $[(\text{MMA})_8(\text{GMA})_4\text{Na}]^+$ -ion. (c) Enhanced view of the mass range from 1550 to 1750 m/z . The peaks are assigned to the number of repeating units of MMA (first number) and GMA (second number), respectively.

The ^1H NMR spectrum of **P1** (Figure 8a) shows, besides the typical resonances for P(MMA) at around $\delta = 1.00$ ppm (CH_3), 1.9 ppm (CH_2), and 3.57 ppm (O-CH_3), respectively, additional resonances that can be assigned to the glycidyl side group of GMA at $\delta = 4.28$ ppm and 3.76 ppm (O-CH_2) and $\delta = 3.19$ ppm, 2.82 ppm and 2.61 ppm (oxirane ring protons). The comparison of integrals that can be clearly assigned to one of the two monomer types, *i.e.* the methyl side group of MMA at $\delta = 3.57$ ppm (I_{MMA}) versus the oxirane ring proton of GMA at $\delta = 3.19$ ppm (I_{GMA}), enables the calculation of the overall monomer fraction of GMA in the polymer, F_y^{exp} , employing Eq. 1.

$$F_y^{\text{exp}} = 3 \cdot \frac{I_{\text{GMA}}}{I_{\text{MMA}}} \cdot \left(1 + 3 \cdot \frac{I_{\text{GMA}}}{I_{\text{MMA}}} \right)^{-1} \quad \text{Eq. 1}$$

The theoretically expected averaged monomer fraction of GMA in the copolymer, F_y^{theo} , can be estimated from the initial monomer composition in the reaction mixture, f , via Eq. 2 with the indices distinguishing the two monomers MMA (x) and GMA (y), respectively, and the copolymerization parameters $r_x = 0.8$ and $r_y = 0.7$ for the binary system.²⁵⁸

$$F_y^{\text{theo}} = \frac{r_y \cdot f_y^2 + f_x \cdot f_y}{r_x \cdot f_x^2 + 2 \cdot f_x \cdot f_y + r_y \cdot f_y^2} \quad \text{Eq. 2}$$

For **P1** (Figure 8a), the molar fraction of GMA, is calculated to be $F_y^{\text{exp}} = 0.38$, which is in good agreement with the theoretically expected value of $F_y^{\text{theo}} = 0.34$.

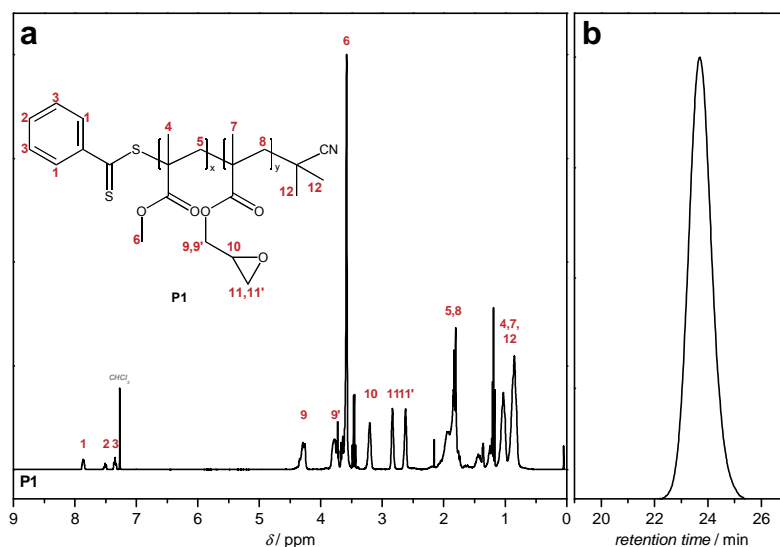


Figure 8. (a) ^1H NMR spectrum of poly(methyl methacrylate-*co*-glycidyl methacrylate), **P1** recorded in CDCl_3 . For resonance assignment see the schematic structure within the figure. (b) GPC elugram of **P1** recorded in THF and calibrated using narrow PMMA standards.

The ^1H NMR spectrum of **P1** (Figure 8a) additionally shows resonances caused by the aromatic ring protons of the CPDB-RAFT endgroup at $\delta = 7.86$, 7.50 and 7.35 ppm. Comparing the integral of the signal at $\delta = 7.50$ ppm (I_{CPDB}) with the integral of the resonance caused by one of the oxirane ring protons at $\delta = 3.21$ ppm (I_{GMA}), the number-averaged molar mass of the polymer (M_n) can be calculated following Eq. 3 with M_x and M_y being the molar masses and F_x and F_y the molar fractions of the two monomers, respectively. F_y can be derived from Eq. 1 and $F_x = 1 - F_y$.

$$M_n^{\text{NMR}} = (F_x \cdot M_x + F_y \cdot M_y) \cdot \frac{I_{\text{GMA}}}{I_{\text{CPDB}} \cdot F_y} \quad \text{Eq. 3}$$

The molecular weight, M_n , derived from the ^1H NMR spectrum depicted in Figure 8a is calculated to be $M_n^{\text{NMR}} = 3700 \text{ g}\cdot\text{mol}^{-1}$ which is in good agreement to the result of the GPC measurement with $M_n^{\text{GPC}} = 3600 \text{ g}\cdot\text{mol}^{-1}$ and $\mathcal{D} = 1.14$. The GPC elugram of **P1** (Figure 8b) shows a monomodal distribution.

The subsequent reaction with sodium azide to yield **P2** (Scheme 29) proceeded in *N,N*-dimethylformamide (DMF) at 50°C . The originally pink colored reaction mixture discolored completely in the course of the reaction, indicating a secondary reaction with involvement of the RAFT-endgroup. A more detailed study of a possible reaction mechanism was conducted and is described in section 3.1.2. Since the nature of the

endgroup is thus only of minor interest for the intended side chain functionalization, the observed side reaction is negligible.

In order to prove complete conversion of the glycidyl moiety into the 2-hydroxy-3-azido side group, a proton NMR spectrum was recorded in CDCl_3 and compared to **P1** (Figure 9). The characteristic peaks of the oxirane ring protons at $\delta = 3.19$ ppm, 2.82 ppm and 2.61 ppm are not visible in the spectrum of **P2**. On the other hand, new resonances at $\delta = 4.04$ ppm and 3.41 ppm are observed that can be assigned to the protons of the new side group evidencing complete conversion. The absence of the aromatic ring protons of the CPDB-endgroup supports the hypothesis of a secondary reaction.

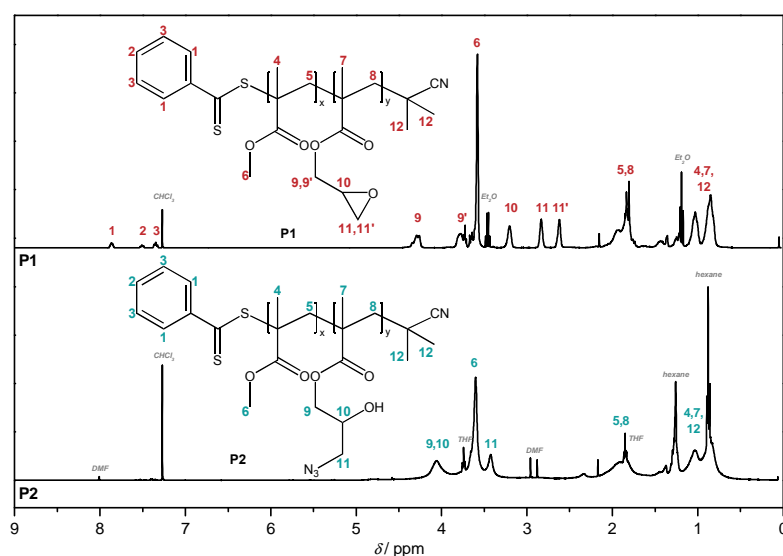


Figure 9. ^1H NMR spectra of **P1** and the product after the reaction with sodium azide, **P2**, recorded in CDCl_3 . For the resonance assignments see the schematic structures within the figure.

Figure 10a shows the infrared (IR) spectra of **P1** and **P2**. A strong new band at 2100 cm^{-1} assigned to the $\text{N}=\text{N}$ stretching vibration attests the presence of azide groups in **P2**. The GPC traces of **P1** and **P2** are shown in Figure 10b. The molar mass is expected to increase slightly due to the addition of an azide group to each glycidyl side group. In comparison to the monomodal and narrow distributed GPC trace of **P1**, **P2** exhibits a broadened trace with a clearly visible shoulder at higher molar masses indicating polymer-polymer coupling in the course of the azide transformation reaction. As a result, polymers synthesized *via* this synthetic route, are not suitable for subsequent ligation reactions. As an alternative route, monomers with azide functionalities were synthesized prior to the polymerization process.

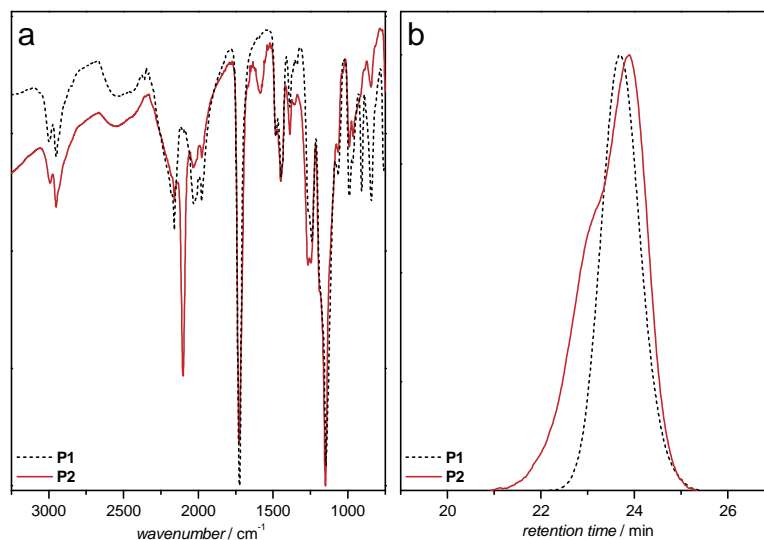
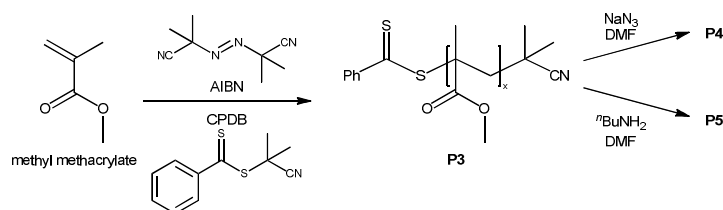


Figure 10. (a) IR spectra of **P1** and **P2**. (b) GPC traces for **P1** and **P2** recorded in THF. Calibration was conducted using narrow PMMA standards.

3.1.2. RAFT-Endgroup Transformation

Although the nature of the polymer endgroup is only of secondary interest for side chain functionalization, the observations described in section 3.1.1 suggest a modification of the RAFT-endgroup during the reaction of **P1** with sodium azide, *i.e.* the discoloring of the reaction solution and the absence of ^1H NMR resonances for the aromatic ring protons in the spectrum of **P2**, a side study investigating the reaction mechanisms was conducted. For this purpose, non-functionalized PMMA, **P3**, was synthesized *via* CPDB-mediated RAFT polymerization and reacted with sodium azide to give **P4**. The analytical results of **P4** are compared to those of **P5** obtained *via* aminolysis of **P3** with *n*-butyl amine (Scheme 30). The SEC-ESI-MS spectra of the derived polymers are depicted in Figure 11.



Scheme 30. RAFT polymerization of MMA with CPDB as the chain transfer agent gives non-functionalized **P3**. The reaction products of **P3** with sodium azide in DMF (**P4**) are compared to the products of the aminolysis of **P3** employing *n*-butyl amine (**P5**).

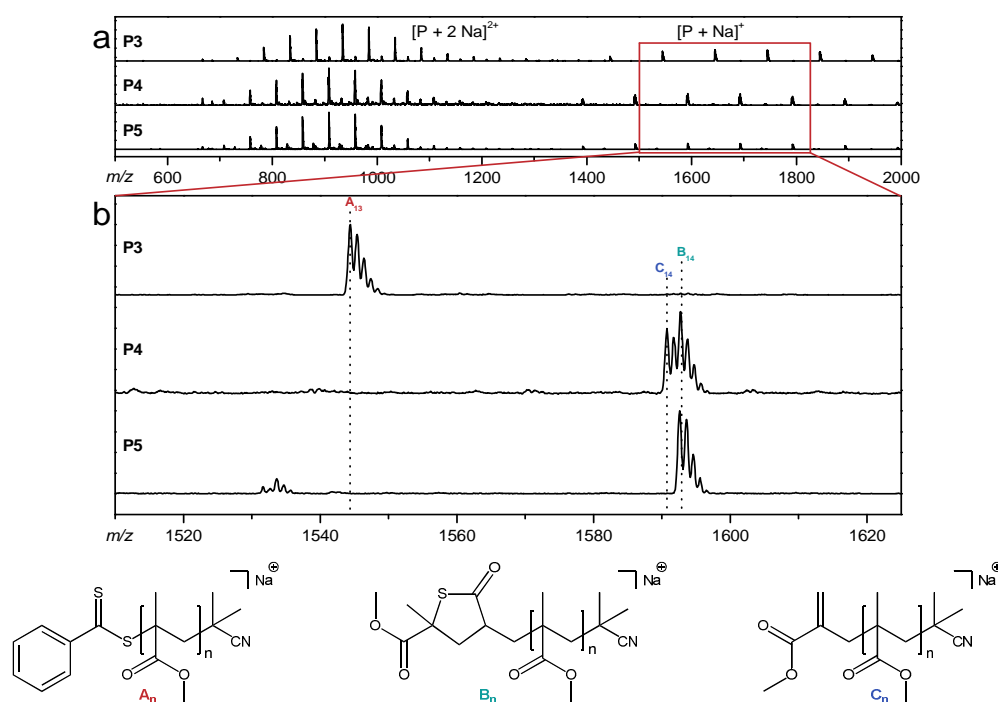


Figure 11. (a) Overall SEC-ESI-MS spectra of the polymers **P3**, **P4** and **P5** and (b) enlarged m/z range from 1510 u to 1625 u. For the peak assignments refer to the schematic drawings below the spectra.

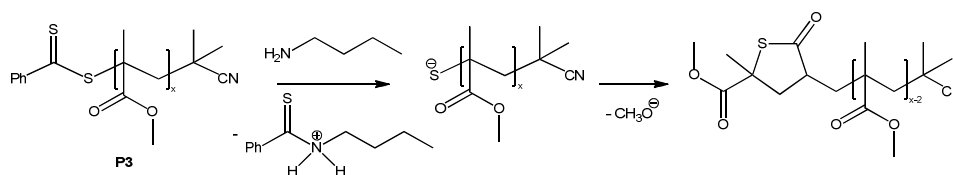
The SEC-ESI-MS spectrum of **P3** shows a single distribution proving the complete functionalization of PMMA with the RAFT endgroup. After the reaction with sodium azide, two product distributions are observed in **P4**. The peaks overlay since they differ only by two mass units. The peaks can be assigned to a thiolactone-encapped and an unsaturated species, respectively. Besides a by-product that could not be identified, the spectrum of **P5** exhibits only one distribution that can be assigned to the thiolactone species as well. Table 2 collates the peak masses depicted in Figure 11b.

Table 2. Experimentally observed and theoretically expected m/z values for polymers **P3**, **P4** and **P5** in the range between 1510 u and 1625 u.

	m/z (exp.)	m/z (theor.)	Δ (m/z)	assignment ^a
P3	1544.42	1544.70	0.28	A ₁₃
P4	1590.75	1590.82	0.07	C ₁₄
	1592.75	1592.78	0.03	B ₁₃
P5	1592.58	1592.78	0.20	B ₁₃

^a For the assignment refer to the schematic drawing within **Figure 11**.

The mechanism of the RAFT-group degradation during the aminolysis reaction was described by Xu *et al.* and includes a ring formation upon the loss of methanol by “backbiting” (Scheme 31).²⁵⁹



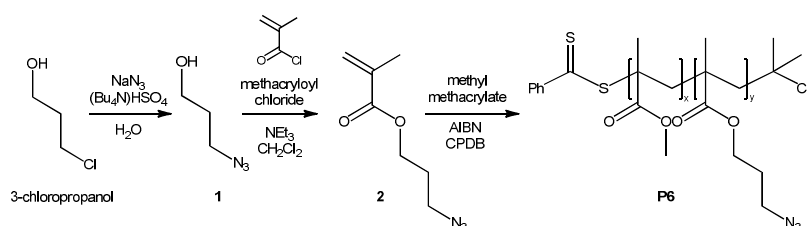
Scheme 31. Reaction mechanism proposed by Xu *et al.* of the aminolysis of thiocarbonylthio endgroup functionalized PMMA.²⁵⁹

A similar reaction mechanism is feasible for the reaction of **P3** with the nucleophilic azide-anion. The generated benzothioyl azide probably undergoes further reactions with the loss of nitrogen. The origin of the unsaturated species could not be finally identified.

The described side reactions can be prevented by the synthesis of azide-containing monomer prior to the polymerization. As a drawback, the ring-opening reaction of glycidyl methacrylate with sodium azide generates an additional secondary hydroxyl group that could potentially affect the next reaction steps. Thus, an alternative strategy was conducted employing 3-azidopropyl functionalized methacrylates to the RAFT polymerization and subsequent functionalization.

3.1.3. 3-Azidopropyl Methacrylate Copolymers

For the direct copolymerization of an azido functionalized monomer, 3-azidopropyl methacrylate (AzPMA, **2**) was synthesized from methacryloyl chloride and 3-azidopropanol (**1**) according to literature.²⁶⁰ The respective copolymer poly(MMA-AzPMA), **P6**, was obtained by polymerization with CPDB as chain-transfer agent (Scheme 32).



Scheme 32. Synthesis of AzPMA (**2**) from 3-azidopropanol (**1**) and methacryloyl chloride. RAFT copolymerization of **2** with MMA affords P(MMA-AzPMA), **P6**.

The variation of the initial monomer composition influences the copolymer composition. Two copolymers, **P6-1** and **P6-2**, featuring different azide contents were synthesized. The theoretically expected molar fraction of azide functionalized monomer, F_y , can be estimated from the initial monomer composition in the reaction mixture, f_x (MMA) and f_y (**2**), and the reactivity ratios r_x and r_y for the binary system following Eq. 4. The reactivity ratios for the system MMA / (**2**) are not determined, thus the parameters for the system MMA / GMA ($r_x = 0.8$, $r_y = 0.7$) were applied as an approximation.²⁵⁸

$$F_y^{\text{theo}} = \frac{r_y \cdot f_y^2 + f_x \cdot f_y}{r_x \cdot f_x^2 + 2 \cdot f_x \cdot f_y + r_y \cdot f_y^2} \quad \text{Eq. 4}$$

Figure 12 shows the proton NMR spectra of the polymers **P6-1** and **P6-2**. The resonances for the CH₂- and CH₃-protons of the polymer backbone can be identified at $\delta = 1.80$ ppm and 0.9 ppm, respectively. The characteristic O-CH₃ signal of the MMA comonomer is located at $\delta = 3.58$ ppm. The resonances of the propyl-CH₂ groups of comonomer **2** exhibit chemical shifts of $\delta = 4.02$ ppm (N₃-CH₂), 3.41 ppm (O-CH₂) and 1.90 ppm (C-CH₂-C). The resonances at $\delta = 7.87$ ppm, 7.51 ppm and 7.34 ppm can be assigned to the aromatic ring protons of the RAFT-endgroup and the multiplet at $\delta = 1.44$ – 1.22 ppm is assigned to the CH₃ protons of the isobutyronitrile endgroup.

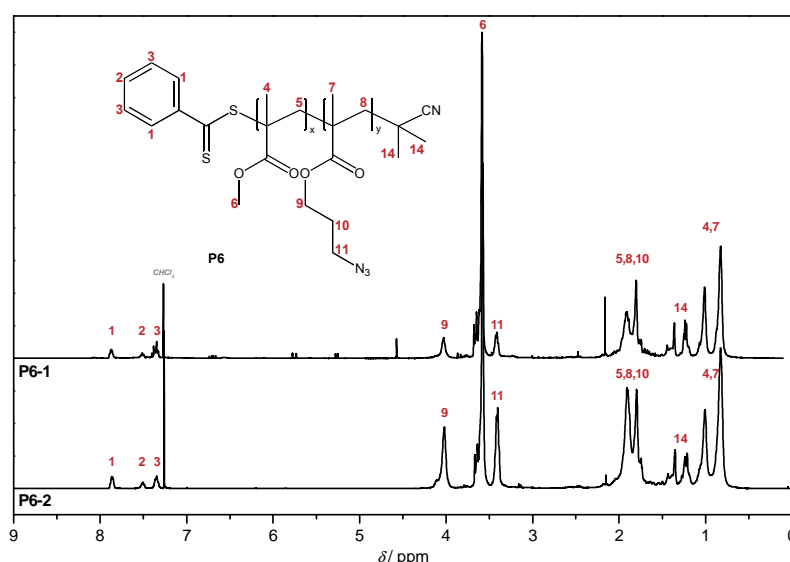


Figure 12. ¹H NMR spectra of the azide-containing polymers **P6-1** and **P6-2** recorded in CDCl₃. For the peak assignments refer to the schematic drawing within the figure.

Comparing the integral of the CH₂ group at $\delta = 4.02$ ppm ($I_{(2)}$) with the integral of the methoxy-group signal at $\delta = 3.58$ ppm (I_{MMA}), the actual molar fraction of (**2**) in the

copolymer can be calculated *via* Eq. 5. For **P6-1**, the theoretically expected molar fraction of azide-containing monomers is calculated to 17.1 %, which is in good agreement with the experimentally obtained value of 16.5 %. Polymer **P6-2** is higher functionalized with a theoretically molar fraction of 34.1 % of (**2**) in the copolymer. From the NMR, F_y is calculated to 34.4 %. Table 3 collates the theoretical expectations and experimental results.

$$F_y^{\text{exp}} = \frac{3}{2} \cdot \frac{I_{(2)}}{I_{\text{MMA}}} \cdot \left(1 + \frac{3}{2} \cdot \frac{I_{(2)}}{I_{\text{MMA}}}\right)^{-1} \quad \text{Eq. 5}$$

The molar mass of the polymer can be calculated *via* Eq. 6 from the integrals of the RAFT endgroup signal at $\delta = 7.87$ ppm and the signal of the CH₂ group of (**2**) at $\delta = 4.02$ ppm with respect to the above calculated molar fraction of (**2**) in the copolymer.

$$M_n^{\text{NMR}} = (F_x \cdot M_x + F_y \cdot M_y) \cdot \frac{I_{\text{GMA}}}{I_{\text{CPDB}} \cdot F_y} \quad \text{Eq. 6}$$

The calculated molar masses of both polymers **P6-1** and **P6-2** from the NMR spectra are in the same mass range with $M_n^{\text{NMR}} = 2700 \text{ g}\cdot\text{mol}^{-1}$ and $2800 \text{ g}\cdot\text{mol}^{-1}$, respectively. These results are in agreement with the results obtained by the GPC measurements in THF after calibration with narrow PMMA standards giving $M_n^{\text{GPC}} = 2700 \text{ g}\cdot\text{mol}^{-1}$ (**P6-1**) and $2800 \text{ g}\cdot\text{mol}^{-1}$ (**P6-2**). The GPC traces are depicted in Figure 13. All determined characteristics of the two copolymers are listed in Table 3.

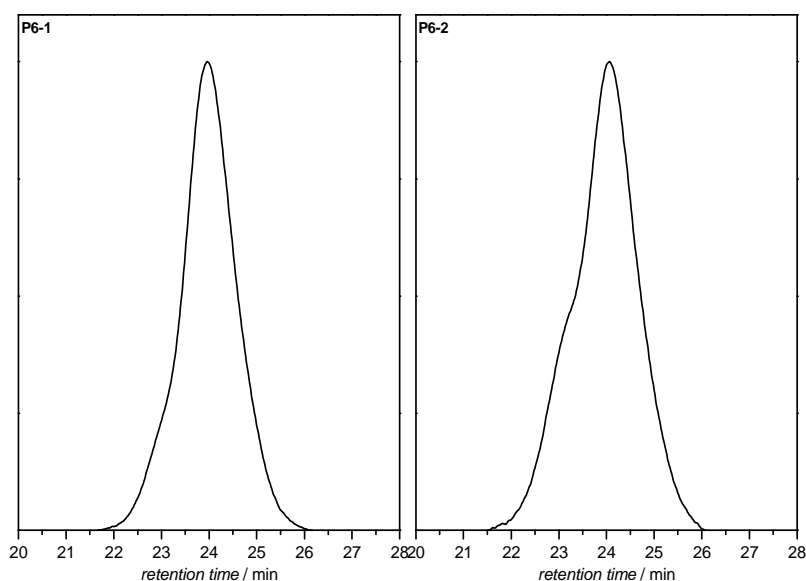


Figure 13. GPC traces of **P6-1** and **P6-2** recorded in THF and calibrated using narrow polystyrene standards.

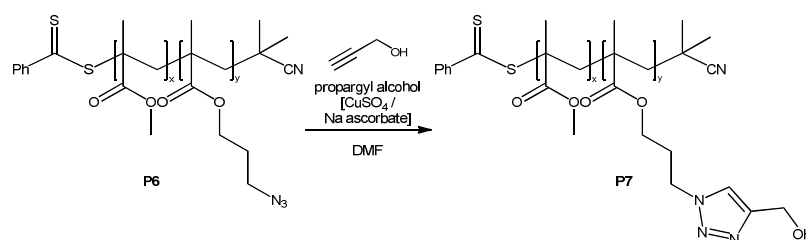
Table 3. Theoretically expected and experimentally determined characteristics of the azide-containing polymers **P6-1** and **P6-2**.

	f_y^a	F_y^{theo}	F_y^{exp}	M_n^{NMR} g·mol ⁻¹	M_n^{GPC} g·mol ⁻¹	\bar{D}
P6-1	0.152	0.171	0.165	2700	2700	1.32
P6-2	0.332	0.341	0.344	2800	2800	1.42

^a molar fraction of (**2**) in the initial reaction mixture.

3.1.4. Test CuAAC Reactions of Azide Functionalized Poly(methacrylate)s with Propargyl alcohol

The efficiency of the obtained azide copolymers in the copper-catalyzed 1,3-dipolar cycloaddition with alkynes is tested with propargyl alcohol as a model substance (Scheme 33). The robust catalyst system, copper (II) sulfate in combination with the reducing agent sodium ascorbate was employed. The catalytic active Cu(I) species is formed *in-situ*, thus the system is insensitive to air.



Scheme 33. Copper catalyzed 1,3-dipolar cycloaddition of polymer **P6** with propargyl alcohol as a model substance yields polymer **P7**.

The obtained products were separated from the copper catalyst by filtration over neutral alumina and reprecipitation from methanol. Figure 14 compares the ¹H NMR spectra of polymer **P6-1** before the reaction and the product **P7-1**. The resonances of the polymer backbone, the MMA comonomer and the RAFT-endgroup retain their chemical shifts. The signals of the propyl-CH₂ groups shift from $\delta = 4.02$ ppm, 3.41 ppm and 1.90 ppm to $\delta = 3.98$ ppm, 3.72 ppm and 2.30 ppm, respectively. No residual signals can be observed in the product spectrum evidencing complete conversion. The additionally observed signals at $\delta = 4.80$ ppm and 4.47 ppm are assigned to the triazolyl ring proton and the additional CH₂ group of propargyl alcohol. The hydroxyl proton is not visible.

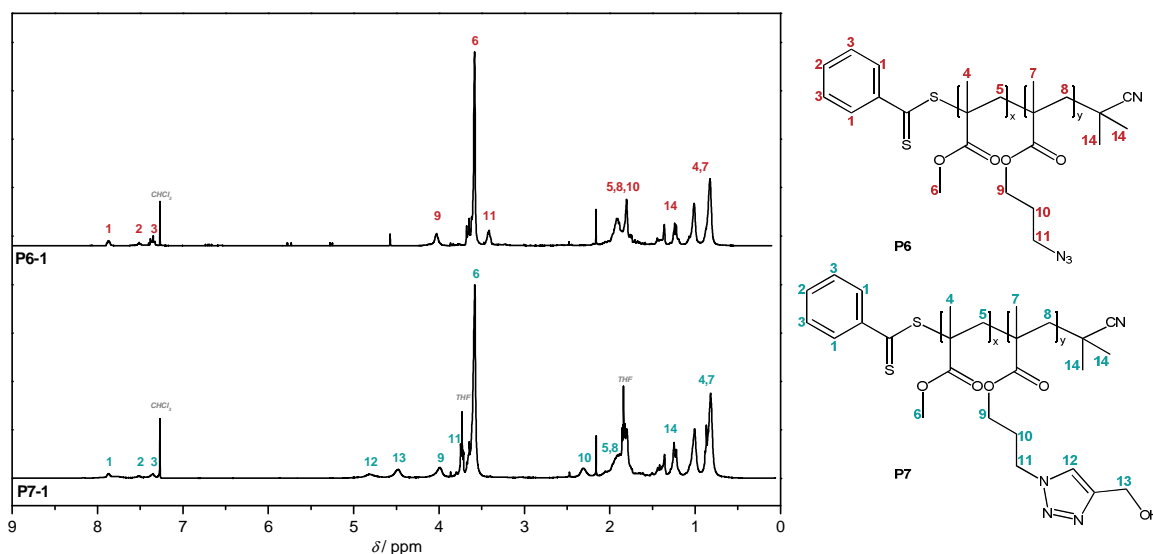


Figure 14. ^1H NMR spectra of polymer **P6-1** and the respective cycloaddition product **P7-1** recorded in CDCl_3 . For the peak assignments see the schematic drawings besides the spectra.

The expected molar mass of the product polymers is calculated *via* Eq. 7, where M_n is the molar mass of the polymers **P6** or **P7** and M and F are the molecular weight and the molar fraction of the respective comonomers. For **P6**, the comonomers are MMA (x) and 3-azidopropyl methacrylate (y) and for **P7** the comonomers are MMA (x) and the cycloadduct (y), respectively.

$$M_n^{\text{P7}} = M_n^{\text{P6}} \cdot \frac{(M_x \cdot F_x + M_y^{\text{P7}} \cdot F_y^{\text{P7}})}{(M_x \cdot F_x + M_y^{\text{P6}} \cdot F_y^{\text{P6}})} \quad \text{Eq. 7}$$

For polymer **P6-1**, the molar mass is expected to increase from $M_n^{\text{P6-1}} = 2700 \text{ g}\cdot\text{mol}^{-1}$ to $M_n^{\text{P7-1}} = 2900 \text{ g}\cdot\text{mol}^{-1}$ in **P7-1**, while the increase for **P6-2** is expected to be higher, namely from $M_n^{\text{P6-2}} = 2800 \text{ g}\cdot\text{mol}^{-1}$ to $M_n^{\text{P7-2}} = 3200 \text{ g}\cdot\text{mol}^{-1}$ in **P7-2** due to the higher fraction of azide functionalized side chains. The GPC results of **P7-1** and **P7-2** are depicted and compared to **P6-1** and **P6-2** in Figure 15. The expected increase in the molar mass cannot be observed. A feasible explanation is a non-linear change in the hydrodynamic volume relative to the change in molar mass of the polymers. A significant broadening of the distribution is not observed.

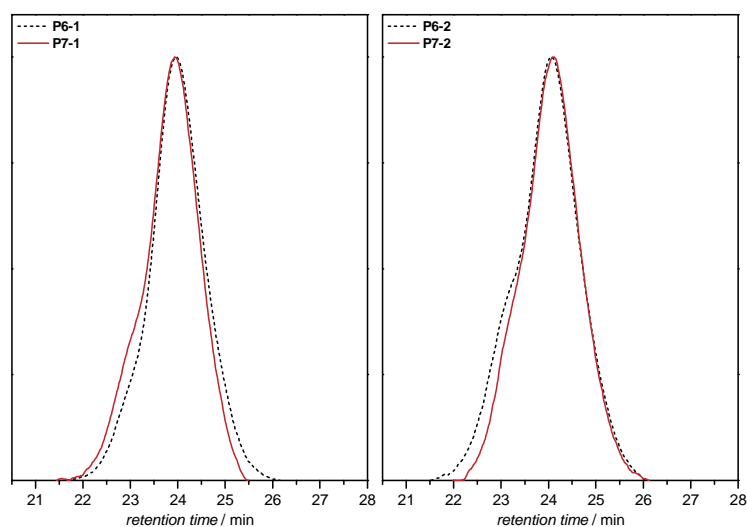


Figure 15. GPC traces of the polymers **P7-1** and **P7-2** after the CuAAC reaction of **P6-1** and **P6-2** with propargyl alcohol, respectively.

The polymers **P6** and **P7** were additionally analyzed by SEC-ESI-MS. The obtained spectra of **P6-2** and **P7-2** are depicted in Figure 16. The overview shows, besides the distribution of the double charged-ions, a distribution of single charged ions that can be assigned to the expected product. The highlighted peaks illustrate the change in molecular weight by cycloaddition of propargyl alcohol for polymer chains including one, two and three azide units, respectively. The explicit m/z values are collated in Table 4 and compared to the theoretically expected values. No residual signals of **P6-2** are observed in the product spectrum of **P7-2** confirming a complete functionalization as already stated by ^1H NMR analysis.

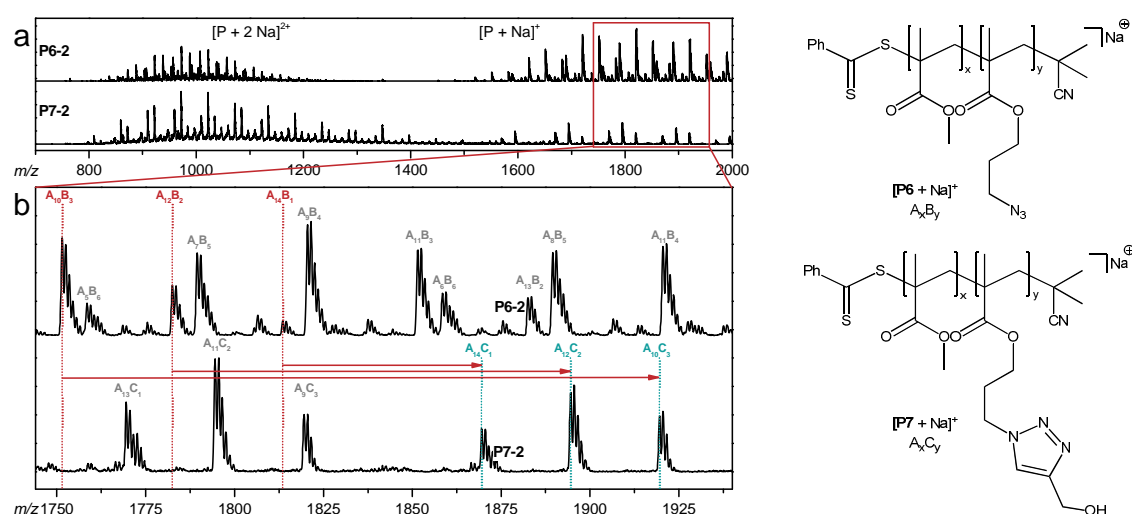


Figure 16. (a) Overview of the SEC-ESI-MS spectra of **P6-2** and **P7-2**. (b) Enlarged m/z range from 1725 u to 1950 u with the highlighted corresponding peaks of three different copolymer compositions. The numerical values are collated in Table 4.

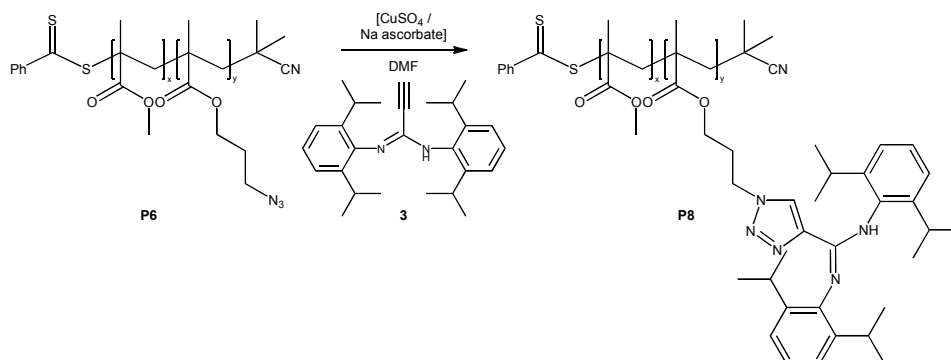
Table 4. Selected experimentally observed and theoretically expected m/z values of the peaks highlighted in the SEC-ESI-MS spectra of **P6-2** and **P7-2** in Figure 16.

	P6-2		P7-2	
m/z^{theo}	1751.80		1919.88	
m/z^{exp}	1751.50	A ₁₀ B ₃	1919.58	A ₁₀ C ₃
Δ	0.30		0.30	
m/z^{theo}	1782.82		1894.87	
m/z^{exp}	1782.50	A ₁₂ B ₂	1894.58	A ₁₂ C ₂
Δ	0.32		0.29	
m/z^{theo}	1813.84		1869.87	
m/z^{exp}	1813.50	A ₁₀ B ₁	1869.58	A ₁₀ C ₁
Δ	0.32		0.29	

Composition nomenclature – A: methyl methacrylate, B: 3-(azidopropyl) methacrylate, C: 3-(1-propyl-1,2,3-triazolyl)4-methanol) methacrylate. All polymerions comprise the CBDP endgroup and a sodium cation.

3.1.5. CuAAC Reaction of Azide Functionalized Poly(methacrylate)s with an Amidine Ligand

The alkyne functionalized metal complexing ligand *N,N'*-bis(2,6-diisopropylphenyl) propiolimidine (**3**) was provided by the institute of inorganic chemistry (S. Gallardo-Gonzalez). The cycloaddition reaction was performed under comparable conditions compared to the test reactions with copper (II) sulfate and sodium ascorbate as the catalytic system at ambient temperature in DMF (Scheme 34).



Scheme 34. Copper-catalyzed cycloaddition of the alkyne functionalized metal ligand *N,N'*-bis(2,6-diisopropylphenyl) propiolimidamide (**3**) with the azide containing polymer **P6** yields the side-chain functionalized polymer **P8**.

The ¹H NMR spectra of the starting materials **P6** and **3** as well as the spectrum of the product **P8** are depicted in Figure 17. The enlarged area in Figure 17b highlights the

shifts of the aromatic protons. In the spectrum of **P6**, the signals of the CPDB-endgroup are visible at $\delta = 7.87$ ppm, 7.52 ppm and 7.34 ppm, respectively. For **3**, a signal close to $\delta = 7.10$ ppm is induced by the phenyl ring protons. The spectrum of **P8** shows both signal groups with no significant difference in the chemical shifts. In the region between $\delta = 4.50$ ppm and 2.50 ppm (Figure 17c), **P6** exhibits an intense signal of the MMA methoxy protons at $\delta = 3.59$ ppm, and additional signals caused by the propyl-CH₂ side groups at $\delta = 4.03$ ppm (CH₂-O) and 3.41 ppm (CH₂-N). In the **P8**, these are shifted to $\delta = 4.25$ ppm and 3.90 ppm, respectively. In the ¹H NMR spectrum of ligand **3**, two signals are observed in the considered area that are assigned to the isopropyl-CH protons ($\delta = 3.25$ ppm) and to the alkyne proton ($\delta = 2.64$ ppm). The first is split into two signals located at $\delta = 3.43$ ppm and 3.02 ppm upon the cycloaddition reaction while the latter is supposed to disappear completely.

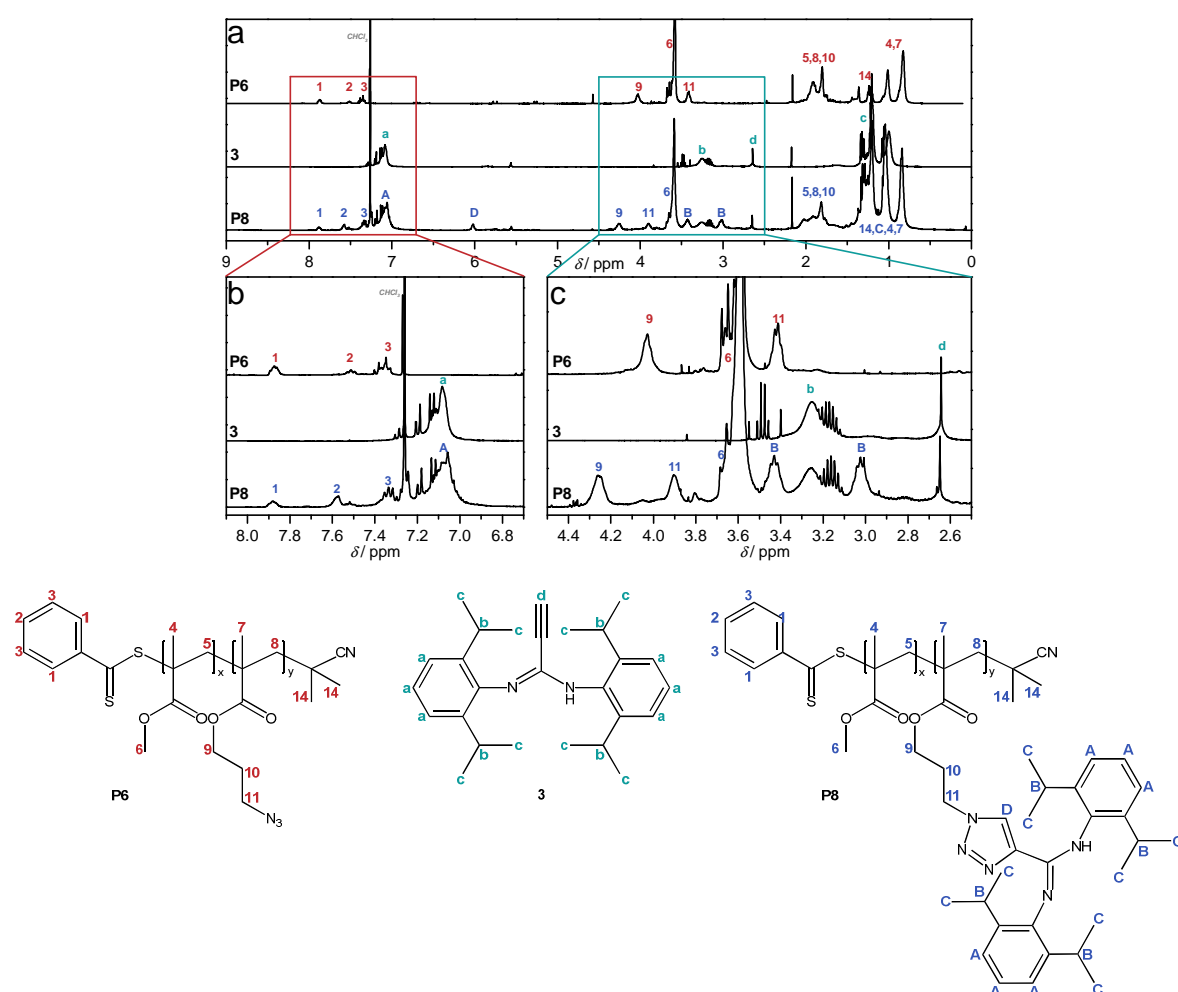


Figure 17. (a) Overall ¹H NMR spectra of **P6**, **3** and **P8** recorded in CDCl₃. (b) Enlarged area between $\delta = 8.25$ ppm and 6.75 ppm. (c) Enlarged area between $\delta = 4.50$ ppm and 2.50 ppm. For the peak assignments refer to the schematic drawings under the figure.

In the ^1H NMR spectrum of **P8**, thus, a residual signals of the alkyne proton and the CH protons are visible indicating residual starting material in the product even after excessive washing and repeated reprecipitation. A full conversion of **P6** cannot be ascertained since the broad adjacent signals could overlay with a residual peak.

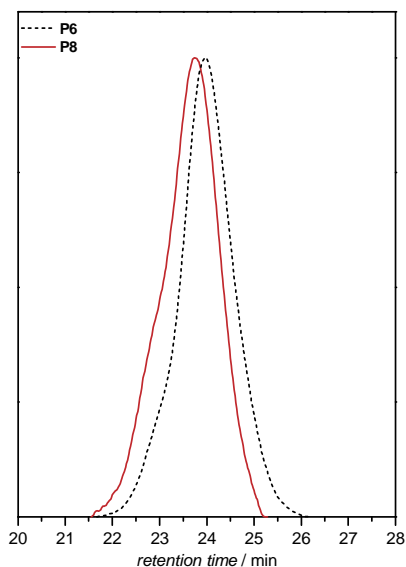


Figure 18. GPC traces of **P6** and **P8** in THF, GPC system was calibrated using narrow PMMA standards.

The results of the GPC measurements of **P6** and **P8** are compared in Figure 18. A clear shift of the molar mass distribution from $M_n = 2700 \text{ g}\cdot\text{mol}^{-1}$ with a dispersity of $\mathcal{D} = 1.32$ in **P6** to $M_n = 3900 \text{ g}\cdot\text{mol}^{-1}$ with a dispersity of $\mathcal{D} = 1.32$ is observed. As already stated for **P7**, the expected number-averaged molar mass of **P8** can be calculated from the initial molar mass of **P6** following Eq. 8 with respect to the ratio of the two comonomers ($F_x = 0.833$ and $F_y^{\text{P6}} = 0.167$) in the copolymer. Assuming complete conversion, F_y^{P8} is equal to F_y^{P6} and the expected molar mass of **P8** is calculated to $M_n = 4300 \text{ g}\cdot\text{mol}^{-1}$.

$$M_n^{\text{P8}} = M_n^{\text{P6}} \cdot \frac{(M_x \cdot F_x + M_y^{\text{P8}} \cdot F_y^{\text{P8}})}{(M_x \cdot F_x + M_y^{\text{P6}} \cdot F_y^{\text{P6}})} \quad \text{Eq. 8}$$

The observed molar mass is lower indicating an incomplete reaction. This suggestion was verified by the SEC-ESI-MS measurements of **P6** and **P8**, depicted in Figure 19. The enlarged view of the two spectra shows the m/z range from 1590 u to 1830 u (Figure 19b). Signals for completely converted species are found, yet also partly or unfunctionalized species can be assigned to the observed peaks.

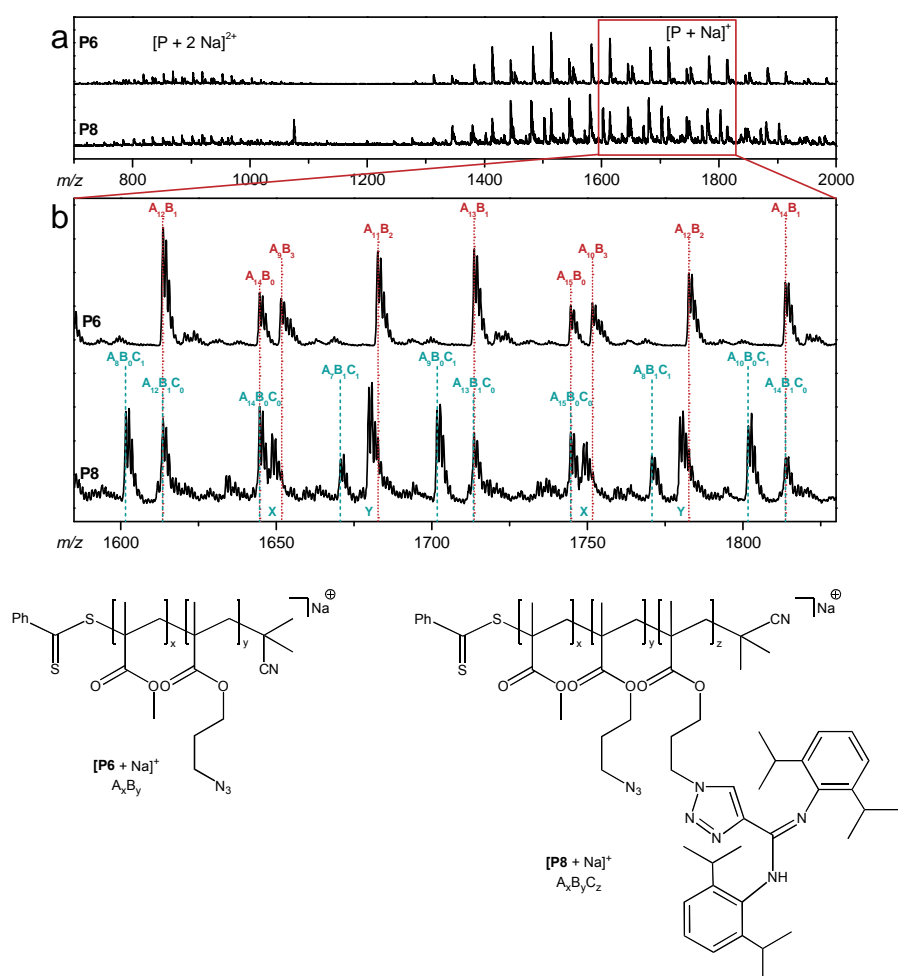


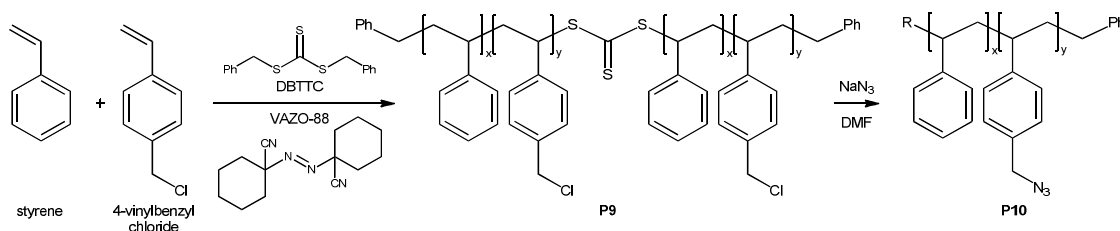
Figure 19. (a) Overview over the SEC-ESI-MS spectra of **P6** and **P8**. (b) Enlarged m/z range between 1590 u and 1830 u. For the peak assignments refer to the schematic drawings below the spectra.

Better results may be obtained by the optimization of the reaction conditions or a variation of the catalytic system. In comparison to the challenging synthesis of the heat and shock sensitive azide-containing monomer **2** as well as the incomplete CuAAC reaction, the approach introduced in section 3.2 was thus preferred.

3.2. Side-Chain Functionalization of Poly(styrene)s

3.2.1. Synthesis of Azide-Containing Polystyrene

For the synthesis of side-chain functionalized polystyrene, the commercially available 4-chloromethyl styrene (CIMSt) was identified as suitable precursor comonomer for a post-polymerization functionalization. The polymerizations were conducted at 80 °C with 1,1'-azobis(cyclohexanecarbonitrile) (VAZO-88) as radical initiator in the presence of the commercially available RAFT agent dibenzyltrithiocarbonate (DBTTC). The subsequent azide-transformation of **P9** was conducted employing sodium azide in DMF at ambient temperature to yield **P10** as depicted in Scheme 35.



Scheme 35. Copolymerization of styrene and CIMSt in the presence of DBTTC as RAFT agent and VAZO-88 as radical initiator at 80 °C. Subsequent reaction of **P9** with sodium azide in DMF gives the azide-functionalized polymer **P10**.

The ^1H NMR spectra of **P9** and **P10** are depicted in Figure 20. The chemical shifts of the resonances assigned to the aromatic protons in the range of $\delta = 7.40$ ppm to 6.00 ppm, and to the aliphatic backbone ranged from $\delta = 2.40$ ppm to 0.80 ppm are not influenced by the substitution reaction. In contrast, the signal of the Ph-CH_2 protons of the functionalized comonomer is shifted from $\delta = 4.54$ ppm in **P9** to $\delta = 4.26$ ppm in **P10**. The endgroup signals overlap with the signals of the polymer precluding the calculation of the molar mass from the NMR spectra. Comparing the integral of the functional side groups (I_y) to the integral of the aromatic protons (I_{Ph}), the determination of the molar fraction of functionalized monomer in the copolymer (F_y) is possible following Eq. 9 with y is $\text{CH}_2\text{-Cl}$ (**P9**) or $\text{CH}_2\text{-N}_3$ (**P10**), respectively.

$$F_y = 5 \cdot \left(2 \cdot \frac{I_y}{I_{\text{Ph}}} + 1 \right)^{-1} \quad \text{Eq. 9}$$

The molar fraction of the polymers **P9** and **P10** depicted in Figure 20 is calculated to be close to $F_y = 0.470$. The complete shift of the benzyl protons confirms the efficient substitution of all side groups.

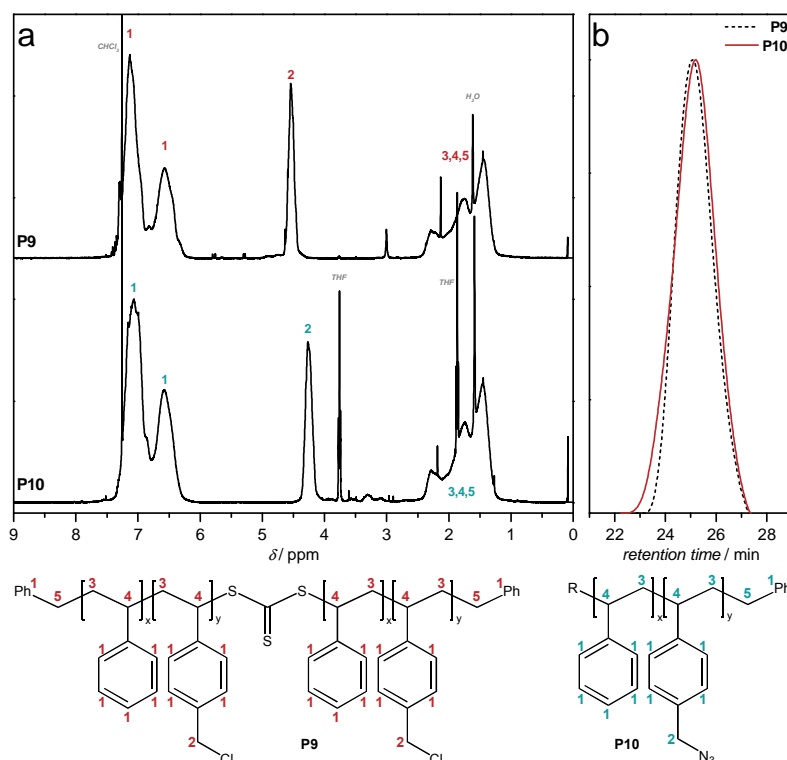


Figure 20. (a) ^1H NMR spectra of **P9** and **P10** recorded in CDCl_3 . For the peak assignments refer to the schematic drawings below the spectra. (b) GPC traces of **P9** and **P10** recorded in THF. Calibration was conducted using narrow polystyrene standards.

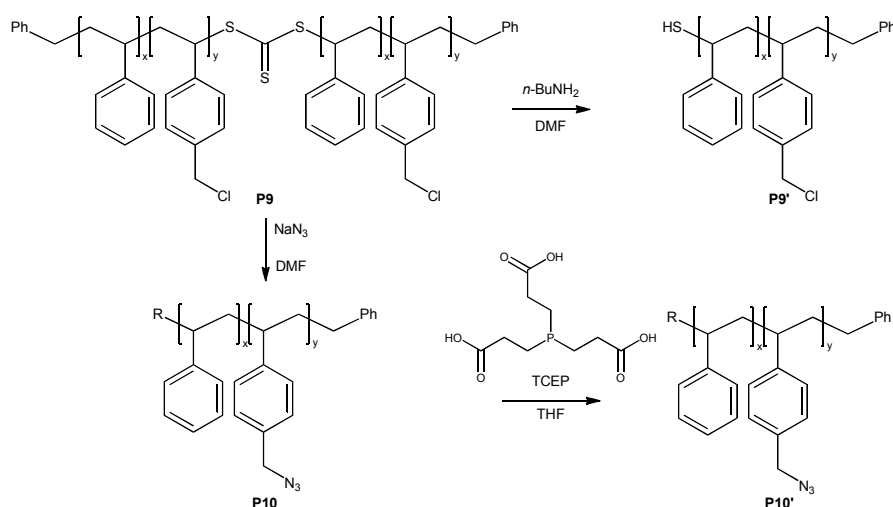
The GPC traces of **P9** and **P10** are compared in Figure 20b. The number-averaged molar mass, M_n , and the dispersity, \mathcal{D} , are not expected to change significantly upon the substitution reaction since the molar mass of Cl compared to N_3 differ only slightly. The molar mass for both **P9** and **P10** is determined by GPC (relative to narrow polystyrene standards) to be $M_n = 3900 \text{ g}\cdot\text{mol}^{-1}$ with a dispersity of $\mathcal{D} = 1.22$ for **P9** and 1.29 for **P10**. Table 5 summarizes the molar mass characteristics of **P9** and **P10**.

Table 5. Molar mass characteristics of the chlorine-functionalized polymer **P9** and the subsequent azide-functionalized polymer **P10**.

	$M_n^a / \text{g}\cdot\text{mol}^{-1}$	\mathcal{D}^a	F_y^b
P9	3900	1.22	0.470
P10	3900	1.29	0.470

^a Derived from GPC measurements in THF. ^b Calculated from ^1H NMR following Eq. 9.

During the reaction of **P9** with sodium azide in DMF the reaction mixture discolored comparable to the observation described in section 3.1.1 for the methacrylate based polymer **P1**. A cleavage of the RAFT endgroup following the same mechanism as suggested for PMMA would thus reduce the molar mass of the azide polymer to a half of the original molar mass. This is due to the mid-chain position of the RAFT group and can be demonstrated by intentionally cleaving the trithiocarbonate group in an aminolysis reaction as depicted in Scheme 36.



Scheme 36. Aminolysis of **P9** with *n*-butylamine to afford the thiol-terminated polymer **P9'** and azide transformation reaction of **P9** yielding **P10**. Treatment of **P10** with tris(2-carboxyethyl)phosphine (TCEP) to give **P10'** was conducted to open presumed disulfide bridges.

The GPC measurements of **P9** before aminolysis and **P9'** after aminolysis are depicted in Figure 21a. For **P9**, the number-averaged molar mass is determined to $M_n = 8400 \text{ g}\cdot\text{mol}^{-1}$ with $\mathcal{D} = 1.20$. After aminolysis, **P9'** features a number-averaged molar mass of $M_n = 2700 \text{ g}\cdot\text{mol}^{-1}$ with $\mathcal{D} = 1.41$. Even though the distribution is slightly broadened by the endgroup transformation, a clear shift to approximately half of the original molar mass is observed. The reaction of **P9** with sodium azide gives the azide side-chain functionalized polymer **P10** with $M_n = 7000 \text{ g}\cdot\text{mol}^{-1}$ and $\mathcal{D} = 1.29$. Sun *et al.* propose a cleaving mechanism of the RAFT endgroup similar to the mechanism of an aminolysis reaction yielding polymers with thiol-endgroups.⁴⁰ However, the molar mass is not reduced by half as observed previously in the aminolysis reaction. The possible coupling of polymer chains *via* disulfide bridges was tested by adding tris(2-carboxyethyl)phosphine (TCEP), a well-known reducing agent, to a solution of **P10** in THF (Scheme 36).²⁶¹ The resulting polymer **P10'** was

analyzed *via* GPC and revealed no change in molar mass or dispersity. The results of the GPC measurements of **P10** and **P10'** are depicted in Figure 21b. However, as in the following only the side groups of the polymers are considered, the identification of the actual mechanism was no longer necessary. The side reaction can be avoided by directly employing the azide functionalized monomers for the polymerization. A significant drawback of this strategy is thus the temperature sensitivity of the azide groups, limiting the applicable polymerization temperature. Thus, the synthetic strategy was not changed accepting the loss of a specific functionality on the chain ends.

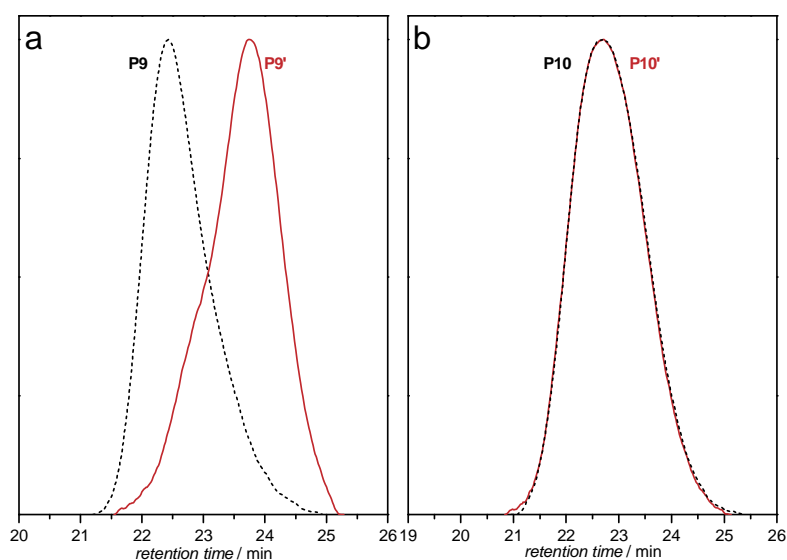


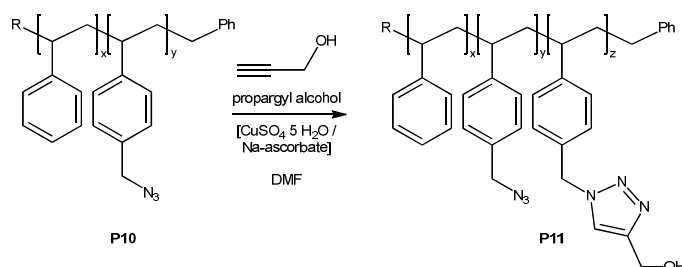
Figure 21. GPC traces recorded in THF. (a) **P9** and **P9'** after the aminolysis. (b) **P10** and **P10'** after treatment with TCEP in THF.

The azide transformation of the chlorine-functionalized polymers was complete in all reactions as evidenced by ^1H NMR analysis. The spectra for the polymers introduced in the following sections will not be explicitly shown.

3.2.2. Reactivity Study of the CuAAC Reaction with Propargyl Alcohol

In a first step, the efficiency of the cycloaddition was tested with propargyl alcohol as a model substance that was added in different ratios ($f_z = 0.3, 0.5, 0.7$ and 1.0) relative to the present azide groups in the polymer. The cycloaddition was catalyzed by the Cu^{I} catalyst formed *in-situ* from copper sulfate by reduction with sodium ascorbate.

Four polymers **P11-1** to **P11-4** were obtained featuring different ratios, F_y and F_z , of residual azide (y) and reacted cycloadduct (z), respectively (Scheme 37).



Scheme 37. Copper catalyzed cycloaddition of propargyl alcohol to the polymer side chains of **P10** in the presence of copper sulfate and sodium ascorbate as the catalyst in DMF gives **P11**.

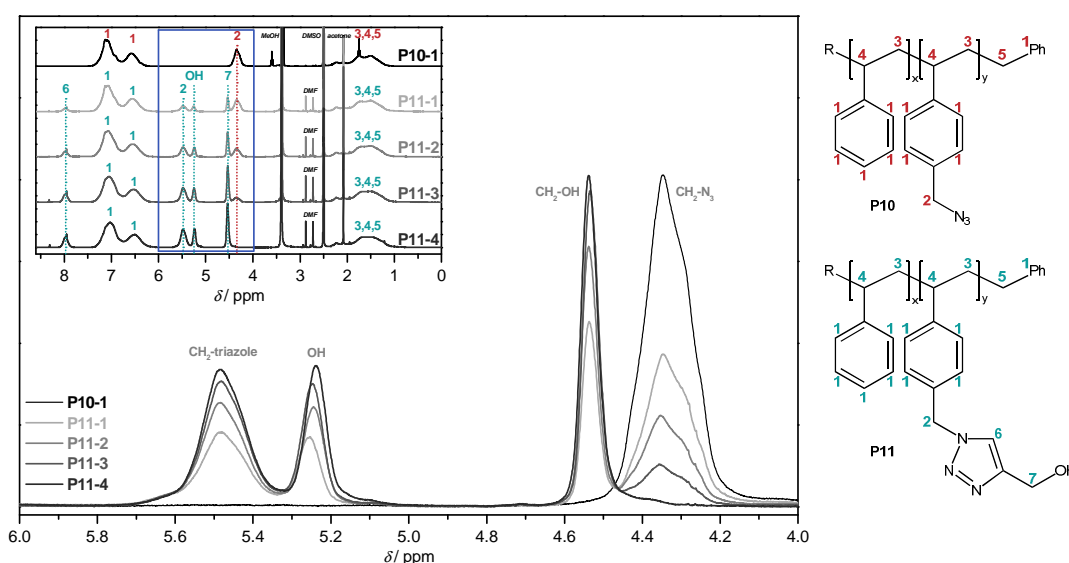


Figure 22. ^1H NMR spectra of **P10** and the subsequent products of the cycloaddition of propargyl alcohol, **P11-1** to **P11-4** recorded in DMSO. The enlarged view ranging from $\delta = 6.0$ ppm to 4.0 ppm, shows the resonances of the $\text{CH}_2\text{-X}$ protons and the hydroxyl group proton. For the peak assignments refer to the schematic drawings besides the figure.

The ^1H NMR spectra of the polymers are depicted in Figure 22. The overview spectra exhibit the non-influenced signals of the aromatic ring protons in the range of $\delta = 7.50$ ppm to 6.15 ppm and the polymer backbone ranging from $\delta = 2.57$ ppm to 1.00 ppm in all spectra. The signal of the $\text{CH}_2\text{-N}_3$ protons decreases with increasing amount of added propargyl alcohol. In contrast, new signals arise that can be assigned to the triazolyl ring proton at $\delta = 7.96$ ppm, the $\text{CH}_2\text{-triazolyl}$ protons at $\delta = 5.48$ ppm, the hydroxy-proton at $\delta = 5.25$ ppm and the $\text{CH}_2\text{-OH}$ protons at $\delta = 4.53$ ppm.

For the calculations of the molar fractions, F_x , F_y and F_z , the integrals of the aromatic ring protons (I_{Ph}), the $\text{CH}_2\text{-triazole}$ (I_{tr}) protons and the $\text{CH}_2\text{-N}_3$ (I_{N_3}) protons are considered. The molar fractions are calculated following Eq. 10 - Eq. 12.

$$F_x = \left(2 \cdot \frac{I_{Ph}}{(I_{tr} + I_{N3})} - 4 \right) \cdot \left(2 \cdot \frac{I_{Ph}}{(I_{tr} + I_{N3})} + 1 \right)^{-1} \quad \text{Eq. 10}$$

$$F_y = (1 - F_x) \cdot \left(\frac{I_{tr}}{I_{N3}} + 1 \right) \quad \text{Eq. 11}$$

$$F_z = 1 - F_x - F_y \quad \text{Eq. 12}$$

The experimentally determined molar fractions are collated in Table 6 and compared to the theoretically expected values assuming complete addition of the added propargyl alcohol. The values for F_z calculated from the ^1H NMR spectra range from appr. 15 % to 50 % of the total copolymer composition and are in good agreement with the theoretically expected values. The amount of functionalization can thus readily be controlled by the employed amount of alkyne. The remaining azide functionalities could be functionalized with a different alkyne in a subsequent reaction step, yielding bifunctionalized polymers.

The molar mass of the polymers was determined *via* GPC measurements in *N,N*-dimethyl acetamide (DMAc) relative to narrow polystyrene standards. The results are depicted in Figure 23 and the obtained molar masses and polydispersities are collated in Table 6. A shift to higher molar masses is observed the more propargyl alcohol was added to the reaction mixture, agreeing with the expected trend.

The theoretically expected molar masses can be calculated from the original number-averaged molar mass of **P10**, M_n^{P10} and the relative molecular weights of the monomers, \overline{M}_m , in **P10** and **P11** with respect to the determined molar fractions of the different comonomers (Eq. 14 and Eq. 15) as defined in Eq. 13. For the values of F_x , F_y and F_z refer to Table 6.

$$M_n^{\text{P11,theo}} = \overline{M}_m^{\text{P11}} \cdot \frac{M_n^{\text{P10}}}{\overline{M}_m^{\text{P10}}} \quad \text{Eq. 13}$$

$$\overline{M}_m^{\text{P10}} = F_x^{\text{P10}} \cdot M_x^{\text{P10}} + F_y^{\text{P10}} \cdot M_y^{\text{P10}} \quad \text{Eq. 14}$$

$$\overline{M}_m^{\text{P11}} = F_x^{\text{P11}} \cdot M_x^{\text{P11}} + F_y^{\text{P11}} \cdot M_y^{\text{P11}} + F_z^{\text{P11}} \cdot M_z^{\text{P11}} \quad \text{Eq. 15}$$

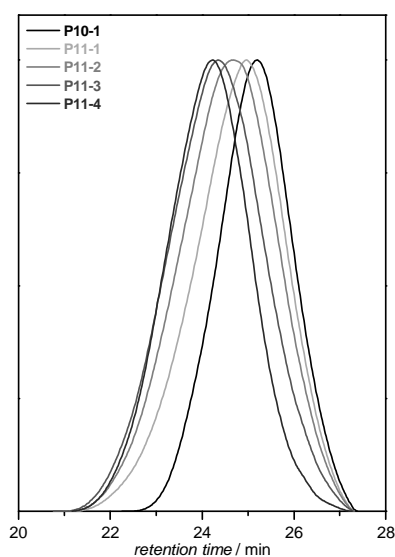


Figure 23. GPC traces of the azide-functionalized polymer **P10-1** and the subsequent cycloaddition products **P11-1** to **P11-4** recorded in DMAc. The determined molar masses, M_n and polydispersities, \mathcal{D} , for all polymers are collated in Table 6.

The molar masses obtained from the GPC measurements are significantly higher than the expected molar masses. This could be due to differences in the hydrodynamic volume induced by the triazolyl methanol group. The increase of the dispersity can be explained by the statistical distribution of functionalized side-groups on the polymer chains whereby some chains bear more than the average number of functionalities and other less. By addition of propargyl alcohol onto some functionalities, this difference increases.

Table 6. Characteristics of the test CuAAC reactions with propargyl alcohol as the model substance. Molar fractions of styrene (x), benzylazide (y) and benzyl triazolyl methanol (z) are calculated following Eq. 10 - Eq. 12.

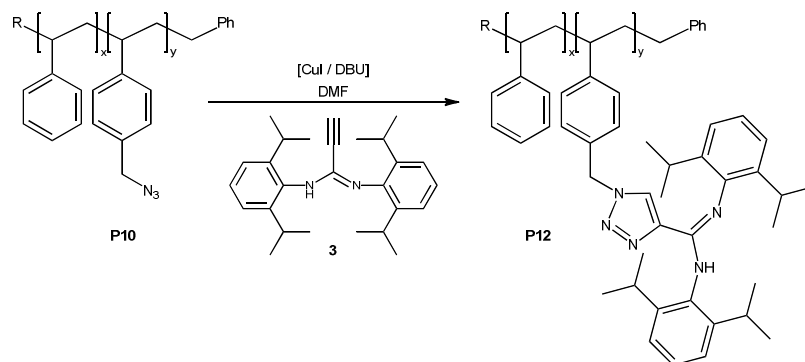
	e_{PgOH}^a	F_x	$F_z^{\text{theo},b}$	F_z^{exp}	$M_n^{\text{theo},c}$ g·mol ⁻¹	$M_n^{\text{exp},d}$ g·mol ⁻¹	\mathcal{D}^d
P10-1	0	0.530	0	0		3900	1.29
P11-1	0.30	0.534	0.141	0.149	4200	4700	1.48
P11-2	0.48	0.534	0.226	0.242	4300	5300	1.52
P11-3	0.70	0.535	0.329	0.339	4500	6100	1.52
P11-4	1.00	0.530	0.470	0.470	4700	7100	1.40

^a Added equivalents of propargyl alcohol in the reaction mixture relative to the azide side groups present in the polymer. ^b Theoretical molar fraction of benzyl triazolyl methanol for complete addition of the added amount of propargyl alcohol. ^c Theoretically expected molar mass calculated following Eq. 13. ^d Determined *via* GPC analysis in DMAc. Calibration was conducted using narrow polystyrene standards.

The partial cycloaddition of propargyl alcohol to the azide side groups of polymer **P10** confirms the efficiency of the CuAAC reaction. While the molar masses measured *via* GPC differ from the expected values, the molar fraction of modified side groups is well predictable and can be controlled *via* ^1H NMR analysis.

3.2.3. CuAAC Reaction with a Rh-Complexing Ligand and Subsequent Rh-Containing Polymers

For the attachment of rhodium on the polymer side-chains, an alkyne functionalized amidine was provided by the institute of inorganic chemistry (S. Gallardo-Gonzalez) that can readily be reduced to the rhodium-complexing amidinato ligand.²⁶²⁻²⁶⁵ The cycloaddition is catalyzed by copper(I)iodide in combination with diazabicycloundecen (DBU) in DMF at ambient temperature (Scheme 40). A potential influence of the spatial proximity of the sterically demanding ligands and their subsequent metal complexes is investigated by the comparison of four polymer sets, **P10-2** to **P10-5** and **P12-1** to **12-4**, respectively. They differ in their relative content of functionalized comonomer, F_y , with the more spatial freedom for the single metal complex, the minor the functional density.



Scheme 38. By copper(I) catalyzed cycloaddition of *N,N'*-bis(2,6-diisopropylphenyl)propiolamidine (**3**) with the azide side chains of polymer **P10**, ligand functionalized polymer **P12** is obtained.

After removal of the copper catalyst, the polymers were analyzed by ^1H NMR analyses. The spectra of the four polymer sets are depicted in Figure 24. The chemical shifts of the phenyl ring protons at $\delta = 7.43$ ppm – 6.16 ppm and the backbone protons at $\delta = 2.46$ ppm – 1.08 ppm are not influenced by the ligation reaction but overlaid by new signals of the diisopropylphenyl groups of the ligand that can be assigned to the phenyl-ring protons in the aromatic shift region or to the

$$F_y = 5 \cdot \left(2 \cdot \frac{I_y}{I_{Ph}} - 2 \right)^{-1} \quad \text{Eq. 16}$$

The molar fractions of the functionalized comonomer range between 17 % and 55 %. There is no significant difference in the calculated values obtained from the ^1H NMR spectra of **P10** compared to those obtained from the spectra of **P12** underpinning the complete conversion of the azide moieties.

Table 7. Characteristics of azide functionalized polymers **P10-2** to **P10-5** and the subsequent cycloadducts **P12-1** to **P12-4**.

	$M_n^{\text{GPC,a}}$ g·mol ⁻¹	\mathcal{D}^a	F_y^b		$M_n^{\text{GPC,a}}$ g·mol ⁻¹	\mathcal{D}^a	F_y^c	$M_n^{\text{theo,d}}$ g·mol ⁻¹	
P10-2	7600	1.34	0.165	→	P12-1	10100	1.30	0.165	11900
P10-3	5200	1.37	0.251	→	P12-2	8000	1.28	0.263	9500
P10-4	7200	1.33	0.450	→	P12-3	12500	1.25	0.454	17000
P10-5	8100	1.33	0.546	→	P12-4	8100	1.33	0.546	20900

^a Determined *via* GPC analysis in THF. Calibration against narrow polystyrene standards. ^b Determined *via* ^1H NMR analysis in CDCl_3 and calculation following Eq. 9. ^c Determined *via* ^1H NMR analysis in CDCl_3 and calculation following Eq. 16. ^d Calculation according to Eq. 19.

The molar mass distribution of the polymers **P10** and **P12** was determined *via* GPC analysis in THF (Figure 25). The number-averaged molar masses, M_n , and the polydispersities, \mathcal{D} , derived after calibration of the GPC system with narrow polystyrene standards are collated in Table 7. Except for polymer **P12-4**, the molar masses increased after the transformation while the dispersity decreased. The expected molar masses, M_n^{theo} , for **P12** are calculated following Eq. 17 with the indices differentiating between styrene (x) and the functionalized comonomer (y). For all polymers a higher molar mass is expected than obtained by GPC, which could be due to a different hydrodynamic volume of the polymers compared to the narrow polystyrene standards or incomplete solubility.

$$M_n^{\text{P12}} = (M_x \cdot F_x + M_y^{\text{P12}} \cdot F_y) \cdot \frac{M_n^{\text{P10}}}{(M_x \cdot F_x + M_y^{\text{P10}} \cdot F_y)} \quad \text{Eq. 17}$$

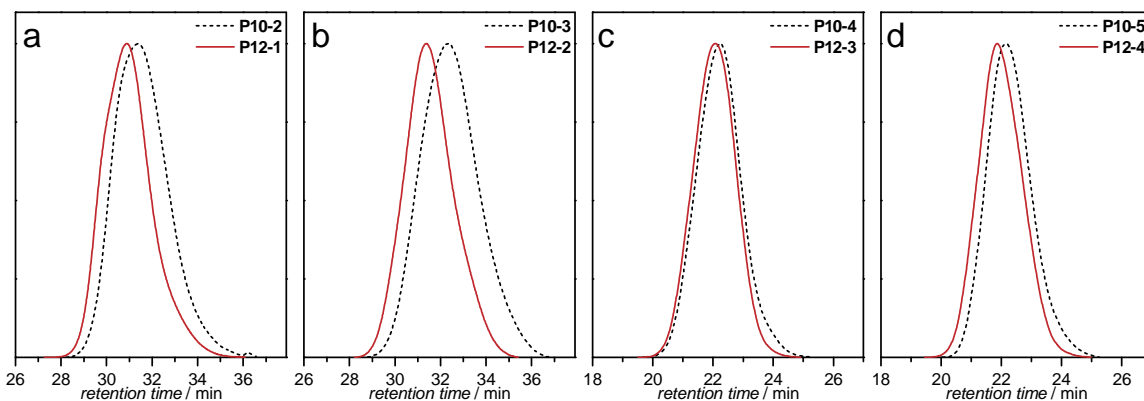


Figure 25. Comparison of the molar mass distributions of **P10-2** to **P10-5** and cycloaddition products **P12-1** to **P12-4** obtained by GPC measurements in THF. Calibration was derived using narrow polystyrene standards; the values for the molar mass and dispersity are collated in Table 7.

The absolute weight-averaged molar mass of the polymers is accessible by static light scattering measurements (SLS). SLS provides information on the time-averaged properties of the system. The apparent weight-averaged molar mass (M_w) can be obtained by the DEBYE relationship (Eq. 18), where c is the concentration, I_r is the relative excess scattering intensity, K gathered optical parameters, R_g is the radius of gyration, q is the scattering wave vector, and A_2 is the second virial coefficient.

$$\frac{K \cdot c}{I_r} = \frac{1}{M_w} \cdot \left(1 + \frac{R_g^2 \cdot q^2}{3} \right) + 2 \cdot A_2 \cdot c \quad \text{Eq. 18}$$

The absolute weight-averaged molar mass, M_w , was obtained by extrapolation of the $(K \cdot c / I_r)$ values to $q = 0$ and $c = 0$. The SLS measurements of the polymers **P12-1** to **P12-4** were conducted in DMAc. The obtained ZIMM-plot of **P12-3** is depicted exemplarily in Figure 26. The results for all polymers are collated in Table 8.

Table 8. Comparison of the theoretically expected weight-averaged molar mass, M_w , versus the results of the respective GPC and SLS measurements for polymers **P12**.

	$M_w^{\text{theo,a}}$	$M_w^{\text{GPC,b}}$	$M_w^{\text{SLS,c}}$
	g·mol ⁻¹	g·mol ⁻¹	g·mol ⁻¹
P12-1	15000	13200	19600
P12-2	17300	10200	17300
P12-3	21000	15600	29400
P12-4	28000	16500	29800

^a Calculated from M_n^{theo} (derived from Eq. 17) by multiplication with \bar{D} from GPC (Table 7).

^b Determined *via* GPC analysis in THF. Calibration against narrow polystyrene standards.

^c Determined *via* SLS in DMAc.

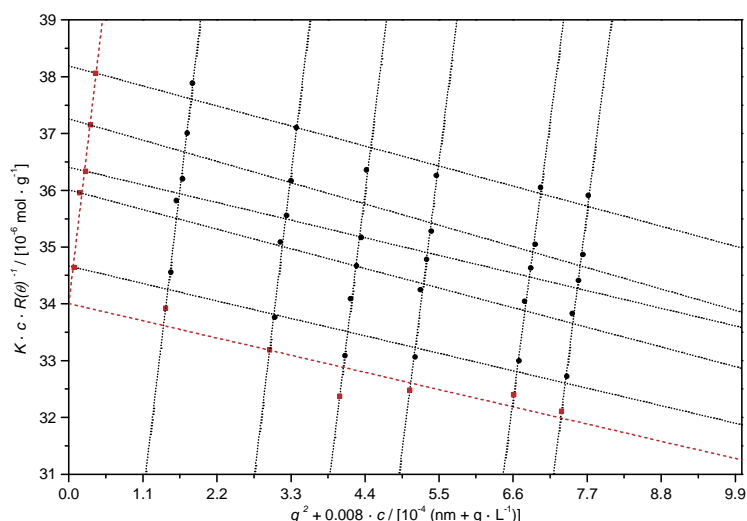
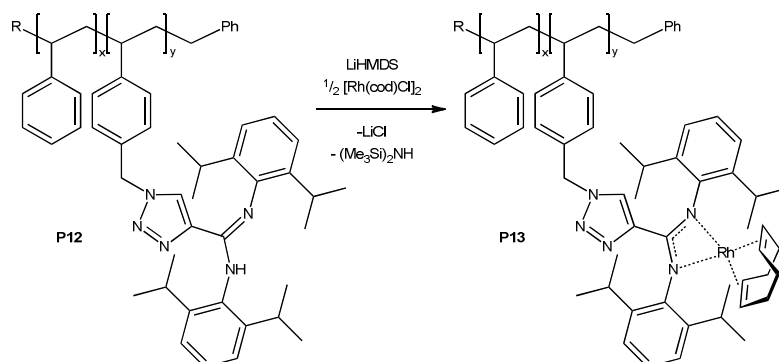


Figure 26. ZIMM-plot of polymer **P12-3** derived from the SLS measurement in DMAc.

The weight-averaged molar masses obtained by SLS range between $17 \text{ kg}\cdot\text{mol}^{-1}$ and $30 \text{ kg}\cdot\text{mol}^{-1}$. They are slightly higher than expected what could be due to the error in the GPC measurements of the precursor polymers **P10** which was not taken into account for the calculation of M_n^{theo} of **P12** (Eq. 17).



Scheme 39. After reduction, the ligand functionalized polymer **P12** reacts with the metal precursor $[\text{Rh}(\text{cod})\text{Cl}]_2$ to give the rhodium loaded polymer **P13**.

The *in-situ* reduction of the ligand moieties in **P12** and subsequent reaction with the metal precursor was conducted by the institute of inorganic chemistry (C. Kiefer) as depicted in Scheme 39. Residual $[\text{Rh}(\text{cod})\text{Cl}]_2$ was removed from the polymer solution by dialysis against THF. After reprecipitation from methanol, the polymers were analyzed *via* ^1H NMR spectroscopy. The obtained spectra of the four polymer sets **P12-1** to **P12-4** with their respective products **P13-1** to **P13-4** are depicted in Figure 27.

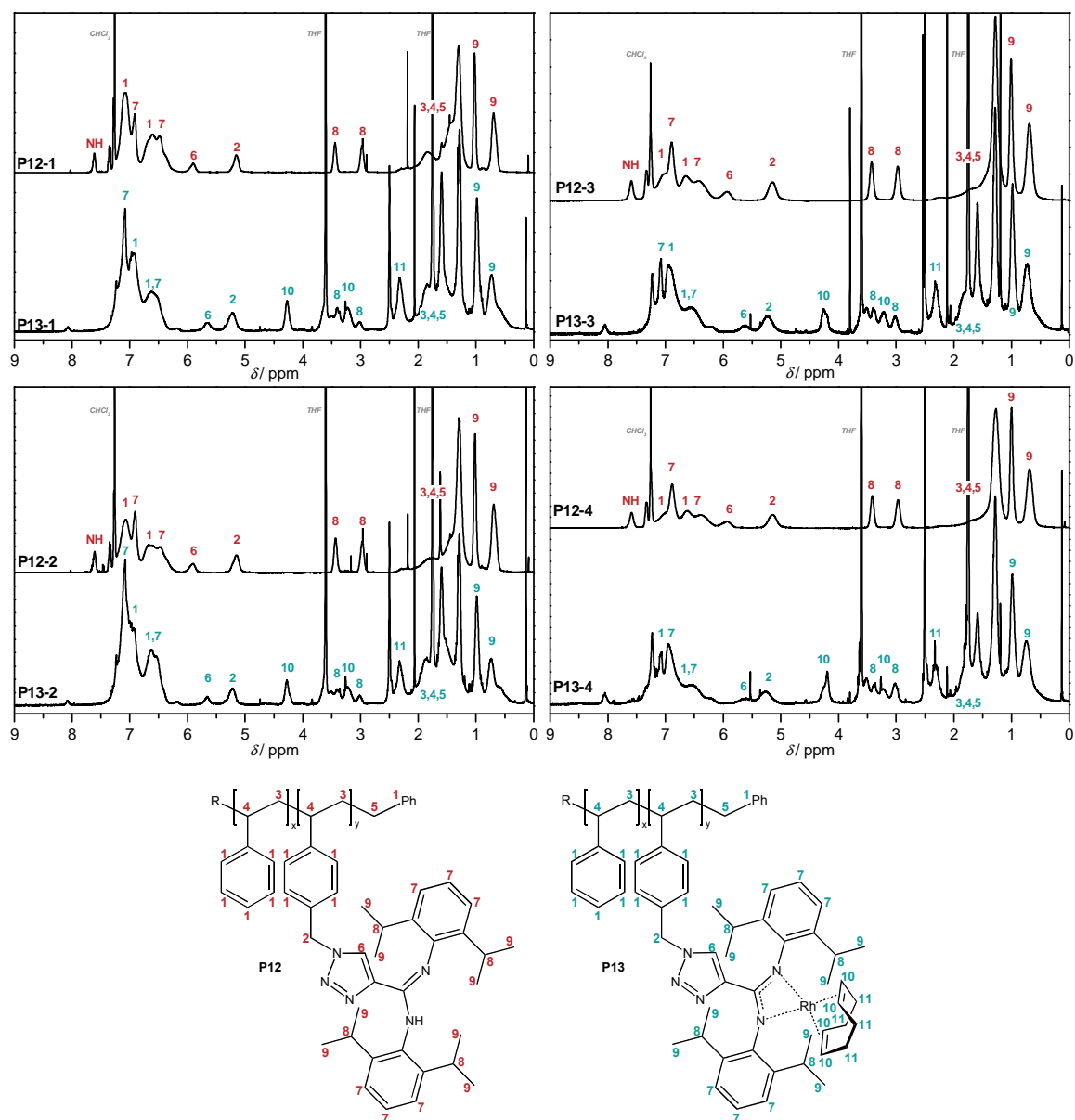


Figure 27. ^1H NMR spectra of the unloaded polymers **P12-1** to **P12-4** recorded in CDCl_3 in comparison to the spectra of the loaded polymers **P13-1** to **P13-4** recorded in THF-d_8 , respectively. For the signal assignments refer to the schematic drawing below the spectra.

The signals of the phenyl ring protons between $\delta = 7.43$ ppm and 6.16 ppm are not influenced in their chemical shift as well as the CH and CH_2 backbone proton signals, generating a broad multiplet signal ranging from $\delta = 2.46$ ppm to 0.44 ppm together with the resonances of the isopropyl- CH_3 protons. The signal of the Ph-CH_2 protons at $\delta = 5.15$ ppm is also not influenced by the loading reaction. The resonances at $\delta = 3.44$ ppm and 2.97 ppm, assigned to the isopropyl-CH protons, are not shifted but overlaid by an additional signal of the cod-CH protons. A second signal of these protons is located at $\delta = 4.27$ ppm. The cod- CH_2 protons induce a new signal at

$\delta = 2.31$ ppm. A clear shift is observed for the triazolyl proton from $\delta = 5.90$ ppm in **P12** to 5.63 ppm in **P13**. The NH signal at $\delta = 7.61$ ppm in **P12** is no longer visible in the respective spectrum of **P13**, evidencing a successful reaction. A quantitative interpretation of the spectra is not possible since the polymers were only partly soluble. A small residual signal of the triazolyl ring proton at $\delta = 5.90$ ppm indicates a small amount of residual unloaded ligand moieties.

The determination of the molar mass distribution of **P13-1** to **P13-4** by GPC analysis was not possible due to insolubility of the polymers. The weight-averaged molar masses could thus be obtained by SLS measurements in DMAc. As an example, the ZIMM-plot derived from extrapolation of the DEBYE relationship (Eq. 18) to $q = 0$ and $c = 0$ is depicted in Figure 28. The results of all SLS measurements are collated in Table 9 for both the polymers **P12-1** to **P12-4** and **P13-1** to **P13-4**.

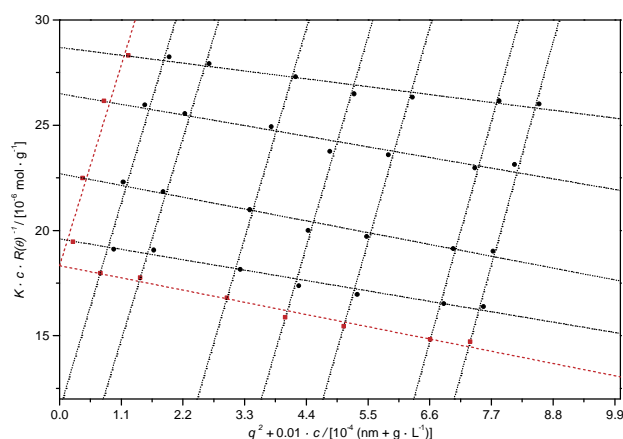


Figure 28. ZIMM-plot of polymer **P13-3** derived from SLS measurement in DMAc.

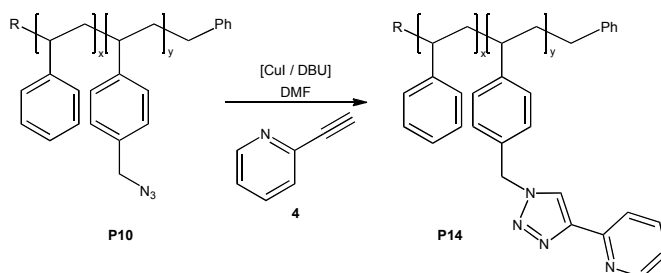
The obtained weight-averaged molar masses for the polymers **P13-1** to **P13-4** range between $M_w = 32 \text{ kg} \cdot \text{mol}^{-1}$ and $46 \text{ kg} \cdot \text{mol}^{-1}$ and are significantly higher compared to their unloaded equivalents **P12-1** to **P12-4**. The specific refractive index increment determined in DMAc increased from around $dn/dc = 0.15 \text{ mL} \cdot \text{g}^{-1}$ in the polymers **P12** to appr. $dn/dc = 0.17 \text{ mL} \cdot \text{g}^{-1}$ in **P13**.

Table 9. Weight-averaged molar masses of the polymers **P12** and **P13** obtained by SLS measurements in DMAc.

	M_w^{SLS} g·mol ⁻¹	dn/dc mL·g ⁻¹		M_w^{SLS} g·mol ⁻¹	dn/dc mL·g ⁻¹
P12-1	19600	0.148	→	P13-1	32100
P12-2	17300	0.139	→	P13-2	46500
P12-3	29400	0.144	→	P13-3	42000
P12-4	29800	0.147	→	P13-4	45600

3.2.4. Generation of a Pd-Complexing Ligand by CuAAC Ligation with 2-Ethynylpyridine and Subsequent Pd-containing Polymers

For the ligation of palladium onto polymer side-chains a very elegant and simple strategy was employed. 2-Ethynylpyridine (**4**) is commercially available and forms – upon cycloaddition with the azide polymer **P10** – a bidentate ligand composed of the pyridine ring nitrogen and one of the triazole ring nitrogen atoms, **P14** (Scheme 40).



Scheme 40. Copper catalyzed cycloaddition of 2-ethynylpyridine (**4**) with azide-functionalized polymer **P10** gives polymer **P14** with a bidentate ligand formed by the triazole ring and the pyridine ring.

Four azide-containing polymers were synthesized featuring different molar ratios of azide functionalities ranging from $F_y = 0.13$ to 0.49 in order to investigate possible influences of the spatial distance between two functionalized side-chains. The polymers were analyzed *via* GPC and ¹H NMR analysis. Table 10 collates the characteristics of the azide-functionalized polymers **P10-6** to **P10-9** and the respective triazolyl pyridinyl functionalized polymers **P14-1** to **P14-4**.

Table 10. Characteristics of azide functionalized polymers **P10-6** to **P10-9** and the subsequent cycloadducts **P14-1** to **P14-4**.

	$M_n^{\text{GPC,a}}$ g·mol ⁻¹	\bar{D}^a	F_y^b		$M_n^{\text{theo,c}}$ g·mol ⁻¹	$M_n^{\text{GPC,a}}$ g·mol ⁻¹	\bar{D}^a	F_y^d	
P10-6	7300	1.29	0.130	→	P14-1	8200	7800	1.27	0.128
P10-7	7100	1.29	0.248	→	P14-2	8600	7700	1.29	0.252
P10-8	5700	1.33	0.387	→	P14-3	7500	6400	1.30	0.386
P10-9	5400	1.35	0.487	→	P14-4	7500	6500	1.25	0.485

^a Determined *via* GPC analysis in DMAc. Calibration against narrow polystyrene standards.

^b Determined *via* ¹H NMR analysis in DMSO-d₆ and calculation following Eq. 9. ^c Calculation according to Eq. 20. ^d Determined *via* ¹H NMR analysis in DMSO-d₆ and calculation following Eq. 19.

The ¹H NMR spectra of the four polymer sets differing in the relative molar fraction of functionalized comonomer are depicted in Figure 29. The chemical shifts of the resonances assigned to the aromatic phenyl ring protons ranging from $\delta = 7.54$ ppm to 6.10 ppm, and to the polymer backbone ranging from $\delta = 2.48$ ppm to 0.87 ppm are not affected by the side-chain modification. The signal assigned to the CH₂N₃ protons in **P10** is shifted from $\delta = 4.26$ ppm downfield to 5.54 ppm in **P14**. The complete shift of this signal proves full conversion of all azide functionalities to the cycloadduct. Additionally, the new signal in the spectrum of **P14** at $\delta = 8.63$ ppm is assigned to the triazolyl ring proton and the signals at $\delta = 8.54$ ppm, 8.05 ppm, 7.80 ppm and 7.25 ppm can be assigned to the pyridinyl ring protons.

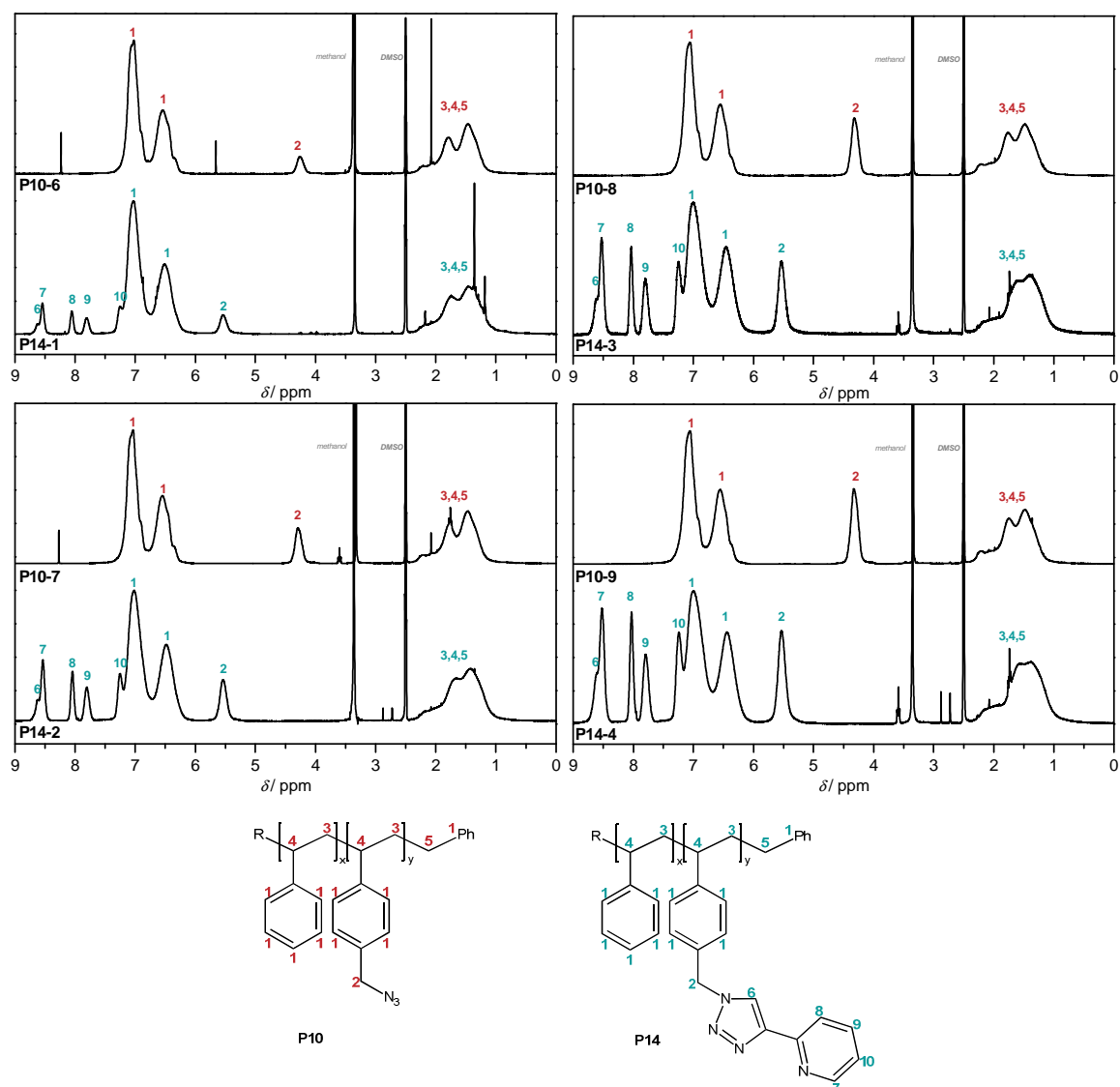


Figure 29. ^1H NMR spectra of **P10-6** to **P10-9** and **P14-1** to **P14-4** recorded in DMSO-d_6 . For the signal assignments refer to the schematic drawing below the spectra.

For the correct assignment of the signals, COESY experiments were conducted as shown exemplarily for **P14-2** in Figure 30. Both protons numbered 7 and 9 induce cross signals with the proton 10 whereas only proton 9 gives a cross signal with proton 8. Proton 6 shows no cross coupling with other signals as expected for the isolated triazolyl proton.

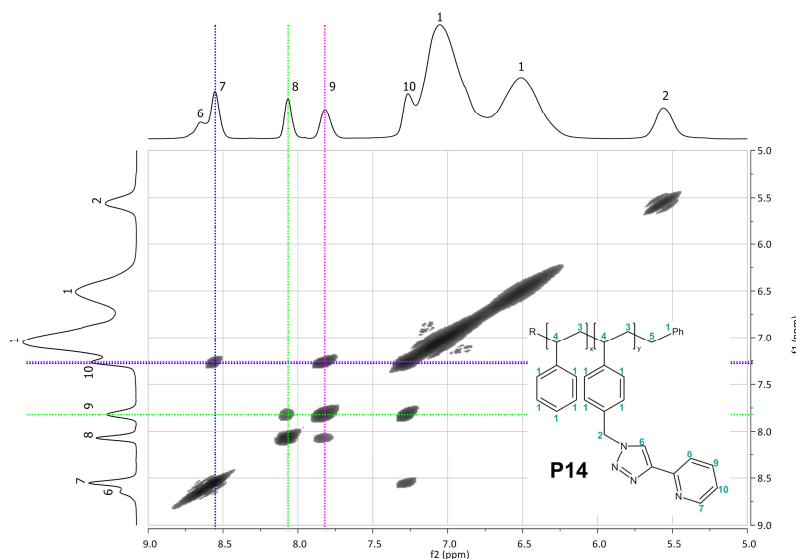


Figure 30. COESY NMR spectrum of **P14-2** in DMSO- d_6 showing the chemical shift range of $\delta = 9.0$ ppm to 5.0 ppm. The cross-resonances allowing for the assignment of the pyridinyl protons and the triazolyl proton, respectively, are highlighted by the dashed lines. For signal assignment refer to the schematic drawing in the figure.

The calculation of the molar fraction of functionalized monomer, F_y , present in the polymer from the integrals of the ^1H NMR spectra of **P14-1** to **P14-4**, takes the overlapping of one pyridinyl ring proton with the signal of the phenyl ring protons into account. F_y can thus be calculated according to Eq. 19 with $y = \text{CH}_2\text{-triazolyl}$. The molar fraction of functionalized comonomer ranging between 13 % and 50 % does not change upon the modification reaction confirming full conversion of the azide side groups (Table 10).

$$F_y^{\text{P14}} = 2.5 \cdot \frac{I_y}{I_{\text{Ph}}} \quad \text{Eq. 19}$$

The molar masses of the polymers were determined *via* GPC measurements in DMAc. Figure 31 depicts the GPC traces of the four polymer sets and Table 10 collates the determined number-averaged molar masses after calibrating the GPC system with narrow polystyrene standards. All distributions show a shift to higher molar masses without broadening. From the molar mass of **P10** a theoretically expected molar mass of **P14** can be calculated following Eq. 20 assuming full conversion as already proofed by the ^1H NMR analyses.

$$M_n^{\text{P14}} = (M_x \cdot F_x + M_y^{\text{P14}} \cdot F_y) \cdot \frac{M_n^{\text{P10}}}{(M_x \cdot F_x + M_y^{\text{P10}} \cdot F_y)} \quad \text{Eq. 20}$$

M_x and F_x are defined as the molecular weight and the molar fraction of the comonomer styrene, M_y^{P10} and F_y referring to the azidomethyl styrene comonomer, and M_y^{P14} and F_y to the pyridinyl triazolyl methyl styrene comonomer, respectively. The number-averaged molar masses of the polymers are specified as M_n^{P10} and M_n^{P14} . In comparison to the theoretically expected molar masses, the determined values are too low, which may be due to a difference in the hydrodynamic radii of the modified polystyrenes compared to the linear narrow polystyrene standards employed for GPC calibration.

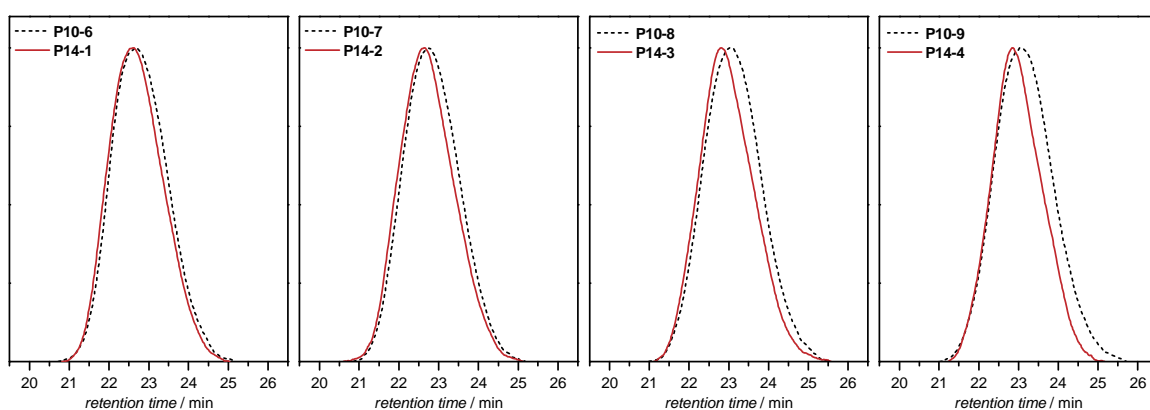


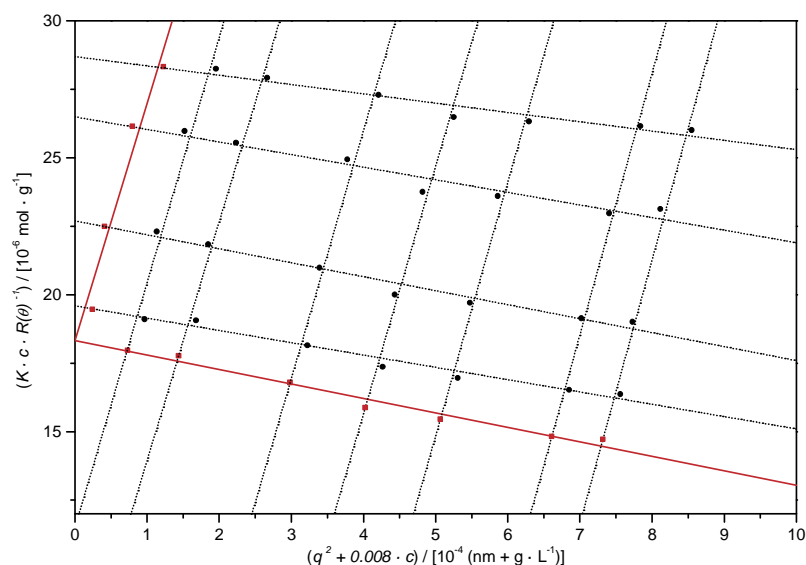
Figure 31. GPC traces of **P10-6** to **P10-9** and **P14-1** to **P14-4** recorded in DMAc. GPC calibration was conducted with narrow polystyrene standards.

The determination of the absolute weight-averaged molar mass, M_w , was conducted *via* SLS measurements in DMAc and subsequent ZIMM-plot analysis with extrapolation of the DEBYE relationship (Eq. 18) to $c = 0$ and $q = 0$. As an example, the obtained ZIMM-plot for polymer **P14-2** is depicted in Figure 32. The ZIMM-plot of polymer **P14-1** could not be evaluated but the weight-averaged molar masses of the polymers **P14-2** to **P14-4** are collated in Table 11. For comparison, the theoretically expected weight-averaged molar mass, M_w^{theo} , was calculated by multiplication of the dispersity, \mathcal{D} , derived from the GPC measurements with the theoretical number-averaged molar mass, M_n^{theo} , obtained *via* Eq. 20. The absolute weight-averaged molar masses determined by SLS range between $13 \text{ kg}\cdot\text{mol}^{-1}$ and $15 \text{ kg}\cdot\text{mol}^{-1}$. They are slightly lower than predicted, yet within the accurateness of the calculation still in good agreement with the expected values.

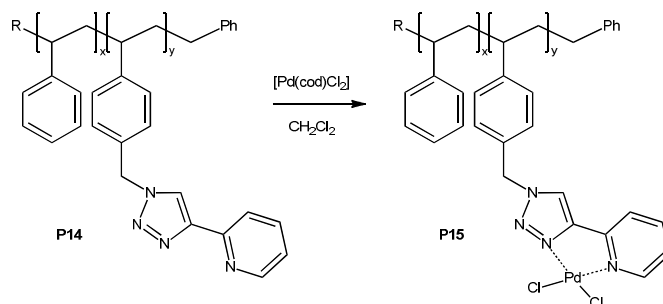
Table 11. Comparison of the theoretically expected weight-averaged molar mass, M_w , versus the results of the respective GPC and SLS measurements for polymers **P14**.

	$M_w^{\text{theo,a}}$	$M_w^{\text{GPC,b}}$	$M_w^{\text{SLS,c}}$
	$\text{g}\cdot\text{mol}^{-1}$	$\text{g}\cdot\text{mol}^{-1}$	$\text{g}\cdot\text{mol}^{-1}$
P14-1	15900	9900	-
P14-2	15900	9900	14600
P14-3	14100	8300	13000
P14-4	13400	8100	13400

^aCalculated from the theoretically expected number-averaged molar mass, M_n^{theo} , (derived from Eq. 20) by multiplication with the dispersity, \mathcal{D} , from GPC as collated in Table 10. ^bDetermined *via* GPC analysis in DMAc. Calibration against narrow polystyrene standards. ^cDetermined *via* SLS and ZIMM-plot analysis in DMAc.

**Figure 32.** ZIMM-plot derived from the SLS measurement of **P14-2** in DMAc for 5 concentrations ranging from 0.5 to 4 $\text{g}\cdot\text{L}^{-1}$.

The subsequent loading of the polymers **P14** with palladium was conducted in the institute of inorganic chemistry (C. Kiefer). The polymer was dissolved in methylene chloride, the precursor $[\text{Pd}(\text{cod})\text{Cl}_2]$ was added and the mixture was stirred at ambient temperature under a nitrogen atmosphere (Scheme 41). The precipitated product was collected by filtration and washed with methylene chloride and *n*-pentane. The obtained products were analyzed *via* ^1H NMR spectroscopy, elemental analysis and static light scattering measurements. Parts of the analyses, especially the elemental analyses, were conducted in the institute of inorganic chemistry. In order to show the entire characterization of the polymers, they will be also presented in the following.



Scheme 41. Palladium loading of **P14** to form **P15**. Reaction was conducted in the institute of inorganic chemistry.

The ^1H NMR spectra of **P15** depicted in Figure 34 show no new signals compared to the spectra of the respective polymers **P14** but a shift to lower fields of the protons in spatial proximity to the bidentate ligand is observed. For the correct assignment of the pyridinyl ring signals two-dimensional COESY NMR measurements were conducted as depicted exemplarily for **P15-2** in Figure 33. For the ringproton 10 at $\delta = 7.61$ ppm, two crosspeaks are observed induced by the adjacent protons 7 at $\delta = 8.95$ ppm and 9 at $\delta = 8.19$ ppm.

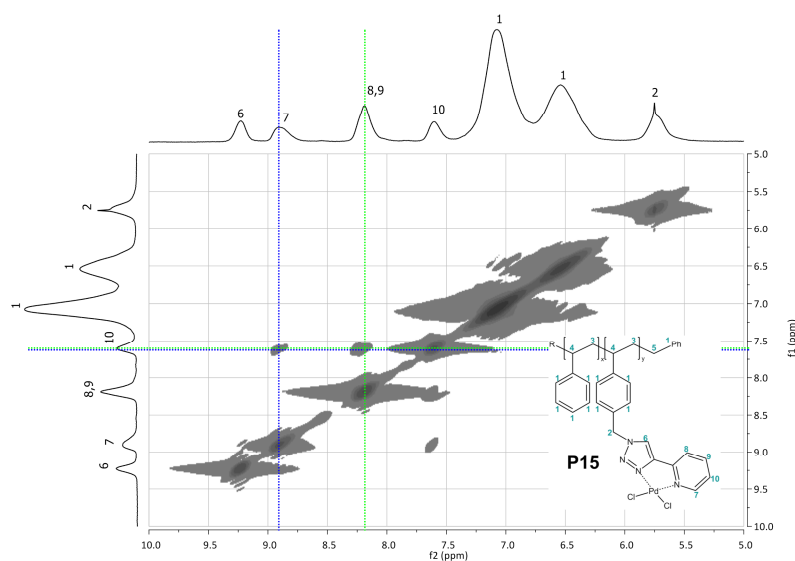


Figure 33. COESY NMR spectrum of **P15-2** in DMSO-d_6 in the range of $\delta = 10.00$ ppm to 5.00 ppm. The crosspeaks allowing for the assignment of the pyridinyl protons are highlighted by the dashed lines. For signal assignment refer to the schematic drawing within the picture.

The triazolyl ring proton is shifted from $\delta = 8.63$ ppm in **P14** to $\delta = 9.22$ ppm in **P15**. The pyridinyl protons are shifted to $\delta = 8.95$ ppm (7), 8.19 ppm (8,9) and 7.61 ppm (10), respectively, with the signals of the ring protons 8 and 9 overlapping with each other. The signal of the CH_2 -triazolyl protons is shifted from $\delta = 5.54$ ppm in **P14** to $\delta = 5.73$ ppm in **P15**. The signals of the phenyl ring protons ($\delta = 7.54$ ppm to

6.10 ppm) and of the polymer backbone ($\delta = 2.48$ ppm to 0.87 ppm) are not influenced in their chemical shifts. Despite the broad signals typically for polymers, a small residual signal of proton 7 in the spectra of **P15** with an identical shift as proton 7 in **P14** can be detected in the enlargement as shown exemplarily for **P15-2** in Figure 34e, indicating incomplete loading of the ligands. Comparing these signals, the loading efficiency, $f_{\text{Pd}^{\text{NMR}}}$, can be calculated.

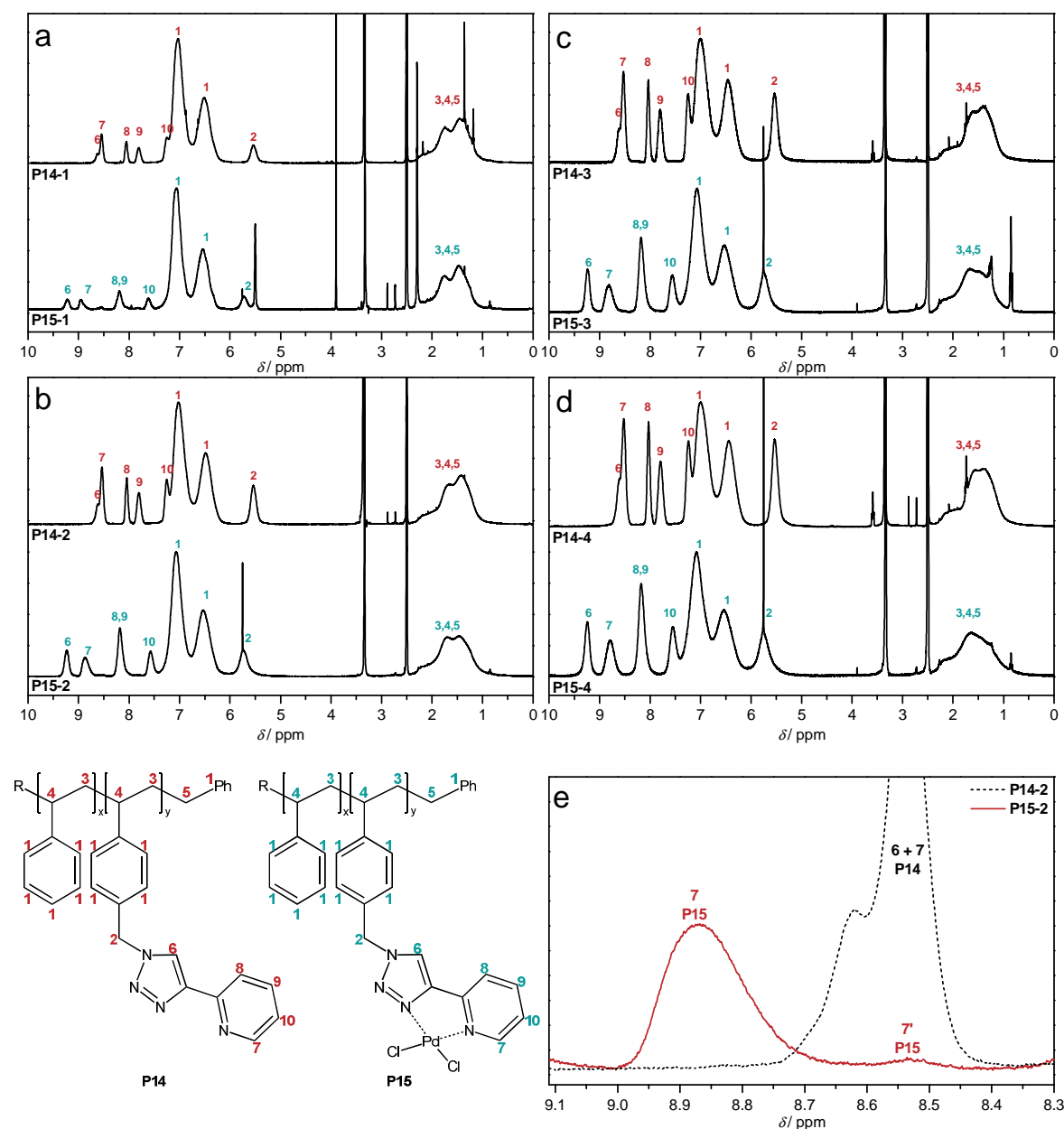


Figure 34. ^1H NMR spectra of **P14-1** to **P14-4** and the subsequent products **P15-1** to **P15-4** recorded in DMSO- d_6 . For the signal assignments refer to the schematic drawings below the spectra. For the calculation of the loading efficiency from the ^1H NMR spectra, the signal of the pyridinyl proton H7 in **P15** is compared to the residual signal of the equivalent signal in **P14** (H7') as highlighted in the lower right figure.

In addition to the determination of the loading efficiency by the ^1H NMR analyses, elemental analyses were conducted determining the relative mass fraction, ω , of the atoms C, H, N and S. The mass content of PdCl_2 in the polymers **P15** is thus the difference of the summarized mass fractions of the detected atoms to 100 %. The resulting mass fraction of Pd in **P15** can subsequently be calculated by Eq. 21.

$$\omega_{\text{Pd}}^{\text{EA}} = \left[1 - \sum \omega(\text{C, H, N, S}) \right] \cdot \frac{M_{\text{Pd}}}{M_{\text{PdCl}_2}} \quad \text{Eq. 21}$$

In comparison, a complete loading would give the theoretically mass fraction of Pd, $\omega_{\text{Pd}}^{\text{theo}}$, that can be calculated following Eq. 22 with the index x referring to styrene and the index y to the palladium functionalized comonomer, respectively.

$$\omega_{\text{Pd}}^{\text{theo}} = \frac{F_y \cdot M_{\text{Pd}}}{F_x \cdot M_x + F_y \cdot M_y} \quad \text{Eq. 22}$$

The loading efficiency is calculated as the quotient of the determined Pd content and the theoretically maximal possible Pd content as described in Eq. 23.

$$f_{\text{Pd}}^{\text{EA}} = \frac{\omega_{\text{Pd}}^{\text{EA}}}{\omega_{\text{Pd}}^{\text{theo}}} \quad \text{Eq. 23}$$

Table 12 summarizes the calculated values for all polymers **P15-1** to **P15-4**. The loading efficiencies derived from either the ^1H NMR spectra or the elemental analyses are in good agreement and range between 70 % and 90 % for all polymers. The incomplete loading is most probably a result of the precipitation of the product during the loading reaction. Better results should be achieved in a suitable solvent that is able to keep the product polymer **P15** in solution. For an application as catalytically active material, the palladium content would thus be sufficient.

Table 12. Summary of the results derived from the ^1H NMR and elemental analyses. Molar fraction of functionalized comonomer, F_y , in P14 and P15, and loading efficiency, f_{Pd} , for the polymers **P15-1** to **P15-4**.

	F_y^{NMR}		F_y^{NMR}	$f_{\text{Pd}}^{\text{NMR}}$	$f_{\text{Pd}}^{\text{EA}}$
P14-1	0.128	→	P15-1	0.107	0.885
P14-2	0.252	→	P15-2	0.248	0.840
P14-3	0.386	→	P15-3	0.378	0.763
P14-4	0.485	→	P15-4	0.458	0.721

The GPC analysis of the palladium functionalized polymers was not possible due to solubility issues and chemical interactions of the palladium-containing polymers with the GPC column material. Alternatively, the absolute weight-averaged molar mass was determined *via* static light scattering measurements in DMAc. The ZIMM-plot was obtained identically to the SLS measurements of **P14** by extrapolation of the DEBYE relationship (Eq. 18) to $c = 0$ and $q = 0$. Exemplarily, the ZIMM-plot of polymer **P15-2** is depicted in Figure 35. The resulting absolute weight-averaged molar masses, M_w^{SLS} , are collated in Table 13 together with the GPC and SLS results of the respective polymers **P14**.

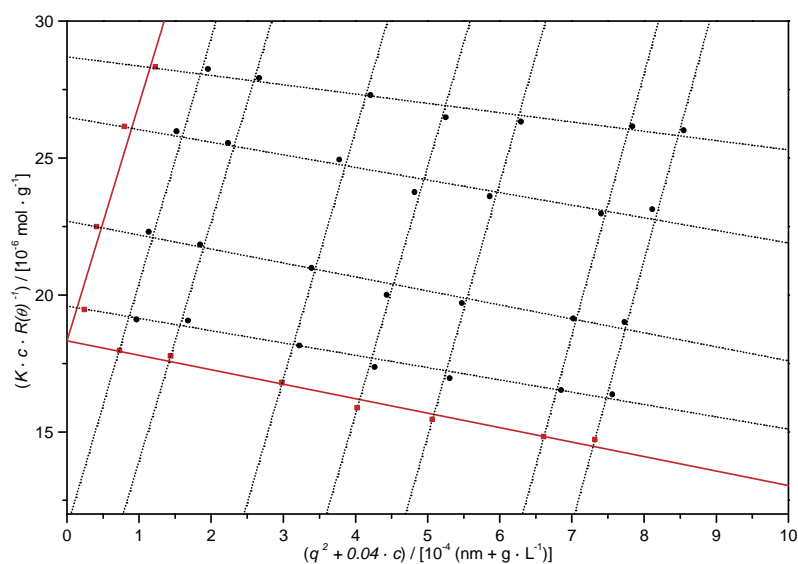


Figure 35. ZIMM-plot derived from the SLS measurements of **P15-2** in DMAc for 5 concentrations ranging from 0.5 to 4 g·L⁻¹.

The molar masses of the polymers **P15** are higher compared to their unloaded equivalents, which is in agreement with the expected behaviour since PdCl₂ is added to the ligands. The resulting molar masses range between 16 and 20 kg·mol⁻¹.

Table 13. Weight-averaged molar masses of the polymers P14 and P15.

	M_w^{GPC}	\mathcal{D}^{GPC}	M_w^{SLS}	dn/dc		M_w^{SLS}	dn/dc	
	g·mol ⁻¹		g·mol ⁻¹	mL·g ⁻¹		g·mol ⁻¹	mL·g ⁻¹	
P14-1	9900	1.27	-	-	→	P15-1	15600	0.1627
P14-2	9900	1.29	14600	0.1452	→	P15-2	20400	0.1636
P14-3	8300	1.30	13000	0.1573	→	P15-3	19100	0.1706
P14-4	8100	1.25	13400	0.1694	→	P15-4	-	-

In summary, the synthesis and characterization of rhodium and palladium containing polystyrenes was shown by a modular approach of side chain-functionalization and subsequent metal loading. Such an approach allows the ligation of various metal complexes onto a pre-synthesized and well-defined polymer chain with excellent control over the molar mass. The spatial distance between two adjacent metal complexes can be controlled by the initial comonomer composition employed in the polymerization reaction. The resulting copolymer composition is well-predictable *via* the copolymerization equation as long as the reactivity ratios of the monomers are known. The determination of the relative molar fractions is enabled by ^1H NMR spectroscopy.

The molar mass distribution can be determined for the precursor polymers by GPC measurements while the final metallopolymers are only slightly soluble in the typical GPC solvents. As an alternative, SLS measurements provide the absolute weight-averaged molar masses of the metallopolymers.

The feasibility of attaching two or more different metal complexes onto a single polymer chain by controlling the employed amount of alkyne species was shown exemplarily with propargyl alcohol.

4

Metal-Containing Main Chain Functionalized Polymers

The high efficiency and orthogonality towards many functional groups of the 1,3-dipolar cycloaddition of azides and alkynes is not only limited to polymer side chain or polymer endgroup modifications, yet can also be employed as a polymerization reaction itself. Not surprisingly the interest of polymer scientists in CuAAC driven polycycloaddition grew strongly since the first attempts in 2004.²⁶⁶ In addition to dendritic polymers²⁶⁷⁻²⁷² or polymer networks,²⁷³⁻²⁷⁷ linear poly(triazole)s featuring specific optical characteristics,²⁷⁸⁻²⁸⁰ thermal stability²⁸⁰⁻²⁸² or biocompatibility²⁸³⁻²⁸⁶ are explored as well as organometallic polymers.^{102,103,287} The 'standard' reaction conditions of the CuAAC reaction, namely the catalysis by

Parts of the test reactions were performed by K. Pahnke in the course of his diploma thesis under supervision of C. Barner-Kowollik and C. Lang. Metal loading and elemental analysis of the polymers were performed in collaboration with C. Kiefer and Prof. P. Roesky (KIT). Parts of the current chapter were reproduced with permission from C. Lang, K. Pahnke, C. Kiefer, A. S. Goldmann, P. W. Roesky and C. Barner-Kowollik, *Polym. Chem.*, 2013, **4**, 5456 (DOI: 10.1039/c3py00648d). Copyright The Royal Society of Chemistry.

in-situ reduced CuSO₄ with sodium ascorbate in water or water/DMF mixtures were rapidly expanded to enable the reaction to proceed in organic solvents. The Cu(I) species are often introduced by Cu(I) salts such as CuBr, CuI or Cu(OAc) and can be stabilized by the addition of multidental *N* donor ligands, *e.g.* PMDETA or DBU.²⁸⁸ Cu(I) complexes with *N* heterocyclic carbenes²⁸⁹⁻²⁹² or polymer supported copper catalysts^{293,294} have also been reported to be active alternatives to the standard system. Employing ruthenium catalysts, the 1,4-regioselectivity can be inverted in order to obtain the 1,5-isomers selectively, having a significant influence on the properties of the poly(triazole).^{295,296} For biosynthetic applications a metal-free cycloaddition of azides and activated alkynes, *e.g.* bis(arylacetylene)s,²⁹⁷ or aroxycarbonylacetylenes,²⁹⁸⁻³⁰⁰ is of special interest.

The synthesis of linear poly(triazole)s affords bifunctional monomers, *i.e.* one molecule featuring one azide and one alkyne functionality (AB) or a mixture of two bifunctionalized monomers each of them bearing two azide (A₂) or two alkyne (B₂) functionalities, respectively. Although the AB system ensures equimolarity in the polymerization reaction, the mixed A₂+B₂ systems are often preferred due to the more facile preparation of homofunctionalized moieties.

In a step-growth polymerization such as polyaddition, the monomers combine firstly to dimers which undergo the next polymerization step and combine to oligomers of three or four monomeric units and so on. Only at high conversions polymer chains are formed. The degree of polymerization, DP_n , is in inverse proportion to $(1 - \chi)$ as described by the CAROTHERS equation,³⁰¹ with χ being the conversion of the two monomers in an equimolar mixture (Eq. 24).

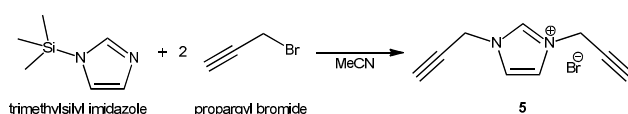
$$DP_n = \frac{1}{1 - \chi} \quad \text{Eq. 24}$$

Consequently, polymers with a high DP_n and thus a high molar mass can only be obtained at very high conversions and the A₂+B₂ system has to comply with strict criteria such as equimolarity of the monomers and no monofunctional species present that could terminate a growing chain. In addition, the employed catalytic system has to be as efficient as possible. For the subsequent loading with metal ions, the copper catalyst needs to be completely removable after the reaction.

In the following, the synthesis of a poly(triazole) featuring chelate ligands directly integrated into the polymer backbone is described. Two bifunctional alkyne monomers, an imidazolium and a pyridinyl derivative, were prepared building a tridentate ligand structure together with the generated triazole rings on both sides of the *N* heterocyclic structure. In a model study with monofunctional azides, the reaction conditions were optimized with regard to the catalytic system and the employed solvent. In addition to the standard CuSO₄ / sodium ascorbate systems, CuBr / PMDETA, CuI / DBU and CuI with a *N* heterocyclic carbene were tested as catalytic systems in DMF and THF. The polymerization reactions were performed employing bifunctional azide linkers together with the dialkynes already used in the test reactions. The solubility of the poly(triazole)s could be enhanced by a fluorene linker equipped with alkyl side chains. The obtained polymers were characterized *via* ¹H NMR, GPC, SLS and elemental analysis. The subsequent metal coordination with a palladium(II) precursor was conducted by the institute of inorganic chemistry (C. Kiefer) and the products were analyzed by ¹H NMR spectroscopy and elemental analysis.

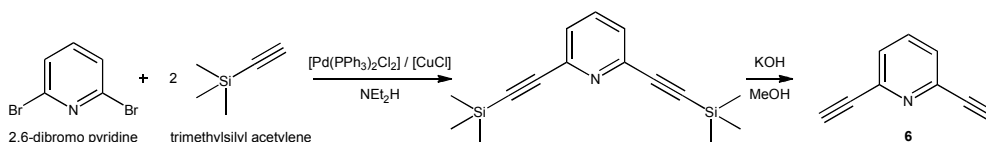
4.1. Synthesis of Suitable Alkyne Monomers

For the incorporation of multidentate metal ligands into a polymeric backbone by poly(CuAAC) polymerization, two suitable bifunctionalized nitrogen-containing heterocyclic compounds were identified, namely 1,3-dipropynyl-imidazolium bromide (**5**) and 2,6-diethynyl pyridine (**6**). The imidazolium salt **5** is accessible in a one-step reaction of trimethylsilyl imidazole with two equivalents of propargyl bromide in acetonitrile (Scheme 42).



Scheme 42. Synthesis of dialkyne-functionalized imidazolium bromide **5** from trimethylsilyl imidazole and two equivalents propargyl bromide in acetonitrile.

The second suitable alkyne moiety was synthesized from 2,6-dibromopyridine and trimethylsilyl acetylene *via* a SONOGASHIRA coupling reaction. The free alkyne **6** was obtained by subsequent removal of the TMS groups in basic methanol (Scheme 43).



Scheme 43. Synthesis of trimethylsilyl (TMS) protected 2,6-diethynyl pyridine by SONOGASHIRA coupling of 2,6-dibromo pyridine and two equivalents of trimethylsilyl acetylene in diethyl amine. Removal of the TMS groups in basic methanol provides 2,6-diethynylpyridine (**6**).

The ^1H NMR spectra of **5** and **6** are depicted in Figure 36. The spectrum of **5** exhibits two signals for the imidazolium protons at $\delta = 9.45$ ppm and 7.89 ppm, a signal induced by the CH_2 group at $\delta = 5.26$ ppm and a signal assigned to the acetylene proton at $\delta = 3.88$ ppm. The spectrum of **6** is composed of the pyridine ring proton signals at $\delta = 7.67$ ppm and 7.44 ppm and the acetylene protons at $\delta = 3.15$ ppm. For the polymerization reactions it is essential that all employed molecules are bifunctionalized, since monofunctionalized species would terminate the chain and thus reduce the conversion preventing the generation of long chain polymers. The integrals of the ^1H NMR resonances assure full functionalization of both the products **5** and **6**.

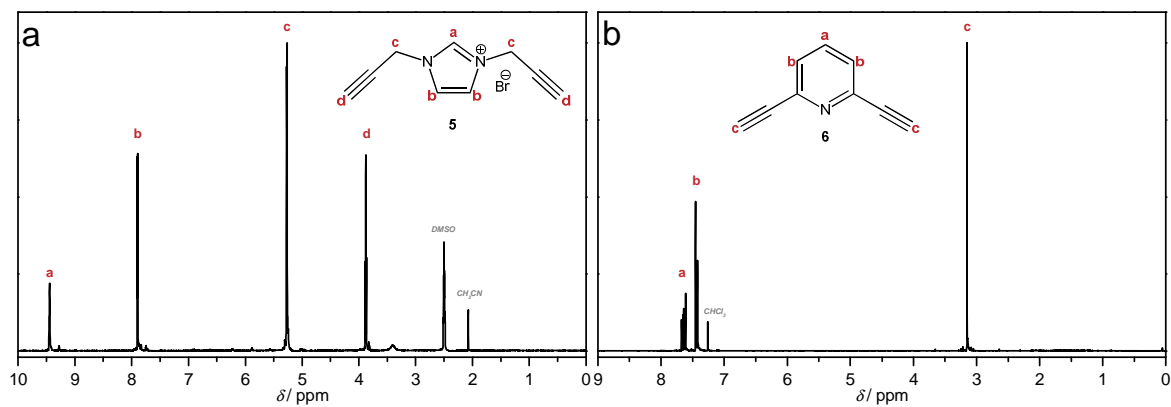
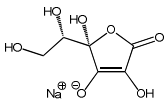
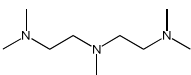
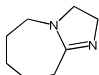
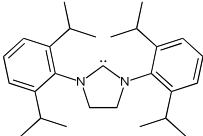


Figure 36. ^1H NMR spectra of **5** (a) in DMSO-d_6 and **6** (b) in CDCl_3 , respectively. For the resonance assignments refer to the schematic drawings within the figure.

4.2. Low-Molecular Model Study for CuAAC Catalyst Activity Testing

The most critical requirement of the step-growth polymerization mechanism following the CAROTHERS equation is achieving high conversion of the monomers.³⁰¹ An equimolar mixture of the two functionalities is a basic requisite as well as the complete bifunctionalization of all molecules. In addition, a successful polymerization requires optimal reaction conditions including a suitable solvent and a very active catalytic system. In order to optimize the reaction conditions for the polymerization reaction, a catalyst study was conducted employing three different catalytic systems for each alkyne monomer. The test reactions of **5** were conducted in DMF as the solvent at ambient temperature with the catalytic systems CuSO₄/sodium ascorbate (**A**), CuBr/*N,N,N',N',N''*-pentamethyldiethylenetriamine (PMDETA) (**B**), and CuI/1,8-diazabicycloundec-7-ene (DBU) (**C**). Due to a better solubility in organic solvents, the test reactions with **6** could be conducted in THF as the solvent. Since copper sulfate is insoluble in THF, the catalytic system (**A**) was replaced by a combination of CuI and a *N*-heterocyclic carbene, 1,3-bis(diisopropylphenyl)ylidene (IPr-NHC), as ligand (**D**). The systems (**B**) and (**C**) could be employed identically to the reactions in DMF. Table 14 collates the four catalytic systems.

Table 14. Overview over the employed catalytic systems for the test reactions.

System	A	B	C	D
Cu^I-source	CuSO ₄ /Na-Asc.	CuBr	CuI	CuI
ligand	-	PMDETA	DBU	IPr-NHC
structure				
solvent	DMF	DMF THF	DMF THF	THF

The monofunctionalized azide moieties 1-azidoundecanol (**7**) and benzyl azide (**8**) were obtained by nucleophilic substitution of the respective bromides with sodium azide in DMF.³⁰² The ¹H NMR spectra of the two azides are depicted in Figure 37. The

spectrum of **7** in CDCl_3 (Figure 37a) exhibits separated resonances for the CH_2 group directly attached to the azide group at $\delta = 3.23$ ppm and for the adjacent CH_2 group at $\delta = 1.57$ ppm as well as for the CH_3 protons at $\delta = 0.87$ ppm. The rest of the alkyl chain CH_2 groups form a multiplet ranging from $\delta = 1.45$ ppm to 1.08 ppm. The spectrum of **8** (Figure 37b) is composed of two signal groups, one assigned to the aromatic ring protons at $\delta = 7.38$ ppm and the other to the benzylic CH_2 protons at $\delta = 4.43$ ppm.

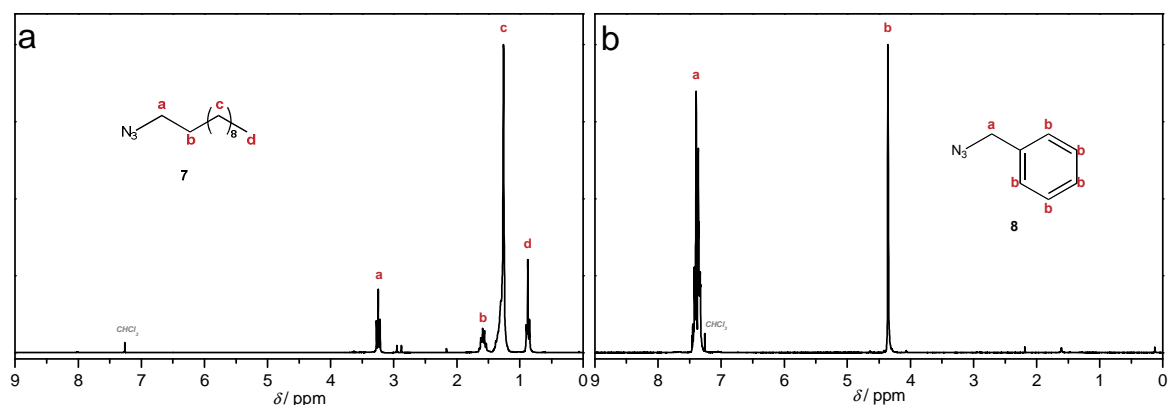
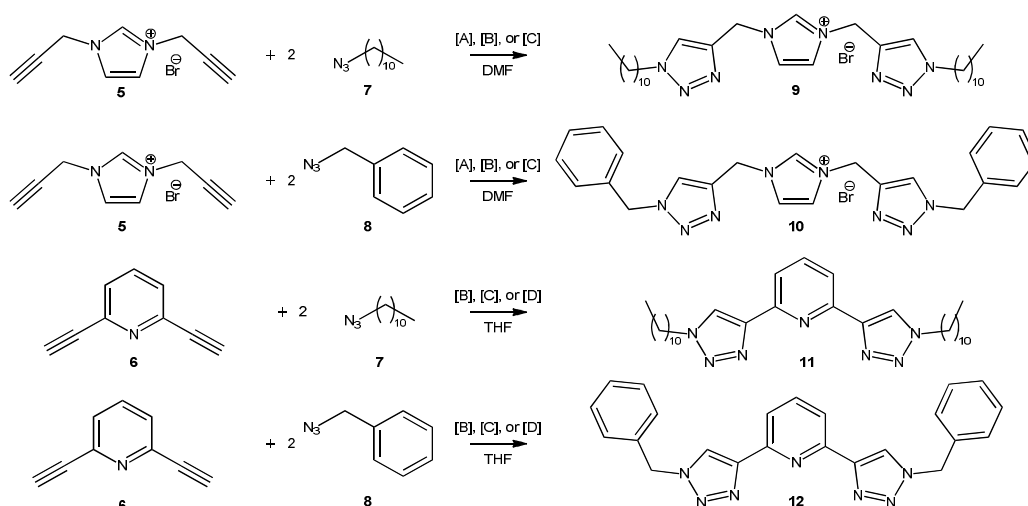


Figure 37. ^1H NMR spectra of (a) 1-azidoundecane (**7**), and (b) benzyl azide (**8**) recorded in CDCl_3 . For the peak assignments refer to the schematic drawing within the figure.

The combination of the two alkynes **5** and **6** with the two azides **7** and **8** affords four test reactions yielding four different products, **9-12** (Scheme 44). For the test reactions two equivalents of the monofunctionalized azide species and 0.2 equivalents of the copper catalyst were employed relative to the bisalkyne.



Scheme 44. The four test reactions resulting from the combination of the two alkynes **5** and **6** with the azide model substances **7** and **8**. The employed catalysts are collated in Table 14.

The reactions were conducted in dry solvents under an inert atmosphere at ambient temperature for 24 h except for the reactions with system **A** that were conducted under air. All products were passed over a small column filled with neutral alumina to remove the catalyst prior to analysis. The efficiency of the CuAAC reaction was monitored by ^1H NMR spectroscopy. The spectra of the products obtained by the different catalysts are depicted in Figure 38 to Figure 41 separately for each reaction mixture.

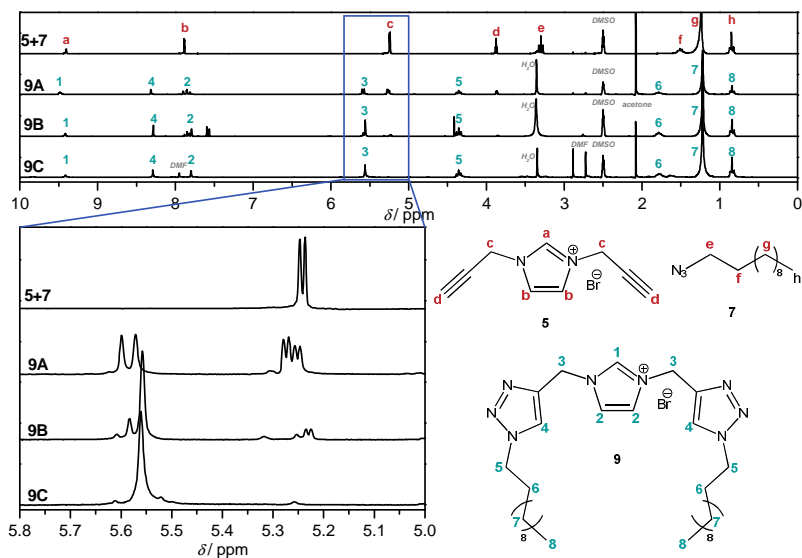


Figure 38. ^1H NMR spectra of the reaction mixture of **5** and **7** and the products **9** obtained by CuAAC reaction catalyzed by (A) $\text{CuSO}_4/\text{Na-ascorbate}$, (B) $\text{CuBr}/\text{PMDETA}$, or (C) CuI/DBU . The enlarged area highlights the signals considered for the determination of the conversion. For the peak assignments refer to the schematic drawings within the figure.

In Figure 38, the ^1H NMR spectra of the reaction mixture composed of **5** and **7** and the subsequent product **9** supported by the different catalysts (**A-C**) are depicted. From the integral ratio of the resonances in the initial reaction mixture, equimolarity of azide and alkyne functional groups is confirmed. The CH_2 proton resonances of **7** directly attached to the azide group are shifted from $\delta = 3.29$ ppm to 4.35 ppm and the signals of the adjacent CH_2 protons are shifted from $\delta = 1.51$ ppm to 1.79 ppm. The other resonances of the alkyl chain protons are not influenced by the ligation reaction exhibiting a chemical shift of $\delta = 1.24$ ppm (CH_2) and 0.85 ppm (CH_3), respectively, both in the spectra of **7** and **9**. The CH protons of **5** with a chemical shift of $\delta = 3.88$ ppm are transformed to the triazolyl protons exhibiting a chemical shift of $\delta = 8.32$ ppm in **9**. The signals of the imidazolium protons in the spectra of **5** or **9**, respectively, at $\delta = 9.40$ ppm and 7.88 ppm are not significantly shifted but a

multiplet generation is observed in the spectra of **9A** and **9B** indicating incomplete ligation. The resonances of the CH₂ protons in **5** are shifted from $\delta = 5.24$ ppm to 5.59 ppm in **9**. The integral of this signal is compared to the integral of the remaining signal of **5** in the reaction mixture as depicted in the enlarged NMR spectra in Figure 38 to give the conversion of the reaction. The results are collated in Table 15. The differences in the obtained conversions and thus in the catalyst activity are significant, ranging from 46 % in **9A** to 85 % in **9B** to 97 % in **9C**.

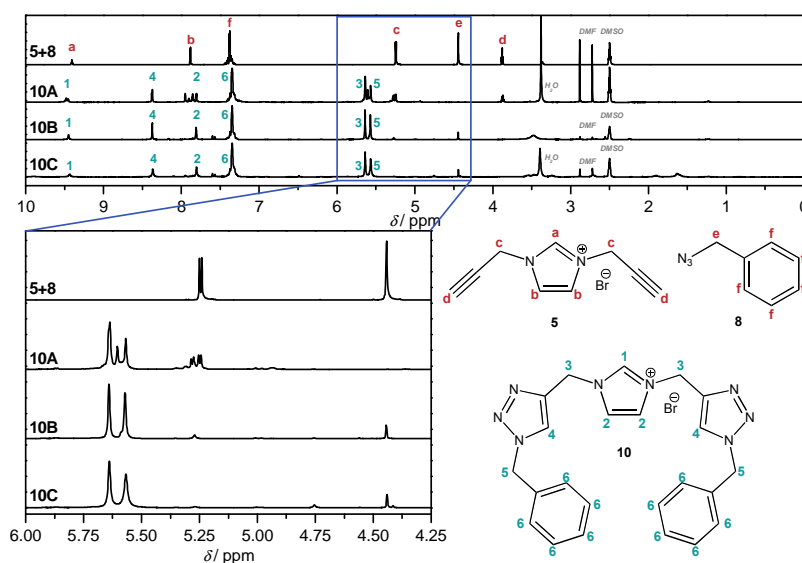


Figure 39. ¹H NMR spectra of the reaction mixture of **5** and **8** and the products **10** obtained by CuAAC reaction catalyzed by (A) CuSO₄/Na-ascorbate, (B) CuBr/PMDETA, or (C) CuI/DBU. The enlarged area highlights the signals considered for the determination of the conversion. For the peak assignments refer to the schematic drawings within the figure.

The CuAAC ligation of **5** and **8** gives the cycloadducts **10**. The ¹H NMR spectra of **10** obtained *via* the three employed catalysts and of the initial reaction mixture are depicted in Figure 39. Equimolarity of the functional groups is verified comparing the integral ratios in the initial reaction mixture of **5** and **8**. The phenyl ring protons of **8** are not influenced by the ligation, retaining their chemical shift at $\delta = 7.38$ ppm. The chemical shifts of the imidazolium ring proton resonances at $\delta = 9.40$ ppm and 7.88 ppm are likewise not influenced, yet a multiplet formation is observed in the spectrum of **10A**. The transformation of the acetylene proton of **5** at $\delta = 3.88$ ppm into a triazolyl ring proton causes a shift to $\delta = 8.37$ ppm in **10**. For the calculation of the conversion, the CH₂ proton resonances of both **5** ($\delta_{\text{CH}_2} = 5.24$ ppm) and **8** ($\delta_{\text{CH}_2} = 4.44$ ppm) have to be taken into account due to an overlay of the respective signals in the

product spectra at $\delta = 5.63$ ppm and 5.56 ppm, respectively. Comparing the sum of the integrals of these peaks, the conversion was calculated to 89 % for **10A**, 93 % for **10B**, and 94 % for **10C**. The ligation was more effective with all employed catalytic systems in comparison to the results for **9**. This may be due to positive influences of the aromatic ring system of **8** or to a negative steric effect of the long alkyl chain of **7**. For a polymerization reaction however, the obtained conversions are still not high enough. Additionally, the low solubility of the products already indicates challenges for generating the targeted polymeric products.

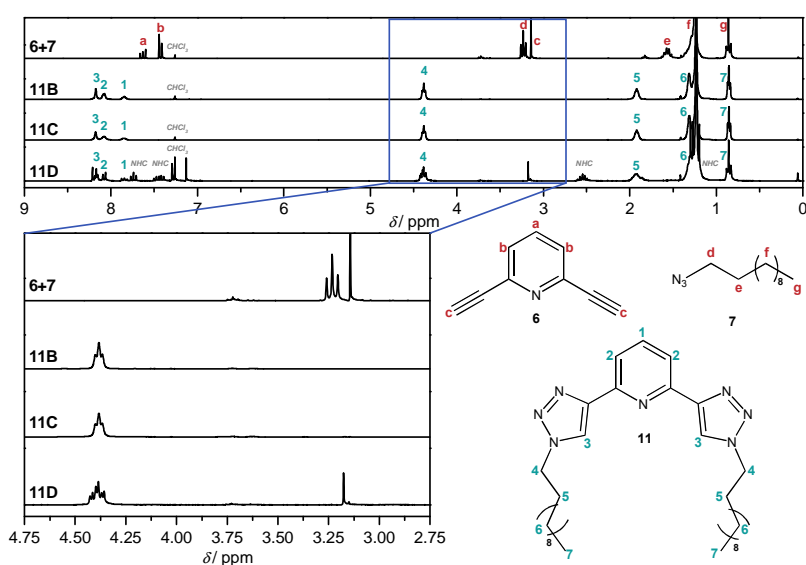


Figure 40. ^1H NMR spectra of the reaction mixture of **6** and **7** and the products **11** obtained by CuAAC reaction catalyzed by (B) CuBr/PMDETA, (C) CuI/DBU, or (D) CuI/IPr-NHC. The enlarged area highlights the signals considered for the determination of the conversion. For the peak assignments refer to the schematic drawings within the figure.

The monomer **6** is in contrast to **5** not ionic and much better soluble in organic solvents. The test reactions could thus be conducted in THF instead of DMF, facilitating the product isolation after the reaction. Moreover, the new catalyst system (D) can be employed in THF. The system (A) was discarded for solubility reasons. The spectrum of the initial equimolar reaction mixture of **6** and **7** and the subsequent product spectra of **11** are depicted in Figure 40. The resonances of the pyridinyl protons in **6** at $\delta = 7.63$ ppm and 7.42 ppm are shifted to $\delta = 7.85$ ppm and 8.08 ppm, respectively. The signal at $\delta = 3.14$ ppm induced by the acetylene proton is shifted to $\delta = 8.18$ ppm upon triazole formation. The CH_2 proton signals of **7** are shifted from $\delta = 3.23$ ppm to $\delta = 4.38$ ppm for the CH_2 group directly attached to the azide or the

subsequent triazole ring, respectively, and from $\delta = 1.57$ ppm to $\delta = 1.92$ ppm for the adjacent CH₂ group. The rest of the CH₂ group proton resonances of the alkyl chain form a multiplet ranging from $\delta = 1.45$ ppm to 1.08 ppm. The chemical shift of this signal as well as the signal of the CH₃ protons at $\delta = 0.86$ ppm are not influenced by the ligation reaction. The NMR spectrum of **11D** exhibits additional resonances assigned to the NHC ligand protons indicating an incomplete removal of the ligand. For all employed catalytic systems, a quantitative conversion was calculated from the integrals of the signals induced by the CH₂ groups directly attached to the azide or triazolyl moiety, respectively.

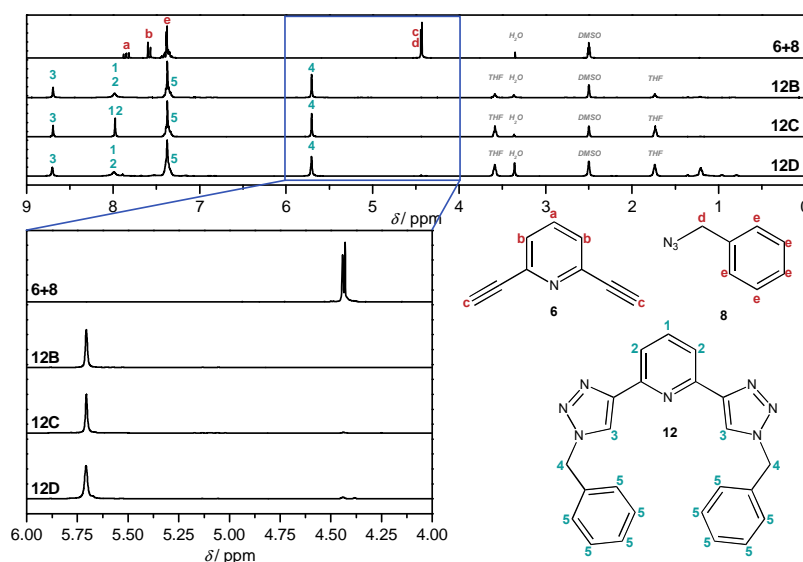


Figure 41. ¹H NMR spectra of the reaction mixture of **6** and **8** and the products **12** obtained by CuAAC reaction catalyzed by (B) CuBr/PMDETA, (C) CuI/DBU, or (D) CuI/IPr-NHC. The enlarged area highlights the signals considered for the determination of the conversion. For the peak assignments refer to the schematic drawings within the figure.

The reaction of **6** and **8** yielding **12** was also conducted in THF. The obtained ¹H NMR spectra of the reaction mixture and the subsequent ligation products are depicted in Figure 41. The pyridinyl proton signals at $\delta = 7.85$ ppm and 7.58 ppm in **6** overlay to one broad signal slightly shifted to lower fields at $\delta = 7.98$ ppm while the aromatic ring protons of **8** at $\delta = 7.38$ ppm are not influenced in their chemical shift. The protons of the acetylene protons of **6** and the CH₂ group of **8** exhibit the same chemical shift at $\delta = 4.43$ ppm. After the ligation reaction, the signal of the triazolyl proton in **12** is located at $\delta = 8.70$ ppm and the CH₂ group protons are shifted to

$\delta = 5.70$ ppm. Comparing the integrals of these signals, complete conversion can be attested for all employed catalysts. Table 15 collates the results of the test reactions.

Table 15. Summary of the conversions obtained in the test reactions depicted in Scheme 44. Conversions were obtained by comparison of the integrals of selected proton resonances in the initial reaction mixture spectrum and the subsequent product spectra. For details refer to the text.

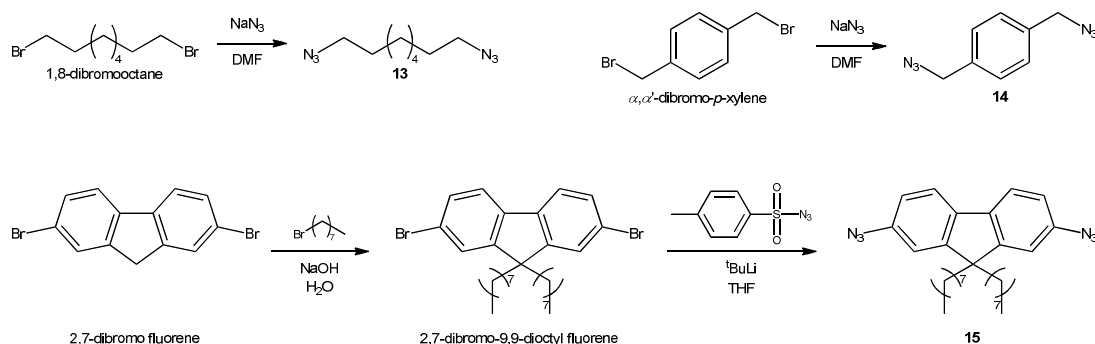
	CuSO₄ Na-ascorbate	CuBr PMDETA	CuI DBU	CuI IPr-NHC
9	0.460	0.847	0.969	n.d.
10	0.885	0.931	0.935	n.d.
11	n.d.	0.998	0.998	0.998
12	n.d.	0.999	0.981	0.966

In summary, the efficiency of the catalysts was higher in THF compared to DMF. In DMF the system (C) composed of CuI and DBU featured the highest efficiency, while there was no difference between the systems noticeable in THF except the incomplete removal of the NHC ligand in **11D**. This was not observed in **12D** and is thus not regarded as a general drawback. In addition, the catalyst efficiency seems to correlate with the nature of the employed azide and alkyne moieties.

4.3. CuAAC Driven Polymerization Reactions

4.3.1. Synthesis of Bifunctionalized Azide Linkers

The polymerization of dialkynes in a poly(CuAAC) ligation requires bifunctionalized azides as second monomer moiety. Since the metal-binding ability is already realized by the combination of the alkyne molecule together with the formed triazolyl rings, the structure of the diazides is variable. The diazides 1,8-diazidooctane (**13**) and α,α' -diazido-*p*-xylene (**14**) were chosen in analogy to the employed mono-functionalized azides **7** and **8** in the test reactions (section 4.2). They are readily available from the respective bromides *via* nucleophilic substitution with sodium azide in DMF (Scheme 45, top).³⁰² As already indicated in section 4.2, the solubility of the polymers is possibly challenging. Thus, a bifunctionalized fluorene (**15**) was synthesized featuring two octyl side chains. This structure already had a positive influence on the solubility of other rigid polymer structures.³⁰³ Starting from 2,7-dibromo fluorene, **15** is obtained in two steps by alkylation of the fluorene and subsequent substitution with tosylazide (Scheme 45, bottom).



Scheme 45. Reaction scheme of the synthesis of 1,8-diazidooctane (**13**), α,α' -diazido-*p*-xylene (**14**), and 2,7-diazido-9,9-dioctyl fluorene (**15**).

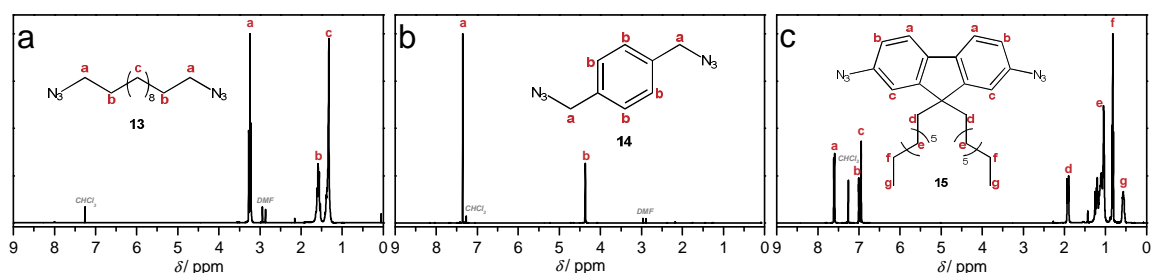
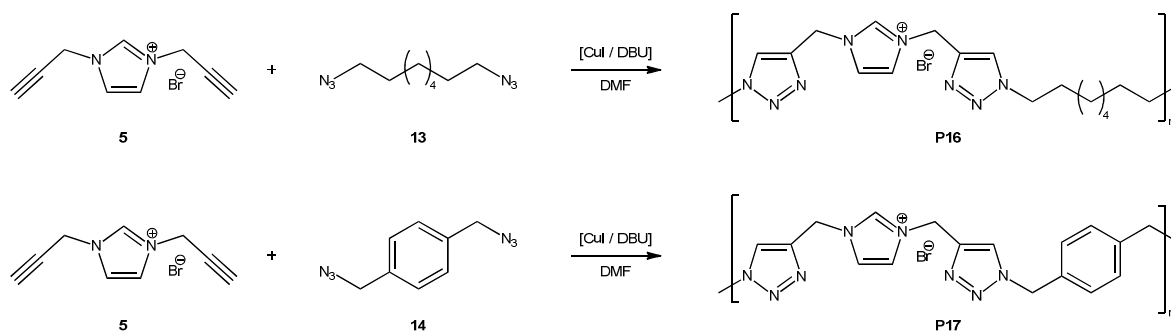


Figure 42. ^1H NMR spectra of the azide linkers. (a) 1,8-diazidooctane (**13**), (b) α,α' -diazido-*p*-xylene (**14**), and (c) 2,7-diazido-9,9-dioctyl fluorene (**15**) recorded in CDCl_3 .

The obtained products were characterized *via* ^1H NMR spectroscopy in CDCl_3 . In the spectrum of **13** (Figure 42a) the signal induced by the CH_2 protons directly attached to the azide group is located at $\delta = 3.24$ ppm and the adjacent CH_2 groups exhibit a signal at $\delta = 1.58$ ppm. The protons of the internal CH_2 groups merge into one signal at $\delta = 1.32$ ppm. The ^1H NMR spectrum of **14** is composed of two signals for the aromatic ring protons at $\delta = 7.35$ ppm and the benzylic CH_2 protons at $\delta = 4.37$ ppm (Figure 42b). In the spectrum of **15**, three signals of the aromatic ring protons are observed at $\delta = 7.60$ ppm, 7.00 ppm and 6.95 ppm. The octyl chain protons exhibit signals at $\delta = 1.92$ ppm, 0.82 ppm, 0.57 ppm and a multiplet ranging from 1.38 ppm to 0.93 ppm (Figure 42c). The chemical shifts and the integrals of the observed signals comply with the expectations for all three compounds. Neither impurities, side-products, nor monofunctionalized products could be observed. The obtained substances are thus suitable for the polyaddition reactions.

4.3.2. CuAAC-Polymerization of 1,3-Dipropynylimidazolium bromide (**5**) with Azide Linkers

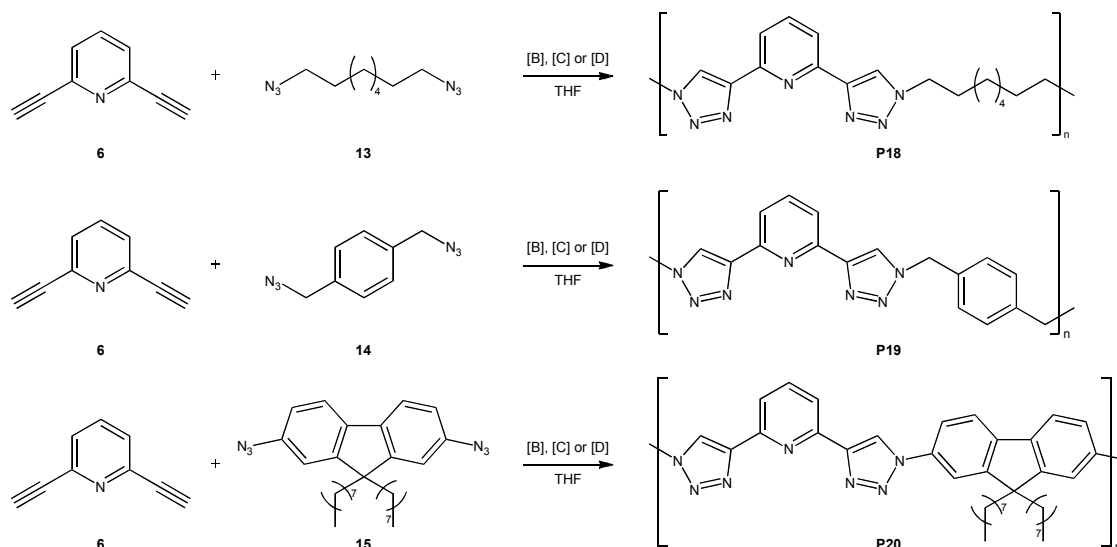
The polymerizations of **5** with the synthesized azide monomers **13** and **14** were conducted in DMF at ambient temperature. According to the results of the test reactions presented in section 4.2, the system composed of CuI and DBU was most effective for the catalysis of the CuAAC ligation of **5** in DMF. Thus, this system was employed for the polymerization reactions with 0.2 equivalents per functional unit (Scheme 46). Subsequently, the reaction mixtures were passed over a small column equipped with neutral alumina prior to solvent removal. Since the obtained solid products were insoluble, further characterization was not possible.



Scheme 46. Reaction scheme of the CuAAC polymerizations with **5** and **13** or **14**, respectively, as the monomers in DMF. As catalyst, CuI / DBU was employed with 0.2 equivalents per functional unit.

4.3.3. CuAAC Polymerization of 2,6-Diethynyl pyridine (**6**) with Azide Linkers

Since the dialkyne **6** exhibited complete conversion in THF with all the employed catalysts in the test reactions, the three catalytic systems CuBr/PMDETA (B), CuI/DBU (C) and CuI/IPr-NHC (D) were employed in the polymerization reactions (Scheme 47). After 24 h reaction time under inert atmosphere at ambient temperature, the catalyst was removed by filtration over neutral alumina and the products were dried *in vacuo*. Comparable to the results of the polymerization of **5**, the products of **P18** and **P19** obtained after catalyst and solvent removal were insoluble and could not be characterized furthermore.



Scheme 47. Polymerization reactions of **6** with **13**, **14**, or **15**, respectively. As catalysts, CuBr/PMDETA (B), CuI/DBU (C), and CuI/IPr-NHC (D) were employed in THF.

However, the polyadduct **P20** from the CuAAC ligation of **6** and **15** was soluble after catalyst and solvent removal in common organic solvents. The products obtained from the catalysis *via* the three catalysts **P20B**, **P20C**, and **P20D** respectively were characterized by GPC analysis in THF. The broad molar mass distributions depicted in Figure 43 are typical for step-growth polymers. The multimodality originates from the oligomers produced in the course of the polyaddition. The molar masses and polydispersities obtained after calibration with narrow polystyrene standards are collated in Table 16.

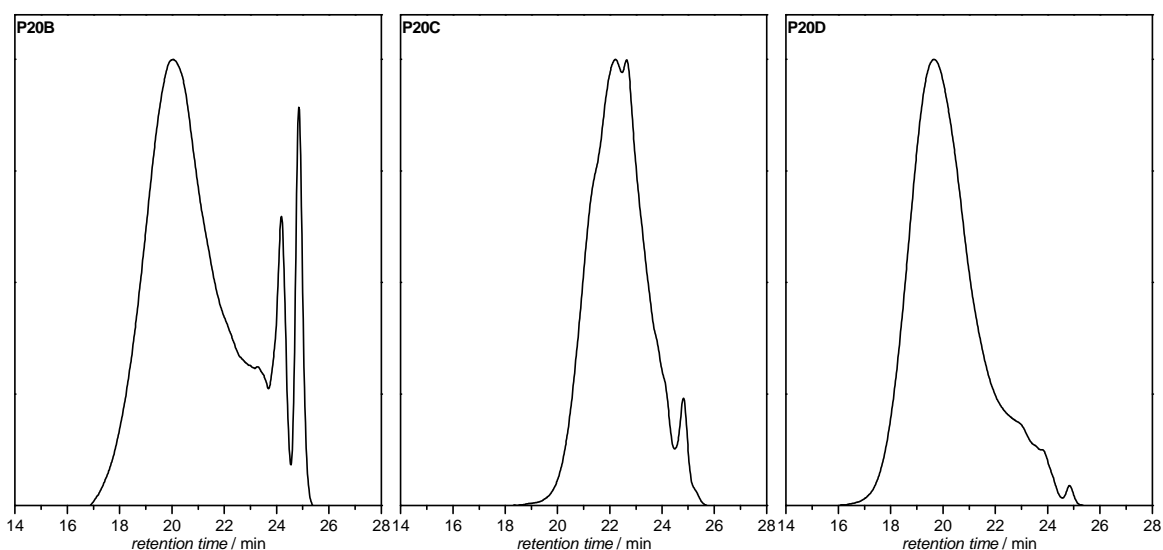


Figure 43. GPC traces of polymer **P20B**, **P20C** and **P20D** in THF. Calibration was based on narrow polystyrene standards.

The highest molar mass, $M_n = 22 \text{ kg}\cdot\text{mol}^{-1}$, was achieved in polymer **P20D**. The other two polymers (**P20B** and **P20C**) have molar masses close to $M_n = 10 \text{ kg}\cdot\text{mol}^{-1}$. The molar mass derived from the GPC measurements is significantly influenced by the calibration. Since no appropriate standards are available for the generated polymer, determination of the absolute weight-averaged molar mass, M_w , was conducted *via* SLS analysis of **P20D** in DMAc. Figure 44 depicts the ZIMM-plot obtained from the extrapolation of the DEBYE relationship (Eq. 18) to $c = 0$ and $q = 0$ as described in section 3.2.3. For **P20D**, the absolute weight-averaged molar mass is determined to be close to $M_w = 55 \text{ kg}\cdot\text{mol}^{-1}$, complying well with the GPC result even though the calibration was conducted with narrow polystyrene standards.

Table 16. Molar masses of the polymers **P20B**, **P20C** and **P20D** obtained *via* GPC measurements in THF. The GPC system was calibrated using narrow polystyrene standards.

	M_n g·mol ⁻¹	M_w g·mol ⁻¹	\bar{D}
P20B	10400	52800	5.07
P20C	8400	14800	1.77
P20D	22400	58200	2.60
		54600 ^a	

^a absolute weight-averaged molar mass determined *via* SLS measurements in DMAc.

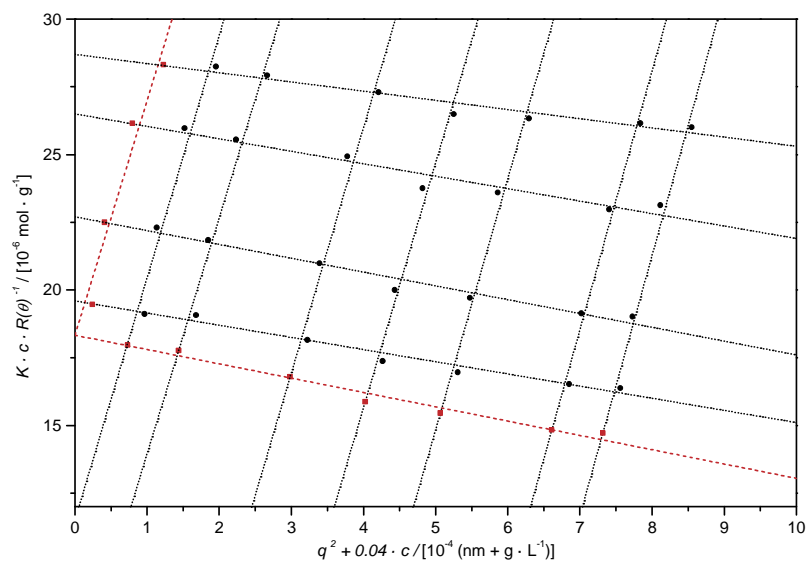


Figure 44. ZIMM-plot obtained from the SLS measurements of **P20D**.

The ^1H NMR spectrum of **P20D** is depicted in Figure 45 together with the spectrum of the initial equimolar monomer mixture composed of **6** and **15**. The aliphatic proton signals of the octyl side-chains in **15** exhibit slight shifts and broadened signals. The resonances of the CH_3 and CH_2 protons at the chain ends at $\delta = 0.80$ ppm and 0.56 ppm merge to a broad multiplet ranging from $\delta = 0.92$ ppm to 0.52 ppm while the inner CH_2 group protons feature a multiplet with a chemical shift between $\delta = 1.79$ ppm and 0.92 ppm. The signal of the CH_2 group protons directly attached to the fluorene is shifted from $\delta = 1.91$ ppm in **15** to 2.12 ppm in the polymer **P20D**. In the aromatic region of the monomer mixture spectrum, three signal groups are observed. The signal at $\delta = 7.59$ ppm is assigned to an overlay of one of the pyridinyl ring protons of **6** and two fluorene ring protons of **15**. The resonances at $\delta = 7.41$ ppm and 6.98 ppm are associated with the residual pyridinyl or fluorene protons, respectively. In the product spectrum, the signals of all fluorene protons and one of the pyridinyl protons are merged to a broad multiplet signal ranging from $\delta = 8.10$ ppm to 7.68 ppm. The second pyridinyl proton signal observed at $\delta = 7.41$ ppm in the monomer mixture is shifted to $\delta = 8.27$ ppm after the polymerization. The signal at $\delta = 3.14$ ppm induced by the alkyne protons disappeared completely in the spectrum of **P20D** and a new signal at $\delta = 8.80$ ppm is observed that can be assigned to the proton of the formed triazolyl units. The integral ratios of the discussed signals in the spectrum of **P20D** are in-line with the expected ratios. A determination of the

molar mass from the NMR spectrum is not possible since the endgroup signals cannot be identified.

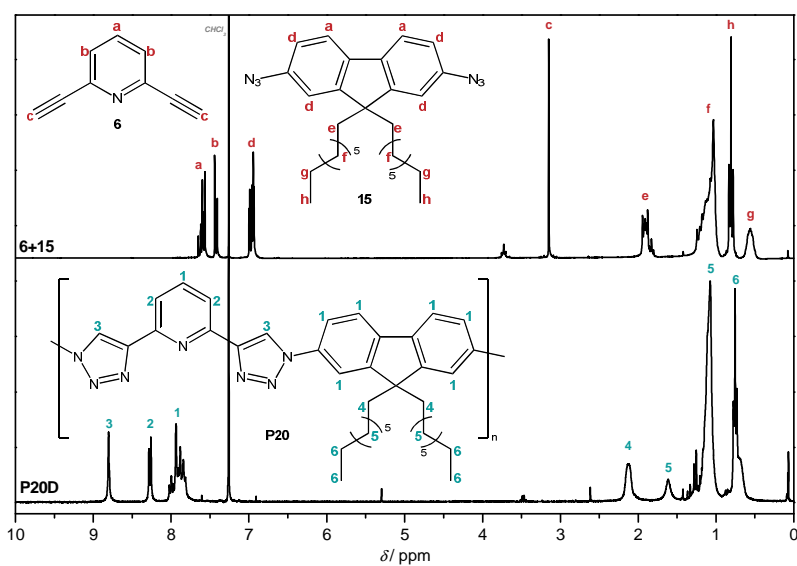
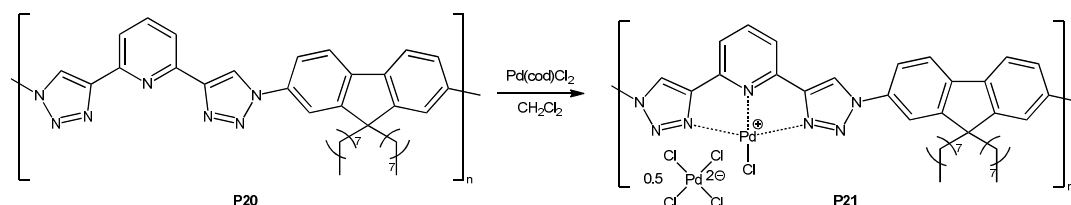


Figure 45. ^1H NMR spectra of the initial equimolar mixture of **6** and **15** (top) and of the subsequent polyadduct **P20D** (bottom) recorded in CDCl_3 . For the signal assignments refer to the schematic drawings within the figure.

4.4. Palladium Loading of the Poly(triazole)

The reaction of the obtained polymer **P20D** with the palladium(II) precursor Pd(cod)Cl₂ in methylene chloride as depicted in Scheme 48 was conducted by the institute of inorganic chemistry (C. Kiefer). The loaded polymer **P21D** precipitated during the reaction and was hardly soluble in a mixture of methylene chloride and DMSO. The ¹H NMR spectra of **P20D** and **P21D** are depicted in Figure 46. Despite the different employed solvents and thus not fully comparable chemical shifts, all signals in the spectrum of **P21D** exhibit a distinct downfield shift compared to the correspondent signals in the spectrum of **P20D**. In detail, the triazolyl protons induce a signal at $\delta = 9.42$ ppm compared to 8.80 ppm in the spectrum of **P20D**, while the aromatic protons shift from $\delta = 8.52$ ppm and 7.91 ppm to 8.52 ppm and 8.26 ppm, respectively. The chemical shifts of the signals assigned to the aliphatic side chains of the fluorene moieties at $\delta = 2.13$ ppm, 1.08 ppm and 0.76 ppm are shifted to $\delta = 2.39$ ppm, 1.33 ppm and 0.98 ppm, respectively. In addition, a broadening of the signals is observed upon palladium ligation.



Scheme 48. Metal loading of polymer **P20** with the palladium(II) precursor Pd(cod)Cl₂ in methylene chloride. The metallopolymer **P21** precipitates from the reaction mixture.

From the NMR spectra, no information on the molar mass or the palladium content of **P21D** can be derived. The low solubility of the polymer precluded the analysis *via* GPC and SLS. However, the determination of the palladium content could be conducted by elemental analysis. Table 17 collates the obtained results of the CHN elemental analysis of **P20D** and **P21D** and the respective theoretically expected values calculated from the repeating unit as depicted in Scheme 48 disregarding the polymer endgroups. For the calculations regarding **P21D**, the formation of an ionic palladium complex with 0.5 equivalents of [PdCl₄]²⁻ as counterion per repeating unit is assumed. Comparable low molecular complexes are known in the literature.³⁰⁴⁻³⁰⁶

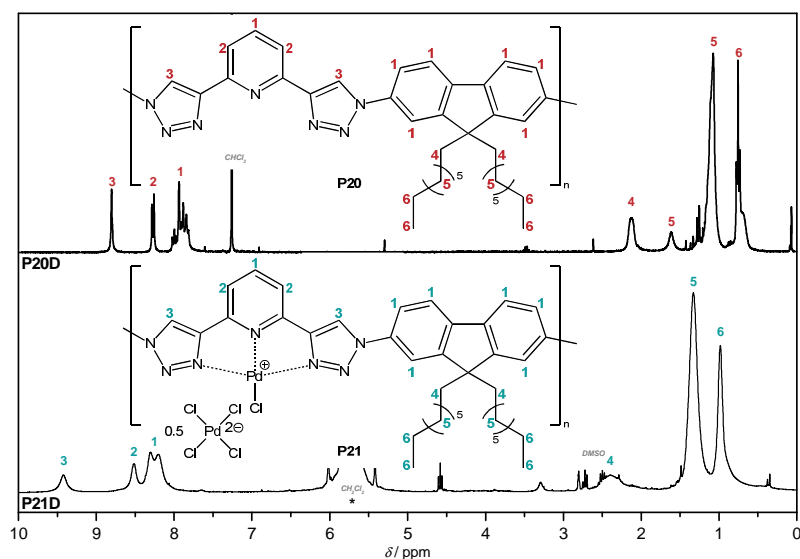


Figure 46. ^1H NMR of the non-loaded polymer **P20D** recorded in CDCl_3 (top) and the product **P21D** after reaction with $\text{Pd}(\text{cod})\text{Cl}_2$ (bottom) recorded in a mixture of methylene chloride and DMSO-d_6 . The methylene chloride solvent peak is partially overlaid by the schematic drawing. For the signal assignments refer to the schematic drawings within the figure.

The obtained elemental mass fractions of C, H and N comply with the expected values with a relative accuracy of 4 % for both **P20D** and **P21D**. In contrast to **P20D**, not all elements present in **P21D** could be detected. The difference to 100 wt% is assigned to the additionally present elements palladium and chlorine. Consequently, the palladium content of the polymer **P21D** is calculated to 17.8 wt% which is in good agreement with the expected value of 18.4 wt%. The absolute number-averaged molar mass of **P21D** can be estimated to $M_n = 30 \text{ kg}\cdot\text{mol}^{-1}$ by addition of $266 \text{ g}\cdot\text{mol}^{-1}$, the molar mass of $[\text{Pd}_{1.5}\text{Cl}_3]$ that is formally added per monomer unit. The degree of polymerization, DP_n^{P21D} , is identical to DP_n^{P20D} and can be calculated from the absolute weight-averaged molar mass of **P20D** determined *via* SLS and the dispersity of **P20D** determined *via* GPC.

Table 17. Comparison of the theoretically expected and experimentally determined mass fractions (in wt%) of the polymers **P20D** and **P21D** obtained *via* elemental analysis.

		C	H	N	$\Sigma(\text{CHN})$	$\text{Pd}_3\text{Cl}_6^{\text{a}}$	Pd^{b}
P20D ($\text{C}_{38}\text{H}_{45}\text{N}_7$)	Cal.	76.09	7.56	16.35	100.00		
	$599.81 \text{ g}\cdot\text{mol}^{-1}$	Exp.	74.28	7.50	15.71	97.49	
P21D ($\text{C}_{38}\text{H}_{45}\text{Cl}_3\text{N}_7\text{Pd}_{1.5}$)	Cal.	52.72	5.24	11.32	69.21	30.79	18.44
	$865.80 \text{ g}\cdot\text{mol}^{-1}$	Exp.	53.53	5.47	11.33	70.33	29.70

^a Difference to 100 %. ^b Mass fraction of Pd assuming 0.5 $[\text{PdCl}_4]^{2-}$ as the counter ion per repeating unit.

In summary, the synthesis of a palladium-containing polymer featuring metal-chelating ligands directly within the polymer backbone *via* the poly(CuAAC) reaction could be demonstrated. Optimal reaction conditions proved to be essential for the successful synthesis of a poly(triazole) and were explored in a model study with bifunctional alkynes and monofunctionalized model azides yielding low molecular bis(triazole)s. ^1H NMR analysis of the obtained product mixtures revealed a higher dependence of the conversion on the employed catalytic systems in DMF compared to THF as the solvent. In DMF the highest conversion of 97 % could be achieved with CuI and DBU as the catalytic system while the model reactions in THF proceeded quantitatively for all investigated catalysts. The polymerization reactions of dipropynyl imidazolium bromide (**5**) with various bifunctional azide linkers provided insoluble products which could not be analyzed while diethynylpyridine (**6**) could be successfully polymerized together with 9,9-dioctyl-2,7-bisazido fluorene (**15**) in THF. The best result was obtained employing CuI and a *N* heterocyclic carbene (IPr-NHC) as the catalytic system giving a readily soluble polymer with $M_n = 22.4 \text{ kg}\cdot\text{mol}^{-1}$ and $D = 2.6$. The polymer was additionally characterized *via* ^1H NMR, SLS and elemental analysis confirming the expected chemical structure. The absolute weight-averaged molar mass of the poly(triazole) was close to $M_w^{\text{abs}} = 54.6 \text{ kg}\cdot\text{mol}^{-1}$. The subsequent metal loading with a palladium precursor provided the targeted metal-containing polymer. ^1H NMR and elemental analysis confirmed full loading of all chelating moieties present alongside the polymer backbone. The limited solubility of the metal-containing polymer precluded the determination of the molar mass *via* GPC or SLS measurements. However, the number-averaged molar mass of the polymer could be estimated to be close to $M_n = 30 \text{ kg}\cdot\text{mol}^{-1}$. The solubility of the polymer *e.g.* in DMAC of $2 \text{ mg}\cdot\text{mol}^{-1}$ would still be sufficiently high for the application as a catalyst.

5

Spatially Controlled Surface Immobilization of Metal Complexes

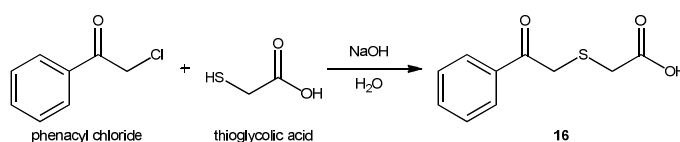
To date, the spatially controlled immobilization of metals or metal complexes on solid substrates could only be realized *via* ink-jet printing with metal-containing inks or lithographic processing of pre-coated polymer supports (please refer to section 2.2.3 for a detailed overview).^{219,225} The versatile photo-induced ligation of metal complexes onto self-assembled monolayers (SAMs) of suitable compounds, *e.g.* photoenols, tetrazoles, or phenacylsulfides, represents a new synthetic approach to obtain spatially resolved surface immobilization with only little instrumental effort.^{153,162} Patterning techniques have already been successfully employed for the derivatization of various substrates with small molecules, polymers, or bioactive substances.^{161,166,307,308} In the following section, the scope and applicability of a photo-

Synthesis and characterization of the PPh_3 -diene and the $\text{Au}(\text{PPh}_3)\text{Cl}$ diene were performed by S. Bestgen in the group of Prof. P. Roesky (KIT). ToF-SIMS measurements were conducted by Dr. A. Welle (KIT).

ligation strategy for the spatially controlled immobilization of metal complexes onto silicon substrates was investigated for the first time. The DIELS–ALDER trapping of *in-situ* formed thioaldehydes from phenacylsulfides upon UV irradiation was selected as suitable ligation strategy. In addition to the required phenacylsulfide derivatives, diene-functionalized ligands and metal complexes were synthesized and characterized *via* ^1H NMR spectroscopy and UV-Vis spectrometry. In addition to the surface modifications, test reactions in solution were conducted with phenacylsulfide benzyl amide and diene-functionalized ligands or complexes, respectively, enabling a product analysis *via* ^1H NMR spectroscopy. The patterned substrates were analyzed by time-of-flight secondary ion mass spectrometry (ToF-SIMS). In contrast to microscopic techniques such as fluorescence microscopy,³⁰⁹ scanning electrochemical microscopy (SEM),³¹⁰ or atomic force microscopy (AFM),³¹¹ ToF-SIMS analysis enables the spatially resolved characterization of compounds immobilized on substrates by the molar mass of charged molecule fragments that are released from the surface upon bombardment with primary ions.^{312,313} The obtained images visualize the relative abundance of a selected fragment ions on the surface. The applicability of ToF-SIMS for the characterization of metal complex-functionalized substrates was previously shown for the analysis of immobilized Fe^{II} supramolecular structures.³¹⁴

5.1. Phenacylsulfide Derivatives

Both the phenacylsulfide benzyl amide (**17**) employed in the test reactions as well as the phenacylsulfide functionalized silane (**18**) employed for the formation of a photoactive self-assembled monolayer on silicon substrates are based on phenacylthio acetic acid (**16**). The synthesis of **16** *via* nucleophilic substitution of phenacyl chloride with thioglycolic acid in basic aqueous solution was conducted following a previously reported procedure (Scheme 49).³¹⁵ After recrystallization from chloroform, the product was characterized *via* ¹H NMR spectroscopy.



Scheme 49. Synthesis of phenacylthio acetic acid (**16**) from phenacyl chloride and thioglycolic acid in aqueous sodium hydroxide solution.

The obtained ¹H NMR spectrum of **16** is depicted in Figure 47. The resonances of the phenyl ring protons exhibit chemical shifts of $\delta = 7.95$ ppm, 7.59 ppm and 7.48 ppm while the resonances of the CH₂ group protons are located at $\delta = 4.05$ ppm and 3.37 ppm, respectively. The pure product was obtained in high yields of appr. 80 %.

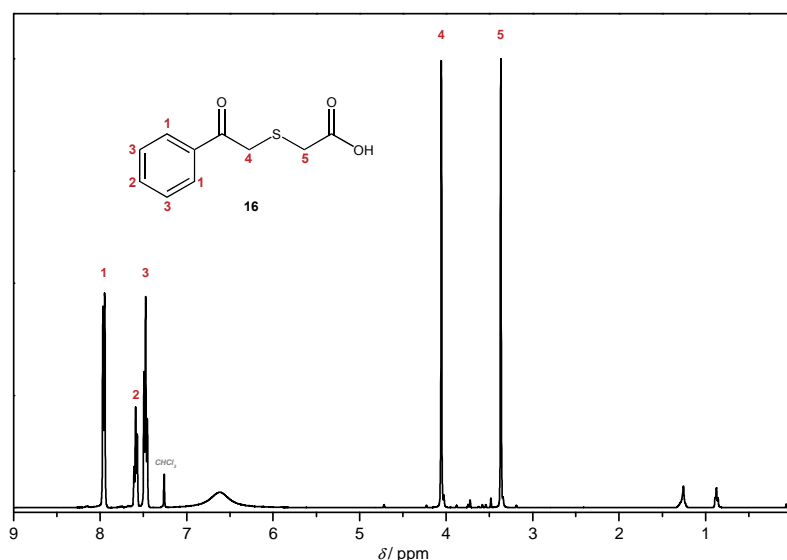
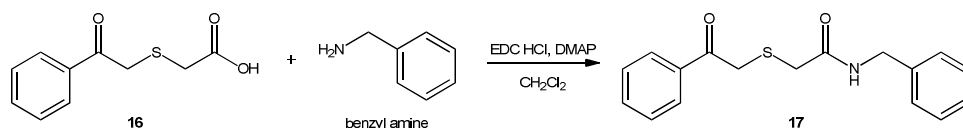


Figure 47. ¹H NMR spectrum of phenacylthio acetic acid (**16**) recorded in CDCl₃. For the signal assignments refer to the schematic drawing.

For the small molecule test reactions, benzyl amine was reacted with the phenacylsulfide acetic acid (**16**) in the presence of 1-ethyl-3-(3-dimethylamino-propyl)carbodiimid hydrochloride (EDC·HCl) and 4-(dimethyl amino)pyridine (DMAP) in methylene chloride at ambient temperature adapting a previously reported procedure (Scheme 50).²¹² The obtained phenacylsulfide benzyl amide (**17**) was characterized *via* ¹H NMR analysis without further purification.



Scheme 50. Synthesis of phenacylsulfide benzyl amide (**17**) *via* amidation of phenacylthio acetic acid (**16**) with benzyl amine in methylene chloride.

The ¹H NMR spectrum of **17** is depicted in Figure 48b. In comparison to the spectrum of **16** (Figure 48a), additional resonances are observed, assigned to the phenyl ring protons at $\delta = 7.30$ ppm, the amine proton ($\delta = 7.16$ ppm) and the newly introduced CH₂ group protons at $\delta = 4.46$ ppm. The resonances of the CH₂ protons of the phenacylsulfide moiety are slightly shifted from $\delta = 4.05$ ppm and 3.37 ppm in **16** to $\delta = 3.94$ ppm and 3.01 ppm in **17**, respectively, while the resonances of the phenacyl ring protons are not influenced.

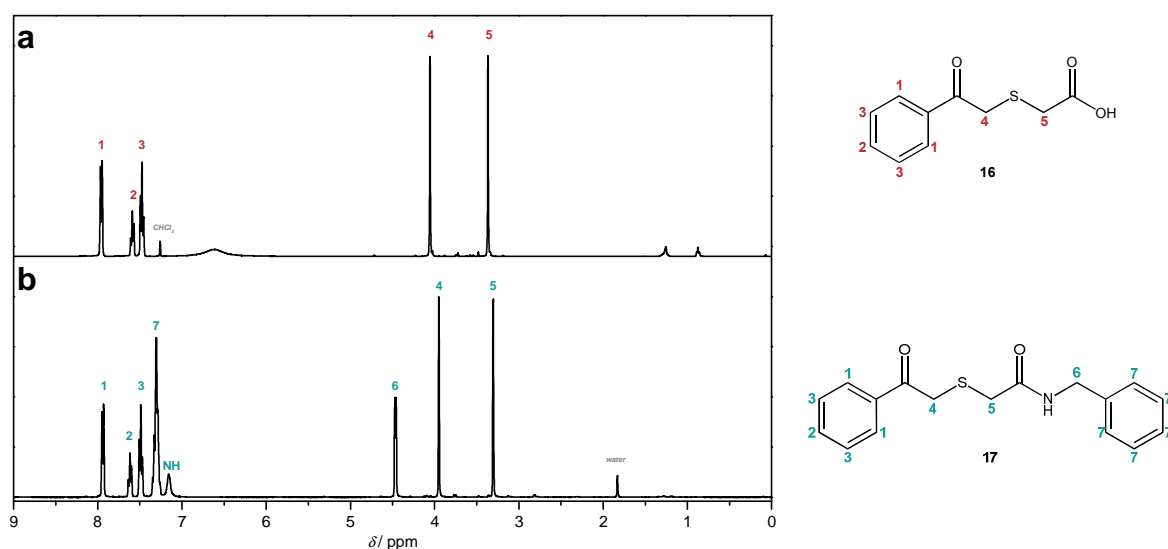
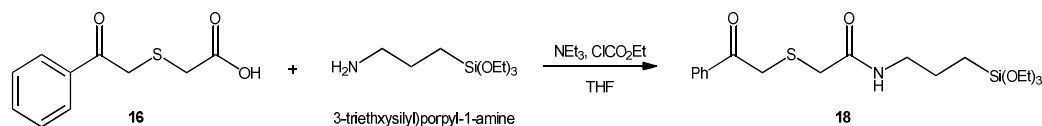


Figure 48. Comparison of the ¹H NMR spectra of **16** (a) and the phenacylsulfide benzyl amide **17** (b) obtained after the amidation reaction of **16** with benzyl amine recorded in CDCl₃. For the signal assignments refer to the schematic drawings below the spectra.

For the surface immobilization of the phenacylsulfide moiety, **16** was reacted with 3-(triethoxysilyl)propyl amine in the presence of triethyl amine and ethyl chloroformate in THF following a previously reported procedure (Scheme 51).¹⁶² Column chromatography afforded the pure silane product in 17 % yield.



Scheme 51. Synthesis of triethoxysilane functionalized phenacylsulfide (**18**) is obtained by the reaction of phenacylthio acetic acid (**16**) with 3-(triethoxysilyl)propyl-1-amine in THF.

The ¹H NMR spectra of **16** and **18** are depicted in Figure 49. The characteristic resonances of the silane-ethoxy groups are observed at chemical shifts ranging from $\delta = 3.88$ ppm and 3.64 ppm (CH₂), as well as at $\delta = 1.24$ ppm (CH₃). The resonances of the propyl protons are located at $\delta = 3.23$ ppm, 1.62 ppm and 0.63 ppm with the first signal overlapping with the resonance of one of the phenacyl-CH₂ groups. All signals are broadened compared to the signals of the initial phenacylthio acetic acid, which could indicate a polymerization of the silane, yet GPC analysis of **18** did not show any polymeric material in the product. The chemical shifts of the residual phenacylsulfide proton resonances are not influenced.

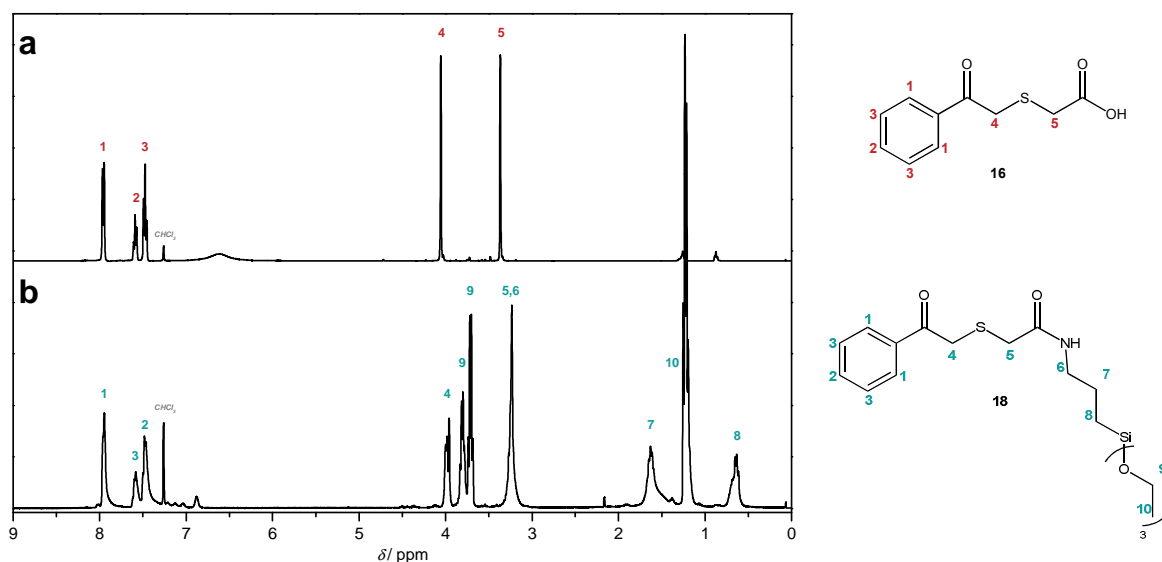


Figure 49. Comparison of the ¹H NMR spectra of phenacylthio acetic acid **16** (a) and the phenacylsulfide silane **18** (b) recorded in CDCl₃. For the signal assignments refer to the schematic drawings.

The UV-Vis absorbance spectra of **16** and **17** in acetonitrile are depicted in Figure 50. Since the subsequent photo-ligations are performed employing a UV lamp with an emission maximum at $\lambda = 355$ nm, the emission spectrum of this lamp was added to the graph illustrating the overlap in the absorbance of the phenacylsulfide containing compounds with the UV emission of the lamp. Both compounds, **16** and **17**, exhibit the same absorption maximum at $\lambda = 330$ nm.

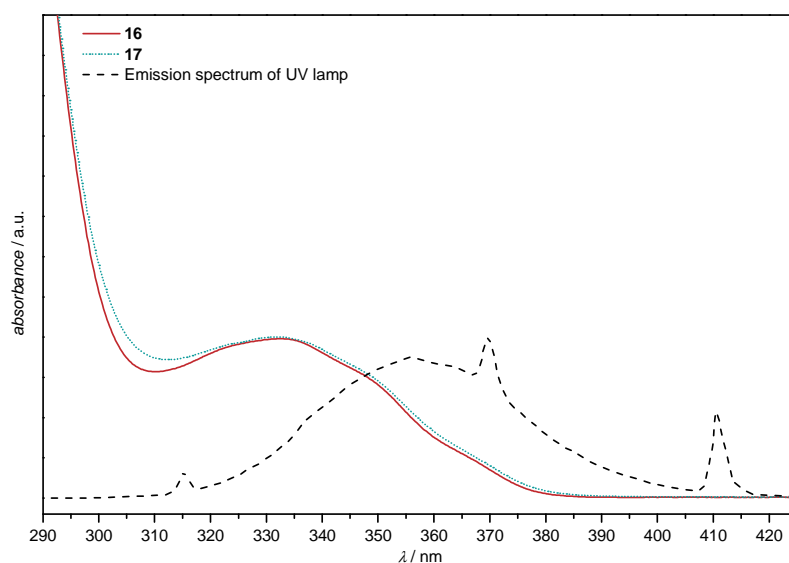
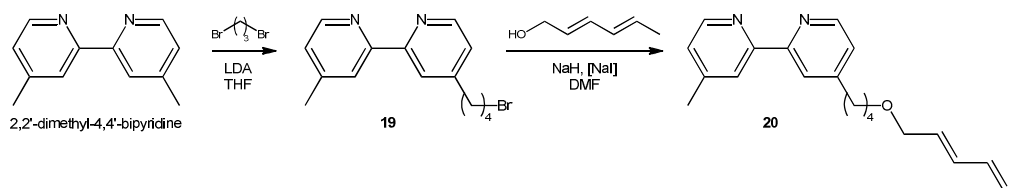


Figure 50. UV-Vis absorbance of the phenacyl derivatives **16** and **17**. For comparison, the emission spectrum of the UV lamp employed in the subsequent photo-ligations is also shown.

5.2. Diene Functionalized Ligands and Metal Complexes

As suitable dienes for both, the photo-ligation and the subsequent complexation of metal ions, 4-(4-((*2E,4E*)-hexa-2,4-dienyloxy)butyl)-4'-methyl-2,2'-bipyridine (**20**) and (*2E,4E*)-hexa-2,4-dienyl-4-(diphenylphosphino)benzoate (**22**) were identified. The compounds feature a linear hexadiene chain suitable for the subsequent DIELS-ALDER ligation with the *in-situ* formed thioaldehyde.

The bipyridine based ligand **20** is obtained from 4,4'-dimethyl-2,2'-bipyridine in a two-step synthesis. In the first step, the bipyridyl-carbanion generated by lithium diisopropyl amine (LDA) reacts with 1,3-dibromopropane to the bromine functionalized **19**. Subsequent nucleophilic substitution with (*2E,4E*)-hexa-2,4-dien-1-ol in the presence of sodium hydride in DMF affords the diene functionalized bipyridine ligand **20** (Scheme 52).



Scheme 52. Synthesis of diene functionalized bipyridine ligand **20**. Addition of 1,6-dibromohexane to 2,2'-dimethyl-4,4'-bipyridine in the presence of lithiumdiisopropyl amine (LDA) affords **19** as intermediate. Subsequent substitution the bromine group of **19** with (*2E,4E*)-hexa-2,4-dien-1-ol affords the diene functionalized product **20**.

The ^1H NMR spectra of 4,4'-dimethyl-2,2'-bipyridine, **19** and **20** are depicted in Figure 51. The chemical shifts of the pyridine ring protons at $\delta = 8.53$ ppm, 8.22 ppm and 7.12 ppm are not influenced by the modification reactions as well as the resonance of the methyl CH_3 group at $\delta = 2.43$ ppm, yet the integral is halved upon the addition of the bromopropyl group to one of the methyl groups. The additional resonances observed in the proton spectrum of **19** at $\delta = 3.43$ ppm, 2.74 ppm are assigned to the protons of the pyridine- CH_2 group or the $\text{CH}_2\text{-Br}$ group, respectively, while the resonances of the two internal CH_2 groups overlap at $\delta = 1.90$ ppm. Except for the latter, all above noted resonances are also observed in the spectrum of **20** with identical chemical shifts and integrals. The resonance of the internal CH_2 groups, however, is slightly shifted to higher fields and overlaps with the resonance of the

newly introduced CH₃ group inducing a multiplet resonance ranging from $\delta = 1.84$ ppm to 1.52 ppm. Additional signals at $\delta = 6.18$ ppm, 6.04 ppm and 5.76 ppm – 5.53 ppm are induced by the vinyl CH protons, while the additional CH₂ group protons exhibit a chemical shift of $\delta = 3.95$ ppm.

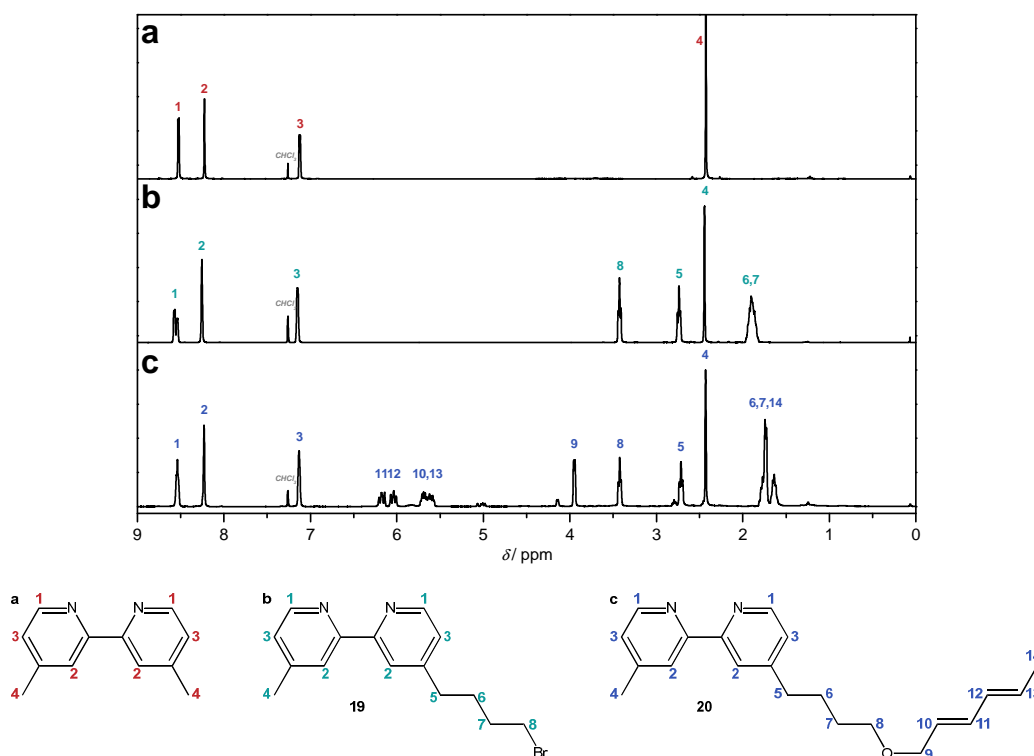


Figure 51. ¹H NMR spectra of 2,2'-dimethyl-4,4'-bipyridine (a), the bromine functionalized intermediate **19** (b) and the diene functionalized bipyridine **20** (c) recorded in CDCl₃. For the peak assignments refer to the schematic drawings below the spectra.

In contrast to the photo-active group, *i.e.* the phenacylsulfide, the diene has to be stable against the irradiated UV light. The absorbance at a specific wavelength indicates electronic changes in the molecule, with a potential negative effect on the subsequent DIELS–ALDER reaction of the diene. The diene should thus not absorb UV light in the relevant range of wavelengths between $\lambda = 320$ nm and 420 nm. The UV-Vis absorption spectrum of **20** is depicted in Figure 52 along with the spectrum of the phenacylsulfide compound **16** and the emission spectrum of the UV lamp employed for the photo-ligation. There is no absorbance in the relevant region observed, which confirms the stability of **20** towards the employed UV irradiation.

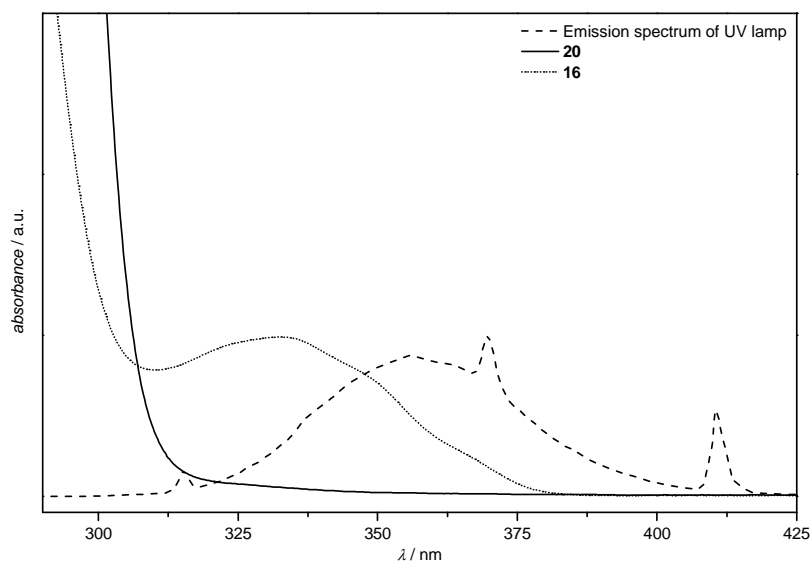
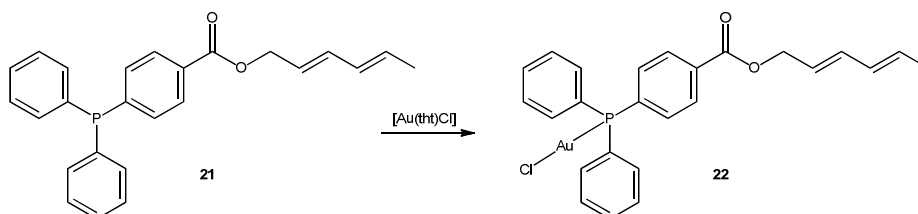


Figure 52. UV absorbance spectra of **16** and **20** recorded in acetonitrile. For comparison the emission spectrum of the UV lamp employed in the photo-ligation reactions is also depicted.

The second ligand based on triphenylphosphine (**21**) and the respective Au complex (**22**) were provided by the institute of inorganic chemistry (S. Bestgen). The complex is formed upon reaction of the pre-synthesized ligand with Au(tht)Cl (tht = tetrahydrothiophen) as the metal precursor (Scheme 53).



Scheme 53. The diene functionalized Au(PPh₃)Cl complex is obtained upon the reaction of the triphenylphosphine ligand **21** with Au(tht)Cl. Both the ligand **21** and its respective Au(PPh₃)Cl complex **22** are provided by the institute of inorganic chemistry (S. Bestgen).

The ¹H NMR spectra of the ligand and the Au-complex are depicted in Figure 53. The chemical shifts of the observed signals are hardly influenced by the complexation of the Au ion. Only the resonances of the phenyl ring protons are slightly shifted from $\delta = 7.99$ ppm and 7.35 ppm in **21** to $\delta = 8.11$ ppm and 7.52 ppm in **22**, respectively. The CH₂ and CH₃ group protons of the hexadiene chain exhibit chemical shifts of $\delta = 4.82$ ppm and 1.77 ppm. The CH protons induce resonances with chemical shifts comparable to the respective resonances in **20** at $\delta = 6.34$ ppm, 6.07 ppm and 5.86 ppm – 5.61 ppm.

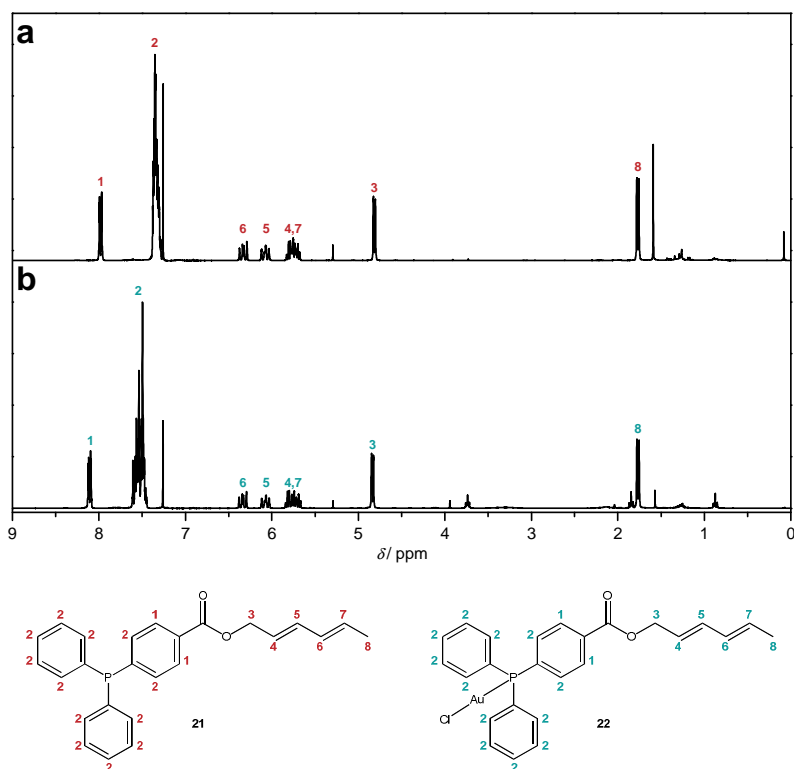


Figure 53. ^1H NMR spectra of the diene functionalized PPh_3 -ligand **21** (a) and the respective $\text{Au}(\text{PPh}_3)\text{Cl}$ -complex **22** (b) recorded in CDCl_3 . For the signal assignments refer to the schematic drawings below the spectra. The spectra were recorded and evaluated by the institute of inorganic chemistry (S. Bestgen).

The UV-Vis absorption spectrum of **22** depicted in Figure 54 only shows little absorbance in the relevant wavelength region between $\lambda = 320$ nm and 420 nm. The Au complex is likely stable under the UV irradiation.

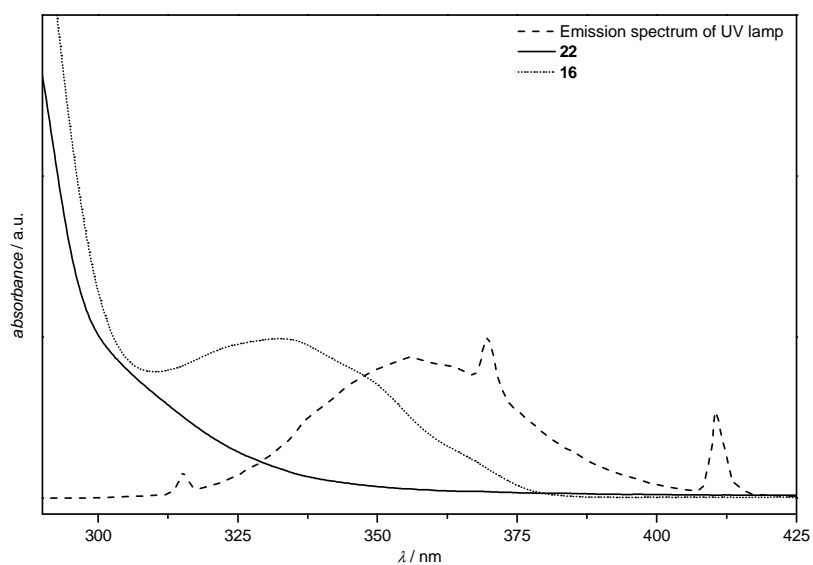


Figure 54. UV-Vis absorbance spectra of **16** and **22** recorded in acetonitrile. For comparison the emission spectrum of the UV lamp employed in the photo-ligation reactions is included.

In order to ensure UV stability, the pure complex **22** was irradiated in deuterated methylene chloride for 2 h and the ^1H , ^{13}C and ^{31}P NMR before and after the irradiation were compared (Figure 55). There are no significant differences in the spectra observed underpinning the stability of the Au complex against UV irradiation in the relevant range ($\lambda = 320$ nm and 420 nm).

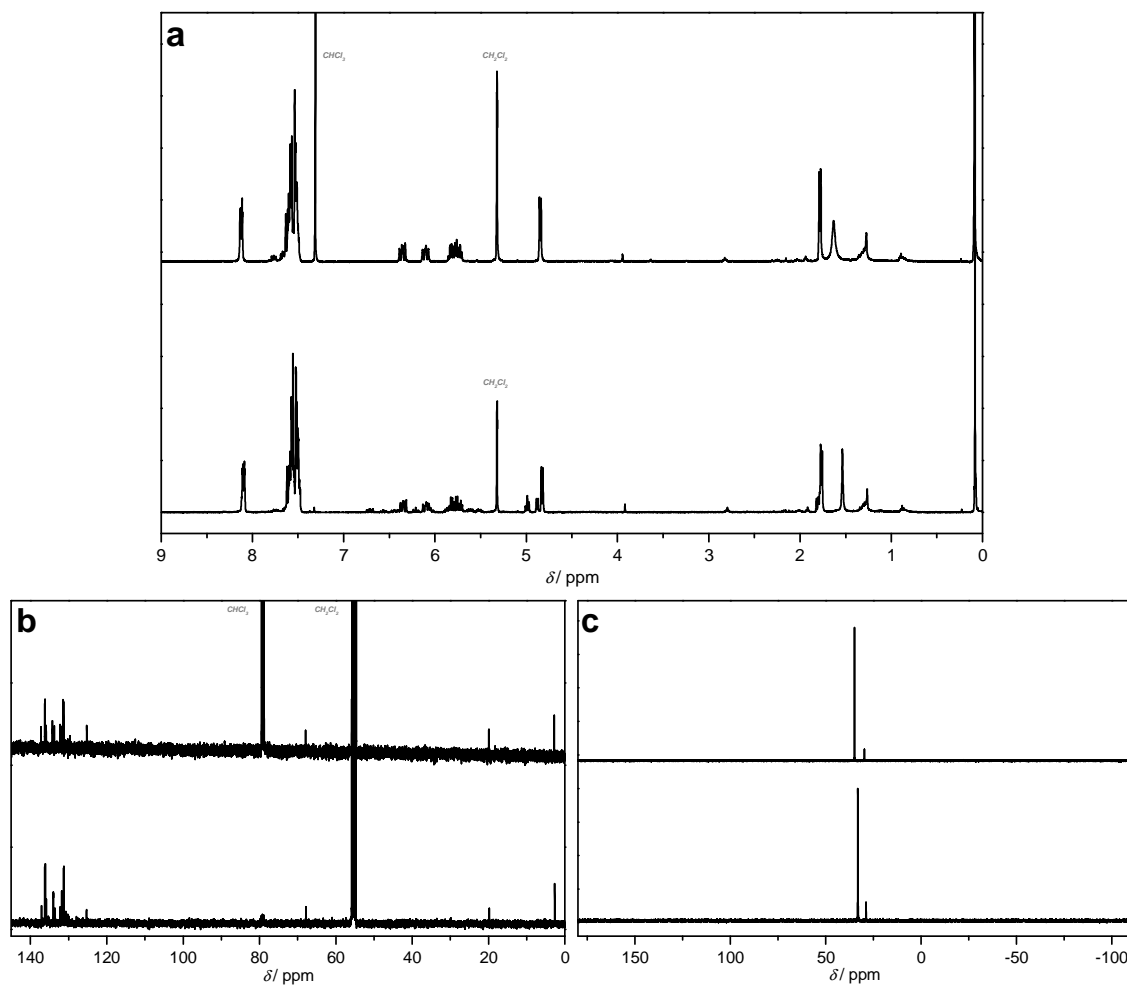
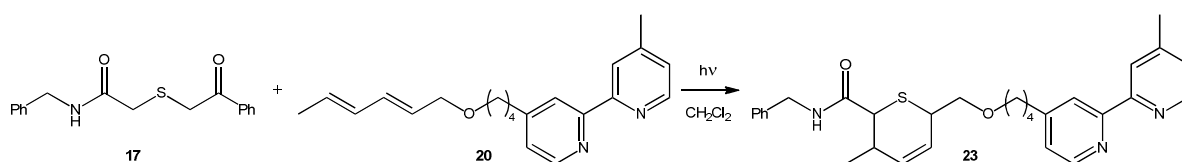


Figure 55. ^1H NMR (a), ^{13}C NMR (b), and ^{31}P NMR (c) of the Au complex **22** before (top) and after irradiation (bottom) with UV ($\lambda = 320$ nm and 420 nm) light for 2 h.

5.3. Photo-Ligation in Solution

Prior to the surface functionalization, test reactions were performed employing phenacylsulfide benzyl amide (**17**) as the photo-reactive compound. This permits a subsequent analysis of the product *via* ^1H NMR analysis.

For the test reactions, a mixture of **17** and the diene functionalized bipyridine ligand **20** or the diene functionalized $\text{Au}(\text{PPh}_3)\text{Cl}$ complex **22**, respectively, was irradiated at $\lambda_{\text{max}} = 355$ nm in methylene chloride for 3 h. The photo-reaction of **17** with **20** is depicted in Scheme 54. After solvent evaporation, the DIELS–ALDER adduct **23** was analyzed *via* ^1H NMR analysis in CDCl_3 (Figure 56).



Scheme 54. Photo-ligation of the diene functionalized bipyridine ligand **20** with phenacylsulfide benzyl amide (**17**) affords the DIELS–ALDER adduct **23**.

In the ^1H NMR spectrum of **23**, the resonances of the benzyl amide moiety are located at $\delta = 7.29$ ppm (Ph-H) and 4.48 ppm (Ph- CH_2) without changes in their chemical shift compared to the proton spectrum of **17**. Most of the resonances associated with the protons of the bipyridyl moiety are also unaffected in their chemical shifts upon the DIELS–ALDER addition of the thioaldehyde. Thus, the pyridine ring proton resonances ($\delta = 8.58$ ppm, 8.28 ppm, 7.17 ppm), the resonances of the butyl- CH_2 groups ($\delta = 3.42$ ppm, 2.72 ppm, 1.83 ppm – 1.51 ppm), the O- CH_2 group ($\delta = 3.97$ ppm), as well as the resonances of the two CH_3 groups ($\delta = 2.47$ ppm and 1.37 ppm) exhibit the same chemical shifts in **23** compared to the respective resonances in **20**. Since the hybridization of the carbon atoms is changed from sp^2 to sp^3 upon the cycloaddition, the resonances of the directly attached protons, H^{10} and H^{13} , are shifted from the multiplet signal ranging from $\delta = 5.76$ ppm to 5.53 ppm in **20** to separated signals at 3.97 ppm (H^{10}), or 2.72 ppm (H^{13}) in **23**, respectively. The shifted signal of H^{10} overlaps with the resonance of the O- CH_2 group protons, while the shifted resonances of H^{13} is overlapping with the signal induced by one of the butyl- CH_2 protons. The internal vinylic carbon atoms retain their sp^2 hybridization and the resonances of the directly attached protons H^{11} and H^{12} at $\delta = 6.18$ ppm and 6.04 ppm in **20** are

combined to a slightly shifted multiplet ranging from $\delta = 5.92$ ppm to 5.57 ppm in **23**, yet a small amount of the residual signals is still visible in the product spectrum. The additionally observed resonances at $\delta = 8.03$ ppm – 7.41 ppm and 2.64 ppm highlighted in Figure 56c are assigned to the by-product acetophenone.

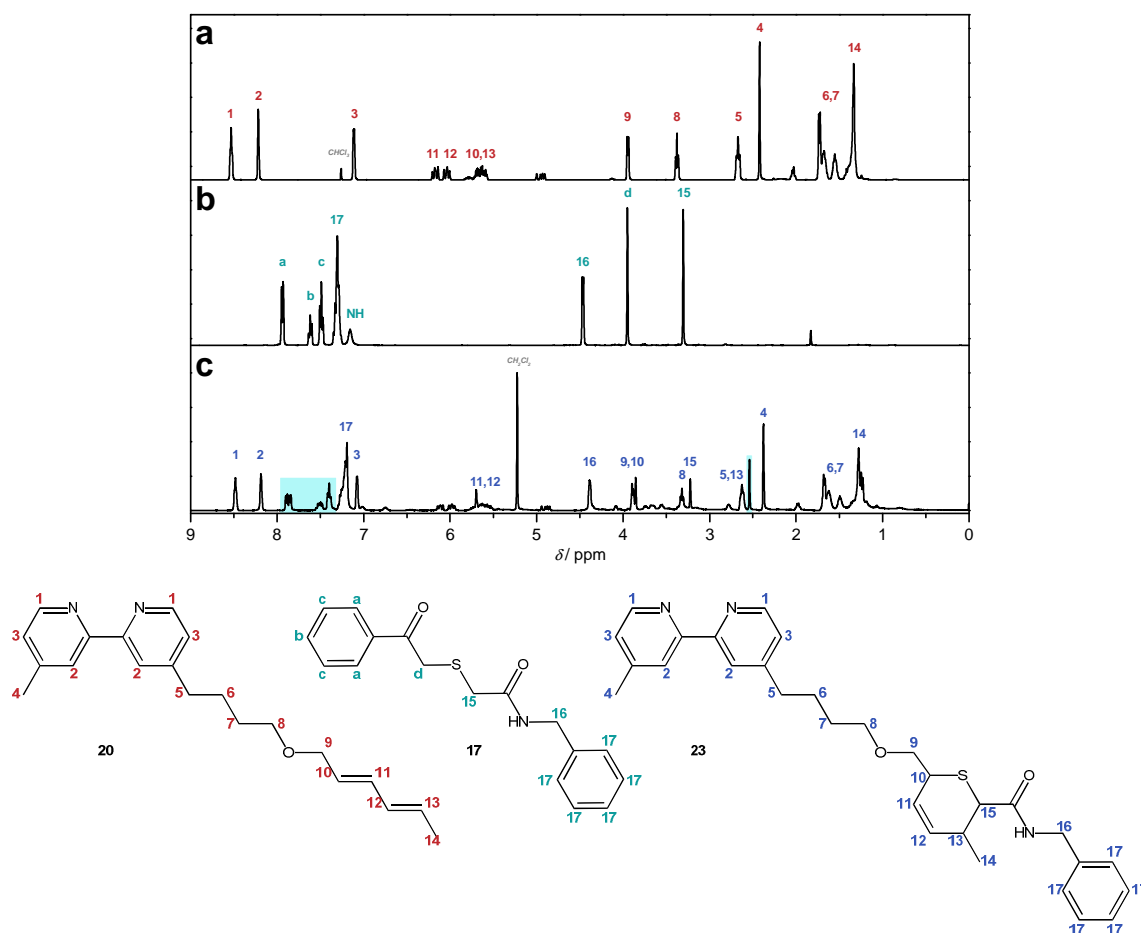
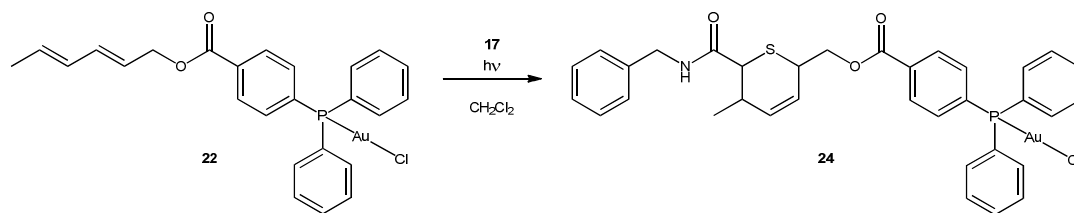


Figure 56. ¹H NMR spectra of the diene-functionalized bipyridine ligand **20** (a), phenacylsulfide benzylamide **17** (b) and the photo-ligation product **23** (c) recorded in CDCl₃. For the signal assignments refer to the schematic drawings below the spectra.

The successful photo-ligation of the bipyridyl diene with a phenacylsulfide model substance in solution could thus be verified. Both, the presence of residual diene as well as the formation of the by-product acetophenone does not affect the subsequent surface modification since these compounds will not be covalently attached to the surface and are thus readily removed by the employed washing procedure.



Scheme 55. Photo-ligation of the diene functionalized Au-complex **22** with **17** at $\lambda_{\text{max}} = 355$ nm in methylene chloride affords the product **24**.

The photo-ligation of **22** with **17** in solution as depicted in Scheme 55 was conducted employing the same conditions as noted above. After solvent removal, the product was analyzed *via* ^1H NMR spectroscopy. Figure 57c depicts the obtained spectrum in comparison to the proton spectra of the diene functionalized Au complex **22** (a) and the phenacylthio benzylamide **17** (b). Besides some signals in the aromatic region, there are no distinct signals observed in the product spectrum preventing both the qualitative as well as a quantitative interpretation of the reactions success. Since the test reaction requires high amounts of the metal complex, a repetition was not conducted in favor of the subsequent surface ligations.

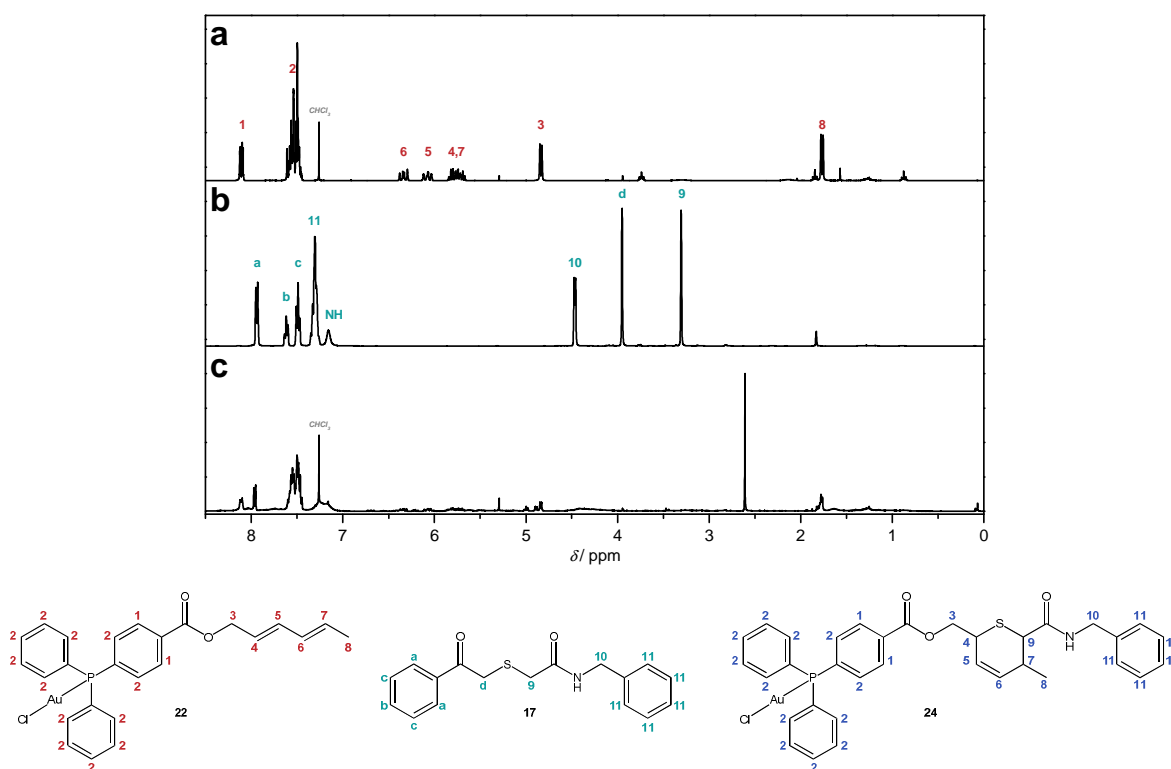
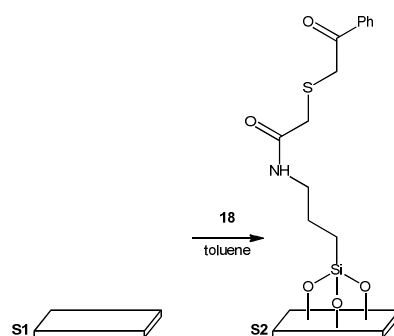


Figure 57. ^1H NMR spectra of the diene-functionalized Au(PPh₃)Cl complex **22** (a), phenacylsulfide benzylamide **17** (b) and the photo-ligation product **24** (c) recorded in CDCl₃. For the signal assignments refer to the schematic drawings below the spectra.

5.4. Surface Patterning

The immobilization of metal complexes on silicon surfaces was realized by two strategies, the modular ligand ligation and subsequent metal loading and the direct ligation of the metal complex. For both strategies, substrate **S1** activated *via* treatment with oxygen plasma was globally pre-functionalized by a self-assembled monolayer of the phenacylsulfide functionalized silane **18** affording the photo-active substrate **S2** (Scheme 57).



Scheme 56. Immobilization of the photo-active self-assembled monolayer on the oxygen plasma-activated silicon substrate **S1** with the phenacylsulfide functionalized silane **18** affording the globally functionalized substrate **S2**.

The spatially resolved photo-ligation of the diene functionalized ligands or metal complexes was conducted covering the surface by a photo-mask (Figure 58a) in a sample holder (b) prior to the addition of the degassed diene solution in methylene chloride. Subsequently, the mixture was irradiated employing a UV lamp emitting in the range of $\lambda = 320$ nm and 420 nm with the maximum emission at $\lambda_{\max} = 355$ nm inside the photo-reactor (c). After irradiation, the substrate was ultrasonicated and thoroughly rinsed with methylene chloride.

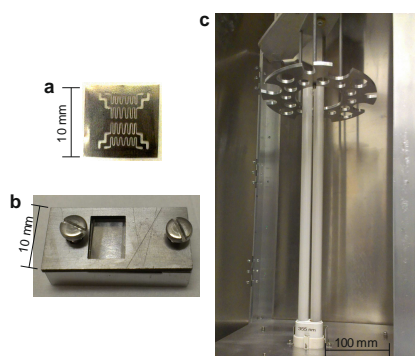
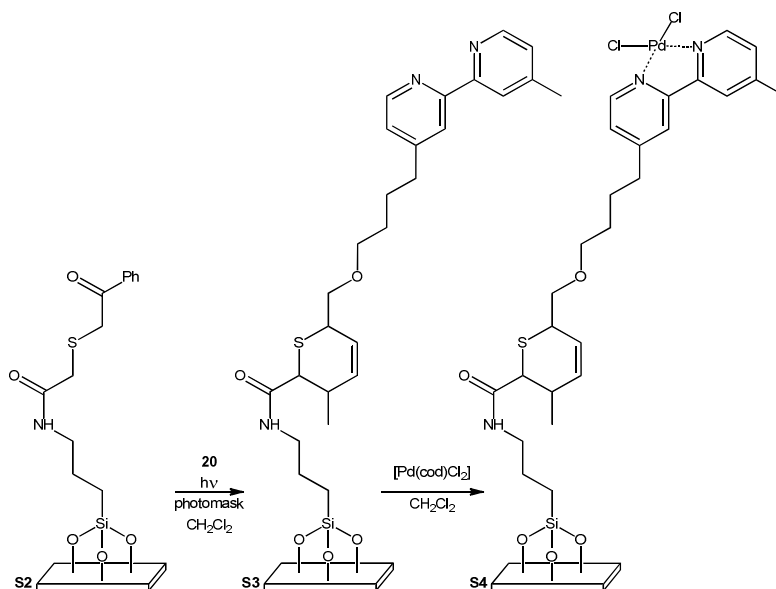


Figure 58. Pictures of the photo-mask (a), the sample holder (b) and the interior of the photo reactor (c) employed for the photo-patterning of the silicon substrates.

The spatially resolved immobilization of the bipyridyl-diene ligand **20** and the successive metal loading with a palladium precursor is depicted in Scheme 57. Both, the ligand-functionalized substrate **S3** as well as the metal-loaded substrate **S4** were analyzed *via* time-of-flight secondary ion mass spectrometry (ToF-SIMS).



Scheme 57. Synthetic strategy for the surface patterning of a silicon wafer with a Pd(bipy) complex. Photo-ligation onto the pre-functionalized substrate **S2** with the bipyridine-diene ligand (**20**) employing a photomask affords the patterned surface **S3**. Successive metal-loading employing Pd(cod)Cl₂ as the metal precursor finally affords **S4** patterned with the metal complex (for clarity reasons, only the ligated species are depicted for **S3** and **S4**).

The ToF-SIMS analysis of the ligand-functionalized substrate **S3** could not determine a patterned ligation of the ligand, yet a slightly visible pattern of the [PdCl₂]⁻ anion on the subsequently metal-loaded substrate **S4** could be imaged (Figure 59). As a consequence, a successful photo-patterning with the bipyridyl-diene ligand in the first step can be assumed. An increased contrast of the patterning could be obtained, however, optimizing the reaction conditions.

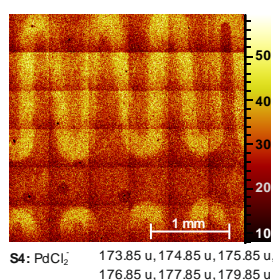
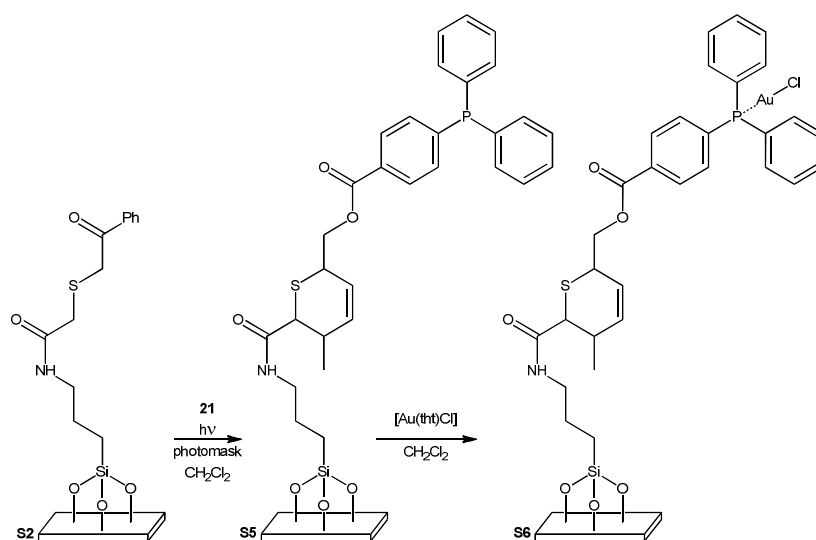


Figure 59. ToF-SIMS image of substrate **S4** visualizing the detected signals of the [PdCl₂]⁻ anion with spatial resolution.

The modular functionalization was also employed for the second system comprised of the triphenylphosphine-diene ligand **21** and Au⁺ as the metal ion. After the photo-patterning (**S5**), the immobilized ligands were loaded with [Au(tht)Cl] as the metal precursor affording **S6** (Scheme 58).



Scheme 58. Irradiation of the phenacylsulfide self-assembled monolayer **S2** in the presence of the diene functionalized triphenylphosphine ligand **21** and a photo-mask affords the patterned substrate **S5**. The metal complex (**S6**) is obtained *via* subsequent metal loading with Au(tht)Cl as the metal precursor (for clarity reasons, only the ligated species are depicted for **S5** and **S6**).

The images obtained from ToF-SIMS analysis of the substrates **S5** and **S6** are depicted in Figure 60. Two positively charged molecule fragments could be imaged from the analysis of **S5**, the 4-(diphenylphosphino)benzoic acid headgroup (Figure 60a) and a phenylphosphine fragment (Figure 60b). After the addition of AuCl, the ToF-SIMS image shows a detectable contrast for the [AuCl]⁻ and the [HAuCl]⁻ anions as depicted in Figure 60c, yet the metal loading was only successful at the edges of the patterned ligand area. In addition, there is no evidence of the [AuCl]⁻ anions being attached to the triphenylphosphine ligand.

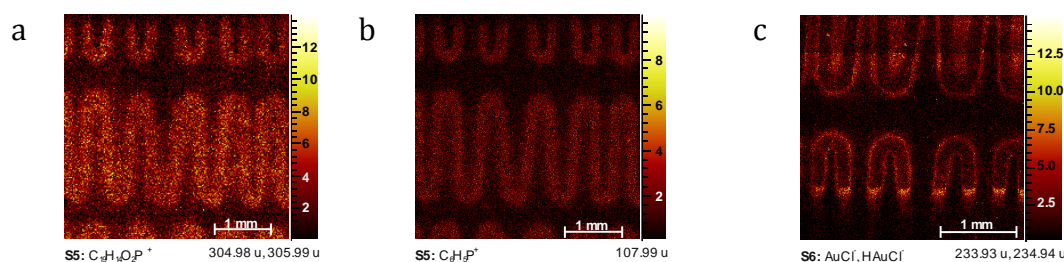
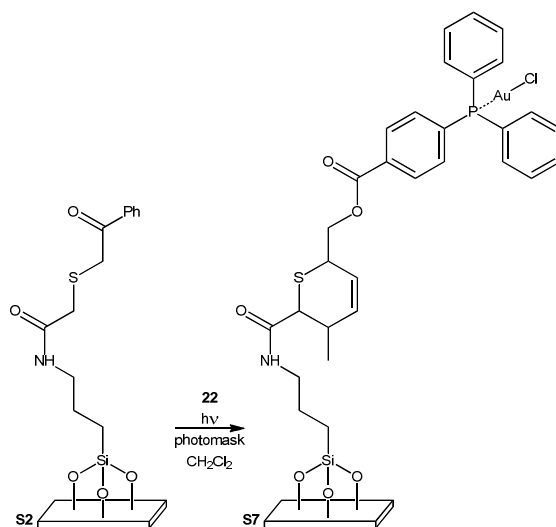


Figure 60. ToF-SIMS images of **S5** (a and b) as well as **S6** (c) patterned with the triphenylphosphine ligand, or the Au(PPh₃)Cl complex, respectively.

The direct use of the metal complex in the photo-patterning reaction ensures the correct binding situation of the metal ions, yet also restricts the choice of the metal complex since it should not absorb in the range of wavelengths irradiated for the photo ligation. The colorless Au^I complex **22** does not absorb in the considered UV regime (Figure 54) and is thus suitable for the direct ligation. Scheme 59 depicts the surface immobilization of **22** *via* DIELS–ALDER reaction with the thioaldehyde formed *in-situ* upon UV irradiation of **S2** affording the patterned substrate **S7**.



Scheme 59. Direct immobilization of an Au(PPh₃)Cl complex *via* partial irradiation of the phenacylsulfide self-assembled monolayer **S2** in the presence of **22** in methylene chloride (for clarity reasons, only the ligated species is depicted in **S7**).

ToF-SIMS analysis of **S7** exhibited spatially resolved contrasts for the Cl⁻ anion (Figure 61a), the Au⁻ (b) and the [AuCl]⁻ / [HAuCl]⁻ (c) anions as well as for the positively charged 4-(diphenylphosphino)benzoic acid fragment [C₁₉H₁₄O₂P]⁺ (d). The best contrast is obtained imaging the Cl⁻ anions introduced by the Au(PPh₃)Cl complex while the contrasts of the other fragments are less intense.

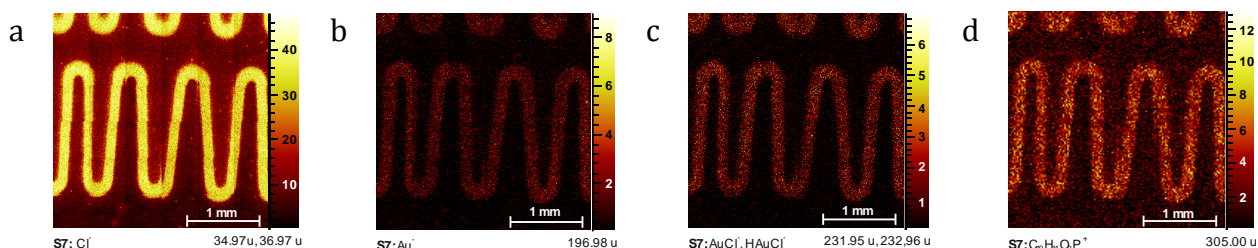


Figure 61. ToF-SIMS images of **S7** visualizing the spatially resolved abundance of Cl⁻ (a), Au⁻ (b), [AuCl]⁻ and [HAuCl]⁻ (c), as well as the 4-(diphenylphosphino)benzoic acid fragment [C₁₉H₁₄O₂P]⁺ (d).

In summary, the principle feasibility to immobilize metal complexes onto a silicon substrate with spatial resolution *via* the photo-induced decomposition of a phenacylsulfide SAM and subsequent DIELS–ALDER trapping of the thioaldehyde could be verified by ToF-SIMS imaging of the patterned surfaces for the first time. For the Pd(bipy) system, a modular approach was pursued with the patterning of the ligand in the first step and subsequent metallation. For the Au(PPh₃)Cl complex, however, better results were obtained when the metal complex was directly immobilized onto the photo-active substrate. However, the ToF-SIMS measurements showed low contrasts which could indicate a low density of functions on the surface. However, the contrast is not necessarily correlated to the amount of immobilized moieties on the surface since only the charged fragments released from the substrate surface are detected by the ToF-SIMS technique.

In addition to the optimization of the reaction conditions for the ligation of the small molar metal complexes, polymer brushes or dendritic structures equipped with multiple metal complexes per surface-ligating unit could be immobilized onto the solid substrates in order to obtain a higher grafting density of the metal complexes. Moreover, the spatially resolved immobilization of two or more metal complexes onto one substrate *via* the photo-triggered ligation could enable the construction of reactors with defined catalytic regimes for the successive catalysis of diverse reactions, *e.g.* in continuous flow reactors.

6

Concluding Remarks and Outlook

The integration of potentially catalytical active metal complexes into polymer side chains was achieved employing the highly efficient copper catalyzed azide alkyne cycloaddition (CuAAC). Using controlled polymerization techniques such as the reversible addition fragmentation chain transfer polymerization (RAFT), polymers with defined molar masses and narrow polydispersities are accessible. The soluble metallopolymers can potentially be employed as catalysts allowing for a facilitated separation from the product after the reaction *via* precipitation of the polymer. The followed modular concept permits the synthesis of a variety of metallopolymers *via* the ligation of the alkyne modified metal complex with the azide functionalized precursor polymer. Thus, the rhodium containing as well as the palladium containing metallopolymers can be obtained starting from the same precursor polymer. In addition, mixed metallopolymers with divers metal complexes on one polymer chain can be synthesized following the partial ligation approach tested with propargyl alcohol in the model study. Accordingly, the relative content of the metal complexes can be controlled by the amount of the added alkyne functionalized metal complexes.

Moreover, the control over the distance between two functional groups *via* the initial monomer composition can be utilized to optimize the amount of present metal ions, while potentially retaining full catalytic activity.

The versatility and high efficiency of the CuAAC ligation was exploited employing it as a polymerization technique. The triazolyl rings formed upon the cycloaddition additionally participated in the complexation of the Pd^{II} ions. While the bisalkyne monomer was introduced for the subsequent metal complexation, the bisazide compound serves to adjust the polymer properties towards the targeted applications. Best solubility was achieved employing a bisazido fluorene. Future attempts could focus on the incorporation of other metal complexes. In addition, studies on the catalytic activity in comparison to the analog side-chain functionalized polymers and low molar catalysts are of interest. Further, multi-functionalized monomers could be employed for the synthesis of dendritic structures or polymer networks with incorporated metal complexes as new catalyst materials.

The spatially resolved immobilization of metal complexes onto photo-active self-assembled monolayers (SAMs) represents a first step towards tailored solid substrate supported catalysts. The UV light-triggered decomposition of phenacylsulfide and subsequent *in-situ* trapping of the generated thioaldehyde with a diene functionalized complex was successfully employed for the surface modification with a Pd^{II} and or an Au^I complex, respectively. Future attempts could be directed towards the immobilization of several metal complexes onto one substrate assembled in spatially defined regimes. In addition, other ligating methods such as the photo-enol DIELS-ALDER, the tetrazole-ene or the light-triggered thiol-yne ligation could be considered as alternative routes for the immobilization of the metal complexes. Furthermore, a higher functional density on the surface could be obtained *via* the immobilization of polymer brushes or dendrons equipped with several metal complexes per surface-ligating unit.

In summary, the achievements presented in the current thesis contribute to the design of new potentially catalytic active materials employing modular and highly efficient ligation methods. The employed synthetic designs enable the transfer of the synthetic strategies to other metal complexes with only minor modifications.

7

Experimental Section

7.1. Materials

If not stated otherwise, the materials were used as received. Acetonitrile (VWR, p.a.), chloroform (VWR, p.a.), diethyl ether (VWR, p.a.), diethylamine (Acros Organics, 99 %), dimethyl acetamide (DMAc, VWR, p.a.), *N,N* dimethylformamide (DMF, Fisher Chemical, p.a.), *N,N*-dimethylformamide anhydrous (Acros Organics), ethyl acetate (VWR, p.a.), *n*-hexane (VWR, p.a.), methanol (VWR, p.a.), methylene chloride (VWR, p.a.), methylene chloride anhydrous (Acros Organics), tetrahydrofuran (THF, VWR, p.a.), tetrahydrofuran anhydrous (Acros Organics), methyl methacrylate (Sigma Aldrich, 99 %) was destabilized by passing through a basic alumina column, glycidyl methacrylate (Sigma Aldrich, 97 %) was destabilized by passing through a basic alumina column, styrene (Acros Organics, 99 % extra pure) was destabilized by passing through a basic alumina column, 4-chloromethyl styrene (Acros Organics, 90 % techn.) was vacuum distilled prior to use, methacryloyl chloride (Sigma Aldrich, 97 %) was destabilized by passing through a basic alumina column, 1,1'-azobis(cyclohexane carbonitrile) (VAZO-88, Sigma Aldrich, 98 %), azoisobutyronitrile (AIBN, Sigma Aldrich) was recrystallized from methanol, dibenzyl trithiocarbonate (DBTTC) was obtained from Orica Pty Ltd., Melbourne Australia as a donation, cyanoisopropyl dithiobenzoate (CPDB) was synthesized according to literature,^{316,317} copper(I) iodide (Sigma Aldrich, 98 %), copper(II) sulfate (Sigma Aldrich, 98 %), copper(I) bromide (Sigma Aldrich, 98 %) was purified by sequential washing with sulfurous acid, acetic acid and ethanol, followed by drying under reduced pressure, 1,8-diazabicyclo[5.4.0]-undec-7-ene (DBU, Fluka, 99 %), *N,N,N',N'',N''*-pentamethyl diethylene triamine (PMDETA, Acros Organics, 99 %), sodium ascorbate (SA, Sigma Aldrich, 98 %), potassium hydroxide (Roth, 85 %), sodium hydroxide (Roth, 99 %), sodium sulfate (Roth, 99 %), sodium azide (Sigma Aldrich, 99 %), tert-butyllithium (Acros, 1.9 M in pentane), tetrabutylammonium iodide (Acros, 98 %), ammonium hydroxide (Fluka, 25 % in water), tetrabutylammonium bisulfate (Sigma Aldrich, 97 %), magnesium sulfate (Roth, dried), sodium chloride (Roth), ammonium chloride (Acros Organics, 99.5 %), sodium hydrogen carbonate (Roth, 99.5 %), neutral alumina (Merck), basic alumina (Merck), potassium phosphate monobasic (Roth), potassium phosphate dibasic (Roth), sodium iodide (Merck, p.a.), *trans*-dichlorobis-

(triphenylphosphine) palladium(II) (ABCR, 99 %), [Pd(cod)Cl]₂ (Alfa Aesar), benzyl chloride (ABCR, 99 %), 1-bromooctane (Alfa Aesar, 98 %), 1-bromoundecane (Fluka, 97 %), 2,7-dibromo fluorene (Acros Organics, 99 %), 2,6-dibromopyridine (Acros Organics, 98 %), 1,8-dibromooctane (Sigma Aldrich, 98 %), α,α' -dibromo-*p*-xylene (Fluka, 98 %), 1,3-dibromopropane (Sigma Aldrich, 99 %), propargyl bromide (Acros Organics, 80% in toluene), 3-chloropropanol (Acros Organics, 98 %), phenacyl chloride (Sigma Aldrich, 98 %), (trimethylsilyl)acetylene (ABCR, 97 %), 1-(trimethylsilyl) imidazole (Alfa Aesar, 97 %), 3-(triethoxysilyl)propyl acetamide (Sigma Aldrich, 99 %), *N*-(3-dimethylaminopropyl)-*N'*-ethyl-carbodiimid hydrochloride (EDC·HCl, Roth, 99 %), 4-dimethylamino pyridin (DMAP, Acros Organics, 98 %), triethylamine (Sigma Aldrich, 99.5 %), diisopropylamine (Acros Organics) was vacuum distilled prior to use, benzyl amine (Fluka, p.a.), *n*-butylamine (Alfa Aesar, 99 %), ethyl chloroformate (Sigma Aldrich, 98 %), hydroquinone (ABCR), hydrochloric acid (Roth, 37 %), thioglycolic acid (Acros Organics, 97 %), *n*-butyllithium (Sigma Aldrich, 1.6 M in hexane), sodium hydride (Sigma Aldrich, 60 % in mineral oil), *trans,trans*-2,4-hexadien-1-ol (Sigma Aldrich, 97 %), 2-ethynylpyridine (ABCR, 95 %), *p*-tosylazide was synthesized according to literature.³¹⁸

Silicon wafers (orientation <100>, B-doped, resistivity 5-20 $\Omega\cdot\text{cm}$) with 50 nm thermal silicon dioxide (SiO₂) over-layer were purchased from Siegert Consulting e.K., Germany.

7.2. Measurements

Nuclear magnetic resonance (NMR) spectra were recorded in CDCl_3 , THF-d_8 , or DMSO-d_6 on a Bruker Avance II NMR spectrometer. Chemical shifts are referenced to internal solvent resonances and are reported relative to tetramethylsilane.

Elemental analyses (EA) were carried out with an Elementar Vario EL.

Molecular weight distributions were measured by size exclusion chromatography (SEC) on a Polymer Laboratories/Varian PL-GPC 50 Plus system comprising a Polymer Laboratories 5.0 μm bead-size guard column ($50 \times 7.5 \text{ mm}^2$), followed by three PL columns and a differential refractive index detector. The eluent was tetrahydrofuran (THF) at 35 °C with a flow rate of $1 \text{ mL}\cdot\text{min}^{-1}$. The SEC system was calibrated using linear polystyrene standards ranging from $2000 \text{ g}\cdot\text{mol}^{-1}$ to $2\cdot 10^6 \text{ g}\cdot\text{mol}^{-1}$ and the Mark-Houwink relationship for polystyrene ($K = 14.1\cdot 10^{-5} \text{ dL}\cdot\text{g}^{-1}$, $\alpha = 0.7$),³¹⁹ or for polymethyl methacrylate ()

Static light scattering (SLS) measurements were performed using a MALLS-detector (multi-angle laser light scattering detector) SLD 7000 from Polymer Standard Services (PSS), Mainz, Germany. Five concentrations of the polymer were employed ranging from $0.5 \text{ g}\cdot\text{L}^{-1}$ to $5 \text{ g}\cdot\text{L}^{-1}$ to determine the weight-averaged molar mass (M_w^{SLS}) and the second virial coefficient (A_2). The solutions were prepared by dissolving the polymer in dimethyl acetamide (DMAc). After a stabilizing period of approx. 60 h, the solutions were filtered over $0.2 \mu\text{L}$ filters and analysed by SLS.

The required dn/dc values were measured employing the same solutions with a refractometer dn/dc 2010 from PSS, Mainz, Germany.

Electrospray ionization mass spectra (ESI-MS) were recorded on a LXQ mass spectrometer (ThermoFisher Scientific, San Jose, CA, USA) equipped with an atmospheric pressure ionization source. The instrument was calibrated in the m/z range 195–1822 using a standard containing caffeine, Met-Arg-Phe-Ala acetate (MRFA) and a mixture of fluorinated phosphazenes (Ultramark 1621) (all from Aldrich). A constant spray voltage of 4.5 kV and a dimensionless sweep gas flowrate of 2 and a dimensionless sheath gas flow-rate of 12 were applied. The capillary

voltage, the tube lens offset voltage and the capillary temperature were set to 60 V, 110 V, and 275.8 °C, respectively.

ToF-SIMS (time-of-flight secondary ion mass spectrometry) was performed on a TOF.SIMS⁵ instrument (ION-TOF GmbH, Münster, Germany), equipped with a Bi cluster liquid metal primary ion source and a non-linear time of flight analyzer. The Bi source was operated in the “bunched” mode providing 0.7 ns Bi¹⁺ ion pulses at 25 keV energy and a lateral resolution of approx. 4 μm. The short pulse length allowed for high mass resolution to analyze the complex mass spectra of the immobilized organic layers. Images larger than the maximum deflection range of the primary ion gun of 500×500 μm² were obtained using the manipulator stage scan mode. Negative polarity spectra were calibrated on the C⁻, C²⁻, and C³⁻ peaks. Positive polarity spectra were calibrated on the C⁺, CH⁺, CH²⁺, and CH³⁺ peaks. Primary ion doses were kept below 10¹¹ ions·cm⁻² (static SIMS limit).

7.3. Syntheses

All manipulations of air-sensitive materials were performed under rigorous exclusion of oxygen and moisture in Schlenk-type glassware on a dual manifold Schlenk line, interfaced to a high vacuum line (10^{-3} torr), or in an argon-filled glove box.

7.3.1. Syntheses of Low Molar Mass Compounds

3-Azidopropanol (1)

To a stirred solution of sodium azide (16.92 g, 260.20 mmol, 1.10 eq) and tetrabutylammonium bisulfate (1.00g, 3.10 ml, 0.01 eq) in 170 mL water, 3-chloropropanol (22.29 g, 235.81 mmol, 1.00 eq) was slowly added. The mixture was heated to 80 °C for 24 h and subsequently stirred at ambient temperature for 16 h. The product was extracted with diethyl ether (3 x 150 mL), the combined organic phases were dried (Na_2SO_4) and the solvent was evaporated. Product purification was conducted *via* vacuum distillation to obtain 20.25 g (85 %) of the pure product as a colorless liquid.²⁶⁰

^1H NMR (250 MHz, CDCl_3) δ / ppm = 3.67 (t, 2H, $\text{CH}_2\text{-OH}$), 3.39 (t, 2H, $\text{CH}_2\text{-N}_3$), 2.78 (s, 1H, OH), 1.84 – 1.71 (m, 2H, C- $\text{CH}_2\text{-C}$).

3-Azidopropyl methacrylate (2)

Triethylamine (15 mL, 108.21 mmol, 1.20 eq) was added to a solution of **1** (8.86 g, 87.66 mmol, 1.00 eq) and hydroquinone (7.65 mg, 0.69 mmol, $7.87 \cdot 10^{-3}$ eq) in 60 mL methylene chloride cooled in an ice-bath. Methacryloyl chloride (20.2 mL, 105.39 mmol, 1.20 eq) was added slowly *via* a dropping funnel. The mixture was stirred at 0 °C for 1 h and subsequently at ambient temperature for 20 h. The reaction mixture was successively washed with 1N hydrochloric acid (2 x 80 mL), water (2 x 80 mL) and 1N aqueous sodium hydroxide solution (2 x 80 mL). The organic phase was dried (MgSO_4) and the solvent was removed *in vacuo*. Vacuum distillation afforded 4.29 g (29 %) of the purified product as a colorless liquid.²⁶⁰

^1H NMR (250 MHz, CDCl_3) δ / ppm = 6.11 – 6.03 (m, 1H, vinyl-CH), 5.58 – 5.50 (m, 1H, vinyl-CH), 4.25 – 4.15 (m, 2H, $\text{CH}_2\text{-O}$), 3.38 (t, 2H, $\text{CH}_2\text{-N}_3$), 1.99 – 1.86 (m, 5H, CH_3 , C- $\text{CH}_2\text{-C}$).

1,3-Dipropargyl imidazolium bromide (5)

Trimethylsilyl imidazole (4.00 g, 28.54 mmol, 1.00 eq) was dissolved in 100 mL acetonitrile and propargyl bromide (7 mL, 64.96 mmol, 2.27 mmol) was added slowly *via* a syringe. The mixture was heated to 95 °C for 48 h and subsequently stored in the freezer. The product crystallized after 5 days from the reaction mixture, was separated by filtration and dried *in vacuo* to obtain 4.00 g (62 %) of the product as a white solid.³²⁰

^1H NMR (250 MHz, DMSO-d_6) δ / ppm = 9.45 (s, 1H, N-CH-N), 7.90 (d, J = 1.6 Hz, 2H, N-CH-CH-N), 5.27 (d, J = 2.6 Hz, 4H, CH_2), 3.88 (t, J = 2.6 Hz, 2H, C-CH).

^{13}C NMR (100 MHz, DMSO-d_6) δ / ppm = 136.2 (N-CH-N), 122.7 (N-CH-CH-N), 79.1 (C_q), 76.0 (CH), 40.2 and 38.8 (CH_2).

2,6-Diethynyl pyridine (6)

In a SCHLENK flask, 2,6-dibromo pyridine (3.25 g, 13.73 mmol, 1.00 eq), ethynyl trimethyl silane (4.1 mL, 29.22 mmol, 2.12 eq), bis(triphenylphosphine)palladium(II) dichloride (0.20 g, 0.29 mmol, 0.02 eq) and copper(I)iodide (21.1 mg, 0.11 mmol, 0.01 eq) were dissolved in 35 mL freshly distilled diethylamine under an argon atmosphere. The mixture was stirred at ambient temperature overnight prior to solvent removal *in vacuo*. The residue was redissolved in 40 mL diethyl ether. After filtration and solvent removal, the product was purified *via* column chromatography (diethyl ether / hexane 1:3, R_f = 0.76). 3.72 g (99 %) of the intermediate trimethylsilyl protected bisalkyne was obtained as a slightly brown solid.^{321,322}

^1H NMR (400 MHz, CDCl_3) δ / ppm = 7.58 (t, J = 7.8 Hz, 1H, Ph-H), 7.37 (d, J = 7.8 Hz, 2H, Ph-H), 0.25 (s, 18H, $\text{Si}(\text{CH}_3)_3$).

The trimethylsilyl protected bisalkyne (4.01 g, 14.78 mmol, 1.00 eq) was dissolved in methanol, potassium hydroxide (2.08 g, 36.99 mmol, 2.50 eq) was added and the reaction mixture was stirred at ambient temperature for 2 h. The solvent was

removed *in vacuo*. Water (50 mL) was added to the residue and the product was extracted with diethyl ether (3 x 50 mL). The combined organic phases were successively washed with water (2 x 50 mL), brine (2 x 50 mL) and water (2 x 50 mL), dried (Na₂SO₄) and the solvent was removed. Column chromatography (diethyl ether / hexane 1:1, *R_f* = 0.35) afforded 1.21 g (64 %) of the pure product as a slightly brown solid.³²¹

¹H NMR (250 MHz, CDCl₃) δ / ppm = 7.64 (dd, 1H, Ph-H), 7.44 (d, 3H, Ph-H), 3.15 (s, 2H, CCH).

¹³C NMR (100 MHz, CDCl₃) δ / ppm = 142.8 (Py(C₂,C₆)), 136.7 (Py(C₄)), 127.2 (Py(C₃,C₅)), 82.2 (C_q), 77.9 (CH).

1-Azidoundecane (7)

A mixture of sodium azide (2.80 g, 43.13 mmol, 2.10 eq) and 1-bromoundecane (5 mL, 20.20 mmol, 1.00 eq) in 75 mL DMF was stirred at ambient temperature for 20 h. Subsequently, water (80 mL) was added and the product was extracted with diethyl ether (3 x 75 mL). The combined organic phases were washed with water (50 mL) and dried (Na₂SO₄). The solvent was removed *in vacuo* to obtain 3.85 g (97 %) of the pure product as a colorless liquid.³⁰²

¹H NMR (250 MHz, CDCl₃) δ / ppm = 3.25 (t, 2H, CH₂-N₃), 1.66 – 1.52 (m, 2H, CH₂-CH₂N₃), 1.44 – 1.17 (m, 16H, CH₂), 0.88 (t, 3H, CH₃).

¹³C NMR (100 MHz, CDCl₃) δ / ppm = 51.7 (C₁), 32.1 (C₂), 29.7 (C₃), 29.7 (C₄), 29.6 (C₅), 29.5 (C₆), 29.3 (C₇), 29.0 (C₈), 26.9 (C₉), 22.8 (C₁₀), 14.3 (C₁₁).

Benzyl azide (8)

A mixture of sodium azide (5.09 g, 78.26 mmol, 1.80 eq) and benzyl chloride (5 mL, 43.45 mmol, 1.00 eq) in 75 mL DMF was stirred at ambient temperature for 20 h. Subsequently, water (80 mL) was added and the product was extracted with diethyl ether (3 x 75 mL). The combined organic phases were washed with water (50 mL) and dried (Na₂SO₄). The solvent was removed *in vacuo* to obtain 2.28 g (39 %) of the pure product as a colorless solid.³⁰²

¹H NMR (250 MHz, CDCl₃) δ / ppm = 7.48 – 7.28 (m, 5H, Ph-H), 4.36 (s, 2H, CH₂-N₃).

^{13}C NMR (100 MHz, CDCl_3) δ / ppm = 135.5 (Ph(C_q)), 129.0 (Ph(C_3, C_5)), 128.5 (Ph(C_2, C_6)), 128.4 (Ph(C_4)), 54.9 (CH_2).

General procedure for the CuAAC ligation of the bifunctionalized alkynes (5,6) with the monofunctionalized azides (7,8) affording 9, 10, 11, or 12

Except the reactions with copper(II) sulfate as the catalyst, all reactions were conducted under an inert atmosphere. All solutions were degassed by percolating with argon. A solution of $0.2 \text{ mol}\cdot\text{L}^{-1}$ dialkyne (**5** or **6**), $0.4 \text{ mol}\cdot\text{L}^{-1}$ monoazide (**7** or **8**) and 0.2 eq of the copper salt and the ligand or base, respectively, in DMF or THF was stirred at ambient temperature for 24 h. Subsequently, aqueous ammonium hydroxide was added to stop the reaction and the reaction mixture was passed over a small column filled with neutral alumina to remove the copper catalyst. The solvent was removed under reduced pressure and conversion was determined *via* ^1H NMR spectroscopy in DMSO-d_6 or CDCl_3 .

NMR data for complete clicked products:

9: ^1H NMR (400 MHz, DMSO-d_6) δ / ppm = 9.49 (s, 1H, N-CH-N), 8.31 (s, 2H, triazole-H), 7.87 (s, 2H, N-CH-CH-N), 5.59 (s, 4H, triazole- CH_2 -imidazole), 4.36 (t, 4H, undecane(H_1)), 1.86-1.70 (m, 4H, undecane(H_2)), 1.22 (s, 32H, undecane(H_3 - H_{10})), 0.84 (t, 6H, undecane(H_{11})).

^{13}C NMR (100 MHz, DMSO-d_6) δ / ppm = 140.8 (N-CH-N), 125.3 (triazole(C_q)), 123.4 (triazole(CH), N-CH-CH-N), 54.3 (undecane(C_1)), 50.5 (triazole- CH_2 -imidazole), 31.9 (undecane(C_2)), 30.2 (undecane(C_3)), 29.6 – 29.2 (m, undecane(C_4 - C_8)), 28.9 (undecane(C_9)), 22.7 (undecane (C_{10})), 14.6 (undecane(C_{11})).

10: ^1H NMR (400 MHz, DMSO-d_6) δ / ppm = 9.36 (s, 1H, N-CH-N), 8.30 (s, 2H, triazole-H), 7.77 (s, 2H, N-CH-CH-N), 7.39-7.31 (m, 10H, Ph-H), 5.63 (s, 4H, Ph- CH_2), 5.53 (s, 4H, triazole- CH_2 -imidazole).

^{13}C NMR (100 MHz, DMSO-d_6) δ / ppm = 140.6 (N-CH-N), 135.7 (Ph(C_q)), 128.8 (triazole(C_q)), 128.3 (Ph(C_3, C_5)), 128.1 (Ph(C_2, C_6)), 124.7 (s, Ph(C_4)), 122.8 (triazole(CH), N-CH-CH-N).

11: ^1H NMR (400 MHz, CDCl_3) δ / ppm = 8.19 (s, 2H, triazole-H), 8.08 (s, 2H, Py(H_3, H_5)), 7.85 (s, 1H, Py(H_4)), 4.37 (t, 4H, undecane(H_1)), 1.91 (s, 4H, undecane(H_2)), 1.32-1.19 (m, 32H, undecane($\text{H}_3\text{-H}_{10}$)), 0.85 (t, 6H, undecane(H_{11})).

^{13}C NMR (100 MHz, CDCl_3) δ / ppm = 150.2 (Py(C_q)), 148.4 (Py(C_4)), 137.8 (triazole(C_q)), 122.0 (triazole(CH)), 119.3 (Py(C_3, C_5)), 50.6 (undecane(C_1)), 32.0 (undecane(C_2)), 30.4 (undecane(C_3)), 29.6 (undecane(C_4)), 29.6 (undecane(C_5)), 29.5 (undecane(C_6)), 29.4 (undecane(C_7)), 29.1 (undecane(C_8)), 26.6 (undecane(C_9)), 22.7 (undecane(C_{10})), 14.18 (undecane(C_{11})).³²³

12: ^1H NMR (400 MHz, DMSO-d_6) δ / ppm = 8.70 (s, 2H, triazole-H), 8.03 (s, 3H, Py-H), 7.42-7.32 (m, 10H, Ph-H), 5.71 (s, CH_2).

^{13}C NMR (100 MHz, DMSO-d_6) δ / ppm = 149.8 (Py(C_q)), 147.4 (Py(C_4)), 138.2 (Ph(C_q)), 135.9 (triazole(C_q)), 128.8 (Ph(C_2, C_6)), 128.2 (Ph(C_4)), 127.9 (Ph(C_3, C_5)), 123.7 (triazole-CH), 118.5 (Py(C_3, C_5)), 53.1 (CH_2).³²⁴

1,8-Diazidooctane (13)

A mixture of sodium azide (3.08 g, 47.40 mmol, 6.22 eq) and 1,8-dibromoundecane (1.4 mL, 7.62 mmol, 1.00 eq) in 40 mL DMF was stirred at ambient temperature for 20 h. Subsequently, water (80 mL) was added and the product was extracted with diethyl ether (3 x 30 mL). The combined organic phases were washed with water (3 x 30 mL) and dried (Na_2SO_4). The solvent was removed *in vacuo* to obtain 1.47 g (99 %) of the pure product as a colorless oil.³⁰²

^1H NMR (400 MHz, CDCl_3) δ / ppm = 3.26 (t, 4H, $\text{CH}_2\text{-N}_3$), 1.60 (quin, 4H, $\text{CH}_2\text{-CH}_2\text{N}_3$), 1.49-1.22 (m, 8H, $(\text{CH}_2)_4$).

^{13}C NMR (100 MHz, CDCl_3) δ / ppm = 51.6 (C_1, C_8), 29.1 (C_2, C_7), 28.9 (C_3, C_6), 26.7 (C_4, C_5).

*α, α' -Diazido-*p*-xylene (14)*

A mixture of sodium azide (4.05 g, 62.30 mmol, 6.20 eq) and α, α' -dibromo-*p*-xylene (2.66 g, 10.06 mmol, 1.00 eq) in 50 mL DMF was stirred at ambient temperature for 20 h. Subsequently, water (80 mL) was added and the product was extracted with diethyl ether (3 x 30 mL). The combined organic phases were washed with water

(30 mL) and dried (Na_2SO_4). The solvent was removed *in vacuo* to obtain 1.72 g (91 %) of the pure product as white crystals.³⁰²

^1H NMR (400 MHz, CDCl_3) δ / ppm = 7.35 (s, 4H, Ph-H), 4.36 (s, 4H, CH_2).

^{13}C NMR (100 MHz, CDCl_3 , δ , ppm): 135.7 (Ph(C_q)), 128.8 (Ph(CH)), 54.5 (CH_2).

2,7-Diazido-9,9-dioctyl fluorene (15)

A mixture of 2,7-dibromo fluorene (3.0 g, 8.98 mmol, 1.0 eq), tetrabutylammonium iodide (334 mg, 0.90 mmol, 0.1 eq) and 30 mL aqueous sodium hydroxide (50%) in a three necked flask and of 1-bromooctane (17.5 g, 90.6 mmol, 10.1 eq) in a second flask was freed from oxygen *via* three consecutive freeze/pump/thaw cycles. The deoxygenized 1-bromooctane was added to the first mixture under an argon atmosphere and the reaction mixture was heated to 70 °C for 2 h under reflux and violent stirring. After cooling to ambient temperature, the aqueous phase was extracted with chloroform (75 mL) and washed with water (3 × 50 mL). The excess of 1-bromooctane was removed by vacuum distillation and the product was purified *via* column chromatography (hexane / chloroform 9:1, R_f = 0.88), affording 5.07 g (99%) of slightly yellow to white crystals of 2,7-dibromo-9,9-dioctyl fluorene.^{303,322}

^1H NMR (400 MHz, CDCl_3) δ / ppm = 7.52 (d, 2H, fluorene- H_3, H_6), 7.45 (d, 4H, fluorene- $\text{H}_1, \text{H}_4, \text{H}_5, \text{H}_8$), 1.99 – 1.84 (m, 4H, fluorene- CH_2), 1.26 – 1.00 (m, 20H, $(\text{CH}_2)_5$), 0.83 (t, 6H, CH_3), 0.65 – 0.50 (m, 2H, $\text{CH}_2\text{-CH}_3$).

^{13}C NMR (100 MHz, CDCl_3) δ / ppm = 152.7 (fluorene($\text{C}_{9a}, \text{C}_{8a}$)), 139.2 (fluorene($\text{C}_{4a}, \text{C}_{4b}$)), 130.3 (fluorene(C_1, C_8)), 126.3 (fluorene(C_4, C_5)), 121.6 (fluorene(C_3, C_6)), 121.3 (fluorene(C_2, C_7)), 55.8 (fluorene(C_9)), 40.3 (octyl(C_1)), 31.9 (octyl(C_6)), 30.0 (octyl(C_3)), 29.3 (d, octyl(C_4, C_5)), 23.8 (octyl(C_2)), 22.7 (octyl(C_7)), 14.2 (octyl(C_8)).

Anhydrous tetrahydrofuran (40 mL) was cooled to -83°C in a flame dried three necked flask under an argon atmosphere when *tert*-butyllithium (14.8 mL, 1.9 M in pentane, 28.1 mmol, 4.6 eq) was added drop wise. After stirring for 15 minutes, 2,7-dibromo-9,9-dioctyl fluorene (3.6 g, 6.6 mmol, 1.0 eq) in 8 mL anhydrous tetrahydrofuran were added drop wise. After an additional 15 min of stirring, *p*-tosylazide (4.4 mL, 28.5 mmol, 4.3 eq) in 3 mL anhydrous THF were slowly added.

The reaction mixture was allowed to stir for 8 h at -83°C; subsequently, 5 mL of a saturated aqueous solution of ammonium chloride was added and the mixture was allowed to warm to ambient temperature overnight. The solvent was removed under reduced pressure, the mixture was extracted with diethyl ether (200 mL) and filtered, washed with brine (3 × 70 mL), dried (Na₂SO₄) and separated from the solvent under reduced pressure. The product was purified *via* column chromatography (hexane, *R_f* = 0.54) and recrystallization from hexane, affording 1.9 g (60%) of **15** as a yellow crystalline product.^{303,322}

¹H NMR (400 MHz, CDCl₃) δ / ppm = 7.60 (d, 2H, fluorene-H₃,H₆), 7.04 – 6.97 (m, 2H, fluorene-H₁,H₈), 6.95 (s, 2H, fluorene-H₄,H₅), 1.98 – 1.86 (m, 4H, fluorene-CH₂), 1.24 – 1.01 (m, 20H, (CH₂)₅), 0.83 (t, 6H, CH₃), 0.64 – 0.51 (m, 4H, CH₂-CH₃).

¹³C NMR (100 MHz, CDCl₃) δ / ppm = 152.7 (fluorene(C_{9a},C_{8a})), 138.9 (fluorene(C_{4a},C_{4b})), 137.8 (fluorene(C₁,C₈)), 120.7 (fluorene(C₄,C₅)), 118.0 (fluorene(C₃,C₆)), 113.7 (fluorene(C₂,C₇)), 55.6 (fluorene(C₉)), 40.5 (octyl(C₁)), 31.9 (octyl(C₆)), 30.0 (octyl(C₃)), 29.3 (octyl(C₄,C₅)), 23.8 (octyl(C₂)), 22.7 (octyl(C₇)), 14.2 (octyl(C₈)).

Phenacylthio acetic acid (16)

Sodium hydroxide (6.2 g, 155.0 mmol, 2.0 eq) was dissolved in 300 mL water, cooled in an ice bath and thioglycolic acid (5.4 mL, 78.0 mmol, 1.0 eq) was slowly added *via* a syringe. Separately, phenacyl chloride (11.9 g, 76.9 mmol, 1.0 eq) was dissolved in 100 mL methanol and slowly added to the reaction mixture. After stirring the mixture at ambient temperature overnight in the dark, it was poured into 200 mL ice and hydrochloric acid (10 mL) was added. The precipitated white solid was separated by filtration, washed with water and dried *in vacuo* to obtain 11.9 g (74 %) of the pure product as a white powder.³¹⁵

¹H NMR (400 MHz, CDCl₃) δ / ppm = 7.96 (d, 2H, Ph-H), 7.59 (t, 1H, Ph-H), 7.48 (t, 2H, Ph-H), 4.06 (s, 2H, CH₂-COOH), 3.37 (s, 2H, CH₂-C(O)-Ph).

Phenacylsulfide benzyl amide (17)

Benzyl amine (2.21 g, 20.67 mmol, 1.1 eq), **16** (4.01 g, 19.07 mmol, 1.0 eq) and 1-ethyl-3-(3-dimethylaminopropyl)carbodiimid hydrochloride (EDC·HCl, 5.51 g,

28.73 mmol, 1.5 eq) were dissolved in 70 mL dried methylene chloride under an argon atmosphere. 4-(dimethyl amino)pyridine (DMAP, 0.28 g, 2.30 mmol, 0.12 eq) was added and the reaction mixture was allowed to stir at ambient temperature for 17 h. Subsequently, water (200 ml) was added, the organic phase was separated and washed with 1N hydrochloric acid (2 x 200 mL), saturated aqueous sodium hydrogen carbonate solution (2 x 200 mL) and dried (MgSO₄). After solvent removal, the product was dried *in vacuo* affording 4.38 g (77 %) of the yellow solid product.²¹²

¹H NMR (400 MHz, CDCl₃) δ / ppm = 7.94 (d, 2H, Ph-H), 7.62 (t, 1H, Ph-H), 7.49 (t, 2H, Ph-H), 7.39 – 7.23 (m, 5H, Ph-H), 7.16 (s, 1H, NH), 4.47 (d, 2H, Ph-C(O)-CH₂), 3.95 (s, 2H, CH₂-C(O)-NH), 3.30 (s, 2H, NH-CH₂-Ph).

Phenacysulfide-N-(3-(triethoxysilyl)propyl)acetamide (18)

In a flame dried SCHLENK flask, **16** (4.94 g, 23.51 mmol, 1.2 eq) was dissolved in 100 mL anhydrous tetrahydrofuran under an argon atmosphere and percolated with nitrogen for 15 min. The mixture was cooled in an ice bath when triethyl amine (2.8 mL, 20.20 mmol, 1.0 eq) and ethyl chloroformate (3.6 mL, 37.82 mmol, 1.9 eq) were slowly added successively, the mixture was stirred for 4 h at 0 °C. After the addition of 3-(triethoxysilyl)propyl)acetamide (4.6 mL, 19.74 mmol, 1.0 eq), the mixture was stirred for 2 h at 0°C and subsequently at ambient temperature overnight. The yellow solution was filtered and the solvent was removed *in vacuo*. The residue was dissolved in ethyl acetate, washed with water, saturated aqueous sodium hydrogen carbonate solution and brine, dried (MgSO₄) and the solvent was removed *in vacuo*. Column chromatography (hexane / ethyl acetate 1:1, R_f = 0.263) afforded 1.074 g (13 %) of the pure product as a colorless oil.¹⁶²

¹H NMR (400 MHz, CDCl₃) δ / ppm = 7.95 (s, 2H, Ph-H), 7.59 (s, 1H, Ph-H), 7.53 – 7.37 (m, 2H, Ph-H), 4.06 – 3.91 (m, 2H, Ph-C(O)-CH₂), 3.90 – 3.60 (m, 6H, Si-O-CH₂), 3.25 (s, 4H, NH-CH₂, CH₂-C(O)-NH), 1.69 – 1.57 (m, 2H, C-CH₂-C), 1.22 (dd, 14.6, 9H, CH₃), 0.75 – 0.57 (m, 2H, CH₂-Si).

¹³C NMR (101 MHz, CDCl₃) δ / ppm = 194.3 (Ph-C(O)), 168.1 (NH-C(O)), 135.2 (Ph(C_q)), 134.0 (Ph-CH), 129.1 – 128.7 (m, Ph(CH)), 58.6 (Si-O-CH₂), 42.4 (NH-CH₂), 38.3 (NH-C(O)-CH₂), 36.1 (Ph-C(O)-CH₂), 23.0 (C-CH₂-C), 18.6 (CH₃), 18.4 (CH₂-Si).

4-(4-Bromobutyl)-4'-methyl-2,2'-bipyridine (19)

In a flame dried three necked round bottom flask, freshly distilled diisopropylamine (0.92 mL, 6.56 mmol, 1.2 eq) was diluted in 7 mL anhydrous tetrahydrofuran under an argon atmosphere and cooled to -83 °C. *n*-Butyllithium (4.12 mL, 1.6 M in hexane, 6.59 mmol, 1.2 eq) was added slowly *via* a syringe. The colorless solution was stirred for 30 min at -83 °C. Subsequently, 1,3-dibromopropane (2.2 mL, 21.67 mmol, 4.0 eq) was added and the mixture was stirred at -83°C for 1 h, then at ambient temperature overnight. After the addition of water (20 mL) and phosphate buffer* (40 mL), the product was extracted with diethyl ether (2 x 100 mL). The combined organic phases were washed with water (100 mL), dried (MgSO₄) and the solvent was evaporated. Column chromatography (ethyl acetate / hexane 1:1, *R_f* = 0.6) afforded 1.19 g (73 %) of the pure product as a colorless solid.³²⁵

*phosphate buffer: 1.06 g potassium phosphate monobasic (KH₂PO₄) and 2.12 g potassium phosphate dibasic (K₂HPO₄) dissolved in 100 mL water.

¹H NMR (400 MHz, CDCl₃) δ / ppm = 8.56 (dd, 2.00H, pyridine-H^{6,6'}), 8.26 (s, 2.00H, pyridine-H^{3,3'}), 7.15 (s, 2.00H, pyridine-H^{5,5'}), 3.43 (t, 2.45H, CH₂Br), 2.74 (t, 2.45H, pyridine-CH₂), 2.44 (s, 2.65H, pyridine-CH₃), 2.02 – 1.74 (m, 4.90H, CH₂).

4-(4-((2E,4E)-Hexa-2,4-dien-1-yloxy)butyl)-4'-methyl-2,2'-bipyridine (20)

A suspension of sodium hydride (0.24 g, 60% in mineral oil, 6.00 mmol, 1.5 eq) in 10 mL DMF was cooled in an ice bath under an argon atmosphere when *trans,trans*-2,4-hexadien-1-ol (0.5 mL, 4.44 mmol, 1.1 eq) was added. The ice bath was removed and the mixture was allowed to stir at ambient temperature for 30 min, then the mixture was again cooled to 0 °C. Sodium iodide (0.03 g, 0.22 mmol, 0.06 eq) and **19** (1.20 g, 3.94 mmol, 1.0 eq) were added. The ice bath was removed and the reaction mixture was stirred at ambient temperature overnight. Phosphate buffer (see synthesis of **19**, 25 mL) were added and the product was extracted with ethyl acetate (3 x 75 mL). The combined organic phases were washed with water (25 mL), dried (Na₂SO₄) and the solvent was evaporated. The crude product was purified *via* column chromatography (hexane / ethyl acetate 1:1, *R_f* = 0.559 and hexane / ethyl acetate 2:1, *R_f* = 0.303) to obtain 0.14 g (11 %) of the pure product as a yellow oil.

^1H NMR (400 MHz, CDCl_3) δ / ppm = 8.54 (s, 2H, pyridine- $\text{H}^{3,3'}$), 8.23 (s, 2H, pyridine- $\text{H}^{6,6'}$), 7.13 (s, 2H, pyridine- $\text{H}^{5,5'}$), 6.24 – 6.11 (m, 1H, vinyl-CH), 6.11 – 5.97 (m, 1H, vinyl-CH), 5.74 – 5.55 (m, 2H, vinyl-CH), 3.95 (d, 2H, O- CH_2 -vinyl), 3.42 (t, 2H, CH_2 -O), 2.72 (t, 2H, pyridine- CH_2), 2.44 (d, 3H, pyridine- CH_3), 1.81-1.59 (m, 7H, CH_2 , CH_3).

^{13}C NMR (101 MHz, CDCl_3) δ / ppm = 156.1 (pyridine- $\text{C}^{2'}$), 156.0 (pyridine- C^2), 152.8 (pyridine- C^4), 149.0 (pyridine- $\text{C}^{6'}$), 149.0 (pyridine- C^6), 148.4 (pyridine- C^4), 133.2 (vinyl-C), 130.9 (vinyl-C), 130.0 (vinyl-C), 127.0 (vinyl-C), 124.8 (pyridine- $\text{C}^{5'}$), 124.1 (pyridine- $\text{C}^{3'}$), 122.2 (pyridine- C^5), 121.5 (pyridine- C^3), 71.4 (O- CH_2 -vinyl), 69.9 (pyridine- CH_2), 35.4 (CH_2 -O), 29.5 (C- CH_2 -C), 27.2 (C- CH_2 -C), 21.3 (pyridine- CH_3), 18.2 (CH_3).

*General procedure for the UV-reaction of **17** with the functionalized dienes (**20** and **22**) affording **23** and **24***

A headspace vial (Pyrex, diameter 20 mm) was equipped with a solution of **17** ($6 \cdot 10^{-5} \text{ mol} \cdot \text{L}^{-1}$) and the diene ($6 \cdot 10^{-5} \text{ mol} \cdot \text{L}^{-1}$) in anhydrous methylene chloride. The vial was crimped air tight and the solution was percolated with argon for 10 min. The solution was irradiated employing a 36 W lamp (Cosmedico, $\lambda_{\text{max}} = 355 \text{ nm}$) for 2 h. After solvent removal, the product was dried *in vacuo*.

23: ^1H NMR (400 MHz, CDCl_3) δ / ppm = 8.85 (s, 2H, pyridine- $\text{H}^{3,3'}$), 8.28 (s, 2H, pyridine- $\text{H}^{6,6'}$), 7.29 (s, 5H, Ph-H), 7.17 (s, 2H, pyridine- $\text{H}^{5,5'}$), 5.92-5.57 (m, 2H, vinyl-CH), 4.48 (s, 2H, Ph- CH_2), 3.97 (s, 3H, thiopyran-CH, O- CH_2), 3.42 (s, 2H, O- CH_2), 2.72 (s, 3H, CH_2 , thiopyran-CH), 2.47 (s, 3H, CH_3), 1.83-1.51 (m, 4H, CH_2), 1.37 (s, 3H, CH_3).

7.3.2. Syntheses of Polymers

P(MMA-GMA)CPDB (P1)

In a SCHLENK flask, methylmethacrylate (MMA, 4.29 g, 30.20 mmol), glycidyl methacrylate (GMA, 6.03 g, 60.22 mmol), azo-bis-(isobutyronitrile) (AIBN, 0.05 g, 0.31 mmol) and cyanoisopropyl dithiobenzoate (CPDB, 0.34 g, 1.52 mmol) were degassed by three consecutive freeze/pump/thaw cycles. The flask was placed in a pre-heated oil bath at 60 °C for 1.5 h. Subsequently, the flask was cooled in liquid nitrogen to stop the polymerization reaction. The polymer was precipitated from diethyl ether, reprecipitated twice (tetrahydrofurane / diethyl ether) and dried *in vacuo*. Conversion (gravimetry) = 38.8 %.

GPC (THF): $M_n = 3600 \text{ g}\cdot\text{mol}^{-1}$, $M_w = 4100 \text{ g}\cdot\text{mol}^{-1}$, $D = 1.14$.

^1H NMR (400 MHz, CDCl_3) δ / ppm = 4.42-4.21 and 3.86-3.70 (m, CO- CH_2 ,_{GMA}), 3.67-3.52 (m, CH_3 ,_{MMA}), 3.20 (s, CH_{GMA}), 2.73 (d, CH_2 ,_{GMA}), 2.11-1.72 (m, CH_2 ,_{backbone}), 1.15-0.74 (m, CH_3 ,_{backbone}).

Molar fraction of GMA comonomer (NMR): 38.1 % (theor.: 34.2 %)

P(MMA-HAzPMA)CPDB (P2)

P(MMA-GMA)CPDB (1.0 g, 3.0 mmol epoxide groups) was dissolved in 100 mL DMF. Sodium azide (1.2 g, 18.1 mmol) and sodium hydrogen carbonate (1.5 g, 18.2 mmol) were added and the mixture was heated at 50 °C for 24 h. The polymer was precipitated from diethyl ether, precipitated twice (tetrahydrofurane / diethyl ether) and dried *in vacuo* to obtain 0.34 g of the product as a white powder.

GPC (THF): $M_n = 4100 \text{ g}\cdot\text{mol}^{-1}$, $M_w = 5300 \text{ g}\cdot\text{mol}^{-1}$, $D = 1.28$.

^1H NMR (400 MHz, CDCl_3) δ / ppm = 4.06 (s, CO- CH_2 and CH-OH), 3.71-3.50 (m, CH_3 ,_{MMA ester}), 3.42 (s, CH_2 - N_3), 2.44-1.67 (m, CH_2 ,_{backbone}), 1.53-0.63 (m, CH_3 ,_{backbone}).

Molar fraction of HAzMA comonomer (NMR): 37.6 % (theor.: 38.1 %)

P(MMA)CPDB (P3)

In a SCHLENK flask, MMA (4.01 g, 40.09 mmol), AIBN (0.013 g, 0.08 mmol) and CPDB (0.11 g, 0.52 mmol) were degassed by three consecutive freeze/pump/thaw cycles. The flask was placed in a pre-heated oil bath at 60 °C for 6 h. Subsequently, the flask

was cooled in liquid nitrogen to stop the polymerization reaction. The polymer was precipitated from hexane, reprecipitated twice (tetrahydrofuran / hexane) and dried *in vacuo*. Conversion (gravimetry) = 44.3 %.

GPC (THF): $M_n = 5000 \text{ g}\cdot\text{mol}^{-1}$, $M_w = 5700 \text{ g}\cdot\text{mol}^{-1}$, $D = 1.15$.

^1H NMR (400 MHz, CDCl_3) δ / ppm = 7.86 (s, Ph-H), 7.65 (d, Ph-H), 7.48 (t, Ph-H), 3.55 (s, $\text{CH}_3\text{-O}$), 2.37 – 0.37 (m, CH, CH_2 backbone, CH_3).

Reaction of **P3** with sodium azide affording **P4**

P3 (250 mg, 0.05 mmol) was dissolved in 1 mL DMF and sodium azide (13 mg, 0.20 mmol) were added. The reaction mixture was allowed to stir for 24 h under ambient conditions until the resulting polymer was precipitated in hexane. The polymer was reprecipitated twice (tetrahydrofuran / hexane) and dried *in vacuo* to obtain 210 mg of a white powder.

GPC (THF): $M_n = 5800 \text{ g}\cdot\text{mol}^{-1}$, $M_w = 7300 \text{ g}\cdot\text{mol}^{-1}$, $D = 1.24$.

^1H NMR (400 MHz, DMSO-d_6) δ / ppm = 7.88 – 7.82 (m, 2.00H, Ph-H), 7.77 – 7.70 (m, 0.98H, Ph-H), 7.63 – 7.56 (m, 2.00H, Ph-H), 3.55 (s, 1229.50H, OCH_3), 2.27 – 0.48 (m, 2167.56H, CH_3 , CH_2 backbone).

Aminolysis of **P3** affording **P5**

In a glass vial, **P3** (200 mg, 0.04 mmol) was dissolved in 1.5 mL anhydrous DMF. The vial was sealed and percolated with argon for 30 min. Subsequently, *n*-butylamine (0.1 mL, 1.01 mmol) was added *via* a syringe. The mixture was allowed to stir at ambient temperature for 24 h. The polymer was precipitated in hexane, reprecipitated twice (tetrahydrofuran / hexane) and dried *in vacuo* to obtain 102 mg of a white powder.

GPC (THF): $M_n = 5100 \text{ g}\cdot\text{mol}^{-1}$, $M_w = 6200 \text{ g}\cdot\text{mol}^{-1}$, $D = 1.23$.

^1H NMR (400 MHz, CDCl_3) δ / ppm = 7.82 – 7.31 (m, Ph-H), 3.69 – 3.46 (m, O- CH_3), 2.10 – 0.61 (m, CH_2 , CH_3 backbone).

P(MMA-AzPMA)CPDB (P6)

In a SCHLENK flask, MMA, 3-azidopropyl methacrylate (AzPMA, **2**), AIBN and CPDB were degassed by three consecutive freeze/pump/thaw cycles. The flask was placed in a pre-heated oil bath at 60 °C for 2 h. Subsequently, the flask was cooled in liquid nitrogen to stop the polymerization reaction. The polymer was precipitated from diethyl ether, reprecipitated twice (THF / diethyl ether) and dried *in vacuo*.

¹H NMR (400 MHz, CDCl₃) δ / ppm = 7.95 – 7.29 (m, Ph-H), 4.15-3.96 (m, O-CH₂, AzPMA), 3.70-3.51 (m, CH₃, MMA), 3.47-3.57 (m, N₃-CH₂, AzPMA), 2.11-1.59 (m, C-CH₂-C_{AzPMA}, CH_{backbone}), 1.14-0.74 (m, CH₃, backbone).

Table 18. Collation of the employed molar amounts of the monomers (MMA, AzPMA), the RAFT agent CPDB and the radical initiator AIBN. Conversion (χ) was determined *via* gravimetry, molar masses and dispersity (M_n , M_w and \mathcal{D}) determined *via* GPC in THF, molar fraction of the functionalized monomer in the copolymer (F_{AzPMA}) was determined *via* ¹H NMR analysis.

	n(MMA)	n(AzPMA)	n(CPDB)	n(AIBN)	χ	M_n	M_w	\mathcal{D}	F_{AzPMA}
	mmol	mmol	mmol	mmol	%	g·mol ⁻¹	g·mol ⁻¹		%
P6-1	40.60	7.25	1.09	0.22	40.1	2700	3500	1.32	16.7
P6-2	45.20	22.43	1.71	0.34	38.7	2800	4000	1.42	34.4

CuAAC Ligation of P6 with propargyl alcohol affording P7

To a solution of copper sulfate (CuSO_4), sodium ascorbate (SA) and **P6** in 4 mL dry DMF, propargyl alcohol (PA) was added. The mixture was allowed to stir at ambient temperature for 24 h, then passed over a short column filled with basic alumina to remove the catalyst. The solvent was evaporated and the product dried *in vacuo*.

^1H NMR (400 MHz, CDCl_3) δ / ppm = 7.95 – 7.29 (m, Ph-H), 4.80 (s, triazole-H), 4.47 (s, $\text{CH}_2\text{-OH}$), 3.98 (s, O- CH_2), 3.72 (m, $\text{CH}_2\text{-triazole}$), 3.67 – 3.47 (m, O- CH_3), 2.30 (s, CH_2), 2.11 – 1.71 (m, $\text{CH}_{\text{backbone}}$), 1.13 – 0.67 (m, $\text{CH}_3, \text{backbone}$).

Table 19. Collation of the employed molar amounts of **P6** (azide groups), CuSO_4 , sodium ascorbate (NA) and propargyl alcohol (PA). Molar masses and dispersity (M_n , M_w and \mathcal{D}) were determined *via* GPC in THF, molar fraction of the functionalized monomer in the copolymer (F_{triazole}) was determined *via* ^1H NMR analysis.

	n(P6-1)	n(P6-2)	n(CuSO₄)	n(NA)	n(PA)	M_n	M_w	\mathcal{D}	F_{triazole}
	mmol	mmol	mmol	mmol	mmol	$\text{g}\cdot\text{mol}^{-1}$	$\text{g}\cdot\text{mol}^{-1}$		%
P7-1	0.43	-	0.044	0.047	0.53	3100	4000	1.31	16.5
P7-2	-	0.42	0.087	0.089	0.46	2700	3600	1.31	34.1

CuAAC Ligation of P6 with 3 affording P8

To a degassed solution of copper iodide (CuI , 4.1 mg, 0.022 mmol), 1,8-diazabicyclo [5.4.0]undec-7-en, (DBU, 8 μL 0.054 mmol) and **P6-1** (50.0 mg, 0.085 mmol azide groups) in 3 mL dry DMF, *N,N'*-bis(2,6-diisopropylphenyl)propiolamidine (**3**, 61.2 mg, 0.103 mmol) was added under an argon atmosphere. The mixture was allowed to stir at ambient temperature for 24 h, then passed over a short column filled with basic alumina to remove the catalyst. The solvent was evaporated and the product dried *in vacuo*.

GPC (THF): $M_n = 3900 \text{ g}\cdot\text{mol}^{-1}$, $M_w = 5100 \text{ g}\cdot\text{mol}^{-1}$, $\mathcal{D} = 1.32$.

P(St-CIMSt)DBTTC (P9)

In a SCHLENK flask, styrene (St), 4-chloromethyl styrene (CIMSt), 1,1'-azobis(cyclohexanecarbonitrile) (VAZO-88) and dibenzyl trithiocarbonate (DBTTC) were degassed by three consecutive freeze/pump/thaw cycles. The flask was placed in a pre-heated oil bath at 80 °C. Subsequently, the flask was cooled in liquid nitrogen to stop the polymerization reaction. The polymer was precipitated from methanol, reprecipitated twice (THF / methanol) and dried *in vacuo*.

¹H NMR (400 MHz, DMSO-d₆) δ / ppm = 7.57 – 6.12 (m, Ph-H), 4.66 (s, CH₂-Cl), 2.45 – 0.81 (m, CH, CH₂ backbone).

Table 20. Collation of the employed molar amounts of the monomers (St, CIMSt), the RAFT agent DBTTC and the radical initiator VAZO-88, as well as the reaction time for the polymerization. Conversion (χ) was determined *via* gravimetry and the molar fraction of the functionalized monomer in the copolymer (F_{Cl}) was determined *via* ¹H NMR analysis.

Polymer	n(St) mmol	n(CIMSt) mmol	n(DBTTC) mmol	n(VAZO-88) mmol	<i>r.t.</i> h	χ %	F_{Cl} %
P9-1	101.0	100.4	3.46	0.70	6	31.4	53.4
P9-2	176.1	30.8	1.03	0.21	20	49.7	17.3
P9-3	144.1	36.0	0.72	0.12	20	n.d.	26.3
P9-4	72.3	48.1	0.60	0.12	20	43.9	45.7
P9-5	57.7	57.7	0.58	0.12	20	51.2	55.6
P9-6	90.2	10.1	0.50	0.10	19.5	54.1	13.4
P9-7	80.1	20.5	0.50	0.10	19.5	48.5	25.7
P9-8	70.1	30.1	0.50	0.10	19.5	39.2	40.1
P9-9	60.1	40.1	0.50	0.10	19	32.3	49.1

Table 21. Molar masses and dispersity (M_n , M_w and \mathcal{D}) of P9 determined *via* GPC in THF,

Polymer	M_n g·mol ⁻¹	M_w g·mol ⁻¹	\mathcal{D}	Polymer	M_n g·mol ⁻¹	M_w g·mol ⁻¹	\mathcal{D}
P9-1	2800	3600	1.29	P9-6	8500	10300	1.21
P9-2	9800	11500	1.18	P9-7	8600	10600	1.23
P9-3	5800	7500	1.29	P9-8	6800	8600	1.26
P9-4	8200	10200	1.25	P9-9	6500	8400	1.29
P9-5	9700	12300	1.27				

P(St-AzMSt) (P10)

A solution of **P9** and sodium azide in DMF was stirred at ambient temperature for 48 h. The polymer was precipitated from methanol, reprecipitated twice (THF / methanol) and dried *in vacuo*.

¹H NMR (400 MHz, DMSO-d₆) δ / ppm = 7.50 – 6.10 (m, Ph-H), 4.33 (s, CH₂-N₃), 2.43 – 0.89 (m, CH, CH₂ backbone).

Table 22. Collation of the employed molar amounts of **P9** (azide groups), sodium azide (NaN₃) and the volume of DMF. Molar masses and dispersity (M_n , M_w and \mathcal{D}) were determined *via* GPC in THF, molar fraction of the functionalized monomer in the copolymer (F_{azide}) was determined *via* ¹H NMR analysis.

Polymer	P9	n(P9) mmol	n(NaN ₃) mmol	V(DMF) mL	M_n g·mol ⁻¹	M_w g·mol ⁻¹	\mathcal{D}	F_{azide} %
P10-1	P9-1	22.6	137.0	150	2800	3800	1.37	48.2
P10-2	P9-2	15.3	98.1	100	7600	10100	1.34	16.5
P10-3	P9-3	7.57	46.9	100	5200	7100	1.37	25.1
P10-4	P9-4	15.3	91.2	150	7200	9700	1.33	45.0
P10-5	P9-5	15.3	138.1	200	8100	10700	1.33	54.6
P10-6	P9-6	3.69	21.7	50	7300	9400	1.29	12.3
P10-7	P9-7	7.0	41.1	80	7100	9300	1.31	24.6
P10-8	P9-8	6.3	37.2	70	5700	7600	1.33	38.5
P10-9	P9-9	7.3	46.5	90	5600	7500	1.35	48.1

Ligation of P10-1 with propargyl alcohol affording P11

To a solution of copper sulfate (CuSO_4), sodium ascorbate (NA) and **P10-1** in 2 mL dry DMF, propargyl alcohol (PA) was added. The mixture was allowed to stir at ambient temperature for 24 h, then passed over a short column filled with basic alumina to remove the catalyst. The polymer was precipitated from water, reprecipitated twice (THF / water) and dried *in vacuo*.

^1H NMR (400 MHz, DMSO-d_6) δ / ppm = 7.97 (s, triazole-H), 7.46 – 5.98 (m, Ph-H), 5.49 (s, CH_2 -triazole), 5.24 (s, OH), 4.54 (s, CH_2 -OH), 2.38-0.69 (m, CH_2 , CH).

Table 23. Collation of the employed molar amounts of **P10-1** (azide groups), CuSO_4 , sodium ascorbate (NA) and propargyl alcohol (PA). Molar masses and dispersity (M_n , M_w and \mathcal{D}) were determined *via* GPC in THF, molar fractions of the ligated monomer (F_{triazole}) and the remaining azide functionalized comonomer (F_{azide}) in the copolymer was determined *via* ^1H NMR analysis.

	n(P10-1)	n(CuSO₄)	n(NA)	n(PA)	M_n	M_w	\mathcal{D}	F_{triazole}	F_{azide}
	mmol	mmol	mmol	mmol	$\text{g}\cdot\text{mol}^{-1}$	$\text{g}\cdot\text{mol}^{-1}$		%	%
P11-1	0.81	0.32	0.32	0.24	4700	6900	1.48	14.9	31.47
P11-2	0.81	0.32	0.32	0.39	5300	8000	1.52	24.2	22.41
P11-3	0.80	0.32	0.33	0.55	6100	9300	1.52	33.9	12.66
P11-4	0.80	0.32	0.32	0.80	7100	9900	1.40	47.0	0

Ligation of **P10-1** with **3** affording **P12**

To a degassed solution of copper iodide (CuI), 1,8-diazabicyclo[5.4.0]undec-7-en, (DBU) and **P10** in a mixture of dry DMF and dry THF, *N,N'*-bis(2,6-diisopropylphenyl) propiolamidine (**3**) was added under an argon atmosphere. The mixture was allowed to stir at ambient temperature for 24 h, then passed over a short column filled with basic alumina to remove the catalyst. The polymer was precipitated from water, reprecipitated twice (THF / water) and dried *in vacuo*. ¹H NMR analysis was conducted by the institute of inorganic chemistry (S. Gallardo-Gonzalez).

¹H-NMR (300 MHz, THF-*d*₈) δ / = 0.73 (br, CH(CH₃)₂), 0.97 (br, CH(CH₃)₂), 1.26 (br, CH(CH₃)₂), 1.50–2.26 (br), 2.99 (br, CH(CH₃)₂), 3.49 (br, CH(CH₃)₂), 5.23 (br, benzyl-CH₂), 6.15 (br, triazole-CH), 6.39–7.21 (br, Ar-H), 8.04 ppm (br, NH).

Table 24. Collation of the employed molar amounts of **P10** (azide groups), CuI, sodium ascorbate (NA) and amidine ligand (**3**) as well as the volume of DMF.

	P10	n(P10) mmol	n(3) mmol	n(CuI) mmol	n(DBU) mmol	V(DMF) mL	V(THF) mL
P12-1	P10-2	2.93	3.65	4.39	4.49	40	15
P12-2	P10-3	2.14	2.68	3.20	3.35	20	15
P12-3	P10-4	1.45	1.47	3.27	1.88	50	15
P12-4	P10-5	1.30	1.43	1.58	1.61	50	15

Table 25. Molar masses and dispersity (M_n , M_w and \mathcal{D}) were determined *via* GPC in THF. Absolute weight-averaged molar masses (M_w^{SLS}) were obtained from SLS measurements. Molar fractions of the ligated monomer (F_3) in the copolymer was determined *via* ¹H NMR analysis

	M_n g·mol ⁻¹	M_w g·mol ⁻¹	\mathcal{D}	M_w^{SLS} g·mol ⁻¹	F_3 %
P12-1	10100	13200	1.30	19600	16.5
P12-2	8000	10200	1.28	17300	26.3
P12-3	12500	15600	1.25	29400	45.4
P12-4	12900	16400	1.27	29800	57.3

Rhodium-loading of P12 affording P13

The loading of the polymers **P12-1** to **P12-4** and the NMR analyses were conducted by the institute of inorganic chemistry (S. Gallardo Gonzalez). The amidine-functionalized polymer **P12** (600 mg, 0.5 mmol) and $\text{LiN}(\text{SiMe}_3)_2 \cdot 0.62 \text{ Et}_2\text{O}$ (107.4 mg, 0.5 mmol) were dissolved in toluene (40 ml) and stirred at room temperature overnight. Then, a solution of $[\text{Rh}(\text{cod})\text{Cl}]_2$ (124.4 mg, 0.25 mmol) in toluene (40 ml) was added at room temperature. After stirring for 72 h, the bright yellow, turbid solution was filtered and washed with a concentrated aqueous solution of NH_4Cl . The organic phase was dried over MgSO_4 , filtered, and the volatiles were evaporated *in vacuo* to leave a thick, yellow film on the glass walls. The residue was redissolved in a mixture of acetone / Et_2O (5:1) and filtered again. After filtration, all volatiles were evaporated *in vacuo* and the residue triturated with methanol overnight, to precipitate **P4** as a fine, yellow powder.

^1H NMR (300 MHz, $\text{THF-}d_8$) δ / ppm = 0.72 (br; $\text{CH}(\text{CH}_3)_2$), 0.95 (br; $\text{CH}(\text{CH}_3)_2$), 1.26 (br; $\text{CH}(\text{CH}_3)_2$), 1.57 (br; $\text{CH}(\text{CH}_3)_2$), 1.78–1.94 (br), 2.29 (br; COD- CH_2), 2.99 (br; $\text{CH}(\text{CH}_3)_2$), 3.18 (br; $\text{CH}(\text{CH}_3)_2$), 3.49 (br; $\text{CH}(\text{CH}_3)_2$), 4.25 (br; COD- CH), 5.20 (br; Benzyl- CH_2), 5.63 (br; triazole- CH), 6.14 (br; triazole- CH), 6.50–7.20 (br, Ar- H); 8.05 (br; NH).

Table 26. Absolute-weight averaged molar masses (M_w^{SLS}) of **P13** obtained *via* SLS.

Polymer	P13-1	P13-2	P13-3	P13-4
$M_w^{\text{SLS}} / \text{g}\cdot\text{mol}^{-1}$	32100	46500	42000	45600

Ligation of P10 with ethynyl pyridine (4) affording P14

To a solution of copper sulfate (CuSO₄), sodium ascorbate (NA) and **P10** in dry DMF, propargyl alcohol (PA) was added. The mixture was allowed to stir at ambient temperature for 24 h, then passed over a short column filled with basic alumina to remove the catalyst. The polymer was precipitated from water, reprecipitated twice (THF / water) and dried *in vacuo*.

¹H NMR (400 MHz, CDCl₃) δ / ppm = 8.55 (s, Py-H), 8.22 (s, Py-H), 8.04 (s, triazole-H), 7.78 (s, Py-H), 7.35 – 6.17 (m, Py-H, Ph-H), 5.44 (s, CH₂-triazole), 2.44 – 1.02 (m, CH₂, CH backbone).

Table 27. Collation of the employed molar amounts of **P10** (azide groups), CuSO₄, sodium ascorbate (NA) and ethynyl pyridine (**3**).

	P10	n(P10) mmol	n(3) mmol	n(CuSO₄) mmol	n(NA) mmol
P14-1	P10-6	0.33	0.42	0.07	0.07
P14-2	P10-7	1.26	1.57	0.25	0.25
P14-3	P10-8	1.85	3.00	0.37	0.37
P14-4	P10-9	2.21	2.76	0.44	0.44

Table 28. Molar masses and dispersity (M_n , M_w and \mathcal{D}) determined *via* GPC in THF, molar fractions of the ligated monomer (F_{triazole}) in the copolymer was determined *via* ¹H NMR analysis. Absolute weight-averaged molar masses (M_w^{SLS}) determined *via* SLS in DMAc.

	M_n g·mol ⁻¹	M_w g·mol ⁻¹	\mathcal{D}	M_w^{SLS} g·mol ⁻¹	F_{triazole} %
P14-1	7600	10000	1.31	n.d.	12.4
P14-2	7900	10100	1.27	14600	24.9
P14-3	6600	8500	1.28	13000	38.6
P14-4	6100	7800	1.27	13400	47.5

Palladium loading of P14 affording P15

The loading of the polymers **P14-1** to **P14-4**, NMR and elemental analyses were conducted by the institute of inorganic chemistry (C. Kiefer). Under a nitrogen atmosphere a mixture of **P14** and [Pd(cod)Cl₂] (1.0 eq relative to pyridine groups) in CH₂Cl₂ was stirred at ambient temperature for 16 h. The formed precipitate was collected by filtration, washed with CH₂Cl₂ and *n*-pentane and dried *in vacuo*.

¹H NMR (DMSO-d₆) δ / ppm = 9.24 (s, triazole-H), 8.79 (s, pyridine-H), 8.17 (s, pyridine-H), 7.78 - 6.10 (m, pyridine-H, Ph-H), 5.76 (s, CH₂-triazole), 2.42 - 0.54 (m, CH₂, CH backbone).

Elemental analysis: **P15-2**: found C, 61.40; H, 4.804; N, 7.50, S, 0.389 %; **P15-3**: found C, 54.67; H, 4.25; N, 9.03; S, 0.395 %; **P15-4**: found C, 51.85; H, 3.99; N, 10.03; S, 0.372 %.

Table 29. Absolute-weight averaged molar masses (M_w^{SLS}) of **P15** determined *via* SLS in DMAc. Molar fraction of the functionalized monomer (F_y) was obtained from ¹H NMR analysis. The loading efficiency was determined *via* NMR (f^{NMR}) and elemental analysis (f^{EA})

Polymer	P15-1	P15-2	P15-3	P15-4
$M_w^{\text{SLS}} / \text{g}\cdot\text{mol}^{-1}$	15600	20400	19100	n.d.
$F_y / \%$	10.7	24.8	37.8	45.8
$f^{\text{NMR}} / \%$	88.5	84.0	76.3	72.1
$f^{\text{EA}} / \%$	n.d.	83.5	76.5	71.1

General procedure for the poly(CuAAC) ligation to afford P16 – P20

Except the reactions with copper(II)sulfate as the catalyst, all reactions were conducted under an inert atmosphere with previously degassed solutions. A solution of 0.2 mol·L⁻¹ dialkyne (**5** or **6**) and 0.2 mol·L⁻¹ diazide (**13**, **14**, or **15**), 0.2 eq of the copper salt and the ligand or base, respectively, in DMF or THF was stirred at ambient temperature for 100 h. Subsequently, aqueous ammonium hydroxide was added to stop the reaction and the reaction mixture was passed over a small column filled with neutral alumina to remove the copper catalyst. The solvent was removed under reduced pressure and the resulting polymers were dried *in vacuo*.

P20: ¹H NMR (400 MHz, CDCl₃) δ / ppm = 8.82 (s, 2H, triazole-H), 8.25 (d, 2H, Py-H), 8.05 – 7.70 (m, 8H, Py-H, fluorene-H), 2.06 (s, 4H, octyl-H), 1.15 – 1.02 (m, 20H, octyl-H), 0.79 – 0.65 (m, 10H, octyl-H).

¹³C NMR (100 MHz, CDCl₃) δ / ppm = 153.2 (fluorene(C_{9a},C_{8a})), 150.0 (Py(C₂,C₆)), 149.0 (Py(C₄)), 140.5 (fluorene(C_{4a},C_{4b})), 138.2 (triazole(C_q)), 136.6 (fluorene(C₁,C₈)), 121.3 (Py(C₃,C₅)), 120.2 (d, triazole(CH), fluorene(C₄,C₅)), 119.5 (fluorene(C₃,C₆)), 115.5 (fluorene(C₂,C₇)), 56.4 (fluorene(C₉)), 40.4 (octyl(C₁)), 31.8 (octyl(C₆)), 30.0 (octyl(C₃)), 29.3 (d, octyl(C₄,C₅)), 24.0 (octyl(C₂)), 22.6 (octyl(C₇)), 14.1 (octyl(C₈)).

Elemental analysis: found C, 74.28; H, 7.50; N, 15.71%, C₃₈H₄₅N₇ requires C, 76.09, H, 7.56; N, 16.35%.

7.3.3. Surface Preparation

Substrate preparation (S1)

One side polished silicon wafers were sonicated in ethyl acetate for 15 min, rinsed with ethyl acetate and acetone and dried in a stream of nitrogen. Dry samples were exposed to air plasma (25 W) for 10 min just before silanization.

Preparation of the phenacylsulfide-SAM (S2)

Silane **18** was dissolved in extra-dry toluene ($1 \text{ mg}\cdot\text{mL}^{-1}$) and percolated with N_2 . The substrate was placed in a headspace vial (Pyrex, diameter 20 mm), crimped air-tight and flushed with nitrogen. 1 mL of the filtered silane solution was added and the sample was heated in the oven at $50 \text{ }^\circ\text{C}$ for 2 h and subsequently at ambient temperature overnight. The wafer was rinsed with toluene, sonicated for 10 min. in toluene, washed with toluene, acetone and water and dried in a stream of nitrogen.

General procedure for the spatially resolved UV-reaction (S3,S5,S7)

The wafer (**S2**) was placed under the shadow mask upright in a headspace vial (Pyrex, diameter 20 mm), crimped air-tight and flushed with nitrogen. The degassed diene solution (5 mL, $2.5 \text{ mg}\cdot\text{mL}^{-1}$ in methylene chloride) was added. The vial was irradiated in the photo-reactor employing a UV lamp (Cosmedico) emitting in the range of $\lambda = 320 \text{ nm}$ and 420 nm with the maximum emission at $\lambda_{\text{max}} = 355 \text{ nm}$. The wafer was washed with CH_2Cl_2 , sonicated in CH_2Cl_2 , rinsed with CH_2Cl_2 and dried in a stream of nitrogen.

Metal loading of the ligand-modified surfaces (S4,S6)

The wafer (**S3** or **S5**) was placed in a headspace vial (Pyrex, diameter 20 mm), crimped air-tight and flushed with nitrogen. The metal solution (1 mL, **S4**: $3 \text{ mg}\cdot\text{mL}^{-1}$ $\text{Pd}(\text{cod})\text{Cl}_2$ in anhydrous methylene chloride; **S6**: $3 \text{ mg}\cdot\text{mL}^{-1}$ $[\text{Au}(\text{tht})\text{Cl}]$ in anhydrous methylene chloride) was added and the mixture was allowed to react overnight. The wafer was washed with CH_2Cl_2 , sonicated in CH_2Cl_2 , rinsed with CH_2Cl_2 and dried in a stream of nitrogen.

References

1. G. Gasser and N. Metzler-Nolte, *Curr. Opin. Chem. Biol.*, **2012**, *16*, 84-91.
2. R. H. Crabtree, *Organometallics*, **2011**, *30*, 17-19.
3. E. A. Hillard and G. r. Jaouen, *Organometallics*, **2011**, *30*, 20-27.
4. A. L. Noffke, A. Habtemariam, A. M. Pizarro and P. J. Sadler, *Chem. Commun.*, **2012**, *48*, 5219-5246.
5. W.-Y. Wong and C.-L. Ho, *Acc. Chem. Res.*, **2010**, *43*, 1246-1256.
6. D. J. Cole-Hamilton, *Science*, **2003**, *299*, 1702-1706.
7. M. Heitbaum, F. Glorius and I. Escher, *Angew. Chem. Int. Ed.*, **2006**, *45*, 4732-4762.
8. A. Zamboulis, N. Moitra, J. J. E. Moreau, X. Cattoen and M. Wong Chi Man, *J. Mater. Chem.*, **2010**, *20*, 9322-9338.
9. A. Schätz, O. Reiser and W. J. Stark, *Chem. Eur. J.*, **2010**, *16*, 8950-8967.
10. H. Li, presented in part at the 2013 10th International Bhurban Conference on Applied Sciences and Technology (IBCAST), 15-19 Jan. 2013, 2013.
11. V. T. Avanesyan and E. G. Vodkailo, *Tech. Phys. Lett.*, **2011**, *37*, 817-819.
12. J. J. Walsh, Q. Zeng, R. J. Forster and T. E. Keyes, *Photochem. Photobiol. Sci.*, **2012**, *11*, 1547-1557.

13. W. Feng, Y. Zhang, Z. Zhang, P. Su, X. Lu, J. Song, D. Fan, W.-K. Wong, R. A. Jones and C. Su, *J. Mater. Chem. C*, **2014**, *2*, 1489-1499.
14. M. Singh, H. M. Haverinen, P. Dhagat and G. E. Jabbour, *Adv. Mater.*, **2010**, *22*, 673-685.
15. D. Qin, Y. Xia and G. M. Whitesides, *Nat. Protocols*, **2010**, *5*, 491-502.
16. C. Weder, *J. Inorg. Organomet. Polym.*, **2006**, *16*, 101-113.
17. D. Astruc, E. Boisselier and C. Ornelas, *Chem. Rev.*, **2010**, *110*, 1857-1959.
18. J. G. Hardy, *Chem. Soc. Rev.*, **2013**, *42*, 7881-7899.
19. C. Tse, K. Cheng and W. Chan, *J. Inorg. Organomet. Polym.*, **2008**, *18*, 59-68.
20. L. Ren, J. Zhang, C. G. Hardy, S. Ma and C. Tang, *Macromol. Rapid Commun.*, **2012**, *33*, 510-516.
21. B. Chen and H. F. Sleiman, *Macromolecules*, **2004**, *37*, 5866-5872.
22. Y. Yang, Z. Xie and C. Wu, *Macromolecules*, **2002**, *35*, 3426-3432.
23. L. Ren, C. G. Hardy, S. Tang, D. B. Doxie, N. Hamidi and C. Tang, *Macromolecules*, **2010**, *43*, 9304-9310.
24. P. Chadha and P. J. Ragogna, *Chem. Commun.*, **2011**, *47*, 5301-5303.
25. C. G. Hardy, L. Ren, T. C. Tamboue and C. Tang, *J. Polym. Sci., Part A: Polym. Chem.*, **2011**, *49*, 1409-1420.
26. C. Herfurth, D. Voll, J. Buller, J. Weiss, C. Barner-Kowollik and A. Laschewsky, *J. Polym. Sci., Part A: Polym. Chem.*, **2012**, *50*, 108-118.
27. Y. Yan, J. Zhang, Y. Qiao and C. Tang, *Macromol. Rapid Commun.*, **2014**, *35*, 254-259.
28. Y. Yan, J. Zhang, Y. Qiao, M. Ganewatta and C. Tang, *Macromolecules*, **2013**, *46*, 8816-8823.
29. G. N. Tew, K. A. Aamer and R. Shunmugam, *Polymer*, **2005**, *46*, 8440-8447.
30. S. Bode, R. K. Bose, S. Matthes, M. Ehrhardt, A. Seifert, F. H. Schacher, R. M. Paulus, S. Stumpf, B. Sandmann, J. Vitz, A. Winter, S. Hoeppener, S. J. Garcia, S. Spange, S. van der Zwaag, M. D. Hager and U. S. Schubert, *Polym. Chem.*, **2013**, *4*, 4966-4973.
31. A. C. Jackson, F. L. Beyer, S. C. Price, B. C. Rinderspacher and R. H. Lambeth, *Macromolecules*, **2013**, *46*, 5416-5422.
32. B. Happ, C. Friebe, A. Winter, M. D. Hager and U. S. Schubert, *Eur. Polym. J.*, **2009**, *45*, 3433-3441.
33. M. Lammens, J. Skey, S. Wallyn, R. O'Reilly and F. Du Prez, *Chem. Commun.*, **2010**, *46*, 8719.
34. C. Ott, C. Ulbricht, R. Hoogenboom and U. S. Schubert, *Macromol. Rapid Commun.*, **2012**, *33*, 556-561.

-
35. L. M. Dupray, M. Devenney, D. R. Striplin and T. J. Meyer, *J. Am. Chem. Soc.*, **1997**, *119*, 10243-10244.
 36. C. N. Fleming, L. M. Dupray, J. M. Papanikolas and T. J. Meyer, *J. Phys. Chem. A*, **2002**, *106*, 2328-2334.
 37. J. N. Younathan, S. F. McClanahan and T. J. Meyer, *Macromolecules*, **1989**, *22*, 1048-1054.
 38. L. M. Dupray and T. J. Meyer, *Inorg. Chem.*, **1996**, *35*, 6299-6307.
 39. X.-Y. Wang, A. Kimyonok and M. Weck, *Chem. Commun.*, **2006**, 3933-3935.
 40. Y. Sun, Z. Chen, E. Puodziukynaite, D. M. Jenkins, J. R. Reynolds and K. S. Schanze, *Macromolecules*, **2012**, *45*, 2632-2642.
 41. J. Karim, S. Binauld, W. Scarano and M. H. Stenzel, *Polym. Chem.*, **2013**.
 42. M. A. R. Meier, B. G. G. Lohmeijer and U. S. Schubert, *Macromol. Rapid Commun.*, **2003**, *24*, 852-857.
 43. G. J. Zhou, W. Y. Wong, C. Ye and Z. Lin, *Adv. Funct. Mater.*, **2007**, *17*, 963-975.
 44. J. Mei, K. Ogawa, Y.-G. Kim, N. C. Heston, D. J. Arenas, Z. Nasrollahi, T. D. McCarley, D. B. Tanner, J. R. Reynolds and K. S. Schanze, *ACS Appl. Mater. Interfaces*, **2009**, *1*, 150-161.
 45. K. Sonogashira, S. Kataoka, S. Takahashi and N. Hagihara, *J. Organomet. Chem.*, **1978**, *160*, 319-327.
 46. S. Takahashi, H. Morimoto, E. Murata, S. Kataoka, K. Sonogashira and N. Hagihara, *J. Polym. Sci.: Polym. Chem. Ed.*, **1982**, *20*, 565-573.
 47. S. Takahashi, E. Murata, K. Sonogashira and N. Hagihara, *J. Polym. Sci.: Polym. Chem. Ed.*, **1980**, *18*, 661-669.
 48. K. Sonogashira, K. Ohga, S. Takahashi and N. Hagihara, *J. Organomet. Chem.*, **1980**, *188*, 237-243.
 49. R. D. Markwell, I. S. Butler, A. K. Kakkar, M. S. Khan, Z. H. Al-Zakwani and J. Lewis, *Organometallics*, **1996**, *15*, 2331-2337.
 50. J. Lewis, M. S. Khan, A. K. Kakkar, B. F. G. Johnson, T. B. Marder, H. B. Fyfe, F. Wittmann, R. H. Friend and A. E. Dray, *J. Organomet. Chem.*, **1992**, *425*, 165-176.
 51. W.-Y. Wong and S.-Y. Poon, *J. Inorg. Organomet. Polym.*, **2008**, *18*, 155-162.
 52. S.-Y. Poon, W.-Y. Wong, K.-W. Cheah and J.-X. Shi, *Chem. Eur. J.*, **2006**, *12*, 2550-2563.
 53. K. A. Bunten and A. K. Kakkar, *J. Mater. Chem.*, **1995**, *5*, 2041-2043.
 54. M. S. Khan, M. R. A. Al-Mandhary, M. K. Al-Suti, A. K. Hisahm, P. R. Raithby, B. Ahrens, M. F. Mahon, L. Male, E. A. Marseglia, E. Tedesco, R. H. Friend, A. Kohler, N. Feeder and S. J. Teat, *J. Chem. Soc., Dalton Trans.*, **2002**, 1358-1368.

55. N. Chawdhury, A. Köhler, R. H. Friend, M. Younus, N. J. Long, P. R. Raithby and J. Lewis, *Macromolecules*, **1998**, *31*, 722-727.
56. N. Chawdhury, A. Köhler, R. H. Friend, W.-Y. Wong, J. Lewis, M. Younus, P.P.Raithby, T. C. Corcoran, M. R. A. Al-Mandhary and M. S. Khna, *J. Chem. Phys.*, **1999**, *110*, 4963-4970.
57. C.-L. Ho and W.-Y. Wong, *Coord. Chem. Rev.*, **2011**, *255*, 2469-2502.
58. N. J. Long and C. K. Williams, *Angew. Chem. Int. Ed.*, **2003**, *42*, 2586-2617.
59. S. Takahashi, Y. Takai, H. Morimoto and K. Sonogashira, *J. Chem. Soc., Chem. Commun.*, **1984**, 3-5.
60. M. S. Khan, N. A. Pasha, A. K. Kakkar, P. R. Raithby, J. Lewis, K. Fuhrmann and R. H. Friend, *J. Mater. Chem.*, **1992**, *2*, 759-760.
61. H. T. Chan, C. S. K. Mak, A. B. Djurišić and W. K. Chan, *Macromol. Chem. Phys.*, **2011**, *212*, 774-784.
62. C. Friebe, H. Görls, M. Jäger and U. S. Schubert, *Eur. J. Inorg. Chem.*, **2013**, *2013*, 4191-4202.
63. C.-S. Wu, Y.-T. Lee and Y. Chen, *Polym. Chem.*, **2012**, *3*, 2776-2784.
64. V. Chandrasekhar and R. Thirumoorathi, *Dalton Trans.*, **2010**, *39*, 2684-2691.
65. D. A. McMorran and P. J. Steel, *Inorg. Chem. Commun.*, **1999**, *2*, 368-370.
66. T. Stoll, M. Gennari, J. Fortage, C. E. Castillo, M. Rebarz, M. Sliwa, O. Poizat, F. Odobel, A. Deronzier and M. N. Collomb, *Angew. Chem. Int. Ed.*, **2014**, *53*, 1654-1658.
67. C.-Q. Zhao, M. Jennings and R. Puddephatt, *J. Inorg. Organomet. Polym.*, **2008**, *18*, 143-148.
68. C. Friebe, A. Wild, J. Perelaer and U. S. Schubert, *Macromol. Rapid Commun.*, **2012**, *33*, 503-509.
69. A. Wild, F. Schlütter, G. M. Pavlov, C. Friebe, G. Festag, A. Winter, M. D. Hager, V. Cimrová and U. S. Schubert, *Macromol. Rapid Commun.*, **2010**, *31*, 868-874.
70. G. Gröger, W. Meyer-Zaika, C. Böttcher, F. Gröhn, C. Ruthard and C. Schmuck, *J. Am. Chem. Soc.*, **2011**, *133*, 8961-8971.
71. F. S. Han, M. Higuchi and D. G. Kurth, *Adv. Mater.*, **2007**, *19*, 3928-3931.
72. I. Welterlich and B. Tieke, *Macromolecules*, **2011**, *44*, 4194-4203.
73. M. Burnworth, L. Tang, J. R. Kumpfer, A. J. Duncan, F. L. Beyer, G. L. Fiore, S. J. Rowan and C. Weder, *Nature*, **2011**, *472*, 334-337.
74. B. Schulze, C. Friebe, S. Hoepfener, G. M. Pavlov, A. Winter, M. D. Hager and U. S. Schubert, *Macromol. Rapid Commun.*, **2012**, *33*, 597-602.

-
75. G. R. Whittell, M. D. Hager, U. S. Schubert and I. Manners, *Nature Materials*, **2011**, *10*, 176-188.
 76. T. J. Kealy and P. L. Pauson, *Nature*, **1951**, 1039-1040.
 77. S. A. Miller, J. A. Tebboth and J. F. Tremaine, *J. Chem. Soc.*, **1952**, 632-635.
 78. V. V. Korshak, S. L. Sosin and V. P. Alekseeva, *Dokl. Akad. Nauk SSSR*, **1960**, *132*, 360.
 79. H. Rosenberg and E. W. Neuse, *J. Organomet. Chem.*, **1966**, *6*, 76-85.
 80. J. B. Gilroy, A. D. Russell, A. J. Stonor, L. Chabanne, S. Baljak, M. F. Haddow and I. Manners, *Chemical Science*, **2012**, *3*, 830-841.
 81. M. Tanabe and I. Manners, *J. Am. Chem. Soc.*, **2004**, *126*, 11434-11435.
 82. M. Erhard, K. Lam, M. Haddow, G. R. Whittell, W. E. Geiger and I. Manners, *Polym. Chem.*, **2014**, *5*, 1264.
 83. K. Temple, F. Jäkle, J. B. Sheridan and I. Manners, *J. Am. Chem. Soc.*, **2001**, *123*, 1355-1364.
 84. Y. Ni, R. Rulken and I. Manners, *J. Am. Chem. Soc.*, **1996**, *118*, 4102-4114.
 85. D. E. Herbert, U. F. J. Mayer, J. B. Gilroy, M. J. López-Gómez, A. J. Lough, J. P. H. Charmant and I. Manners, *Chem. Eur. J.*, **2009**, *15*, 12234-12246.
 86. W. Y. Chan, A. J. Lough and I. Manners, *Organometallics*, **2007**, *26*, 1217-1225.
 87. S. K. Patra, G. R. Whittell, S. Nagiah, C. L. Ho, W. Y. Wong and I. Manners, *Chem. Eur. J.*, **2010**, *16*, 3240-3250.
 88. N. S. Jeong and I. Manners, *Macromol. Chem. Phys.*, **2009**, *210*, 1080-1086.
 89. A. Bartole-Scott, H. Braunschweig, T. Kupfer, M. Lutz, I. Manners, T. L. Nguyen, K. Radacki and F. Seeler, *Chemistry*, **2006**, *12*, 1266-1273.
 90. M. Tamm, A. Kunst and E. Herdtweck, *Chem. Commun.*, **2005**, 1729-1731.
 91. H. Braunschweig, C. J. Adams, T. Kupfer, I. Manners, R. M. Richardson and G. R. Whittell, *Angew. Chem. Intern. Ed.*, **2008**, *47*, 3826-3829.
 92. U. Vogel, A. J. Lough and I. Manners, *Angew. Chem. Int. Ed.*, **2004**, *43*, 3321-3325.
 93. U. F. J. Mayer, J. B. Gilroy, D. O'Hare and I. Manners, *J. Am. Chem. Soc.*, **2009**, *131*, 10382-10383.
 94. J. B. Gilroy, S. K. Patra, J. M. Mitchels, M. A. Winnik and I. Manners, *Angew. Chem. Int. Ed.*, **2011**, *50*, 5851-5855.
 95. M. A. Buretea and T. D. Tilley, *Organometallics*, **1997**, 1507-1510.
 96. G. Masson, A. J. Lough and I. Manners, *Macromolecules*, **2008**, *41*, 539-547.
 97. H. Ebadi-Dehaghani and S. Mehdipour-Ataei, *J. Inorg. Organomet. Polym.*, **2011**, *22*, 223-234.
 98. C. M. Casado, M. Moran, J. Losada and I. Cuadrado, *Inorg. Chem.*, **1995**, *34*, 1668-1680.

99. M. Cazacu, A. Vlad, M. Marcu, C. Racles, A. Airinei and G. Munteanu, *Macromolecules*, **2006**, 3786-3793.
100. D. Chao, X. Lu, J. Chen, X. Liu, W. Zhang and Y. Wei, *Polymer*, **2006**, 47, 2643-2648.
101. J. Ma, M. Vollmann, H. Menzel, S. Pohle and H. Butenschön, *J. Inorg. Organomet. Polym.*, **2008**, 18, 41-50.
102. S. E. Brady, G. V. Shultz and D. R. Tyler, *J. Inorg. Organomet. Polym.*, **2010**, 20, 511-518.
103. C. Lang, D. Voll, A. J. Inglis, N. Dingenouts, A. S. Goldmann, L. Barner and C. Barner-Kowollik, *Macromol. Chem. Phys.*, **2011**, 212, 831-839.
104. D. Astruc, C. Ornelas and J. Ruiz Aranzaes, *J. Inorg. Organomet. Polym.*, **2008**, 18, 4-17.
105. A. W. Leung and M. MacLachlan, *J. Inorg. Organomet. Polym.*, **2007**, 17, 57-89.
106. K. Yagi, M. Ito and H. Houjou, *Macromol. Rapid Commun.*, **2012**, 33, 540-544.
107. A. C. W. Leung, J. K. H. Hui, J. H. Chong and M. J. MacLachlan, *Dalton Trans.*, **2009**, 5199-5210.
108. R. I. Kureshy, N.-u. H. Khan, S. H. R. Abdi, S. Singh, I. Ahmed and R. V. Jasra, *J. Mol. Catal. A: Chem.*, **2004**, 218, 141-146.
109. A. C. W. Leung and M. J. MacLachlan, *J. Mater. Chem.*, **2007**, 17, 1923-1932.
110. J. Jiang, A. C. W. Leung and M. J. MacLachlan, *Dalton Trans.*, **2010**, 39, 6503-6508.
111. B. J. Holliday, T. B. Stanford and T. M. Swager, *Chem. Mater.*, **2006**, 18, 5649-5651.
112. M. L. Mejía, K. Agapiou, X. Yang and B. J. Holliday, *J. Am. Chem. Soc.*, **2009**, 131, 18196-18197.
113. M. Cazacu, M. Marcu, A. Vlad and M. Vasiliu, *J. Macromol. Sci. Part A*, **2004**, 41, 565-575.
114. E. Scamporrino, S. Bazzano, D. Vitalini and P. Mineo, *Macromol. Rapid Commun.*, **2003**, 24, 236-241.
115. N. Senthilkumar, A. Raghavan and A. S. Nasar, *Macromol. Chem. Phys.*, **2005**, 206, 2490-2500.
116. A. B. Powell, B. C.W. and A. H. Cowley, *J. Am. Chem. Soc.*, **2009**, 131, 18232-18233.
117. A. B. Powell, C. W. Bielawski and A. H. Cowley, *J. Am. Chem. Soc.*, **2010**, 132, 10184-10194.
118. S. He, A. A. Buelt, J. M. Hanley, B. P. Morgan, A. G. Tennyson and R. C. Smith, *Macromolecules*, **2012**, 45, 6344-6352.
119. W. K. Cheung, C. S. Mak and W. K. Chan, *Macromol Rapid Commun*, **2012**, 33, 585-591.
120. S. C. Yu, S. Hou and W. K. Chan, *Macromolecules*, **1999**, 32, 5251-5256.
121. W. Kin Chan, P. King Ng, X. Gong and S. Hou, *J. Mater. Chem.*, **1999**, 9, 2103-2108.
122. Q. Wang, L. Wang and L. Yu, *J. Am. Chem. Soc.*, **1998**, 120, 12860-12868.

-
123. L. Trouillet, A. De Nicola and S. Guillerez, *Chem. Mater.*, **2000**, *12*, 1611-1621.
 124. K. D. Ley, C. E. Whittle, M. D. Bartberger and K. S. Schanze, *J. Am. Chem. Soc.*, **1997**, *119*, 3423-3424.
 125. P. K. Ng, X. Gong, S. H. Chan, L. S. M. Lam and W. K. Chan, *Chem. Eur. J.*, **2001**, *7*, 4358-4367.
 126. S. C. Yu, X. Gong and W. K. Chan, *Macromolecules*, **1998**, *31*, 5639-5646.
 127. G. C. Cameron and G. P. Pickup, *Chem. Commun.*, **1997**, 303-304.
 128. S. C. Yu, S. Hou and W. K. Chan, *Macromolecules*, **2000**, *33*, 3259-3273.
 129. E. Stratakis, A. Ranella and C. Fotakis, *Biomicrofluidics*, **2011**, *5*, 13411.
 130. H. Kaji, G. Camci-Unal, R. Langer and A. Khademhosseini, *Biochimica et Biophysica Acta 1810*, **2011**, *1810*, 239-250.
 131. T. J. Park, K.-B. Lee, S. J. Lee, J. P. Park, Z.-W. Lee, S. Y. Lee and I. S. Choi, *J. Am. Chem. Soc.*, **2004**, *126*, 10512-10513.
 132. T. J. Park, S. Y. Lee, S. J. Lee, J. P. Park, K. S. Yang, K.-B. Lee, S. Ko, J. B. Park, T. Kim, S. K. Kim, Y. B. Shin, B. H. Chung, S.-J. Ku, D. H. Kim and I. S. Choi, *Anal. Chem.*, **2006**, *78*, 7197-7205.
 133. T. Chen, R. Ferris, J. Zhang, R. Ducker and S. Zauscher, *Prog. Polym. Sci.*, **2010**, *35*, 94-112.
 134. E. Ueda and P. A. Levkin, *Adv. Mater.*, **2013**, *25*, 1234-1247.
 135. J. Gunho, C. Minhyeok, C. Chu-Young, K. J. Ho, P. Woojin, L. Sangchul, H. Woong-Ki, K. Tae-Wook, P. Seong-Ju, H. B. Hee, K. Y. Ho and L. Takhee, *Nanotechnology*, **2010**, *21*, 175201.
 136. J. J. Gassensmith, P. M. Erne, W. F. Paxton, M. Frasconi, M. D. Donakowski and J. F. Stoddart, *Adv. Mater.*, **2013**, *25*, 223-226.
 137. J. T. Fourkas, *J. Phys. Chem. Lett.*, **2010**, *1*, 1221-1227.
 138. B. Derby, *Annu. Rev. Mater. Res.*, **2010**, *40*, 395-414.
 139. Z. P. Tolstyka, W. Richardson, E. Bat, C. J. Stevens, D. P. Parra, J. K. Dozier, M. D. Distefano, B. Dunn and H. D. Maynard, *ChemBioChem*, **2013**, *14*, 2464-2471.
 140. T. Gao, X. Wang, B. Yu, Q. Wei, Y. Xia and F. Zhou, *Langmuir*, **2013**, *29*, 1054-1060.
 141. Y. Kikkawa, M. Fukuda, N. Ichikawa, A. Kashiwada, K. Matsuda, M. Kaneshato and T. Hiraishi, *J. Mater. Chem. A*, **2013**, *1*, 4667-4670.
 142. K. Ueno, S. Takabatake, K. Onishi, H. Itoh, Y. Nishijima and H. Misawa, *Appl. Phys. Lett.*, **2011**, *99*.
 143. Y. Hoshi, Y. Xu and C. K. Ober, *Polymer*, **2013**, *54*, 1762-1767.

144. T. A. Martin, S. R. Caliyari, P. D. Williford, B. A. Harley and R. C. Bailey, *Biomaterials*, **2011**, *32*, 3949-3957.
145. A. Bernard, J. P. Renault, B. Michel, H. R. Bosshard and E. Delamarque, *Adv. Mater.*, **2000**, *12*, 1067-1070.
146. J.-L. Zhuang, D. Ar, X.-J. Yu, J.-X. Liu and A. Terfort, *Adv. Mater.*, **2013**, *25*, 4631-4635.
147. A. Garcia, N. Hanifi, B. Joussetme, P. Jégou, S. Palacin, P. Viel and T. Berthelot, *Adv. Funct. Mater.*, **2013**, *23*, 3668-3674.
148. N. Komuro, S. Takaki, K. Suzuki and D. Citterio, *Anal. Bioanal. Chem.*, **2013**, *405*, 5785-5805.
149. Y. Hu, J. S. Li, W. T. Yang and F. J. Xu, *Thin Solid Films*, **2013**, *534*, 325-333.
150. R. T. Chen, S. Marchesan, R. A. Evans, K. E. Styan, G. K. Such, A. Postma, K. M. McLean, B. W. Muir and F. Caruso, *Biomacromolecules*, **2012**, *13*, 889-895.
151. R. Ganesan, S. Y. Yoo, J.-H. Choi, S. Y. Lee and J.-B. Kim, *J. Mater. Chem.*, **2008**, *18*, 703-709.
152. O. Norberg, I. H. Lee, T. Aastrup, M. Yan and O. Ramström, *Biosens. Bioelectron.*, **2012**, *34*, 51-56.
153. T. Tischer, T. K. Claus, M. Bruns, V. Trouillet, K. Linkert, C. Rodriguez-Emmenegger, A. S. Goldmann, S. Perrier, H. G. Börner and C. Barner-Kowollik, *Biomacromolecules*, **2013**, *14*, 4340-4350.
154. S. Hansson, T. Tischer, A. S. Goldmann, A. Carlmark, C. Barner-Kowollik and E. Malmstrom, *Polym. Chem.*, **2012**, *3*, 307-309.
155. T. M. Herne and M. J. Tarlov, *J. Am. Chem. Soc.*, **1997**, *119*, 8916-8920.
156. E. W. L. Chan and L. Yu, *Langmuir*, **2001**, *18*, 311-313.
157. M. J. Salierno, A. J. García and A. del Campo, *Adv. Funct. Mater.*, **2013**, *23*, 5974-5980.
158. O. El Zubir, I. Barlow, E. Ul-Haq, H. A. Tajuddin, N. H. Williams and G. J. Leggett, *Langmuir*, **2012**, *29*, 1083-1092.
159. R. M. Hensarling, V. A. Doughty, J. W. Chan and D. L. Patton, *J. Am. Chem. Soc.*, **2009**, *131*, 14673-14675.
160. P. Jonkheijm, D. Weinrich, M. Köhn, H. Engelkamp, P. C. M. Christianen, J. Kuhlmann, J. C. Maan, D. Nüsse, H. Schroeder, R. Wacker, R. Breinbauer, C. M. Niemeyer and H. Waldmann, *Angew. Chem. Int. Ed.*, **2008**, *47*, 4421-4424.
161. T. Pauloehrl, G. Delaittre, V. Winkler, A. Welle, M. Bruns, H. G. Börner, A. M. Greiner, M. Bastmeyer and C. Barner-Kowollik, *Angew. Chem. Int. Ed.*, **2012**, *51*, 1071-1074.
162. M. Glassner, K. K. Oehlenschlaeger, A. Welle, M. Bruns and C. Barner-Kowollik, *Chem. Commun.*, **2013**, *49*, 633-635.

-
163. M. Dietrich, G. Delaittre, J. P. Blinco, A. J. Inglis, M. Bruns and C. Barner-Kowollik, *Adv. Funct. Mater.*, **2012**, *22*, 304-312.
164. E. Blasco, M. Piñol, L. Oriol, B. V. K. J. Schmidt, A. Welle, V. Trouillet, M. Bruns and C. Barner-Kowollik, *Adv. Funct. Mater.*, **2013**, *23*, 4011-4019.
165. S. V. Orski, A. A. Poloukhine, S. Arumugam, L. Mao, V. V. Popik and J. Locklin, *J. Am. Chem. Soc.*, **2010**, *132*, 11024-11026.
166. C. M. Preuss, T. Tischer, C. Rodriguez-Emmenegger, M. M. Zieger, M. Bruns, A. S. Goldmann and C. Barner-Kowollik, *J. Mater. Chem. B*, **2014**, *2*, 36-40.
167. C. N. Bowman, B. D. Fairbanks, N. B. Cramer and K. S. Anseth, *Polymer Preprints*, **2010**, *51*, 703-704.
168. F. Goethals, S. Martens, P. Espeel, O. van den Berg and F. E. Du Prez, *Macromolecules*, **2013**, *47*, 61-69.
169. D. P. Nair, N. B. Cramer, T. F. Scott, R. Shandas and C. N. Bowman, *Polymer Preprints*, **2011**, *52*, 391-392.
170. D. J. Hall, H. M. Van Den Berghe and A. P. Dove, *Polym. Int.*, **2011**, *60*, 1149-1157.
171. A. H. Soeriyadi, G.-Z. Li, S. Slavin, M. W. Jones, C. M. Amos, C. R. Becer, M. R. Whittaker, D. M. Haddleton, C. Boyer and T. P. Davis, *Polym. Chem.*, **2011**, *2*, 815-822.
172. R. Pötzsch, H. Komber, B. C. Stahl, C. J. Hawker and B. I. Voit, *Macromol. Rapid Commun.*, **2013**, *34*, 1772-1778.
173. C. E. Hoyle and C. N. Bowman, *Angew. Chem.*, **2010**, *122*, 1584-1617.
174. A. B. Lowe, *Polym. Chem.*, **2010**, *1*, 17-36.
175. A. B. Lowe, C. E. Hoyle and C. N. Bowman, *J. Mater. Chem.*, **2010**, *20*, 4745-4750.
176. M. J. Kade, D. J. Burke and C. J. Hawker, *J. Polym. Sci., Part A: Polym. Chem.*, **2010**, *48*, 743-750.
177. A. Dondoni, *Angew. Chem. Int. Ed.*, **2008**, *47*, 8995-8997.
178. B. D. Fairbanks, E. A. Sims, K. S. Anseth and C. N. Bowman, *Macromolecules*, **2010**, *43*, 4113-4119.
179. L. M. Campos, K. L. Killops, R. Sakai, J. M. J. Paulusse, D. Damiron, E. Drockenmuller, B. W. Messmore and C. J. Hawker, *Macromolecules*, **2008**, *41*, 7063-7070.
180. K. L. Killops, L. M. Campos and C. J. Hawker, *J. Am. Chem. Soc.*, **2008**, *130*, 5062-5064.
181. T. R. Hayes, P. A. Lyon, E. Silva-Lopez, B. Twamley and P. D. Benny, *Inorg. Chem.*, **2013**, *52*, 3259-3267.
182. N. B. Cramer, J. P. Scott and C. N. Bowman, *Macromolecules*, **2002**, *35*, 5361-5365.
183. N. B. Cramer, S. K. Reddy, M. Cole, C. Hoyle and C. N. Bowman, *J. Polym. Sci., Part A: Polym. Chem.*, **2004**, *42*, 5817-5826.

184. J. P. Lafleur, R. Kwapiszewski, T. G. Jensen and J. P. Kutter, *Analyst*, **2013**, *138*, 845-849.
185. A. S. Goldmann, M. Glassner, A. J. Inglis and C. Barner-Kowollik, *Macromol. Rapid Commun.*, **2013**, *34*, 810-849.
186. J. E. Hein and V. V. Fokin, *Chem. Soc. Rev.*, **2010**, *39*, 1302-1315.
187. J. A. Johnson, M. G. Finn, J. T. Koberstein and N. J. Turro, *Macromol. Rapid Commun.*, **2008**, *29*, 1052-1072.
188. B. J. Adzima, Y. Tao, C. J. Kloxin, C. A. DeForest, K. S. Anseth and C. N. Bowman, *Nature Chemistry*, **2011**, *3*, 256-259.
189. J. S. Clovis, A. Eckell, R. Huisgen and R. Sustmann, *Chem. Ber.*, **1967**, *100*, 60-70.
190. W. Song, Y. Wang, J. Qu and Q. Lin, *J. Am. Chem. Soc.*, **2008**, *130*, 9654-9655.
191. W. Song, Y. Wang, J. Qu, M. M. Madden and Q. Lin, *Angew. Chem. Int. Ed.*, **2008**, *47*, 2832-2835.
192. J. Wang, W. Zhang, W. Song, Y. Wang, Z. Yu, J. Li, M. Wu, L. Wang, J. Zang and Q. Lin, *J. Am. Chem. Soc.*, **2010**, *132*, 14812-14818.
193. Y. Wang, W. Song, W. J. Hu and Q. Lin, *Angew. Chem. Int. Ed.*, **2009**, *48*, 5330-5333.
194. M. M. Madden, C. I. Rivera Vera, W. Song and Q. Lin, *Chem. Commun.*, **2009**, 5588-5590.
195. Y. Wang, C. I. Rivera Vera and Q. Lin, *Org. Lett.*, **2007**, *9*, 4155-4158.
196. Y. Wang, W. J. Hu, W. Song, R. K. V. Lim and Q. Lin, *Org. Lett.*, **2008**, *10*, 3725-3728.
197. S. Ito, Y. Tanaka, A. Kakehi and K.-i. Kondo, *Bull. Chem. Soc. Jpn.*, **1976**, *49*, 1920-1923.
198. C. Rodriguez-Emmenegger, C. M. Preuss, B. Yameen, O. Pop-Georgievski, M. Bachmann, J. O. Mueller, M. Bruns, A. S. Goldmann, M. Bastmeyer and C. Barner-Kowollik, *Adv. Mater.*, **2013**, *25*, 6123-6127.
199. H. C. Kolb, M. G. Finn and K. B. Sharpless, *Angew. Chem.*, **2001**, *113*, 2056-2075.
200. C. Barner-Kowollik, F. E. Du Prez, P. Espeel, C. J. Hawker, T. Junkers, H. Schlaad and W. van Camp, *Angew. Chem. Int. Ed.*, **2011**, *50*, 60-62.
201. X.-L. Sun, C. L. Stabler, C. S. Cazalis and E. L. Chaikof, *Bioconjugate Chem.*, **2005**, *17*, 52-57.
202. G. Jarre, Y. Liang, P. Betz, D. Lang and A. Krueger, *Chem. Commun.*, **2011**, *47*, 544-546.
203. H. Kaper, A. Grandjean, C. Weidenthaler, F. Schüth and F. Goettmann, *Chem. Eur. J.*, **2012**, *18*, 4099-4106.
204. P. G. Sammes, *Tetrahedron*, **1976**, *32*, 405-422.
205. J. L. Charlton and M. M. Alauddin, *Tetrahedron*, **1987**, *43*, 2873-2889.
206. J. L. Segura and N. Martín, *Chem. Rev.*, **1999**, *99*, 3199-3246.

-
207. S. M. Mellows and P. G. Sammes, *J. Chem. Soc. D*, **1971**, 21-22.
208. S. Arumugam and V. V. Popik, *J. Am. Chem. Soc.*, **2011**, *133*, 5573-5579.
209. T. Gruending, K. K. Oehlenschlaeger, E. Frick, M. Glassner, C. Schmid and C. Barner-Kowollik, *Macromol. Rapid Commun.*, **2011**, *32*, 807-812.
210. M. Glassner, K. K. Oehlenschlaeger, T. Gruending and C. Barner-Kowollik, *Macromolecules*, **2011**, *44*, 4681-4689.
211. M. Winkler, J. O. Mueller, K. K. Oehlenschlaeger, L. Montero de Espinosa, M. A. R. Meier and C. Barner-Kowollik, *Macromolecules*, **2012**, *45*, 5012-5019.
212. T. Pauloehrl, A. Welle, K. K. Oehlenschlaeger and C. Barner-Kowollik, *Chemical Science*, **2013**, *4*, 3503-3507.
213. K. Kalyanasundaram and M. Grätzel, *Coord. Chem. Rev.*, **1998**, *177*, 347-414.
214. C. del Pozo, A. Corma, M. Iglesias and F. I. Sánchez, *Organometallics*, **2010**, *29*, 4491-4498.
215. A. Fernandes, P. Hensenne, B. Mathy, W. Guo, B. Nysten, A. M. Jonas and O. Riant, *Chem. Eur. J.*, **2012**, *18*, 788-792.
216. K. S. Joya, N. K. Subbaiyan, F. D'Souza and H. J. M. de Groot, *Angew. Chem. Int. Ed.*, **2012**, *51*, 9601-9605.
217. J. D. Slinker, A. A. Gorodetsky, M. S. Lowry, J. Wang, S. Parker, R. Rohl, S. Bernhard and G. G. Malliaras, *J. Am. Chem. Soc.*, **2004**, *126*, 2763-2767.
218. S. Kabehie, A. Z. Stieg, M. Xue, M. Liong, K. L. Wang and J. I. Zink, *J. Phys. Chem. Lett.*, **2010**, *1*, 589-593.
219. P. Calvert, *Chem. Mater.*, **2001**, *13*, 3299-3305.
220. H.-H. Lee, K.-S. Chou and K.-C. Huang, *Nanotechnology*, **2005**, *16*, 2436.
221. B. K. Park, D. Kim, S. Jeong, J. Moon and J. S. Kim, *Thin Solid Films*, **2007**, *515*, 7706-7711.
222. S. H. Ko, H. Pan, C. P. Grigoropoulos, C. K. Luscombe, J. M. J. Fréchet and D. Poulikakos, *Nanotechnology*, **2007**, *18*, 345202.
223. M. K. Corbierre, J. Beerens and R. B. Lennox, *Chem. Mater.*, **2005**, *17*, 5774-5779.
224. T. Bhuvana and G. U. Kulkarni, *ACS Nano*, **2008**, *2*, 457-462.
225. B. Radha, S. Kiruthika and G. U. Kulkarni, *J. Am. Chem. Soc.*, **2011**, *133*, 12706-12713.
226. H. Xu, R. Hong, X. Wang, R. Arvizo, C. You, B. Samanta, D. Patra, M. T. Tuominen and V. M. Rotello, *Adv. Mater.*, **2007**, *19*, 1383-1386.
227. M. Kimura, H. Yamagiwa, D. Asakawa, M. Noguchi, T. Kurashina, T. Fukawa and H. Shirai, *ACS Appl. Mater. Interfaces*, **2010**, *2*, 3714-3717.

228. T. Koepplmayr, M. Cardinale, T. Rath, G. Trimmel, S. Rentenberger, E. Zojer, W. Kern and T. Griesser, *Macromol. Chem. Phys.*, **2012**, *213*, 367-373.
229. M. Miyachi, M. Ohta, M. Nakai, Y. Kubota, Y. Yamanoi, T. Yonezawa and H. Nishihara, *Chem. Lett.*, **2008**, *37*, 404-405.
230. C. Haensch, M. Chipper, C. Ulbricht, A. Winter, S. Hoepfener and U. S. Schubert, *Langmuir*, **2008**, *24*, 12981-12985.
231. L. Kosbar, C. Srinivasan, A. Afzali, T. Graham, M. Copel and L. Krusin-Elbaum, *Langmuir*, **2006**, *22*, 7631-7638.
232. P. C. Mondal, J. Yekkoni Lakshmanan, H. Hamoudi, M. Zharnikov and T. Gupta, *J. Phys. Chem. C*, **2011**, *115*, 16398-16404.
233. P. F. Driscoll, E. F. Douglass, M. Phewluangdee, E. R. Soto, C. G. F. Cooper, J. C. MacDonald, C. R. Lambert and W. G. McGimpsey, *Langmuir*, **2008**, *24*, 5140-5145.
234. C. Duan, K.-S. Chen, F. Huang, H.-L. Yip, S. Liu, J. Zhang, A. K. Y. Jen and Y. Cao, *Chem. Mater.*, **2010**, *22*, 6444-6452.
235. T. Bilkay, K. Schulze, T. Egorov-Brening, A. Bohn and S. Janietz, *Macromol. Chem. Phys.*, **2012**, *213*, 1970-1978.
236. H.-Y. Yu, Z.-Y. Qin, L.-F. Wang and Z. Zhou, *Carbohydr. Polym.*, **2012**, *87*, 2447-2454.
237. Y. Li, Y. Qian, T. Liu, G. Zhang and S. Liu, *Biomacromolecules*, **2012**, *13*, 3877-3886.
238. G. D. Fu, L. Q. Xu, F. Yao, K. Zhang, X. F. Wang, M. F. Zhu and S. Z. Nie, *ACS Appl. Mater. Interfaces*, **2009**, *1*, 239-243.
239. C.-J. Huang and F.-C. Chang, *Macromolecules*, **2009**, *42*, 5155-5166.
240. C. Li, Z. Ge, J. Fang and S. Liu, *Macromolecules*, **2009**, *42*, 2916-2924.
241. F. D. Jochum and P. Theato, *Chem. Soc. Rev.*, **2013**, *42*, 7468-7483.
242. V. Ladmiral, G. Mantovani, G. J. Clarkson, S. Cauet, J. L. Irwin and D. M. Haddleton, *J. Am. Chem. Soc.*, **2006**, *128*, 4823-4830.
243. K. A. Aamer and G. N. Tew, *J. Polym. Sci., Part A: Polym. Chem.*, **2007**, *45*, 5618-5625.
244. R. Kakuchi and P. Theato, *Macromolecules*, **2012**, *45*, 1331-1338.
245. J. Liu, R. C. Li, G. J. Sand, V. Bulmus, T. P. Davis and H. D. Maynard, *Macromolecules*, **2012**, *46*, 8-14.
246. J. D. Flores, J. Shin, C. E. Hoyle and C. L. McCormick, *Polym. Chem.*, **2010**, *1*, 213-220.
247. G. M. Miyake, R. A. Weitekamp, V. A. Piunova and R. H. Grubbs, *J. Am. Chem. Soc.*, **2012**, *134*, 14249-14254.
248. E. Yavuz, Y. Gursel and B. F. Senkal, *Desalination*, **2013**, *310*, 145-150.
249. Y. Tang, L. Liu, J. Wu and J. Duan, *J. Colloid Interface Sci.*, **2013**, *397*, 24-31.

-
250. B. Gacal, H. Durmaz, M. A. Tasdelen, G. Hizal, U. Tunca, Y. Yagci and A. L. Demirel, *Macromolecules*, **2006**, *39*, 5330-5336.
251. T. Dispinar, R. Sanyal and A. Sanyal, *J. Polym. Sci., Part A: Polym. Chem.*, **2007**, *45*, 4545-4551.
252. O. Altintas, J. Willenbacher, K. N. R. Wuest, K. K. Oehlenschlaeger, P. Krolla-Sidenstein, H. Gliemann and C. Barner-Kowollik, *Macromolecules*, **2013**, *46*, 8092-8101.
253. M. Tonga, N. Cengiz, M. M. Kose, T. Dede and A. Sanyal, *J. Polym. Sci., Part A: Polym. Chem.*, **2010**, *48*, 410-416.
254. A. Bousquet, C. Barner-Kowollik and M. H. Stenzel, *J. Polym. Sci., Part A: Polym. Chem.*, **2010**, *48*, 1773-1781.
255. A. Dag, H. Durmaz, E. Demir, G. Hizal and U. Tunca, *J. Polym. Sci., Part A: Polym. Chem.*, **2008**, *46*, 6969-6977.
256. G. Delaittre, T. Pauloehrl, M. Bastmeyer and C. Barner-Kowollik, *Macromolecules*, **2012**, *45*, 1792-1802.
257. J. Ma, J. W. Bartels, Z. Li, K. Zhang, C. Cheng and K. L. Wooley, *Aust. J. Chem.*, **2010**, *63*, 1159-1163.
258. S. Paul and B. Rånby, *J. Polym. Sci.: Polym. Chem. Ed.*, **1976**, *14*, 2449-2461.
259. J. Xu, J. He, D. Fan, X. Wang and Y. Yang, *Macromolecules*, **2006**, *39*, 8616-8624.
260. B. S. Sumerlin, N. V. Tsarevsky, G. Louche, R. Y. Lee and K. Matyjaszewski, *Macromolecules*, **2005**, *38*, 7540-7545.
261. A. P. Vogt and B. S. Sumerlin, *Soft Matter*, **2009**, *5*, 2347-2351.
262. J. R. Hagadorn and J. Arnold, *J. Organomet. Chem.*, **2001**, *637-639*, 521-530.
263. C. Jones, D. P. Mills and A. Stasch, *Dalton Trans.*, **2008**, 4799-4804.
264. F. J. Lahoz, A. Tiripicchio, M. T. Camellini, L. A. Oro and M. T. Pinillos, *J. Chem. Soc., Dalton Trans.*, **1985**, 1487-1493.
265. D. Matioszek, N. Saffon, J.-M. Sotiropoulos, K. Miqueu, A. Castel and J. Escudié, *Inorg. Chem.*, **2012**, *51*, 11716-11721.
266. A. J. Scheel, H. Komber and B. I. Voit, *Macromol. Rapid Commun.*, **2004**, *25*, 1175-1180.
267. D. Astruc, L. Liang, A. Rapakousiou and J. Ruiz, *Acc. Chem. Res.*, **2011**, *45*, 630-640.
268. A. Carlmark, C. Hawker, A. Hult and M. Malkoch, *Chem. Soc. Rev.*, **2009**, *38*, 352-362.
269. P. Antoni, D. Nystrom, C. J. Hawker, A. Hult and M. Malkoch, *Chem. Commun.*, **2007**, 2249-2251.
270. P. Antoni, M. J. Robb, L. Campos, M. Montanez, A. Hult, E. Malmström, M. Malkoch and C. J. Hawker, *Macromolecules*, **2010**, *43*, 6625-6631.

271. C. N. Urbani, C. A. Bell, D. Lonsdale, M. R. Whittaker and M. J. Monteiro, *Macromolecules*, **2007**, *41*, 76-86.
272. C. Ornelas, J. Ruiz Aranzaes, E. Cloutet, S. Alves and D. Astruc, *Angew. Chem. Int. Ed.*, **2007**, *46*, 872-877.
273. K. Oberg, Y. Hed, I. Joelsson Rahmn, J. Kelly, P. Lowenhielm and M. Malkoch, *Chem. Commun.*, **2013**, *49*, 6938-6940.
274. H. W. Ooi, K. S. Jack, H. Peng and A. K. Whittaker, *Polym. Chem.*, **2013**, *4*, 4788-4800.
275. H. Altin, I. Kosif and R. Sanyal, *Macromolecules*, **2010**, *43*, 3801-3808.
276. Y. Tang, C. K. W. Jim, Y. Liu, L. Ye, A. Qin, J. W. Y. Lam, C. Zhao and B. Z. Tang, *Appl. Mater. Interf.*, **2010**, *2*, 566-574.
277. J. M. Spruell, M. Wolffs, F. A. Leibfarth, B. C. Stahl, J. Heo, L. A. Connal, J. Hu and C. J. Hawker, *J. Am. Chem. Soc.*, **2011**, *133*, 16698-16706.
278. M. A. Karim, Y.-R. Cho, J. S. Park, S. C. Kim, H. J. Kim, J. W. Lee, Y.-S. Gal and S.-H. Jin, *Chem. Comm.*, **2008**, *16*, 1929.
279. B. Kolli, S. P. Mishra, M. P. Joshi, S. R. Mohan, T. S. Dhami and A. B. Samui, *Advanced Materials Research*, **2012**, *584*, 8-12.
280. Z. Chen, D. R. Dreyer, Z.-q. Wu, K. M. Wiggins, Z. Jiang and C. W. Bielawski, *J. Polym. Sci., Part A: Polym. Chem.*, **2011**, *49*, 1421-1426.
281. Y. Nagao and A. Takasu, *J. Polym. Sci., Part A: Polym. Chem.*, **2010**, *48*, 4207-4218.
282. I. Molina-Pinilla, M. Bueno-Martínez, K. Hakkou and J. A. Galbis, *J. Polym. Sci., Part A: Polym. Chem.*, **2014**, *52*, 629-638.
283. W. Li, T. Tian, W. Zhu, J. Cui, Y. Ju and G. Li, *Polym. Chem.*, **2013**, *4*, 3057-3068.
284. F. Deng, B. Xu, Y. Gao, Z. Liu, D. Yang and H. Li, *J. Polym. Sci., Part A: Polym. Chem.*, **2012**, *50*, 3767-3774.
285. Y. Gao, L. Chen, Z. Zhang, W. Gu and Y. Li, *Biomacromolecules*, **2010**, *11*, 3102-3111.
286. N. G. Angelo and P. S. Arora, *J. Am. Chem. Soc.*, **2005**, *127*, 17134-17135.
287. Y. Wang, D. Wang, J. Han and S. Feng, *J. Organomet. Chem.*, **2011**, *696*, 1874-1878.
288. P. L. Golas, N. V. Tsarevsky, B. S. Sumerlin and K. Matyjaszewski, *Macromolecules*, **2006**, *39*, 6451-6457.
289. S. Diez-Gonzalez, E. C. Escudero-Adan, J. Benet-Buchholz, E. D. Stevens, A. M. Z. Slawin and S. P. Nolan, *Dalton Trans.*, **2010**, *39*, 7595-7606.
290. S. Hohloch, D. Scheiffele and B. Sarkar, *Eur. J. Inorg. Chem.*, **2013**, *22-23*, 3956-3965.
291. S. Hohloch, C.-Y. Su and B. Sarkar, *Eur. J. Inorg. Chem.*, **2011**, *20*, 3067-3075.
292. C. Gibard, D. Avignant, F. Cisnetti and A. Gautier, *Organometallics*, **2012**, *31*, 7902-7908.

-
293. J. M. Collinson, J. D. Wilton-Ely and S. Diez-Gonzalez, *Chem. Commun.*, **2013**, 49, 11358-11360.
294. C. Girard, E. Önen, M. Aufort, S. Beauviere, E. Samson and J. Herscovici, *Org. Lett.*, **2006**, 8, 1689-1692.
295. B. C. Boren, S. Narayan, L. K. Rasmussen, L. Zhang, H. Zhao, Z. Lin, G. Jia and V. V. Fokin, *J. Am. Chem. Soc.*, **2008**, 130, 8923-8930.
296. A. Qin, J. W. Y. Lam, C. K. W. Jim, L. Zhang, J. Yan, M. Häussler, J. Liu, Y. Dong, D. Liang, E. Chen, G. Jia and B. Z. Tang, *Macromolecules*, **2008**, 41, 3808-3822.
297. A. Qin, C. K. W. Jim, W. Lu, J. W. Y. Lam, M. Häussler, Y. Dong, H. H. Y. Sung, I. D. Williams, G. K. L. Wong and B. Z. Tang, *Macromolecules*, **2007**, 40, 2308-2317.
298. H. Li, H. Wu, E. Zhao, J. Li, J. Z. Sun, A. Qin and B. Z. Tang, *Macromolecules*, **2013**, 46, 3907-3914.
299. H. Li, J. Mei, J. Wang, S. Zhang, Q. Zhao, Q. Wei, A. Qin, J. Sun and B. Z. Tang, *Sci. China Chem.*, **2011**, 54, 611-616.
300. A. Qin, L. Tang, J. W. Y. Lam, C. K. W. Jim, Y. Yu, H. Zhao, J. Sun and B. Z. Tang, *Adv. Funct. Mater.*, **2009**, 19, 1891-1900.
301. P. J. Flory, *Chem. Rev.*, **1946**, 39, 137-197.
302. J. R. Thomas, X. Liu and P. J. Hergenrother, *J. Am. Chem. Soc.*, **2005**, 127, 12434-12435.
303. P. Gerstel, S. Klumpp, F. Hennrich, O. Altintas, T. R. Eaton, M. Mayor, C. Barner-Kowollik and M. M. Kappes, *Polym. Chem.*, **2012**, 3, 1966-1970.
304. M. Alajarin, C. Lopez-Leonardo, P. Llamas-Lorente, D. Bautista and P. G. Jones, *Dalton Trans.*, **2003**, 426-434.
305. S. Jie, P. Ai, Q. Zhou and B.-G. Li, *J. Organomet. Chem.*, **2011**, 696, 1465-1473.
306. D. Das, G. K. Rao and A. K. Singh, *Organometallics*, **2009**, 28, 6054-6058.
307. T. Pauloehrl, A. Welle, M. Bruns, K. Linkert, H. G. Börner, M. Bastmeyer, G. Delaittre and C. Barner-Kowollik, *Angew. Chem. Int. Ed.*, **2013**, 52, 9714-9718.
308. P. Hazarika, J. M. Behrendt, L. Petersson, C. Wingren and M. L. Turner, *Biosens. Bioelectron.*, **2014**, 53, 82-89.
309. L. Schermelleh, R. Heintzmann and H. Leonhardt, *J. Cell Biol.*, **2010**, 190, 165-175.
310. G. Wittstock, M. Burchardt, S. E. Pust, Y. Shen and C. Zhao, *Angew. Chem. Int. Ed.*, **2007**, 46, 1584-1617.
311. I. A. Mahmood, S. O. R. Moheimani and B. Bhikkaji, *IEEE Transactions on Nanotechnology*, **2011**, 10, 203-216.
312. R. N. S. Sodhi, *Analyst*, **2004**, 129, 483-487.

313. T. L. Colliver, C. L. Brummel, M. L. Pacholski, F. D. Swanek, A. G. Ewing and N. Winograd, *Anal. Chem.*, **1997**, *69*, 2225-2231.
314. V. Spampinato, S. Vitale, S. Quici, A. Torrisi, V. Stepanenko, F. Würthner and A. Licciardello, *Surf. Interface Anal.*, **2013**, *45*, 206-210.
315. G. A.-N. Gohar, S. N. Khattab, O. O. Farahat and H. H. Khalil, *J. Phys. Org. Chem.*, **2012**, *25*, 343-350.
316. S. Perrier, C. Barner-Kowollik, J. F. Quinn, P. Vana and T. P. Davis, *Macromolecules*, **2002**, *35*, 8300-8306.
317. Y. K. Chong, J. Krstina, T. P. T. Le, G. Moad, A. Postma, E. Rizzardo and S. H. Thang, *Macromolecules*, **2003**, *36*, 2256-2272.
318. T. J. Curphey, *Org. Prep. Proced. Int.*, **1981**, *13*, 112-115.
319. H. L. Wagner, *J. Phys. Chem. Ref. Data*, **1985**, *14*, 1101-1106.
320. Z. Fei, D. Zhao, R. Scopelliti and P. J. Dyson, *Organometallics*, **2004**, *23*, 1622-1628.
321. K. A. Bunten and A. K. Kakkar, *Macromolecules*, **1996**, *29*, 2885-2893.
322. G. Saikia and P. K. Iyer, *J. Org. Chem.*, **2010**, *75*, 2714-2717.
323. B. Schulze, D. Escudero, C. Friebe, R. Siebert, H. Görls, U. Köhn, E. Altuntas, A. Baumgaertel, M. D. Hager, A. Winter, B. Dietzek, J. Popp, L. González and U. S. Schubert, *Chem. Eur. J.*, **2011**, *17*, 5494-5498.
324. M. Majek and A. Jacobi von Wangelin, *Angew. Chem. Int. Ed.*, **2013**.
325. V. Marin, E. Holder and U. S. Schubert, *J. Polym. Sci., Part A: Polym. Chem.*, **2004**, *42*, 374-385.

List of Publications

- 1 C. Lang, D. Voll, A. J. Inglis, N. Dingenouts, A. S. Goldmann, L. Barner and C. Barner-Kowollik, *Macromol. Chem. Phys.*, 2011, 212, 831-839.
- 2 C. Lang, C. Kiefer, E. Lejeune, A. S. Goldmann, F. Breher, P. W. Roesky and C. Barner-Kowollik, *Polym. Chem.*, 2012, 3, 2413-2420.
- 3 C. Lang, K. Pahnke, C. Kiefer, A. S. Goldmann, P. W. Roesky and C. Barner-Kowollik, *Polym. Chem.*, 2013, 4, 5456.

Conference Contributions

- 1 *Palladium-Containing Polymers via a Combination of RAFT and Triazole Chemistry*

Christiane Lang, Claude Kiefer, Elise Lejeune, Anja S. Goldmann, Frank Breher, Peter W. Roesky, Christopher Barner-Kowollik, *MacroBEGE*, Houffalize, Decemeber **2012**.

Danksagung

Eine schöne Zeit geht zu Ende. Ich blicke zurück auf drei Jahre voller Herausforderungen, einigen Niederlagen, glücklicherweise aber mehr Erfolgen. Auf diesem Weg haben mich viele Menschen auf die unterschiedlichste Art und Weise begleitet, unterstützt, gefordert und gefördert, denen ich nun danken möchte.

Prof. Christopher Barner-Kowollik danke ich für das entgegengebrachte Vertrauen in meine Fähigkeiten, für die Ratschläge und den Ansporn, den er jedem einzelnen in der Arbeitsgruppe zuteil werden lässt. Auch an Dr. Anja Goldmann richtet sich an dieser Stelle mein Dank für die vielfältige Unterstützung sowohl in wissenschaftlichen als auch in administrativen Fragen.

Für die gute Zusammenarbeit möchte ich mich bei meinen Kooperationspartnern aus der anorganischen Chemie, Tanja Wolfer (AK Breher), Dr. Sandra Gallardo-Gonzalez (AK Breher), Claude Kiefer (AK Roesky) und Sebastian Bestgen (AK Roesky), sowie bei den betreuenden Professoren, Herrn Prof. Breher und Herrn Prof Roesky, ganz herzlich bedanken.

Ebenso danke ich Kai Pahnke für die hilfreiche Unterstützung während seiner Diplomarbeit und Alexander Welle für die ToF-SIMS Messungen.

Teile dieser Arbeit wurden durch das Bundesministerium für Bildung und Forschung (BMBF) unter der Fördernummer 13N11312 finanziell gefördert und entstanden im Rahmen eines Kooperationsprojektes des Karlsruher Instituts für Technologie (KIT) mit der Universität Hamburg, dem Leibniz-Institut für Katalyse (LIKAT) in Rostock, und dem Fraunhofer Institut für Chemische Technologie (ICT) in Berghausen. Für die fruchtbaren Diskussionen bedanke ich mich bei allen Beteiligten.

Den Sekretariats-Mitarbeiterinnen Gabriele Herrmann und Evelyn Stühning, sowie Peter Gerstel, Vincent Schüler und Dr. Maria Schneider danke ich für die Unterstützung in all den administrativen und organisatorischen Bereichen.

Die Einrichtung der neuen Außenstelle „Westhochschule“ war eine der großen Herausforderungen, die in dieser Arbeit nicht zur Geltung kommen und doch für mich persönlich sehr wichtig sind. An dieser Stelle gilt mein ganz besonderer Dank den Helden der ersten Stunde Dr. Sebastian Emmerling und Dr. Christoph Dürr, sowie

Dr. Maria Schneider, die sich mit all den Bestellungen, Reklamationen und Änderungswünschen herumärgern musste. Aber auch den späteren „Westies“ Dr. Lebohang Hlalele, Kai Pahnke, Dr. Andrew Vogt, Dr. Keita Fuchise und Tanja Claus danke ich für die tolle Atmosphäre.

Kai Pahnke, Doris Abt, Jan Müller und Dr. Dominik Voll danke ich für das aufmerksame Korrekturlesen meiner Arbeit. Besonders hervorheben möchte ich an dieser Stelle auch Michael Kaupp und Thomas Tischer – meinen Mitstreitern in Sachen Doktorarbeit und den Mitgestaltern der legen... es kommt gleich...dären PhD Party!

Für die vielen wissenschaftlichen Anregungen und Diskussionen bedanke ich mich bei allen ehemaligen und gegenwärtigen macroarc-Mitarbeitern. Aber zum Glück stand nicht immer nur die Arbeit im Vordergrund; viele Geburtstagsfeiern, Barbecues, Summertrips und Weihnachtsfeiern, Doktorwagenbau-Aktionen und Doktorfeiern bereicherten stets den Arbeitsalltag und schafften einen angenehmen Ausgleich. Ich hoffe, dass diese Tradition auch weiterhin so fortgeführt wird.

Mit einem „Dreifach kräftig Wasser Marsch“ danke ich allen Feuerwehrangehörigen der Freiwilligen Feuerwehr Eggenstein-Leopoldshafen – meiner zweiten Familie. Im Besonderen danke ich meinen Kids der Jugendfeuerwehr für die tollen Jugenddienste und allen Jugendbetreuern, aber auch der „Gold-Gruppe“.

Es gibt Menschen, die einen ganz besonders beeindruckten und beeinflussen. Alexandra Till, Julian Will, Christian Nagel, Anja Goldmann, Corinna Preuß und Jan Müller haben das auf ihre ganz eigene Art und Weise getan. Dafür schulde ich ihnen mehr als nur meinen Dank.

Ich danke meiner Familie, meinen Eltern Ute und Karl-Heinz Lang, sowie meinem Bruder Stephan dafür, dass sie mich immer unterstützt haben, immer ein offenes Ohr hatten und mich immer wieder aufgebaut haben, wenn es nötig war. Ebenfalls bedanken möchte ich mich bei meinem Onkel Jürgen und seiner Familie. Ich denke an meine geliebten Großeltern, von denen ich mich viel zu früh verabschieden musste. Nicht zuletzt gilt ein riesengroßer Dank Martin Nagel. Es ist schön, einen Menschen an meiner Seite zu wissen, der sowohl schlechte Zeiten als auch gute Zeiten mit mir durchlebt – egal ob zwischen dem Wechsel nur Minuten oder ganze Wochen liegen.